



**OPTIMISATION OF VERTICAL AXIS WIND
TURBINE BY USE INOVATIVE DESIGN**

**2022
PhD THESIS
ENERGY SYSTEM ENGINEERING**

Hashem Ibrahim M. ABUSANNUGA

**Thesis Advisor
Prof. Dr. Mehmet ÖZKAYMAK**

**OPTIMIZATION THE PERFORMANCE OF A UNIQUE AND
DEVELOPED TYPE OF VERTICAL TURBINE USING THEORETICAL
AND EXPERIMENTAL TECHNIQUES**

Hashem Ibrahim M. ABUSANNUGA

**T.C.
Karabuk University
Institute of Graduate Programs
Department of Energy System Engineering
Prepared as
PhD Thesis**

**Thesis Advisor
Prof. Dr. Mehmet ÖZKAYMAK**

**KARABUK
January 2022**

I certify that in my opinion the thesis submitted by HASHEM ABUSANNUGA titled “OPTIMISATION OF VERTICAL AXIS WIND TURBINE BY USE INOVATIVE DESIGN” Is fully adequate in scope and in quality as a thesis for the degree of Doctoral of Engineering.

Prof. Dr. Mehmet ÖZKAYMAK
Thesis Advisor, Energy Systems Engineering Department

This thesis is accepted by the examining committee with a unanimous vote in the Department of Energy System Engineering as a Doctoral thesis. January 28, 2022

Examining Committee Members (Institutions) Signature

Chairman: Prof. Dr. Kurtuluş BORAN (GÜ)

Member : Prof. Dr. Mehmet ÖZKAYMAK (KBÜ)

Member : Assist. Prof. Dr. Engin GEDİK (IBÜ)

Member : Assist. Prof. Dr. Erhan KAYABAŞI (KBÜ)

Member : Assoc. Prof. Dr. Bayram KÖSE (KBÜ)

The degree of Doctoral of Engineering by the thesis submitted is approved by the Administrative Board of the Institute of Graduate Programs, Karabük University.

Prof. Dr. Hasan SOLMAZ
Director of the Institute of Graduate Programs

“I declare that all the information within this thesis has been gathered and presented in accordance with academic regulations and ethical principles and I have according to the requirements of these regulations and principles cited all those which do not originate in this work as well.”

Hashem Ibrahim M. ABUSANNUGA

ABSTRACT

Ph.D. Thesis

OPTIMISATION OF VERTICAL AXIS WIND TURBINE BY USE INOVATIVE DESIGN

Hashem Ibrahim M. ABUSANNUGA

**Karabük University
Institute of Graduate Programs
The Department of Energy System Engineering**

Thesis Advisor:

Prof. Dr. Mehmet ÖZKAYMAK

January 2022, 175 pages

In the context of interests in the sector of renewable energies in general and wind energy in particular, the topic of this thesis revolved around the design and manufacture of a unique system of vertical axis wind turbines and its comparison with other systems known to specialists and those interested in the sector of wind energy. This thesis is divided into seven stages, which are sequenced as follows. Work began with the selection of an appropriate analytical mathematical model. The *Multi-Stream Tube* model was chosen, where modifications were made to match the target study cases. In the second stage, a programming process for the *Multi-Stream Tube* model was carried out by *Microsoft Visual Software*, Therefore, the computer program was designed and called *Al-Hashem VAWT Soft*. Before starting the third stage, the quality of the results of the computer program was verified by comparing its theoretical results with previous reliable laboratory results. The third stage included a pneumatic kinematic analysis using the designed computer program,

where three engineering designs of vertical axis propellers were studied, and they are the original *Darrieus* rotor in the shape of a parabolic, the modified *Darrieus* rotor that takes the shape of rectangle or square and an innovative air rotor in this thesis where half of its area is the upper is similar to the trapezoid, as well as the lower. Fourth stage the *Solidwork* program was used to design three types of wind rotor with different geometric shapes in order to be used in the fifth stage. The three designs are slant straight blade vertical axis wind turbine with inclination angles *35 Degree*, *55 Degree* and *85 Degree*. In the fifth stage, a computer program called *Ansys Fluent* was used in order to work on physical modeling of designs extracted from *Solidworks* and to compare them physically in terms of the effect of aerodynamic on them during their rotation. Based on all of the above stages, a prototype was manufactured, which is an innovative vertical axis air fan. During this thesis, its geometric shape can change to *64* configurations by changing the angles of its blades. In the context of this thesis, it was called *Sannuga system SS-VAWT 01*, where “*Sannuga*” is relative to the surname of the author of this thesis, “*SS*” stands for Slant Street Blade, “*VAWT*” is a vertical axis wind turbine and “*01*” indicates that this is the first version of the design. In the eighth and final phase, preliminary field tests of the *Sannuga system SS-VAWT 01* prototype were conducted. A comparison was made between the findings of some of the eight stages, the results were compatible, and one of the most important results obtained was to determine the optimal geometric shape of a vertical axis wind rotor in terms of aerodynamic efficiency.

Key Words : Wind turbine, VAWT, aerodynamic performance, multi-stream tube, self-starting problem,

Science Code : 92806

ÖZET

Doktora Tezi

DÜŞEY EKSENLİ RÜZGAR TÜRBİNİNİN YENİLİKÇİ TASARIM KULLANIMIYLA OPTİMİZASYONU

Hashem Ibrahim M. ABUSANNUGA

Karabük Üniversitesi

Lisansüstü Eğitim Enstitüsü

Enerji Sistemleri Mühendisliği Anabilimdalı

Tez Danışmanı:

Prof. Dr. Mehmet ÖZKAYMAK

Ocak 2021, 175 sayfa

Genel olarak yenilenebilir enerjiler ve özel olarak rüzgar enerjisi alanındaki ilgiler bağlamında, bu tezin konusu, benzersiz bir dikey eksenli rüzgar türbini sisteminin tasarımı ve üretimi ve bunun uzmanlar tarafından bilinen diğer sistemlerle ve diğer sistemlerle karşılaştırılması etrafında dönüyordu. rüzgar enerjisi alanına ilgi duymaktadır. Bu tez, aşağıdaki gibi sıralanan yedi aşamaya ayrılmıştır. Çalışma, uygun bir analitik matematiksel modelin seçilmesiyle başladı. Hedef çalışma durumlarını eşleştirmek için değişikliklerin yapıldığı Multi-Stream Tube modeli seçildi. İkinci aşamada, Multi-Stream Tube modeli için Microsoft Visual Software tarafından bir programlama işlemi gerçekleştirilmiştir, bu nedenle bilgisayar programı tasarlanmış ve Al-Hashem VAWT Soft olarak adlandırılmıştır. Üçüncü aşamaya başlamadan önce, bilgisayar programının sonuçlarının kalitesi, teorik sonuçları ile önceki güvenilir laboratuvar sonuçları karşılaştırılarak doğrulandı. Üçüncü aşama, dikey eksenli pervanelerin üç mühendislik tasarımının incelendiği ve

bunların bir parabolik şeklindeki orijinal Darrieus rotoru, dikdörtgen veya dikdörtgen şeklini alan modifiye Darrieus rotoru olduğu, tasarlanan bilgisayar programını kullanan bir pnömatik kinematik analizi içeriyordu. Alanının yarısının üstte olduğu bu tezde kare ve yenilikçi bir hava rotoru, yamuğun yanı sıra altta da benzer. Dördüncü aşamada Solidwork programı kullanılarak, beşinci aşamada kullanılmak üzere farklı geometrik şekillere sahip üç tip rüzgar rotoru tasarlanmıştır. Üç tasarım, eğim melekleri 35 Derece, 55 Derece ve 85 Derece ile eğimli düz kanatlı dikey eksenli rüzgar türbinidir. Beşinci aşamada, Solidworks'ten çıkarılan tasarımların fiziksel modellemesi üzerinde çalışmak ve dönmeleri sırasında aerodinamiğin üzerlerindeki etkisi açısından fiziksel olarak karşılaştırmak için Ansys Fluent adlı bir bilgisayar programı kullanılmıştır. Yukarıdaki aşamaların tümüne dayanarak, yenilikçi bir dikey eksenli hava fanı olan bir prototip üretildi. Bu tez sırasında, kanatlarının açıları değiştirilerek geometrik şekli 64 konfigürasyona dönüşebilir. Bu tez bağlamında, Sannuga sistemi SS-VAWT 01 olarak adlandırılmıştır, burada “Sannuga” bu tezin yazarının soyadına göredir, “SS” Slant Street Blade anlamına gelir, “VAWT” dikey eksenli bir rüzgardır. türbin ve “01”, bunun tasarımın ilk versiyonu olduğunu gösterir. Sekizinci ve son aşamada, Sannuga sistemi SS-VAWT 01 prototipinin ön saha testleri yapıldı. Sekiz aşamadan bazılarının sonuçları arasında bir karşılaştırma yapıldı, sonuçlar uyumluydu ve elde edilen en önemli sonuçlardan biri, aerodinamik verimlilik açısından dikey eksenli bir rüzgar rotorunun optimal geometrik şeklini belirlemektir.

Anahtar Kelimeler : Rüzgar türbini, VAWT, aerodinamik performans, çoklu akış tüpü, kendi kendine başlama sorunu

Bilim Kodu : 92806

ACKNOWLEDGEMENT

First of all, in veneration and honor of my parents, I present to them this achievement as a very modest gift from me, in recognition of their tireless effort and endless giving. I also thank my wife for her support and patience with me. Sincere thanks to the Libyan “Center for Solar Energy Research and Studies” for granting Scholarship to do a PhD in Turkey. I would also like to express my sincere gratitude, appreciation and thanks to my advisor, Prof. Dr. Mehmet ÖZKAYMAK, for his skillful supervision of this thesis and his valuable advice and guidance. Furthermore, extend my thanks and gratitude to the Karabuk University staff for the quality of services and the provision of appropriate condition for student.

CONTENTS

	<u>Page</u>
APPROVAL.....	ii
ABSTRACT.....	iv
ÖZET.....	vi
ACKNOWLEDGEMENT	viii
LIST OF FIGURES	xiii
LIST OF TABLES	xviii
SYMBOLS AND ABBREVIATIONS INDEX	xviii
PART 1	1
INTRODUCTION	1
1.1. WIND POWER	1
1.2. WIND TURBINES	3
1.2.1. Horizontal Axis Wind Turbine “HAWT”	4
1.2.2. Vertical Axis Wind Turbine “VAWT”	5
1.3. PROBLEM STATEMENT	7
1.4. THESIS OBJECTIVES	8
1.5. THESIS OUTLINE	9
PART 2	10
LITERATURE REVIEW.....	10
2.1. A BRIEF HISTORY OF VAWT WIND TURBINES.....	10
2.2. ADVANTAGES AND DISADVANTAGES OF VAWTs.....	33
2.3. TYPES OF VAWTs	34
2.3.1. Straight Bladed Darrieus Turbine.....	34
2.3.2. Curved Bladed Turbine.....	35
2.3.3. Hybrid Savonius-Darrieus Turbine.....	35
2.3.4. Blade Pitching Darrieus Turbine	37
2.3.5. Helical Turbine	38
2.4. AERODYNAMICS OF VAWTs	40

	<u>Page</u>
PART 3	45
METHODOLOGY AND METHODS.....	45
3.1. SLANT-STRAIGHT BLADE ROTOR (SS-VAWT).....	45
3.1.1. Geometric Details of SS-VAWT	45
3.1.2. Performance Optimization of SS-VAWT.....	46
3.2. MODIFIED MULTI STREAM TUBE MODEL.....	48
3.2.1. Overview.....	48
3.2.2. Multiple Streamtube Model.....	49
3.3. DESIGNED ANALYSIS SOFTWARE.....	59
3.3.1. Overview.....	59
3.3.2. Mathematical Commands Used in AL Hashem VAWT Soft.....	63
3.4. PERFORMANCE COMPARISON OF PARABOLIC-DARRIEUS, STRAIGHT BLADE DARRIEUS AND SLANTING STRAIGHT BLADE-DARRIEUS	64
3.5. SIMULATION USEING ANSYS FLUENT	65
3.5.1. Pre-Processing	66
3.5.2. Processing	88
3.5.3. Post-Processing.....	88
3.6. DETAILED ENGINEERING DESIGN OF (SS-VAWT).....	89
3.6.1. Using the Wind Energy Equation for (SS-VAWT).....	89
3.6.2. Determine the Value of the Rotor Area (A)	90
3.6.3. Choosing the Type of Airfoil.....	93
3.6.4. Geometric Dimensions Values of the SS-VAWT	94
3.7. SANNUGA SYSTEM SS-VAWT 01	94
3.7.1. Solidworks Software Design	96
3.7.2. System Manufacturing Process	96
 PART 4	 99
RESULTS AND DISCUSSION	99
4.1. EFFECT OF GEOMETRIC SHAPE OF SS-VAWT ON ITS PERFORMANCE (Case: 25DEG).....	99
4.1.1. Rotor Hight Effect (H).....	99
4.1.2. Rotor Radius Effect (R).....	99

	<u>Page</u>
4.1.3. Number of Blade Effect (N)	99
4.1.4. Airfoil Chord Length Effect (C)	100
4.2. EFFECT OF GEOMETRIC SHAPE OF SS-ROTOR ON ITS PERFORMANCE (Case: 45DEG).....	102
4.2.1. Rotor Hight Effect (H).....	102
4.2.2. Rotor Radius Effect (R)	102
4.2.3. Number of Blade Effect (N)	102
4.2.4. Airfoil Chord Length Effect (C)	102
4.3. EFFECT OF GEOMETRIC SHAPE OF SS-ROTOR ON ITS PERFORMANCE (Case: 65DEG).....	105
4.3.1. Rotor Hight Effect (H).....	105
4.3.2. Rotor Radius Effect (R)	105
4.3.3. Number of Blade Effect (N)	105
4.3.4. Airfoil Chord Length Effect (C)	105
4.4. EFFECT OF GEOMETRIC SHAPE OF SS-ROTOR ON ITS PERFORMANCE (Case: 85DEG).....	108
4.4.1. Rotor Hight Effect (H).....	108
4.4.2. Rotor Radius Effect (R)	108
4.4.3. Number of Blade Effect (N)	108
4.4.4. Airfoil Chord Length Effect (C)	108
4.5. FOUR CASES COMPARISON FOR THE SS-VAWT ROTOR.....	111
4.5.1. Influence of β On C_p at Different H Values.....	111
4.5.2. Influence of β On C_p at Different R Values	111
4.5.3. Influence of β on C_p at different N values	112
4.5.4. Influence of β On C_p at Different R Values	112
4.6. REYNOLDS NUMBER EFFECT	115
4.7. PERFORMANCE OF SS-VAWT vs, S & PB-DARRIEUS	115
4.8. WORK WITHIN THREE SPECIFIC ANGLES [35Deg 55Deg 85Deg]....	118
4.8.1. The Case Study 35Deg	118
4.8.2. The Case Study 55Deg	118
4.8.3. The Case Study 85Deg	118
4.9. ANSYS FLUENT POST PROCESSING	120
4.9.1. Aerodynamic Investigations of Physical Phenomena.....	120

	<u>Page</u>
4.9.2. Aerodynamic Forces for the Three Cases [35Deg, 55Deg, 85Deg].....	125
4.9.3. Forces Effects Comparison of Three Cases [35Deg, 55Deg, 85Deg] ..	126
4.9.4. Power Output for The Three Cases [<i>35Deg, 55Deg, 85Deg</i>].....	128
PART 5	131
CONCLUSION	131
5.1. FUTURE WORK	132
REFERENCES	134
APPENDIX A. “AL-HASHEM VAWT” MICROSOFT VISUAL SOFTWARE..	146
APPENDIX B. “SANNUGA SYSTEM SS-VAWT 01” SOLIDWORKS DESIGN.....	156
APPENDIX C. PROTOTYPE MANUFACTURING	166
APPENDIX D. SANNUGA SYSTEM SS-VAWT 01	171
APPENDIX E. PUBLICATIONS.....	173
RESUME	175

LIST OF FIGURES

	<u>Page</u>
Figure 1.1. Significant achievements by the wind sector since 1982.....	1
Figure 1.2. Wind power installation in the worldwide in 2020	2
Figure 1.3. Tow basic configurations of the wind turbine.	3
Figure 1.4. horizontal axis wind turbines.	5
Figure 1.5. Vertical axis wind turbines.	7
Figure 2.1. a) Original three-bladed phi, b) First Darrieus style of VAWTs, c) Darrieus on rooftop of NRC.	11
Figure 2.2. a) 230kW-Darrieus, was installed in the Magladen Islands, b) 500kW-Darrieus was produced by DAF Indal, c) 50kW-Darrieus was produced by DAF Indal.	13
Figure 2.3. a) Sandia 17-m with strutted, b) Sandia 17-m without strutted, c) Sandia 34-metre with two blades.	15
Figure 2.4. a) ALCOA 8kW capacity, b) ALCOA 500KW-VAWT model.	16
Figure 2.5. a) Wind Turbines of CWT Power, b) Turbine from CWT Power, c) 9-kW double-bladed turbine produced by Bjervig.....	17
Figure 2.6. Sandia FlowWind model.	19
Figure 2.7. EOLE model with 3.8MW capacity.	20
Figure 2.8. a) Musgrove wind turbine 30KW, b) Musgrove wind turbine 500KW.	22
Figure 2.9. a) NOVA-VAWT with sails, b) 10MW offshore V-shaped VAWT.....	23
Figure 2.10. Vertical Wind AB 200KW prototype.....	25
Figure 2.11. a) Combines wind and tidal energy in a single unit, b) Gearbox and generator of (Skwid) system.....	27
Figure 2.12. Offshore VertAx wind turbine.....	29
Figure 2.13. Vertiwind -VAWT.....	31
Figure 2.14. a) 15 KW ANEW-S1, b) 1.5 MW ANEW-B1.....	33
Figure 2.15. Dornier Darrieus/Savonius 5.5KW.	37
Figure 2.16. Helical Turbine with three blades.....	40
Figure 2.17. Multi-streamtube model.....	41
Figure 2.18. Double multi-streamtube model	42
Figure 2.19. The vortex model basics.	43
Figure 3.1. Changing the Angle of Inclination of the Rotor Blade SS-VAWT.....	45

	<u>Page</u>
Figure 3.2. Geometric Variables of the SS-VAWT.....	46
Figure 3.3. The System Is in Several Geometric Shapes.....	47
Figure 3.4. Geometrical Aspects of Multiple Streamtube Model and Relevant Velocities.....	50
Figure 3.5. Blade-element position.....	51
Figure 3.6. Wind velocity component normal to blade element surface ($V \sin \theta \sin \beta$).....	52
Figure 3.7. Velocity Triangle at a Blade-Element.....	53
Figure 3.8. Forces Acting on a Blade-Element.....	53
Figure 3.9. Power Coefficient as Function of Tip Speed Ratio.....	57
Figure 3.10. Input Window of AL Hashem VAWT Program.....	60
Figure 3.11. AL Hashem VAWT Program Flowchart.....	61
Figure 3.12. Validation of the Results of the Al-Hashem program.....	64
Figure 3.13. Sketch for Three Types of Vertical Wind Rotor.....	65
Figure 3.14. The model before mesh step.....	66
Figure 3.15. Creating Domine for the Model.....	67
Figure 3.16. Imported the Model into “Ansys Design Modeler”.....	67
Figure 3.17. The model in “Ansys Design Modeler”.....	68
Figure 3.18. Creating <i>Booleans</i> for the model.....	69
Figure 3.19. <i>CFD mesh</i> for the flow domain.....	70
Figure 3.20. Primary surface mesh.....	70
Figure 3.21. Mesh refinement the turbine and sliding interface.....	71
Figure 3.22. Element quality.....	72
Figure 3.23. Aspect ratio.....	72
Figure 3.24. Skewness.....	73
Figure 3.25. The step of choosing the type of solver.....	75
Figure 3.26. Step of choosing the type of physical model.....	78
Figure 3.27. Step of choosing materials and properties.....	80
Figure 3.28. The cell zones slide.....	81
Figure 3.29. Velocity inlet in boundary condition step.....	83
Figure 3.30. Pressure output in boundary condition step.....	84
Figure 3.31. Symmetry boundary conditions.....	85
Figure 3.32. Solution method step.....	86
Figure 3.33. Solution initialization step.....	87

	<u>Page</u>
Figure 3.34. Run calculations step.....	88
Figure 3.36. Five different geometrical shape of SS-VAWT.....	92
Figure 3.37. Average wind speeds for a year in the "Bala" region.....	92
Figure 3.38. "bala" Location on the Map.....	93
Figure 3.39. Airfoil "NACA 0015" with Dimensions.....	93
Figure 3.40. General design details of the system.....	95
Figure 3.41. Some Important parts of the system.....	95
Figure 3.42. Sannuga system SS-VAWT 01.....	97
Figure 3.43. Five geometrical configurations of the System.....	98
Figure 4.1. Height change effect, case: 25Deg.....	100
Figure 4.2. Radius change effect, case: 25Deg.....	100
Figure 4.3. Blades number change effect, case: 25Deg.....	101
Figure 4.4. Chord length change effect, case: 25Deg.....	101
Figure 4.5. Hight change effect, case: 45Deg.....	103
Figure 4.6. Radius change effect, case: 45Deg.....	103
Figure 4.7. Blades number change effect, case: 45Deg.....	104
Figure 4.8. Chord length change effect, case: 45Deg.....	104
Figure 4.9. Height change effect, case: 65Deg.....	106
Figure 4.10. Radius change effect, case: 65Deg.....	106
Figure 4.11. Blades number change effect, case: 65Deg.....	107
Figure 4.12. Chord length change effect, case: 65Deg.....	107
Figure 4.13. Height change effect, case: 85Deg.....	109
Figure 4.14. Radius change effect, case: 85Deg.....	109
Figure 4.15. Blades number change effect, case: 85Deg.....	110
Figure 4.16. Chord length change effect, case: 85Deg.....	110
Figure 4.17. Influence of β on C_p at different H values.....	113
Figure 4.18. Influence of β on C_p at different R values.....	113
Figure 4.19. Influence of β on C_p at different N values.....	114
Figure 4.20. Influence of β on C_p at different C values.....	114
Figure 4.21. Reynolds number effect on power factor.....	115
Figure 4.22. Comparison when changing the height of the three models.....	116
Figure 4.23. Comparison when changing the radius of the three models.....	116
Figure 4.24. Comparison when changing the blades number of the three cases.....	117

	<u>Page</u>
Figure 4.25. Comparison when changing the chord length of the three models.....	117
Figure 4.26. Power factor behavior in case of 35Deg.....	119
Figure 4.27. Power factor behavior in case of 55Deg.....	119
Figure 4.28. Power factor behavior in case of 85Deg.....	120
Figure 4.29. Velocity vectors behavior for three cases of SS-VAWT.....	121
Figure 4.30. Stream lines behavior for three cases of SS-VAWT.	122
Figure 4.31. Velocity vectors behavior for three cases of SS-VAWT domine.....	122
Figure 4.32. Pressure behavior for three cases of SS-VAWT.....	123
Figure 4.33. Pressure counter of three cases of SS-VAWT.....	123
Figure 4.34. Velocity counter of three cases of SS-VAWT.....	124
Figure 4.35. Wall shear due to aerodynamic forces.....	124
Figure 4.36. Force effect in three directions for case study 35deg.....	125
Figure 4.37. Force effect in three directions for case study 55deg.....	125
Figure 4.38. Force effect in three directions for case study 85deg.....	126
Figure 4.39. X-Force comparison.....	127
Figure 4.40. Y-Force comparison.....	127
Figure 4.41. Z-Force comparison.....	128
Figure 4.42. Power output for case 35Deg.....	128
Figure 4.43. Power output for case 55Deg.....	129
Figure 4.44. Power output for case 85Deg.....	129
Figure 4.45. Output power comparison of cases [35Deg, 55Deg, 85Deg].....	130
Figure Appendix B.1. “Sannuga System VAWT 01” Engineering Drawings.....	157
Figure Appendix C.1. Blades Tamblet.....	167
Figure Appendix C.2. Initial Blade.....	167
Figure Appendix C.3. Airfoil Tamblets.....	167
Figure Appendix C.4. Aluminyum Supports.....	168
Figure Appendix C.5. Blades Production.....	168
Figure Appendix C.6. Blades are Ready.....	168
Figure Appendix C.7. Metal joints for fixing blades.....	169
Figure Appendix C.8. Aluminum Struts Connecting Blades to the Discs.....	169
Figure Appendix C.9. Iron Discs Connecting Struts to the Shaft.....	169
Figure Appendix C.10. Iron Rotating Shaft.....	170
Figure Appendix C.11. Bearing Covers.....	170

	<u>Page</u>
Figure Appendix C.12. The Tower and Its Upper Base.....	170
Figure Appendix D.1. Multi Shape of “Sannuga System SS-VAWT 01”.....	172

LIST OF TABLES

	<u>Page</u>
Table 3.1. Four groups of SS-VAWT geometrical variables parameters	47
Table 3.2. Initial design input	90
Table 3.3. Value of aera for each case.	90
Table 3.4. Value of aera for each case.	94

SYMBOLS AND ABBREVIATIONS INDEX

SYMBOLS

A	: rotor swept area
A_b	: blade planform area
A_S	: cross-sectional area of streamtube
a	: Induced velocity area
C	: blade chord
C_d	: drag coefficient
C_l	: lift coefficient
C_m	: torque coefficient
C_n	: $C_l \cos\alpha + C_d \sin\alpha$
C_p	: power coefficient
C_{p_m}	: maximum power coefficient
C_t	: $C_l \sin\alpha - C_d \cos\alpha$
d	: rotor diameter
dD	: element drag force
df	: elemental axial force acting on one blade-element
dF_r	: element radial force
dF_t	: element tangential force
df_x	: elemental axial force acting on streamtube
dL	: elemental lift force
ds	: blade-element length
f_x^*	: $\left[\frac{Ndf}{2\pi r \rho V_1^2 \sin \theta dz} \right]$
H	: rotor half height
h	: rotor height
M	: moment
N	: number of blades
P	: power

R : maximum rotor radius
 Re : Reynolds number
 V : air velocity in rotor plane
 V_1 : free stream velocity
 V_2 : wake velocity
 ΔV : $V_1 - V_2$
 W : resultant velocity
 α : angle of attack
 β : blade inclination angle
 λ_0 : tip speed ratio
 θ : azimuth angle
 ρ : air density
 ω : angular velocity
 σ : solidity
 r : radius at z

PART 1

INTRODUCTION

1.1. WIND POWER

In recent years, wind power has been a leading technological innovation. Wind power, after hydroelectric power, is the leading renewable power technology in terms of overall generation capacity, with more than half a terawatt installed at the end of 2018. Along with hydro, wind accounted for the majority of overall renewable energy adds in 2018, with about 43 GW added globally. Figure 1.1 show significant achievements by the wind sector since 1982. [1]

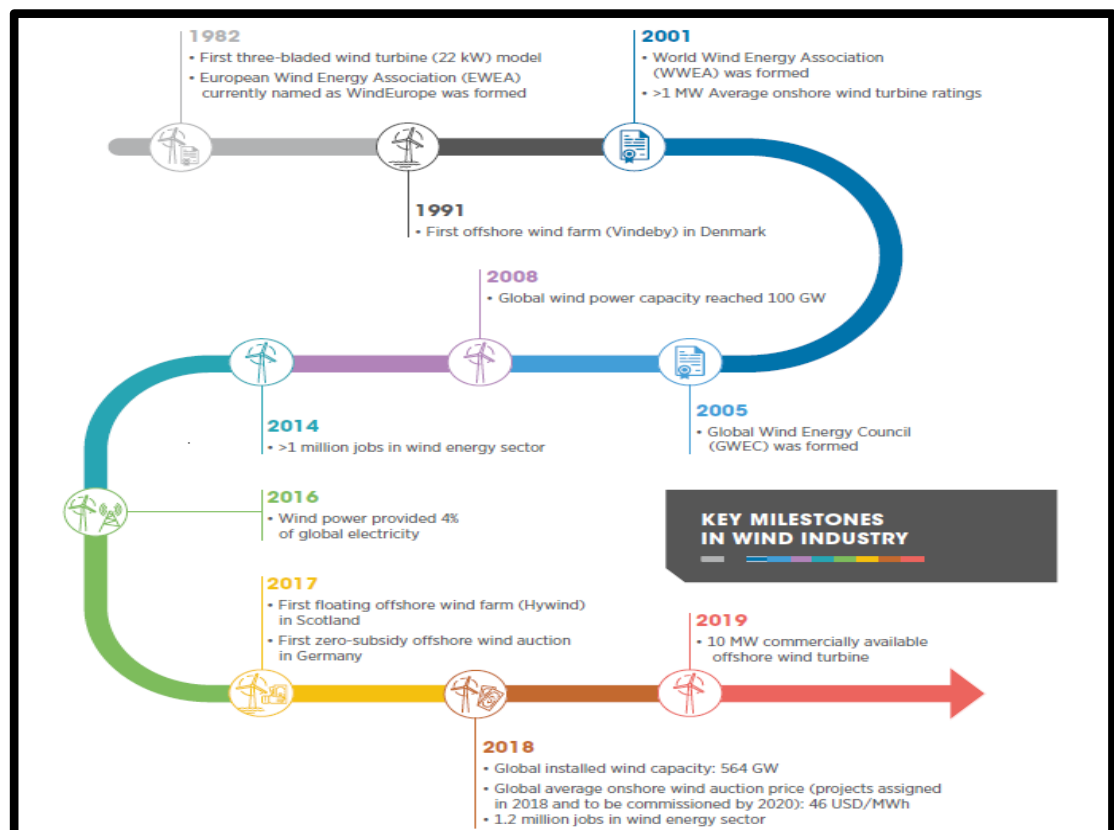


Figure 1.1. Significant achievements by the wind sector since 1982 [1].

Global new wind power projects exceeded 90 GW in 2020, up 53% from year earlier, taking overall generating capacity to 743 GW, up 14% from year earlier. The onshore wind market saw 86.9 GW of system upgrades, whereas the offshore wind market saw 6.1 GW, 2020 will be the first and second-largest year for wind power projects in history, respectively. The Asia Pacific needs to keep in global wind power production, with its market share in the global rising by 8.5 percent last year due to this rapid increase of installations in China. North America 18.4 % has surpassed Europe 15.9% as the second-largest geographic market for new installations due to a record year of installations throughout the United States. In 2020, Latin America will maintain its position as the world's fourth largest geographical market 5.0 %, led by Africa and the Middle East 0.9%. China, USA, Brazil, the Netherlands, and Germany became the top five regions for new installations in 2020. Last year, these five markets accounted for 80.6 % of global installations, an increase of even more than 10% from 2019, Figure 2 shows wind power installation in the worldwide in 2020. [2]



Figure 1.2. Wind power installation in the worldwide in 2020 [2].

1.2. WIND TURBINES

Through the use of blades and a pole, a wind system transforms fluid energy into mechanical energy, which is then converted into electrical energy by a generator. The type of a wind machine is specified by whether the stream is corresponding to the hub of turn (pivotal stream) or opposite (spiral stream), Figure 1.3 exhibit tow basic types of wind turbine. Each design of wind turbine has its own set of advantages and disadvantages; however, in the end, all wind turbines work in a similar way [3].

Based on their blade design and function, wind systems are split into two species. The horizontal axis wind turbine “HAWT” is the first kind. It is the most typical kind of wind turbine and can be found scattered around the countryside in areas with relatively flat terrain and consistent year-round wind patterns. HAWTs are made up of a pair of blades that rotate around an axis in the opposite direction of flow and are supported by a tall tower. For decades, these wind turbines have been the focus of wind turbine research, owing to their similar procedure and characteristics to rotational aircraft [4].

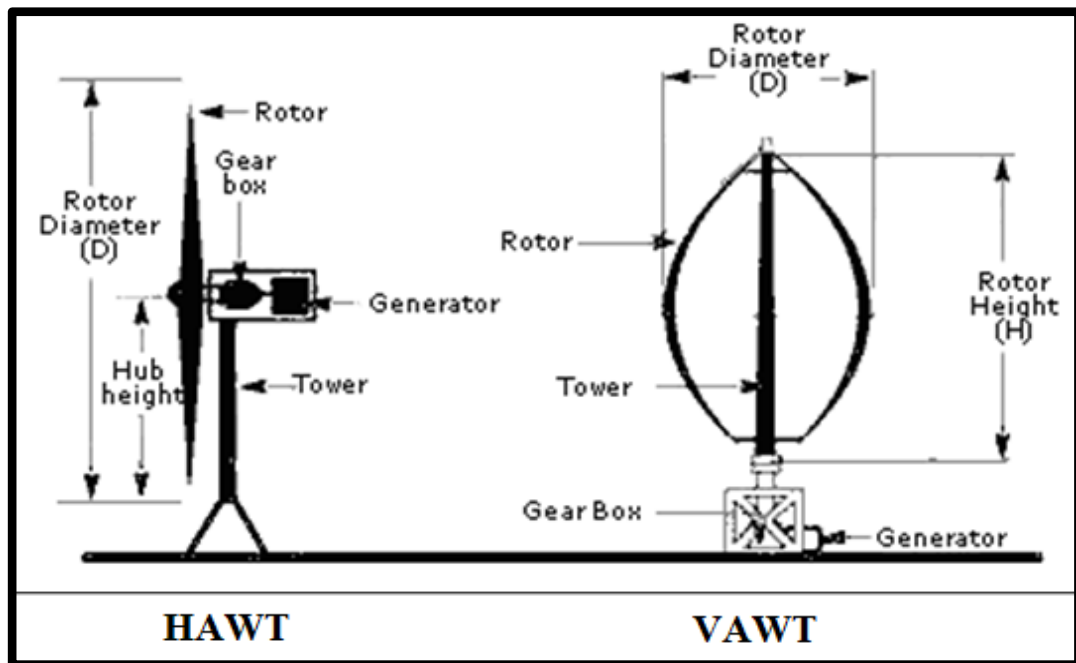


Figure 1.3. Tow basic configurations of the wind turbine.

The vertical axis wind turbine is the second most common kind of wind turbine “VAWT”. This model of wind turbine circulates around a perpendicular axis to the

approaching surge, allowing it to capture wind from either direction. Darrieus rotor and the Savonius rotor are the two main forms of VAWTs. Darrieus wind turbine “VAWT” that rotates around a central axis due to the lift provided by spinning airfoils, while the Savonius rotor rotates because of the drag generated by their blades. A new kind of VAWT is emerging inside the wind energy science which is a combination of the Darrieus and Savonius designs. The multiple kinds of wind turbines are shown in Figure 1.3 [5]. In this figure, the difference between vertical and horizontal axis fans is shown in terms of geometry and the distribution of components such as electrical materials and gearbox.

1.2.1. Horizontal Axis Wind Turbine “HAWT”

The HAWT has been the most commonly used and efficient wind turbine. Vestas, Siemens, and GE companies are among the world's leading and most efficient wind turbine companies, developing and deploying HAWTs in worldwide. These businesses are supported by wind turbine technologies based on knowledge and experience gained from rotor and rotational aircraft. Any big wind turbine on the planet employs a large number of HAWTs who work together to help produce energy for rural-urban areas [6], Figure 1.4 shows horizontal axis wind turbines.

A HAWT's blades generate lift to capture power from the wind, compared with a net torque along the shaft. The gearbox accelerates the slow spinning of such wind turbine blades to produce electricity via a generator, which generates torque. Active pitch controls are also used to assure that every blade is balanced to retain an optimum angle of attack for maximum energy production for a specific speed, which is particularly important for large HAWTs. To deliberately yaw the blades towards the wind, a yaw controller is sometimes used. Such active controllers, on the other hand, are much more complicated and require several movable parts and time to build than a VAWT system, in which the rotor has been the only moving part, and thus the rest of the parts are placed just at the turbine's base [7].

A HAWT blade is difficult to build and manufacture because of its narrowness and pervaded with differing cross-sections to attain optimal aerodynamic efficiency. The

difference of the relative velocity factor W causes the blade's cross-section and twist to shift from both the roots to tips. The blade's twist is facile, and the cross-section is narrow since the tip turns even faster than that of the base. The resulting force F operating upon the blade segment is incredibly high because of high relative velocity just at the tip, but only a small proportion of such a drag force is controlling the rotation. According to the current blade's design, the narrow blade profile with such a low angle of twist at the tip provides approximately the same amount of torque as that of the blade's root due to the wide-moment arm. The blade profile seems to be much thicker at the base, with a higher angle of twist, than at the tip, due to slower rotation speed. Because of this configuration, a major percentage of the resulting force is directed in the rotational direction. The torque distribution around the blade is somewhat linear because of the lower moment arm at the root. [8]



Figure 1.4. horizontal axis wind turbines.

1.2.2. Vertical Axis Wind Turbine “VAWT”

VAWTs have progressively increased in popularity as people become more interested in self-renewable energy sources. Such new devices, such as *Helix Wind Turbine*, *Urban Green Energy*, and *Wind spire*, are being promoted by small businesses around the world. As a means of supplying local and personal wind

energy, VAWTs target individual residences, farmland, or small residential areas. This eliminates the target individual's reliance on external energy sources while still opening up a wider demand for renewable energy technologies. Since VAWTs are compact, discreet, simple to mount, could capture wind direction, yet work effectively in high turbulence circumstances, a new field of wind turbine research has emerged to address the needs of people who want to monitor and engage in compact wind power technologies [9-12].

The system is itself extremely easy. The wind turbine's most complicated components, such as the gearbox and engine, are mounted at the bottom, leaving just the rotor as the main moving part. Installing a VAWT becomes a simple and fast process as a result of this. Because of the continuous cross-section blades, designing a VAWT is so much easier than HAWT. The VAWT is ideal for the domestic sector for its easy process of production and installation [13-14], Figure 1.5 shows horizontal axis wind turbines.

The VAWT rotor that is made up of series of blades of the same cross-section is equipped to have strong aerodynamic properties at different angles of attack α . A VAWT, in contrast to a HAWT, rotates perpendicular to a flow, allowing its blades to oscillate in torque along the axis of rotation. Blade's local angle of attack is a function of its azimuthal position. The average torque is primarily supported as an objective function since each blade has a specific angle of attack at a certain given moment. Despite the fact that the HAWT blades would have different cross-sections and twists, they have to perform at a constant angle of attack for the duration of a rotation. VAWT blades, oppositely, are engineered to provide good aerodynamic efficiency during a rotation at the different angles of attack they encounter, resulting in high time-averaged torque [15-16].



Figure 1.5. Vertical axis wind turbines.

1.3. PROBLEM STATEMENT

Electric energy is one of the most important components of life and finding sources for it and devising technologies to generate it is one of the most important endeavors of all countries of the world. Wind is one of the most important sources of energy that has flourished greatly in the last two decades, as it is one of the types of renewable energies. Wind energy is converted into electrical energy by systems called wind turbines. Thus, the electrical energy extracted from the wind depends on two basic factors, the first of which is the wind, and the second is a system for converting the kinetic energy of wind into electrical energy. The first factor (wind) is a gift from God and man cannot interfere with it and influence it. Consequently, countries have invested many capabilities of scientists, researchers and funds to develop wind turbines to be suitable in terms of performance for the available winds and their physical conditions such as speed, direction, turbulence and eddies. On the other hand, taking into account the cost of application and manufacturing. There are two types of wind turbines, one of which is called the horizontal axis wind turbine, which is popular and strongly present in the global market despite its very high initial cost, and the second type is called vertical axis wind turbine, one of the most important characteristics of it is that the cost of its manufacture and operation is low compared to the horizontal axis wind turbine. On the other hand, it is less efficient and cannot acquire its rotational motion from the wind without an external influence

that is integrated with it or with one of its components. From this standpoint, scientists and researchers have been developing these systems in order to raise their efficiency, increase the productive capacity and overcome the problem of starting self-movement. Based on the aforementioned, this thesis contributes significantly to raising the efficiency of vertical-axis wind turbines and reducing the problem of self-movement initiation through the design, pneumatic kinematic analysis, performance evaluation and manufacture of a wind turbine called “*Sannuga System SS-VAWT 01*”. Since the most important design problem for a wind turbine is to reach the optimum model that would have a low manufacturing cost and high efficiency, the design compatibility between its engineering design parameters is very difficult due to the use of mathematical and analytical models, high-efficiency software. In addition to manufacturing processes and laboratory or field trials.

1.4. THESIS OBJECTIVES

This research will suggest some solutions for raising the efficiency Vertical Axis Wind Turbines and to look into its self-starting problem. Whereas, use one of the most accurate and effective aerodynamic methods and applying it in the form of a computer program, after making some modifications to it to be suitable for this work. Moreover, the use of the “*Ansys Fluent*” software is known to be effective in design, simulation and performance evaluation, will result in high quality results and thus a valuable search. Furthermore it, a complete and detailed design of the “*Sannuga system SS-VAWT 01*” was done by the “*Solidworks*”. Since most of the work in this thesis was centered around the innovative system called “*Sannuga system SS-VAWT 01*”, then the most important objectives of this thesis are as follows:

- To contribute to the improvement of the power coefficient C_p of vertical axis wind turbines.
- To investigate of self-starting problem of SS-VAWT.
- To design and manufacture an effective SS-VAWT.
- To look into of optimization of SS-VAWT.
- To make comparisons between SS-VAWT, Parabolic Darrieus, H-Darrieus.

1.5. THESIS OUTLINE

Part 1: Introduction. This part showed a general explanation of wind energy and wind turbines, their types and components, and the differences between their two main types. It also shows the problem statement and the objectives to be achieved.

Part 2: Literature Review. This section provides a clear and detailed explanation of the wind turbine's history in terms of their various designs and development processes. This part also showed the innovative analytical methods during the previous years for evaluating the performance of wind turbines.

Part 3: Methodology and Methods. In this part of the thesis, an extensive explanation of the work methodology and methods used to reach the target results were provided. An explanation of the modified Multi-Stream Tube model was presented, as well as the physical modeling processes using Ansys-Fluent, in addition to the presentation of the design of the *Solidworks* for the innovative wind turbine in this thesis, moreover, the procedures and steps for making the prototype are explained in this part.

Part 4: Results and Discussion. In this part of the thesis, all the results obtained from the processes of analysis, evaluation and design were shown with the various means used, whether mathematical models, physical models or experimental.

Part 5: Conclusion. The outcome of the thesis is summarized in this chapter.

PART 2

LITERATURE REVIEW

2.1. A BRIEF HISTORY OF VAWT WIND TURBINES

Prior to the invention of Darrieus turbine, drag-based Savonius turbines were employed as a means of mechanical energy instead of producing electricity over the last decade. Machines that are powerful and elevated are in high demand because of the use of electricity. As a result, lift-based machines are discussed as a potential replacement for drag machines. Darrieus style wind turbines were patented in 1931 by French aeronautical engineer *Georges Jean Marie Darrieus* [17]. A vertical shaft uses two or more of the airfoil blades, in the form of a bow, with tips of each of the blade fixed to a shaft's two ends. The rotational movement is caused by the blades moving against by the wind, creating an aerodynamic force that acts upon the shaft. For his workers, Compagnie Electro mécanique CEM in Bourget, outside of Paris, *George Darrieus* refined vital parameters on his VAWT and constructed many innovative wind turbines. The approved pattern is a three-bladed phi arrangement, as seen in Figure 2.1 a. Darrieus wind turbines for electricity production were reintroduced in 1966 by South. P and Rangi. R in Canada National Research Council CNRC. South. P and Rangi. R created the Darrieus VAWTs in Canada, which have been mounted mostly on the roof of the National Research Council NRC [18] as in Figure 2.1 c. Thanks here to oil chock later in 1973, nations were looking at alternative's forms of fossil fuels as a source of energy. Raj and South continued to study those turbines, while Dominion Aluminum Fabrication Ltd. DAF was hired to manufacture them [19]. As illustrate in Figure 2.1 b, the very first pieces of machinery designed by DAF was exported to the Defense Research Establishment in Ottawa and installed therein the Arctic. For a decade, the CNRC was at the forefront of Darrieus turbine research. In 1970, Sandia National Laboratories SNL in the United States implemented *Darrieus* system concept, which contributed further to

research into different configurations. Following that, in 2019, the VAWT grew in magnitude, eventually reaching 3.8 megawatts.

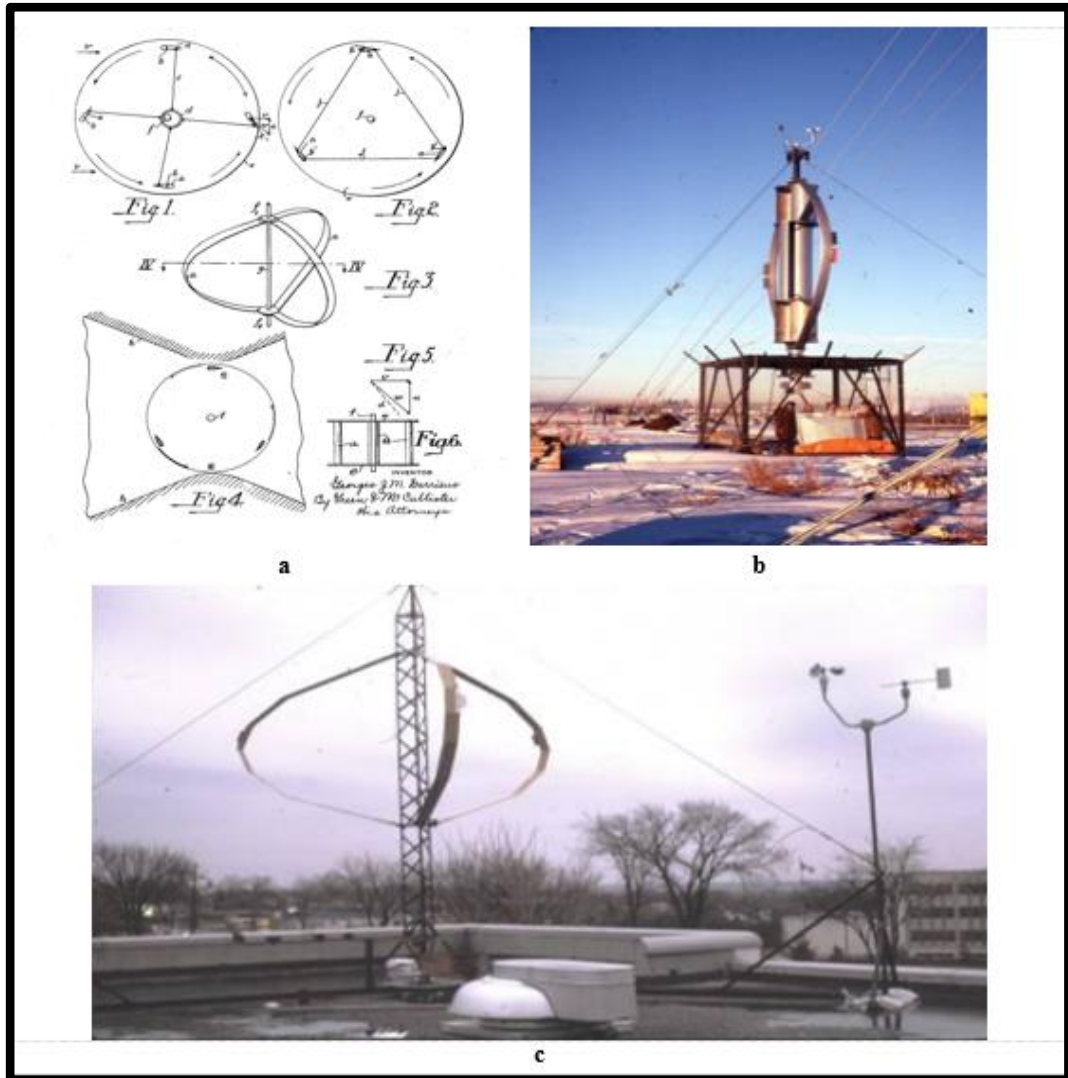


Figure 2.1. a) Original three-bladed phi, b) First Darrieus style of VAWTs, c) Darrieus on rooftop of NRC.

Figure 2.2 a display the very first huge turbine, which came with a 230-kW rated capacity in Canada. The turbine was designed by DAF Indal, an aluminum component manufacturer, in collaboration with Hydro Quebec and with CNRC supervision. The rotor had a diameter of 24 meters [20] and 595 square feet of cross-sectional area. The two-bladed turbine's constant velocity was fitted with a belt-driven induction engine. The brake mounted on the turbine blades (i.e., spoiler) has been studied in depth and shown in the following Figure 2.2c. The spoilers are

positioned in the center of the blade, but their durability has been questioned. The turbine, on the other hand, needed hydraulic braking and could not depend on their on-air brakes alone [21]. If the turbine was not connected to the driving train, it would collapse. Mostly on the plus side, the turbine's self-starting capacity was shown, despite the reality that it was widely thought that because the turbine couldn't work on its own the turbine was decommissioned in 1988 after 11 years of operation [18].

DAF Indal manufactured the 6400 model, which had a 500-kW rated power in 1984 [22], as illustrate in Figure 2.2 b. Southern California Edison Company SCE owned the very first unit in this chain, which was placed in the vicinity of Palm Springs, California. Another unit, operated by CNRC, was located at the Atlantic wind testing site in Prince Edward Island, Canada [23] and had a 36-meter-diameter rotor that rotates on the hydraulic bottom and top bearings. The gearbox was acting as the pedestal and was protected by three pairs of galvanized bridge strand guy wires. The blades are *NACA 0015* profile aluminum extrusions. The rotor moves the bull gear, allowing for a single transmission to reach the necessary generator rpm. The bull gear also serves as a brake disc, with 16 hydraulic brakes actuating it. The pinion gear mesh becomes spray lubricated mechanically, and the constraint is placed in self-aligning spherical seats. Two separates centrifugally controlled Overspeed valves are attached on the rotor column [24].

The valves let go hydraulic support pressure throughout the moment of rotor Overspeed and breakdown of the main Overspeed sensing and safety mechanism, allowing the brakes to be activated [25]. Aside from the 500-kW design, DAF Indal also produced 50-kW turbine that was also popular for their dependability, as seen in Figure 2.2 c [26]. Over the past 16 years, the turbine on Vancouver Island is in service [27]. The Darrieus turbine production through DAF Indal came to an end in 1985 when the blades on turbine mounted on Prince Edward Island failed. With the exception of blade failure and torque wave, that are intrinsic to Darrieus turbines, DAF Indal turbines appear to be promising.

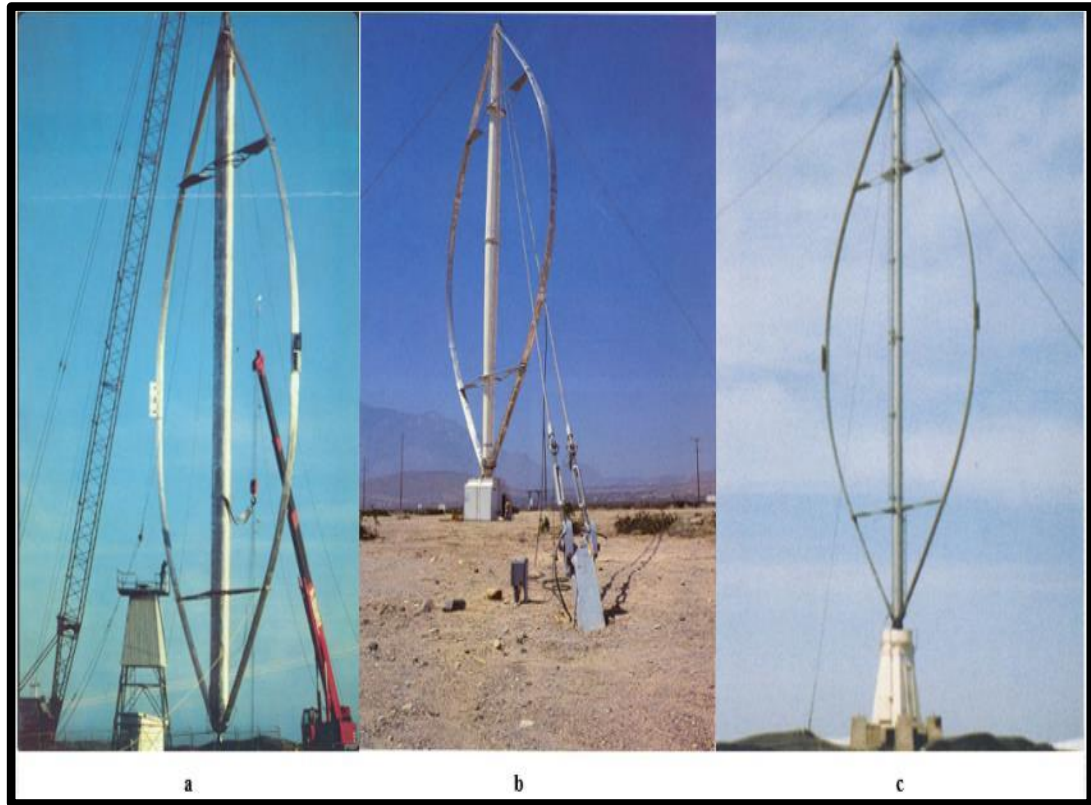


Figure 2.2. a) 230kW-Darrieus, was installed in the Magladden Islands, b) 500kW-Darrieus was produced by DAF Indal, c) 50kW-Darrieus was produced by DAF Indal.

The US Department of Energy (DOE) tasked Sandia National Laboratories with conducting studies into fossil fuel substitutes. In 1970 Wind turbine research began with an emphasis on Savonius and Darrieus turbines, with SNL focusing on Darrieus turbines because of their reliability shortly afterward. Darrieus turbines in various designs are analyzed and evaluated using models. With small modifications, two popular models are commercialized by private companies such as FloWind. The two-bladed 17 m prototype may produce 60 kW at quite a wind speed of 13 m/s [28]. Both ends thrust bearings support the rotor. A timing belt connects the spinning tower shaft to a gearbox, which in turn connects to the synchronous generator. Both aluminum and carbon blades have been used to evaluate the turbine [29]. The carbon blades have a NACA0012 profile, while the aluminum extrusion blades have a NACA0015 profile. The output of aluminum and carbon blades is nearly identical, with no discernible distinction. The blades on the blade shaft needed to be supported by pin joint supports and struts [30].

Since the aluminum extrusion blades are thicker than carbon blades, they provide substantial cost savings and eliminate the requirement for struts [31]. The struts have a common airfoil profile that reaches up to 67 % of a radius of the diameter. When strutted and unreliable blades were compared, it was discovered that struts induce substantial parasitic drag, resulting in a loss of coefficient of performance C_p . The aerodynamic efficiency of the *Sandia 17-m* VAWT equipped with unreliable and swaggered blades, as seen in Figure 2.3 a and b, respectively, shows a clear alteration. As opposed to strutted carbon blades, extruded unreliable aluminum blades have a higher power coefficient C_p . Sandia went on to develop a massive Darrieus turbine of *34-meter* diameter underneath the “Test-bed” program in 1988 after successfully testing the *17-meter* model [32]. A two-bladed turbine with an alternator and speed control gearbox is valued at *500 kW* at *12.5 m/s*, as shown in Figure 2.3 c [33]. The turbines turn at *1800 rpm* and the turbine can be abandoned *29.6* to *59.5 rpm* in 13 stages on account of the pulleys, belt, and transmission proportions. The three parts of the guy-wired phi rotor blades are prepared from aluminum extrusion. *NACA 0021*, *SNL 0018/15*, and *SNL 0018/50* are used for the root, transformation, and equatorial portions, respectively [34]. The tailored airfoil for various parts improves mechanical rigidity by reducing localized lateral folding, blade strain, and aerodynamic efficiency [35]. The unreliable architecture now has the most extreme power coefficient of 0.43 [36]. as a result of these changes. In past years, the SNL received a *\$4.1 million* award [37] for the construction of a multi-megawatt Darrieus turbine for offshore power production.

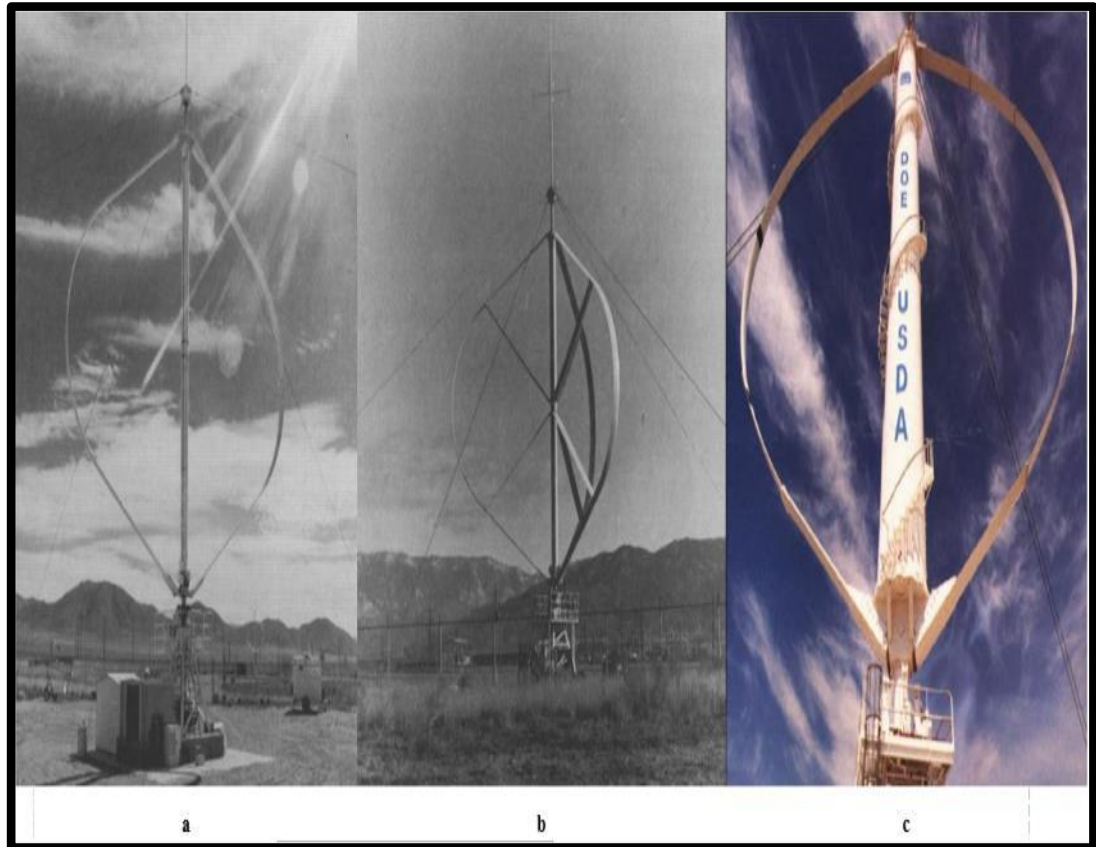


Figure 2.3. a) *Sandia 17-m with strutted*, b) *Sandia 17-m without strutted*, c) *Sandia 34-metre with two blades*.

In 1975, the Aluminum Company of America ALCOA, that had previously produced blades for SNL, started producing VAWT constructed on SNL technology. As seen in Figure 2.4 a, ALCOA built ALVAWT, an 8-kW capacity turbine having rated speed at 15.2 m/s. An induction motor with a constant speed gearbox is utilized in the three-bladed turbines. Perhaps their famous models, the *ALVAWT 100*, was able to run safely in bad weather. In 1981, ALCOA produced the *ALVAWT 500*, a rotor with a diameter of 25meters and a height of 37.5 meters. ALCOA built it is before creation of the 25-meter, 500 kW model for the Eugene Water and Electric Board close to Newport, Oregon, around 1979 and 1981, as found in Figure 2.4 b. because of the control malfunction, the three-bladed machines based in Pittsburg, USA, crashed. Early failures forced ALCOA to withdraw its turbines, effectively ending VAWT production [38].



Figure 2.4. a) ALCOA 8kW capacity, b) ALCOA 500KW-VAWT model.

In the 1980s, Adecon began producing VAWTs under the course of Peter South. To save space, the original 125kW machine had a 17-meter diameter and was assisted by lattice masts rather than guy cables. The turbine, like other turbine types, fell due to over speeding. Later, CWT Power revamped the rotor with four blades and a cross section base, which supplanted the torque tube with grid poles. As found in Figure 2.5 a and b, ten of these turbines were built in Alberta, Canada, and two of them fell down due to lattice frame turbulence and metallurgical defects, effectively ending Adecon's construction of VAWTs [39], as shown in Figure 2.5 a. VAWTPOWER produced 185 kW and mounted 40 turbines that were all operational till 1985. Figure 2.6 b [40] shows the latest cycle of the cantilevered model, which is tried at 60 kW. The 9-kW double-bladed turbine produced by Bjervig and was afterwards purchased by Vestas, as found in Figure 2.5 c [41], is a mystery c [41].

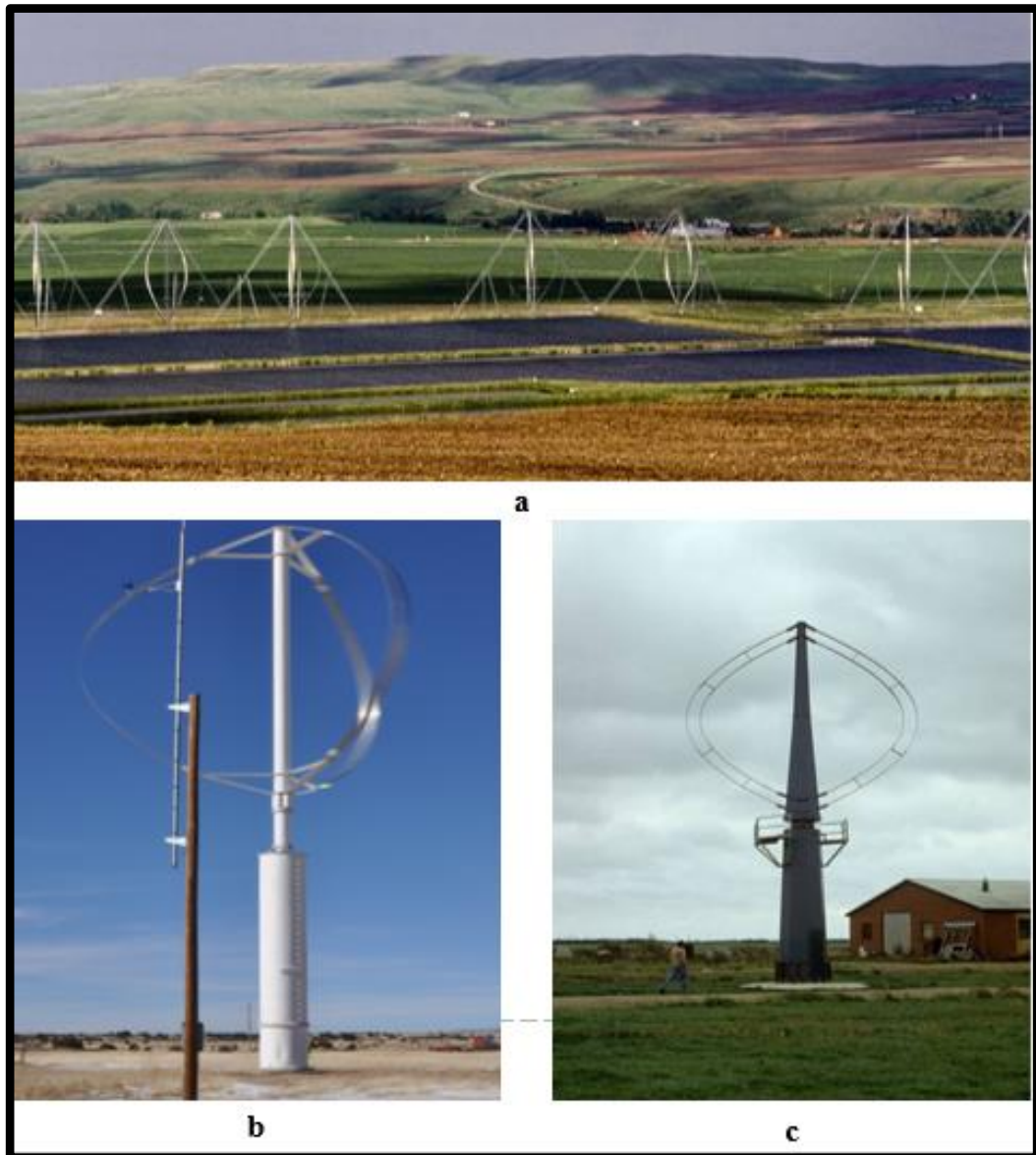


Figure 2.5. a) Wind Turbines of CWT Power, b) Turbine from CWT Power, c) 9-kW double-bladed turbine produced by Bjervig.

The Sandia Test-bed software was successfully tested in 1989, as well as the idea was commercialized. The point model was indeed the pre-commercial prototype, and it had been applied to the private sector. The 17 m and 19 m models were designed and run by *FloWind* using SNL technology [42]. The 17 m refers to the rotor diameter, which sweeps a 260-meter square field at the height of 23 meter. The 19-meter model cleared 316-meter square and had a greatest limit of 300 kW at 20 m/s. The most extreme wind speeds of 17 m/s and 20 m/s for the 17 meter and 19-meter models are nearly higher for coastal turbines, and the turbines never arrived at their

normal capacity during their working time. Figure 2.6 [43] shows the details of the tower, rotor, and drive train. An SNLA 2150 airfoil and a retrofit gearbox improved the turbine's rotational speed to 60 rpm [44]. were used during the 300kW machine. The Retrofit gearbox failed early on, leading to the replacement of prototypes with initial *F-19* gearboxes that limited the rpm to 52 rpm . The *S82435* airfoil was created after the *SNLA 2150* airfoil failed to fulfill the FloWind specifications. Since the blade dividers were extremely powerless to bear the curve set up and working pressing factors, the primary cycle of *S82435* wedged. The blades were modified with denser walls, and industrial blades of such a type have been used. The rotor needed to be stabilized, so struts were built in a V-shape and rim to the tower. The pipe struts with diameters of 80 and 102 mm were not aerodynamically faired, resulting in substantial aerodynamic drag, which reduced output power by 25% at average wind speeds [45]. The productivity of the vehicle improves by around 15% as it is aerodynamically faired. The expanded height to diameter EHD model was created to boost the rotor's power output. The EHD design increased the cleaned area of the rotor by extending it vertically instead of raising its diameter. As contrasted to a rotor with a low height-to-diameter ratio, the EHD configuration reduced bend-in-place static stresses. The brake system was among the most expensive parts of the *FloWind* fleet to maintain. Two sets of hydraulically operated brakes have been used in an ultimate system configuration. The braking system also included a third fail-safe parking brake package. Commercial turbine blades made of aluminum are prone to fatigue loss due to cyclical pressure [46]. The absence of blades in the 19 m model ruined the company's image and brought it close to bankruptcy. During its high time, FloWind manufactured and worked around 500 turbines by Altamont Pass in California. By 2004 , all of the FloWind generators had been decommissioned, and the latest was removed in 2010 to be supplemented through Vestas HAWTs. [47]



Figure 2.6. Sandia FlowWind model.

The EOLE, the world's biggest VAWT, was installed in Quebec in 1987. The direct-drive synchronous generator is valued at 3.8MW and runs at 14 rpm [48]. The blades have a metal frame and are valued at 3.8MW . Despite operating at a decreased rpm of 12, the loss of the lower part causes the turbine to stop, as found in Figure 2.7 [49]. A two-bladed direct drive 300 kW system with the spinning tower was designed by Heidelberg Motor GmbH [46]. The enormous diameter ground-mounted generator obviated the need for a transmission infrastructure. Later revisions included the addition of a permanent magnet generator to the tripod's top. One of the five turbines installed self-destructed owing to strut welding failure. Due to the parasitic drag created by the struts, the aerodynamic efficiency of the tripod-based machine is significantly reduced. Heidelberg then created 20 kW machines that were put in Rwanda and the German Alps and functioned for over 15 years [50]. Heidelberg then developed 20 kW machines that were installed in Rwanda and the German Alps and operated for over 15 years.



Figure 2.7. EOLE model with 3.8MW capacity.

In 1975, Peter Musgrove started research on the H-rotor at the University of Reading in the United Kingdom. Musgrove [51] endorsed the innovative idea of regulating H-rotor over speeding and its viability for multi-megawatt turbines with his student Ian Mays. The British Aerospace Aircraft Group (Bristol), Taylor Woodrow Construction Ltd., and Reading University [52] collaborated on the original VAWT design and production work. The leading Musgrove turbine designed and verified at Reading University has a diameter of 3-meter, which is constrained via the magnitude of the wind tunnel offered at the university. At 11 m/s , the adjustable geometry two-bladed turbine produced 130 kW . The rotor has a diameter of 25 meters and a swept surface of 450 square meters. The turbine will spin at an extreme rpm of 27 using a standard *NACA 0015* airfoil with an 18-meter blade length. The transmitting and power facilities are mounted on the floors. The turbine shaft was attached to two 75 kW and 30 kW induction generators [53]. When the wind speed was low, the 30-kW generator is used, and when the wind speed was high, both

generators are used. If the wind speed exceeds 30 m/s , the turbine's automated reefing mechanism would reef the blades into the form of a double-headed arrow, essentially reducing the swept section. Figure 2.8 a [54] shows the turbine in the reefed position. However, data obtained from 200 sensors over a two-year cycle in 1988 showed that the reefing mechanism was overly complicated, as power balance was naturally accomplished by airfoils' inherent passive-stalling, even in heavy winds with the blades being vertical. As a result, when the design was scaled up to 500 kW , the variable geometry device was removed VAWT-850. In the interim, VAWT Ltd. introduced a 17 m width, 100 kW VAWT-260 exhibit project on the Isles of Scilly and Sardinia [55] prior to introducing the VAWT-850 turbine. Since the Isles of Scilly were not connected to the matrix, depending on a diesel generator for desalination was restrictively expensive. The 500 kW VAWT 850 model was planned and introduced at the Carmarthen test in 1990 with help from the European Commission. Figure 2.8 b [56] depicts the VAWT 850– 500 kW turbine. A higher wind speed of 18 m/s [57], which is just conceivable in seaward areas, is important to achieve the appraised 500 kW turbine with a rotor diameter of 38 m . The turbine was only functional before *February 26, 1991*, until one of the blades separated because of a manufacturing flaw in the fiberglass blades. Notwithstanding its oversimplified design, the VAWT 850 model may not be however practical as it might have been recently accepted. The big concrete tower must be able to handle the blades' cyclical loads. Eventually, Musgrove stressed that for turbines with capacities greater than 20 MW , the VAWT with blade pitch power is more cost-effective than that of the HAWT.



Figure 2.8. a) Musgrove wind turbine 30KW, b) Musgrove wind turbine 500KW.

David Sharpe suggested the Aerogenerator idea, which had been later accepted by Wind Power Ltd. Aerogenerator arose from David Sharpe and Derek Taylor's effective evaluation of a 5 kW two-bladed V-rotor prototype in 1987. They additionally proposed a mono V-VAWT, involving one slanted blade with relating adjusting loads fixed on a teetered hub point over a similarly short support frame, following the testing of the twin-bladed unit. It was expected that the only cantilevered blade would increase efficiency while lowering manufacturing costs. The patent for aerogenerator is generally owned by Wind Power Ltd., and it has been later created by the Novel Offshore Vertical Axis turbine NOVA venture [58]. Figure 2.9 a [59] depicted the actual NOVA design, which had four sails for every appendage, orchestrated so that no sails covered at a specific higher area to keep away from errors because of sail wake connections [60]. Nevertheless, because of the large quantity of junction areas, low-aspect-ratio sails are even less effective due to increased persuaded drag and tip failures, as well as greater interference drag. Moreover, because of the reduced height and angular velocity, the lower sails add considerably less torque under this profile. As a result, all optimization research is based on single and double-sail designs. The aim is to build a 10MW offshore premium wind turbine with enhanced power output for 5 GW wind farms expected to be completed by 2020. Initially, two support systems for the aerogenerator were taken into account: a fixed jacket design for low water profundity seaward areas and a semi-sub plan for more noteworthy water profundity seaward areas. Both

prototypes are tested for rough waves crashing and hurricane levels up to *70 meters* per second [61]. The discoveries show that all through the endurance mode, the drive train or course could be evaded by basically rivaling the drive shaft. Furthermore, it was discovered that perhaps the slope and depth of the airfoil have no noticeable effect on efficiency so that the aerogenerator is preferred over the traditional symmetric NACA series. The designed *10 MW* aerogenerator is *270 meters* in diameter and *120 meters* in height, with a *13 m/s* rated speed and an *88 percent* drive train performance. A *5kW* model was installed to certify the design, as can be found in Figure 2.9 b [59]. The *5kW* model is made up of two V-shaped arms of four sails, each one with guy wires linking them to minimize bending stress. The full-scale model improved by Grimshaw architects, on the other hand, does not even have guy cables. In contrast with a current Repower *5MW* HAWT turbine it last *10 MW* aerogenerator setup was diminished to a *5 MW* plan during the plan cycle. With a power coefficient of *0.38* and considerably lower bending moments and center of gravity than that of the VAWT, the aerogenerator configuration achieves acceptable aerodynamic performance when operating at a slightly lower height. [61]



Figure 2.9. a) NOVA-VAWT with sails, b) *10MW* offshore *V-shaped* VAWT.

Vertical Wind AB [62], which would be a spinoff by Uppsala University, built a *200kW* prototype in *2010*. After a year of work on H-rotors, a *200kW* prototype was constructed and deployed in Falkenberg, Sweden's west coast. Figure 2.10 [63] shows a turbine with a diameter of *26 meter* and a blade length of *24 meter* that

sweeps a region of *624-meter square*. The main fault in VAWT, according to analysts at Uppsala University, is the gearbox, and removing the gearbox would reduce downtime and repair costs. As a result, the emphasis is on developing direct-drive synchronous generators that are ideal for H-rotors. To endure the high overload power, the 36-pole generator built [63], was designed with a neodymium-iron-boron permanent magnet rotor. Fixing the generator to the recurrence drive takes into account variable speed balance. On such a turbine, the idea of using a generator as a motor to operate the turbine was thoroughly investigated. Moreover, the key winding, a specific auxiliary winding [64] through electrical connectors has now been added to switch among running the generator and regular operation. The auxiliary winding that allows a turbine to begin at 0.5m/s was successfully demonstrated in the *12kW* prototype. In comparison, in case of a crisis or while stopping, the motor fills in as the fundamental brake while applying the hydraulic brake. The steel shaft linking the rotor to a generator was already attached on the surface and is fixed in place by rotating on the two ends. The tower is prepared from wood coated in fiberglass, while the blades and struts are prepared of fiberglass. Because of the cheaper cost ratio, it can endure heavy wind forces throughout storms. Within the fact that the original plan did not have guy cables, three have been inserted when cracks occur on the wood-laminated tower as a result of the incorrect glue application. Multiple techniques have been utilized to reduce resonances caused by complex loads while building a wind turbine stack. The tower must be stiffened or softened to change the eigenfrequency that was more than three times the rotational rpm or in the rated rpm range. Guy wires reduce the overall rpm from 33 to 23, which is restricted by the eigenfrequency [65]. The noise produced by the turbine has been thoroughly investigated. The noise level of a *200-kW* turbine would be in the range of *600–1200 Hz* [66], which is similar to the frequency of ambient noise. The level of noise around 8 m/s at 10 meters above the ground is 96.2 dBA, while it is *94.1 dBA* at 6 m/s. The central factor of noise within the H-rotor was discovered to be the trailing edge vortex as well as turbulence [67]. The noise amplification analysis reveals that when contrasted to a comparable scale HAWT, VAWT noise reduces significantly [68]. Whenever a major investor walked out, the project ground to a halt. Vertical Wind AB is primarily engaged in the development of generators for many other wind turbine companies.



Figure 2.10. Vertical Wind AB 200KW prototype.

Savonius Keel & Wind Turbine Darrieus (Skwid) [69] was built by Mitsui Ocean Development & Engineering Company (MODEC), an offshore technology firm specializing in offshore oil and gas platforms. By exploiting their experience in building floating systems, the turbine has been designed for offshore power production. The turbine is remarkable in many respects, including the fact that it is revolutionary at the time to combine wind and tidal energy in a single unit (see Figure 2.11 a [69]). As per MODEC, the energy utilization yields up to a factor of two, making it a practical seaward methodology. A Darrieus rotor removes the wind energy, while a two-stage Savonius rotor tackles the force from the weak sea flows.

Two stages improve the path capacity and smoother torque generation. The Darrieus rotor's rotating tower and the Savonius rotor's rotating tower are aligned and attached over the gearbox. The Savonius rotor will start a rotation in the Darrieus rotor that improves beginning efficiency and then proceed to produce power as a stand-alone device. Although the actually rated capacities of the turbines are unknown, the hybrid turbine's total rated power is stated as *500 kW* at *13 m/s*, whereas the Savonius turbine is rated at *60 kW*. The weight of a high-density material the Darrieus rotor is held erect by a Savonius rotor with lower endplates acting as ballast. As found in Figure 2.11 b, a gearbox and generator are located within the moving dock and linked to the spinning tower by a gimbal-like arrangement. Although being moored to the seabed by mooring lines, this helps a platform to sync with waves. The experts claim that the Savonius turbine is suitable for aquatic life because it has a low tip speed ratio. To endure the harsh seaward climate, every blade of a Darrieus rotor is facilitated by five struts. Regardless of the way that the plan was innovative, severe failures throughout construction put the turbine's production on hold. The Skwid installation site will be on the coastline of Japan's Kabe Island. Although the Savonius rotor is noted for its heavy thrust loads [70], the rotor shaft broke and sunk in the sea when being dragged to the location [71], as found in Figure 2.11 b. In 2014, the rotor was recovered and refitted [72], and a second try at installation was produced. However, owing to unstable angling, the entire platform sunk, prompting concerns about the turbine's suitability for offshore weather. In *May 2015*, MODEC stated that the design had been safely recovered, so the project had been canceled. Novel models for low-current power production, including turbines with trapped vortex airfoils [73], may theoretically substitute Savonius turbines. On the off chance that it was introduced and worked appropriately; the turbine might have been a distinct advantage as a practical seaward VAWT.

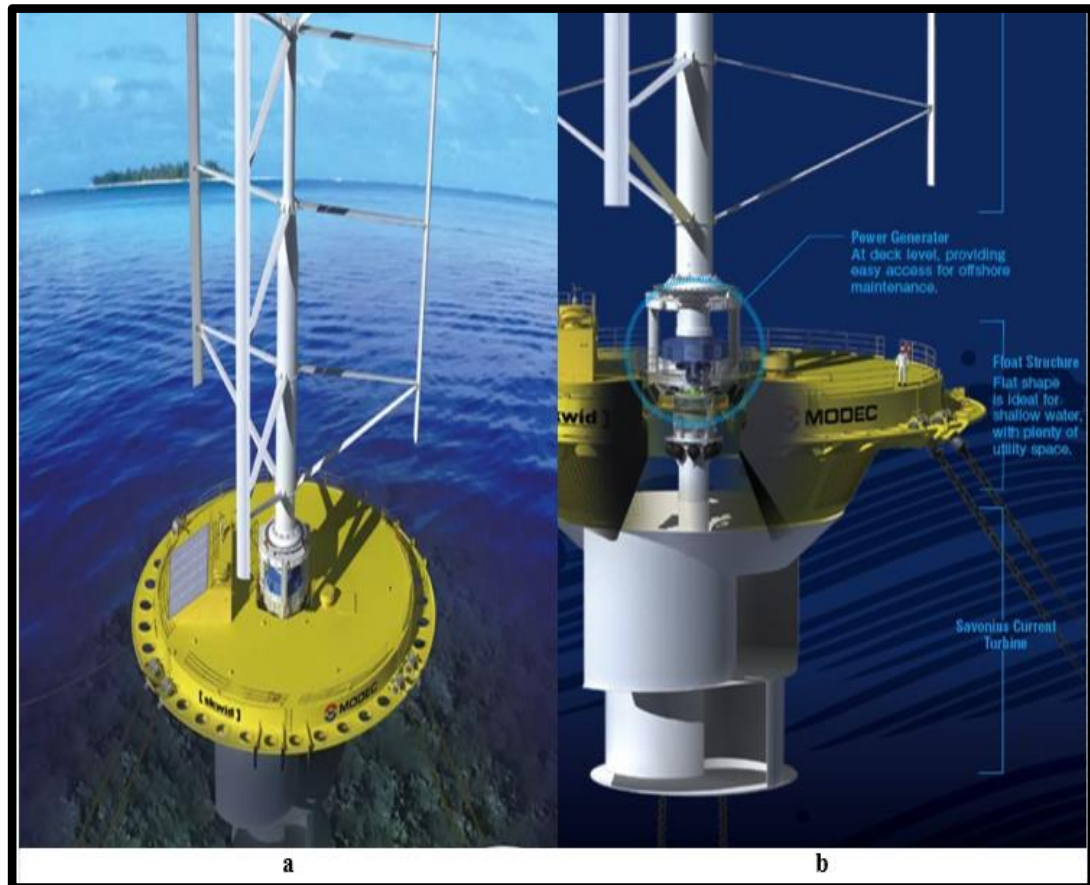


Figure 2.11. a) Combines wind and tidal energy in a single unit, b) Gearbox and generator of (Skwid) system.

VertAx wind [74] limited was founded in 2007 with the aim of building an offshore wind turbine through significant cost savings and re-establishing wind turbine production in UK. Low cost of maintenance, resilience, and durability are all important areas of study. The group was created with the goal of concentrating on each component of the turbine and using experience to create a dependable offshore turbine. As found in Figure 2.12, the suggested three-bladed Darrieus VAWT seems to have a rotor diameter of *140 meters* and a blade height of *110 meters*, with such a maximum power potential of *10 MW*. For blade production, VertAx Wind partnered with Slings by Composites and the Northwest Composite Hub. The blades are completed in *11-meter* lengths and installed on-site to make logistics easier. To minimize mass and parasitic drag, the supporting arms are often made of composites. The University of Leeds [75] performs blade modeling and aerodynamic optimization. Via a novel blade design, VertAx wind seems to have reduced the vortex-shedding impact. Collaboration with the University of Edinburg has resulted

in significant advancements in generator architecture. Mark Muller's C-Gen technology [76] was used in this project. The stator discs move through the C-limbs of the compact permanent magnet ring generator that has a C-shaped composite material [77]. The cogging torque has a major impact on VAWT beginning features. The greater cogging torque from the generator may be explicitly attributed to the low startup capacity. The minimal cogging torque of the C-Gen generator allows the turbine to operate earlier, raising the total annual yield. The C-Gen is a well-known generator for marine turbines and waves energy invertors, with capacities ranging from *15 kW* to *1 MW*. Two generators, each rated at *5 MW* and spinning at *4 RPM*, get a strut joining section. For multi-megawatt VAWTs, producing ring bearings is a problem that has been overcome through utilizing rollers and track. The struts rotate all around the tower and are attached to a roller frame. The University of Cranfield performed dynamic modeling of a VertAx turbine tower and structure. The turbine is built to last for at least 25 years and has an onboard machine for blade and roller installation [78]. The crane's hydraulic ram is installed generally on the tower top deprived of interfering with the turbine's various parts. Mostly on top of a tower, there is a helipad that can handle a *4–6-seater* helicopter. The turbine could be installed entirely on it and shipped to the desired spot. Although this turbine rotating platform had been extensively debated, a separate spar type is preferred over jointed multi-spar due to lower overturning moment. The VertAx *10 MW* turbine is yet to be built.



Figure 2.12. Offshore VertAx wind turbine.

During the year 2011, the government of French launched the Vertiwind program. The aim is to create a more powerful and cost-effective offshore wind turbine than the traditional HAWT. Technip, a major oil and gas corporation with experience in offshore engineering, partnered with Nenuphar, a group of expertise in wind power research supervised by EDF Energies, to form the partnership. The model construction of a 35 kW Darrieus VAWT onshore turbine, kicks off the study mostly on the production of 2 MW turbines. The prototype's purpose is to evaluate the changed blade physical parameters as well as the struts. Torque movement and parasitic drag owing to studs are two key problems that the Vertiwind developer described as needing to be overcome in able to manufacture a stable and effective offshore turbine. The parasitic drag caused by the supportive arms is reduced by an

innovative, supportive mechanism where the lower one-third of a blade is rigorously protected by arms, while the upper two-thirds of blades are held by struts to counteract blades' centrifugal force. While Vertiwind claimed to have decreased parasitic drag, owing to vibration from unstable blade length, the proposed concept wasn't really transferred onto the 2 MW turbine. As a result, the 2 MW turbine provides standard supporting weaponry. In comparison to the cyclical torque variations of straight-bladed Giromills, helical rotors are noted for their steady torque production. Owing to the higher cost of blade manufacture and transportation, using a helical blade with multi-megawatt blades is not feasible. As a result, Vertiwind uses multipole sections of straight blades to create a close structure. Figure 2.13 [79] shows the designed helicoidal-shaped blades with a floating platform. The revised architecture, according to Vertiwind, has changed mechanical and aerodynamic characteristics. A significant portion of a gross turbine cost is shared by the floating base of an offshore turbine. The overturning moment on the platform determines the platform's height. The overturning moment is strong in HAWT since the thrust force works just at the hub, while the thrust force in Darrieus VAWT is uniformly spread over the whole blade range. By switching to a vertical mode, an over turbine moment is said to be halved. The nacelle mass has an effect on the ballast mass and platform size. Throughout the situation of HAWT, a heavier ballast is needed for turbine stability since the generator and gearbox are situated on the top of the tower, while in the situation of Vertiwind turbines, the drive train modules are installed at 20 meter above mean sea level, reducing the platform size to just 9 meters below sea level. Vertiwind estimates the above modifications would decrease the expense by 25% [80] compared to significant material savings. Given such accomplishments, Nenuphar was unable to secure funding for the construction of a 2 MW turbine and was subsequently forced to liquidate in 2019 [81].

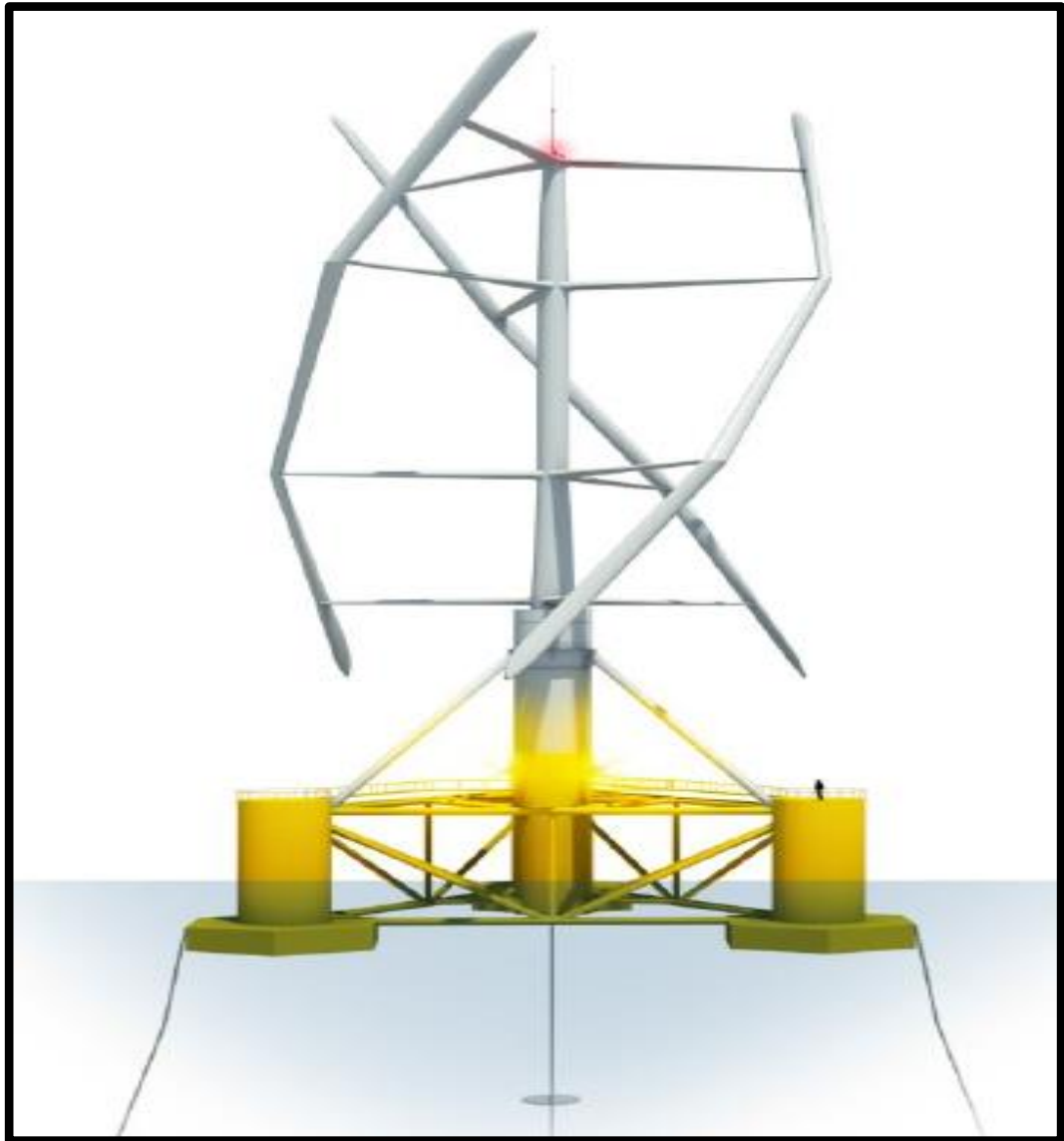


Figure 2.13. Vertiwind -VAWT.

With the help of Stalprodukt S.A., a new Polish research center is operational on the construction of multi-megawatt Darrieus turbines. Figure 2.14 a [82] shows the first version, the *15 KW ANEW-S1* [82] model, which is three-bladed and designed for low wind speeds around $3\text{--}9\text{ m/s}$. Residences and field use are the main markets for such turbines. The separate structs of each blade, as well as the V-shaped blades, grab attention and serve as the foundation for Anew Institute's multi-megawatt turbines. The V-shaped blades are attractive and have been shown to minimize noise. Research teams from the Anew Institute illustrated a Darrieus-type multi-stage rotor to solve the torque variations that plague single-stage rotors. The two-stage rotor was discovered to advance the turbine's operating capabilities by replacing the dead

group. The testing analysis indicates that a multi-stage rotor's performance is significantly decreased due to blade tip failure as contrasting to a single-stage rotor. The ANEW-performance S1's led to the launch of the *200 kW ANEW-M1* [83], which is rated at *200 kW* at *12 m/s*. Wind speed was estimated to be reduced by *3.2 m/s*, which is also the minimum for Darrieus turbines of this scale. To minimize weight, the struts and blades are made of fiberglass. Large diameter generator configuration provides minimal cogging torque. Vertical Wind AB [84] produced the generator, which is a direct drive type. And at a lower RPM of *34*, the turbine will produce a voltage output of *400 VAC*. The tower configuration of the *200 KW ANEW-M1* is special, with half a strut for easier generator installation and half monopole for less friction on the blades. The struts rollers are driven on tracks, mostly on support rings, removing a need for large bearings. The tower is securely anchored to the supporting ring. ANEW-M1 was expanded to *1.5 MW ANEW-B1*, as shown in Figure 2.14 b [85], which has been in use since 2017. The whole strut configuration of the tower was comprised of six pyramid-shaped pillars. The turbine is reported to produce *1.5 MW* at *13 m/s*, with a diameter of *52 meters* and an output power of *1700 meter square*. The blade's top angular speed is *44 m/s*, with a maximum RPM of *16*. About the fact that turbines are among the most attractive candidates for megawatt-scale power production, the overall power coefficient obtained is debatable because of substantial blade tip failure owing to the unavailability of endplates. Removing one strut resulted in a substantial decrease in parasitic drag, and substantial product and manufacturing overall costs. The blades must be repaired or redesigned after *10* years, as per the producer, which may result in repair costs. This could be because of blade exhaustion and rotating tension, which is a Darrieus rotor feature.



Figure 2.14. a) 15 KW ANEW-S1, b) 1.5 MW ANEW-B1.

2.2. ADVANTAGES AND DISADVANTAGES OF VAWTs

The vertical axis windmill has the capability to have a low-cost and easy wind energy conversion system. Multiple facets of the basic architecture contribute to the opportunity for cost savings. Firstly, since the windmill's axis is vertical, direct shafting to generating machinery on the field is possible. This results in a support system that is lighter in weight. Secondly, while the blades must have an airfoil appearance to work well, they do not have to be twisted, and mass manufacturing of a blade seems to be financially viable. Third, because of the windmill! It is Omni-directional in reference of wind direction; it's doesn't need a system to ensure any specific wind direction inclination. Fourth, since the main blade loads are generated by centrifugal forces that are basically constant in definition, material failure ought to be minimal. The traditional vertical axis principle has a major flaw that it is not self-starting and needs some kind of system to restart it when winds fall below a certain threshold [15], [86-90].

2.3. TYPES OF VAWTs

2.3.1. Straight Bladed Darrieus Turbine

The Darrieus turbine with straight blades seems to be the easiest of three types subsequently it is simpler to produce, ship, and install on the turbine. The quantity of blades required for a particular installed capacity is resolute by the average wind speed at the site location, the machine's *rpm*, and also the machine's startup parameters. H-Rotor [91] refers to a Darrieus rotor with two straight blades, and Giromill [92] refers to a turbine with more than two blades. While the blades for most of the rotors are parallel to the axis of rotation, the blades of a delta rotor, diamond rotor, *V*, or *Y* rotor were stated to be oriented to the axis of rotation. A straight-bladed turbine's maximum coefficient of performance C_p is between 0.25 to 0.35. The rigidity of a turbine, which is determined by the proportion of blade area to swept area, has a significant impact on its C_p . Increase the quantity of blades and the chord length of a blade to maximize their rigidity. The rigidity of a Darrieus rotor with straight blades has a significant effect on a turbine's startup properties. Baker's research program [93] reveals that three-bladed turbines have an advanced static torque coefficient than two-bladed turbines. Steel tubes could be utilized for the blade mounting struts, which decreases construction costs and come in a variability of diameters and widths. Darrieus turbines with straight blades were not recommended for industrial applications due to their weak results in low and erratic weather. The inability to self-start at wind speeds less than $4m/s$ [94] is a big downside that prevents these turbines from being mounted on rooftops. Previous self-starting research has shown that flow withdrawal from blades at low Reynolds numbers Re and high Angles of Attack α results in the poor lift, which reduces net torque considerably [95]. The rotating speed of smaller Darrieus turbines is yet another flaw. Darrieus turbines have a slower rpm than HAWT turbines. Cogging torque increases with expanded generator size with the same power output [96], resulting in higher resistive torque opposite rotation. Despite these disadvantages, the advancement of advanced small-scale Darrieus wind turbines was aided by their aesthetically appealing and straightforward design. Darrieus turbines with straight blades are widely viable in power capacities ranging from $500 W$ to $1.5 MW$.

2.3.2. Curved Bladed Turbine

The curved bladed rotor was inspired by a *phi* rotor [97], which was created during VAWT's early days. The only contrast between the curved bladed rotor and the *phi* rotor would be that the *phi* rotor's blade edges are fixed to a tower, while the curved bladed rotor's blade ends are open. Struts [98] fix its curved blades to a tower. The existence of struts seems to have a significant impact on torque production due to parasitic drag's resistive torque. To minimize parasitic drag in massive turbines, struts are constructed from symmetrical airfoils. The tower may be revolving or not rotating in all scenarios. The *phi* rotor model is common for turbines with a power greater than 50 kW , while curved rotor models are ideal for turbines with a power lower than 10 kW . The struts are linked directly to an axial flux generator's top flange. The ring bearing inside the generator may withstand a higher moment load, unlike similar-sized deep groove ball bearings. The curved rotor and also the H-rotor vary significantly in terms of aerodynamics. The Re of H-rotor blades becomes constant over their length, while the Re of curved blades is stronger within the middle of a blade length [99]. The shifts in Re cause a complex stall closer to a root to occur sooner. As a consequence, there are other blade tip vortices, resulting in a lower C_p . Curved bladed rotors are more visually attractive than H-rotors, making them a good option for rooftop applications. Producing curved blades is more difficult than straight blades. Glass fiber is utilized to make smaller angled blades in a molding operation [100]. Extrusion is used to create larger angled blades, which are then bent by a competent professional. Although larger curved blades are made in parts, various airfoils may be utilized for different parts [101]. Greef produces small-scale curved blades equal to 2 kW , as found in Figure 6. The blades of a 2-kW turbine have a top rpm of 160 and are made of Fiber Reinforced Plastic (FRP). The average wind speed is 11 m/s , however the starting wind speed is 2.8 m/s . It was believed that the starting torque needed to rotate the rotor is much less than 0.3 Nm .

2.3.3. Hybrid Savonius-Darrieus Turbine

The Savonius turbines have a greater startup torque than Darrieus turbines, which have a lower startup torque. The unusual concept is to merge both of Darrieus and

Savonius rotors to complement one another [102], Figure 2.15 shows combined system called Dornier [103]. When the wind speed is weak 3 m/s , a combined machine behaves like a Savonius rotor, but when the wind speed is strong ($>4 \text{ m/s}$), the combined machine behaves like a traditional Darrieus rotor. Combining a Savonius and Darrieus rotor is accessible in two setups. The Savonius rotor could be positioned on or around the Darrieus rotor or can be enclosed within the Darrieus rotor. The Savonius rotor's location from outside the Darrieus rotor continues to lengthen the spinning shaft, resulting in vibration. As a consequence, the Savonius rotor should be combined with the Darrieus rotor. A variety of previous experiments and analytical research were carried out founded on the above definition. The aim of each of this research is to maximize the Savonius rotor diameter for optimum low-wind output while reducing the strain of the Savonius rotor on the Darrieus rotor's C_p in strong winds. The findings demonstrate that the combined machine's startup torque seems to be much greater than the Darrieus rotor and also that the maximum C_p is reached at low tip speed ratio λ_o . [104]. The combined machine's maximum working λ_o is 1 to 1.2 . It's worth noting that a Savonius rotor's total λ_o is 1 , but any effort to work above λ_o 1 might lead to negative torque. The Darrieus rotor has a λ_o range of 3 to 6 [105]. This discrepancy in peak output among two rotors is a major stumbling block to the production of hybrid turbines. As the Darrieus rotor speeds up past λ_o 1 , Mousavi [106] suggested disengaging the rotors. Although this approach is theoretically feasible, the power collected by the Savonius rotor after retrenchment would not add to the total power generation, and the Savonius rotor's wake would remain [107]. This hybrid rotor would be marketed as a possible option for low-speed wind service, thanks to a viable approach to remove the Savonius rotor's wake.



Figure 2.15. Dornier Darrieus/Savonius 5.5KW.

2.3.4. Blade Pitching Darrieus Turbine

Blade pitching had first been introduced for large wind turbines because installing the device inside a small wind turbine is expensive and complicated. Pitching systems could then be used in small Darrieus turbines with capacities as low as *10 kW*, because of the advancement of activation frameworks [108] and furthermore the lower costs of related gadgets. Although this Darrieus rotor appears to be simple, its

aerodynamics are far more complicated than HAWT. Leading to variations in relative velocity, its fixed blades face a large spectrum of angle of attack α around 0 deg to 360 deg . The blades are continuously stalling due to the large α . And if the α decreases, the flow can be disconnected owing to hysteresis inflow. Blade pitching is a feasible way to keep blades at optimal α . The result of blade pitching has been thoroughly investigated using a Double Multiple Stream Tube DMST [109]. The blades may be aggressively or unconsciously pitched. For small wind turbines, aggressive pitching is accomplished that used a closed-loop mechanism operated by an engine. The motor needs a significant amount of power to operate. Active pitching has a benefit over passive pitching except that the blades can be pitched independently [110]. The wind velocity is monitored by the closed-loop mechanism, which pitches the blade respectively. Since both of the blades are involved in torque production, the startup torque is greater [111]. A brief glance only at torque produced by a single blade with a complete revolution shows that the upwind half generates the most positive torque, while the downwind half generates the least. Specific blade pitching, which is not feasible through passive pitching, tends to minimize negative torque [112]. The curved blade is enabled to offset in such a balanced manner during passive pitching, relying on a centrifugal force of a blade. The negative torque may raise with passive pitching; however, the positive torque may rise further [113]. As a consequence, active pitching improves the turbine's efficiency. According to a previous analysis by Paraschivoiu [114], good throwing will raise the total annual yield by 30%. Blade pitching systems will be used on potential big Darrieus turn turbines for their benefits.

2.3.5. Helical Turbine

Gorlov introduced the helical turbine in 1995 [115], Figure 2.16 shows one of Helical turbines with 3 blades. Helical bladed turbines have a number of benefits over straight bladed turbines, including improved self-starting capacity, lower noise, longer blade span, lower vibrations, and lower peak tension in the blades [116]. The capacity of the blades to speed past the dead band, as well as the decrease of a, increase the self-starting functionality [117]. The stall angle is greatly increased to boundary layer connection caused by the application of spanwise flow by a helical

blade, as shown by previous studies. Tailored airfoils have been suggested to delay stall. [118] the stall angle is also influenced by the helical angle of a blade. The observational analysis of a straight-bladed Darrieus turbine with a helical turbine shows that the helical turbine's maximum C_p is considerably lower than that of the straight-bladed turbine. In the scenario of a Darrieus turbine with straight blades, motions are minimized by constant wake instead of vortices [119]. On the downside, the expense of making helical blades is greater than straight blades. The only way to make a helical blade is to use a mold, while straight blades could be made using aluminum extrusion. While three-bladed helical turbines are perhaps the most common, two-bladed and five-bladed turbines, have also been registered. The working Tip Speed Ratio continues to decrease while the quantity of blades increases λ_0 . For turbines of three or even more blades, blade tip failure and blade wake interactions seem to be very noticeable. Industrial helical turbines with an energy capacity of 2 to 10 kW are popular. VWT Power produced a 7.5 kW model known as the Qr6 [120], which is the latest generation of turbines. The three-bladed turbines have such a swept area of about 16-meter square and a top rpm of 260, with a survival wind speed of around 52.5 m/s. The blade fixation arms are crafted of carbon fiber that lowers the rotor's mass and, as a result, helps self-starting by lowering inertia [121]. Another related helical turbine producer is "Turby" [122], which seems to be a Delft University of Technology study result. At 14 m/s, the 2.5 kW turbine achieves its maximum capacity. Even with the warped flow, the turbine is designed for rooftop installation, achieving a 40 percent performance.



Figure 2.16. Helical Turbine with three blades.

2.4. AERODYNAMICS OF VAWTs

A wind turbine's aerodynamic research has two primary goals. Firstly, to determine the turbine's aerodynamic efficiency, and secondly, to determine the wind loads which will affect on the turbine. In most cases, certain templates are used to achieve these goals [123-124].

Streamtube ideas are utilized in the simplified VAWT aerodynamic models. The change in wind velocity in a stream tube is equated to a time-averaged force mostly on blades throughout the stream tube in such models. To evaluate uniform velocities and pressures, experimentation is needed, and two-dimensional airfoil lift and drag parameters are being used to calculate blade forces. These equations can easily account for wind shear or local Reynolds number variations. The turbine is assigned to a particular stream tube, several stream tubes that discriminate among upwind and downwind blades throughout the different versions, Figures 2.17 and

2.18 show multi-streamtube MST and double-multi streamtube models DMST [125-126].

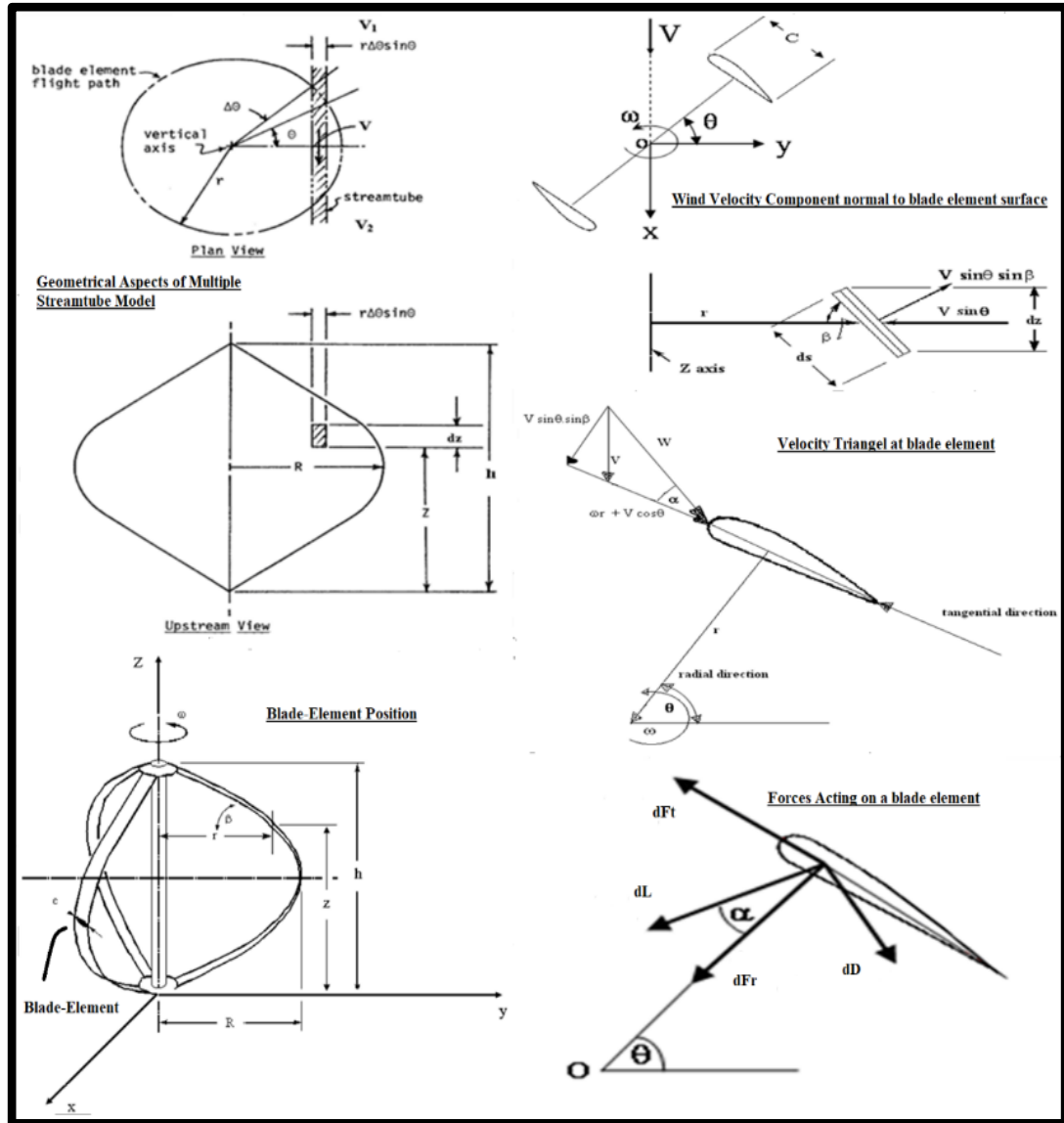


Figure 2.17. Multi-streamtube model.

For three major aspects, multiple steam tube techniques are typically common among wind turbine designers. First, they are being shown to reliably model turbine output for a broad spectrum of rotors and flow properties. Second, they are easy to understand or use and can be installed on almost any desktop machine. Third, they operate very fast. However, time-averaged approaches neglect most of the fluid

dynamics inside the rotor and hence cannot be able to forecast unstable results or comprehensive loads reliably [127-128].

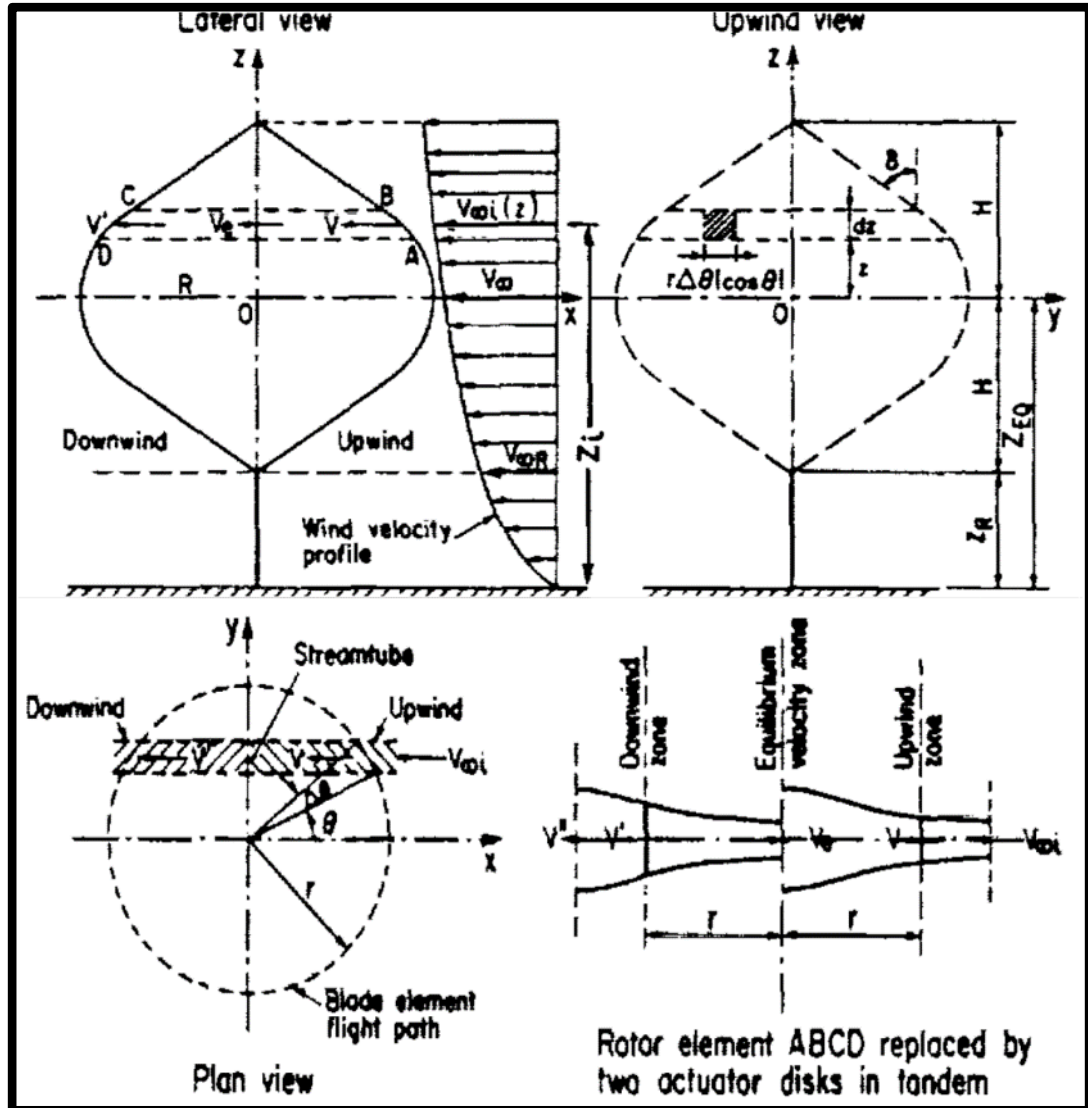


Figure 2.18. Double multi-streamtube model [128].

By deciding the extent of vorticity within turbine wake, vortex methods conduct precise measurements of an induced velocity field centered on a certain type of vorticity equation, Figure 2.19 shows the vortex model basics. Vortex models could use both lifting line and lifting surface formulations for such blades, including free wake or fixed (or prescribed) wake models, but there are several variants. The far more technically feasible model is indeed the three-dimensional, lifting floor, free wake formulation, but no programs are presently available that can operate such

a model in a timely manner, irrespective of the type of machine being used. With vortex codes, the challenge is to strike the right balance between model simplification and runtime [129].

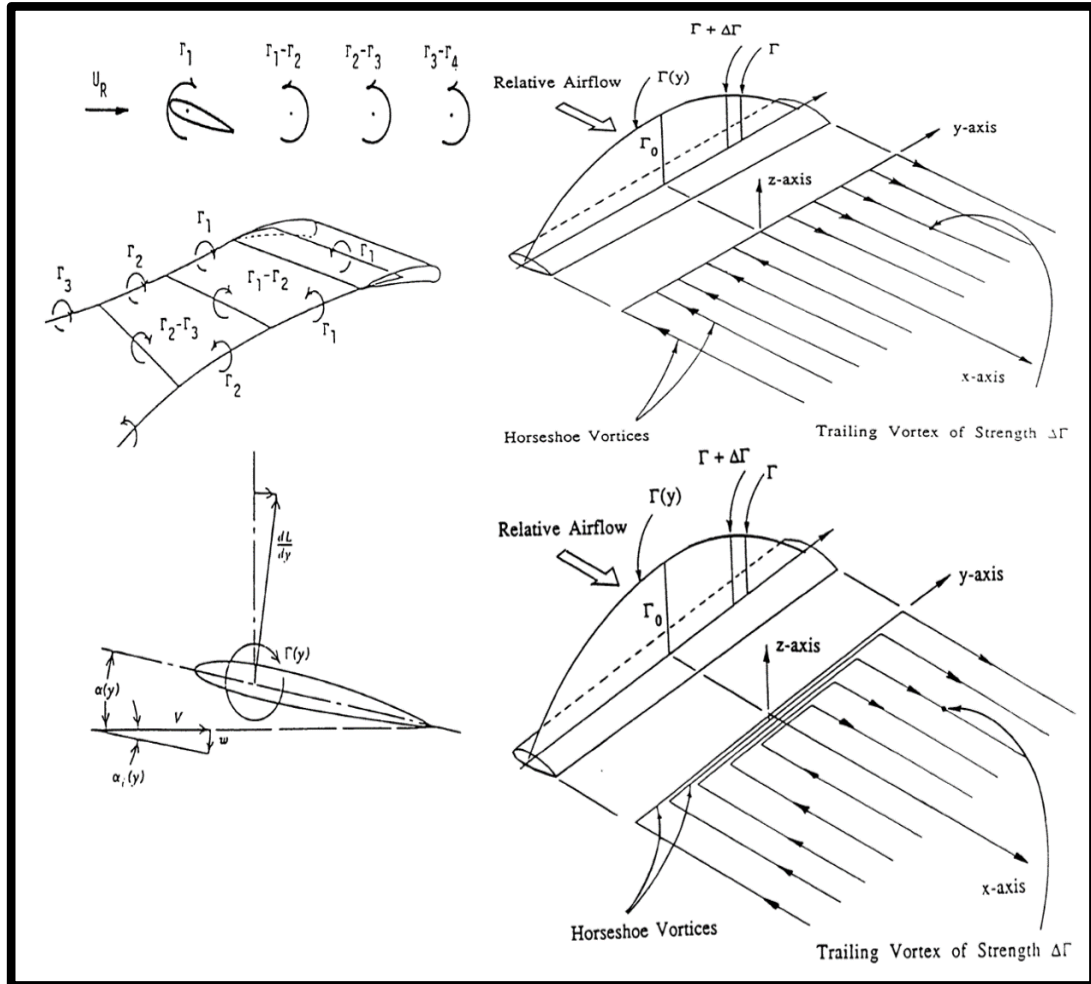


Figure 2.19. The vortex model basics.

The momentum and vortex models are combined in the local circulation model LCM. The LCM uses a momentum equilibrium between both the impact on a blade and the shift of wind momentum when it flows via the rotor, comparable to the stream tube versions. The blade, on the other hand, is depicted as an amplitude of hypothetical blades with elliptical circulation intervals of various spans. Local propagation models can be used to assess flow behavior and can provide details on flow field velocity and blade loads. The LCM has better results than momentum models, eliminates the vortex models' convergence issues, and needs much less

computing time for an adequate wake model against the vortex models. This model, however, isn't as easy to appreciate as stream tubes or vortex ones, yet it hasn't been widely used to date [130].

To calculate blade loads and turbine output, all current aerodynamic models include airfoil section phenomenon tables (lift and drag coefficients as properties of the angle of attack and Reynolds number). Two-dimensional, static wind tunnel experiments or two-dimensional, static airfoil design modules are commonly used to obtain airfoil section results. These are therefore updated using empirical, semi-empirical, or analytic approaches to approximate blade loads within three-dimensional, severe situations, such as dynamic stall. Determining the necessary airfoil section properties for the operating area is the most challenging part of providing correct assumptions [131-134].

PART 3

METHODOLOGY AND METHODS

3.1. SLANT-STRAIGHT BLADE ROTOR (SS-VAWT)

3.1.1. Geometric Details of SS-VAWT

Figures 1 and 2 illustrate the geometric variables of the SS-VAWT turbine, which include the height $2H$, diameter $2R$, and angle of inclination of the blades β . These variables, in addition to the length of the blade cord line C and the number of blades N are what this study aimed to verify their influence on the performance of the SS-VAWT.

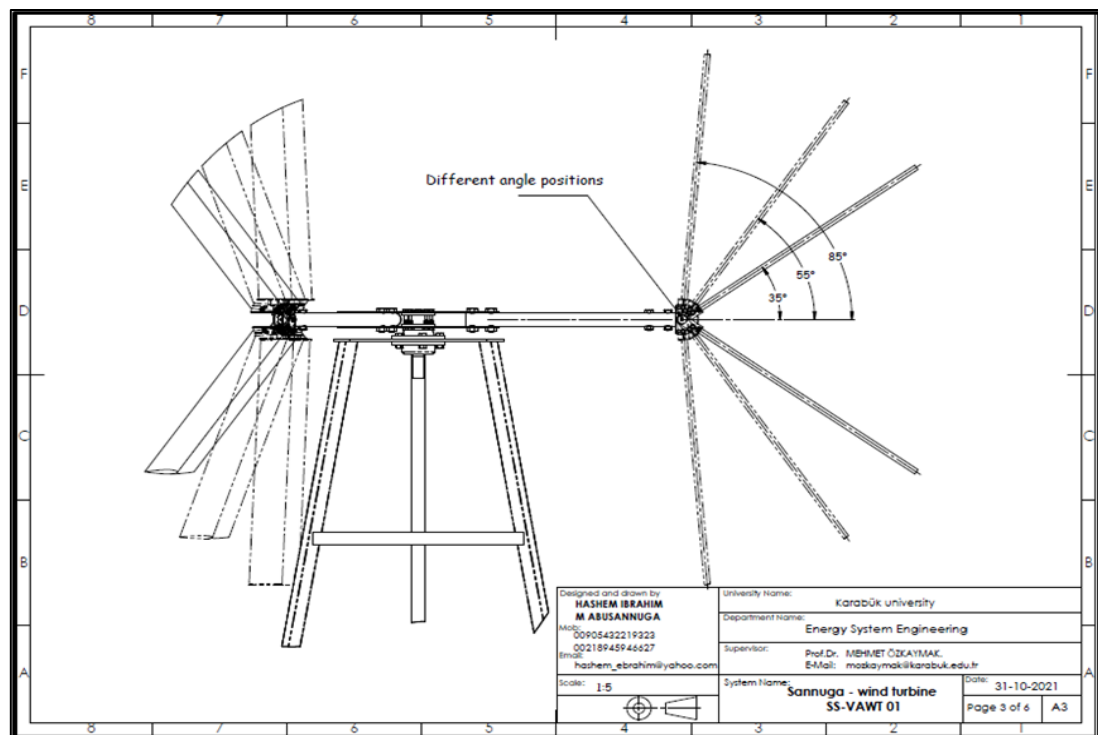


Figure 3.1. Changing the Angle of Inclination of the Rotor Blade SS-VAWT.

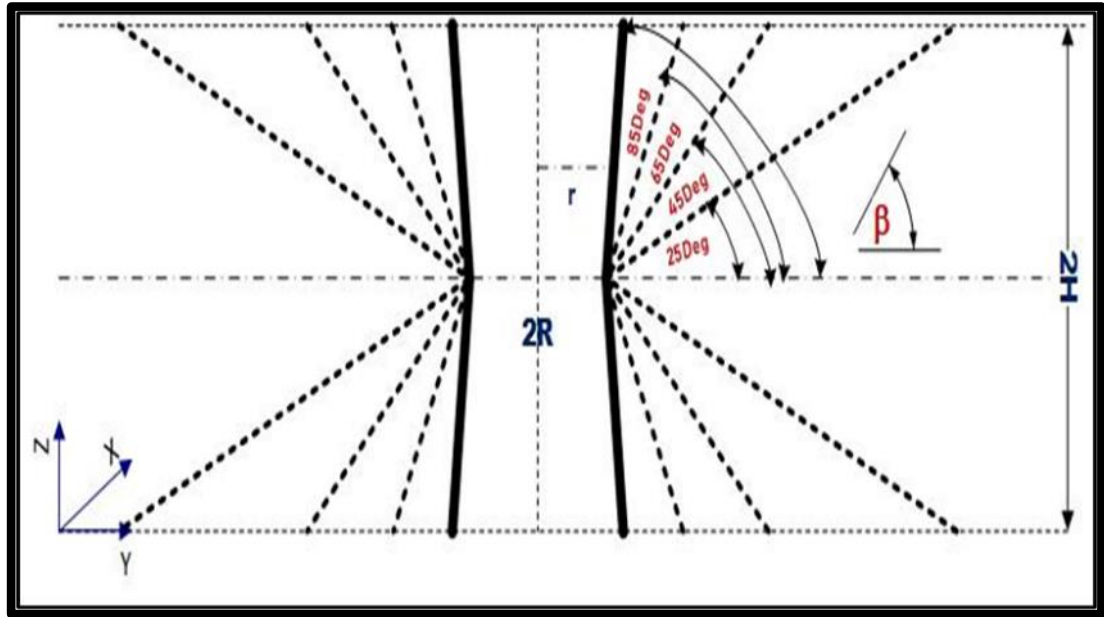


Figure 3.2. Geometric Variables of the SS-VAWT.

3.1.2. Performance Optimization of SS-VAWT

The effect of variable blade inclination angle or angle of blade slant on power factor C_p of straight blades- vertical axis wind turbine has been studied. Where a slop of angle on the horizontal plane was changed from an angle of *25 degrees* to an angle of *85 degrees* with the amount of change is equal to *20 degrees*. Within the scope of this thesis, the wind rotor was given the name "*straight-slant vertical axis wind turbine*" (SS-VAWT). The mathematical model "*Multi Stream Tube*" was modified and then applied in the form of a computer program by using "*Microsoft Visual program*", with regard to checking the effectiveness of this program, it was done by comparing its theoretical results with previous laboratory results from another researches, as it proved its effectiveness in achieving satisfactory results that fit the aim of this study.

As part of this Thesis analysis was conducted on twelve configurations of SS-VAWT as shown in Table 3.1, which were divided into four groups which are (*H group*), (*R group*), (*N group*) and (*C Group*) to study the effect of blade inclination angle at different values of rotor height H , rotor radius R , rotor blades number N and blade airfoil length C respectively and separately. The results are expressed by power

curves as a function of tip speed ratio. As the results indicated that angle of blade slant range from 45 degrees to 65 degrees is the best range for rotor blade inclination in terms of obtaining the highest power factor Cp_M in addition to the largest range of tip speed ratio and moreover the angle 45 degree has the advantage of limiting the problem of starting a self-motion.

Table 3.1. Four groups of SS-VAWT geometrical variables parameters.

Group 1- "H" variable				Group 3 "N" variable			
N	R(m)	H(m)	C(m)	N	R(m)	H(m)	C(m)
3	1	0.5	0.12	2	1	1	0.12
3	1	1	0.12	3	1	1	0.12
3	1	1.5	0.12	4	1	1	0.12
Group 2 "R" variable				Group 4 "C" variable			
N	R(m)	H(m)	C(m)	N	R(m)	H(m)	C(m)
3	0.5	1	0.12	3	1	1	0.06
3	1	1	0.12	3	1	1	0.12
3	1.5	1	0.12	3	1	1	0.18

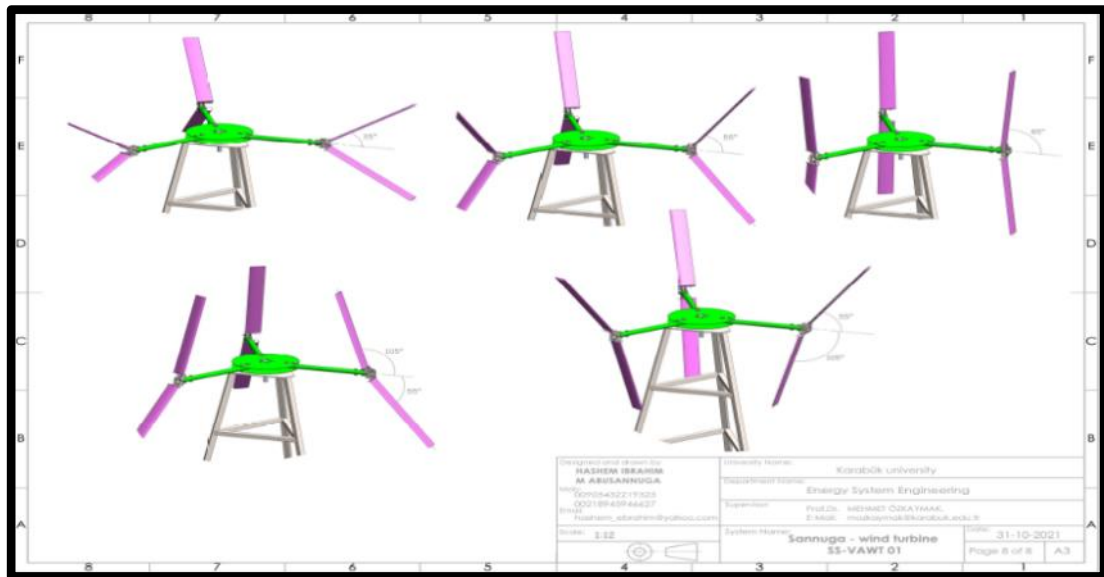


Figure 3.3. The System Is in Several Geometric Shapes.

3.2. MODIFIED MULTI STREAM TUBE MODEL

3.2.1. Overview

There are numerous mathematical concepts for the operational and reliability evaluation of Darrieus Wind Rotor (DWR), according to the available investigation. Most of these concepts aim to figure out how the air traveling through the rotor is distributed in velocity. Though such a distribution is known, the aerodynamic forces impacting upon the blades of the rotor can be determined, as well as the axial and torque force impacting on the rotor might well be derived as a result. The initial mathematical frameworks, known as blade-element momentum methods (BEM), can be clustered together historically. Such models work by correlating the axial part of the aerodynamic force occurring on the blades with the change rate of axial energy to calculate flowing velocities across the rotor.

Templin [16] presented what got described as the "one stream-tube model" in 1974. The rotors, he imagined, were contained within a single stream tube. Templin substituted the wind rotors with such an "actuator disc" into which the stream velocity is supposed to be constant, based on the "Glauert Actuator Disc Hypothesis." The velocity of air through the rotor is calculated by correlating the axial force exerted on the rotors with the change rate of axial momentum throughout the disc.

Lissaman and Wilson [124] and afterward Strickland [127] introduced what is described as the "many streams tube models," which significantly refined this prototype. A sequence of neighboring aerodynamically autonomous parallel stream tubes flows through to the rotor rather than a unified stream tube encircling the entire rotor inside the new approach. The BEM method is used to measure the velocity variation of the air moving past the rotor once more. When contrasted to empirical results, this significantly achieves the prior model, particularly in terms of the greatest output coefficient values. In section 3.2.2 of this thesis, Strickland's, numerous stream tube mathematical model is covered in depth. Paraschivoiu [128] proposed the "dual multiple stream tube model" later on. The velocity of flow in the

upstream half of such rotor is expected to be varied from the downstream half throughout this model. This necessitates the utilization of two actuator discs working together. Despite the fact that this approach is more precise than earlier models in terms of predicting local aerodynamics blade energies, it concludes that the proposed power coefficient for higher-solidity rotors.

In [129], an entirely distinct strategy from earlier BEM approaches was described, dubbed the "Vortex model." The element of the rotor blade is substituted with "trailing" and "bound" vortices throughout this methodology, which is similar to the "vortex-lattice approach" used for airplane wings. The influenced velocities, as well as the consequent flow velocity as well as approach angle, are therefore estimated as an outcome of this system of the vortex. As a result, the aerodynamic forces, and thus the torque as well as axial force, can be calculated. Mandal and Hirsch [135] developed a "cascade model" based on the techniques of cascade flow analysis often used in the domain of turbo-machinery. The parts of the rotor blade in this paradigm are considered to be on a plane area, with a blade gap equivalent to the circumference of the rotor split by the blade's numbers. The vortex, cascade as well as double multiple stream tube models are all within the focus of this thesis.

3.2.2. Multiple Streamtube Model

In what follows, a brief account of a multiple streamtube model due to Strickland [127] is briefly described. In this method, the formulas of the turbine geometry, torque formulas and aerodynamic forces acting on the turbine are combined. This method is known to satisfactorily and adequately predict the total value of the power factor, Moreover, it is easy to convert it into a computer program. In this thesis, the requirements of this method have been modified according to the requirements of the work.

3.2.2.1. Induced Velocity Factor

As shown in Figure 3.4, the wind rotor is replaced by what is termed actuator disc through which a number of aerodynamically independent streamtubes pass.

The velocity through disc plane is expected to vary from one streamtube to the other. Moreover, the axial air velocity is also expected to vary from its freestream value V_1 to its value at the plane, V , and finally reaching a value V_2 far behind the rotor. This continuous reduction of velocity is obviously due to the fact that the rotor extracts part of the kinetic energy of the wind. An induced velocity factor, a , is defined as follows:

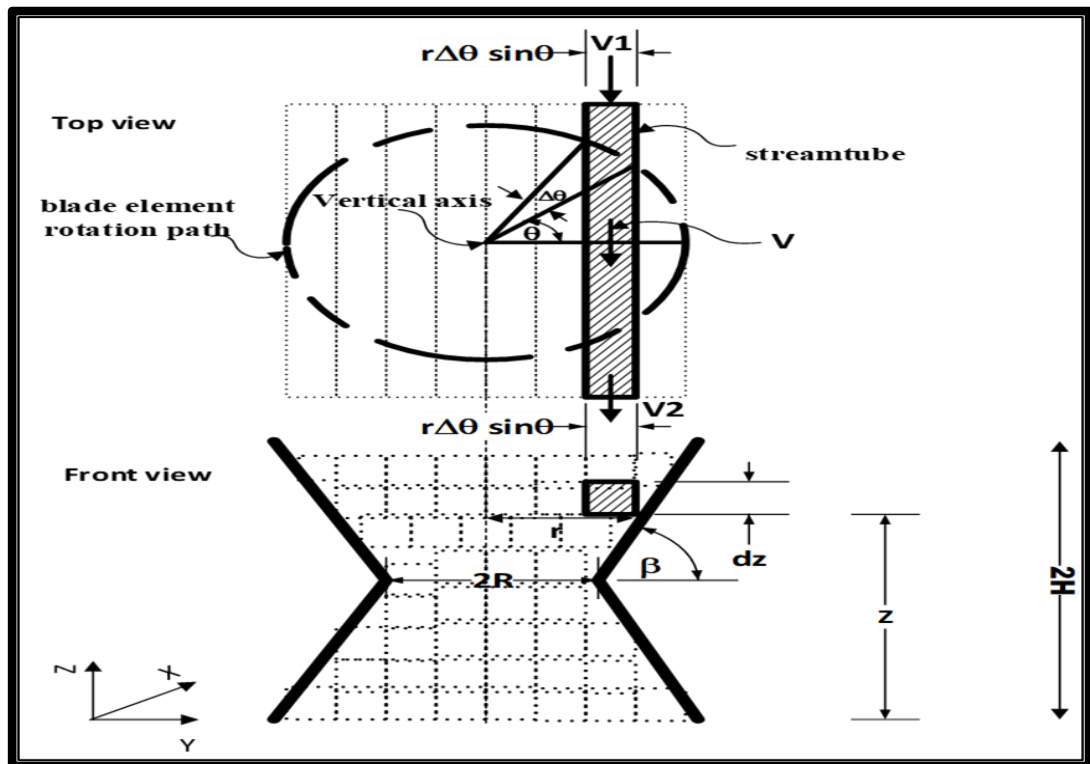


Figure 3.4. Geometrical Aspects of Multiple Streamtube Model and Relevant Velocities.

$$V = V_1(1 - a) \quad (3.1)$$

Now according to the actuator disc theory, half of the net change in axial velocity occurs at the disc plane and therefore

$$V_2 = V_1(1 - 2a) \quad (3.2)$$

In the following analysis, the airflow is assumed to be steady, uniform at any section, incompressible, and purely axial.

3.2.2.2. Force Acting on the Rotor

Figure 3.5 schematically shows a “*slant straight blade-vertical axis wind turbine*” (SS-VAWT) subjected to a wind velocity V_I which makes it rotate at a rotational speed ω . Also shown is the cartesian coordinate system (x, y, z) used in the analysis.

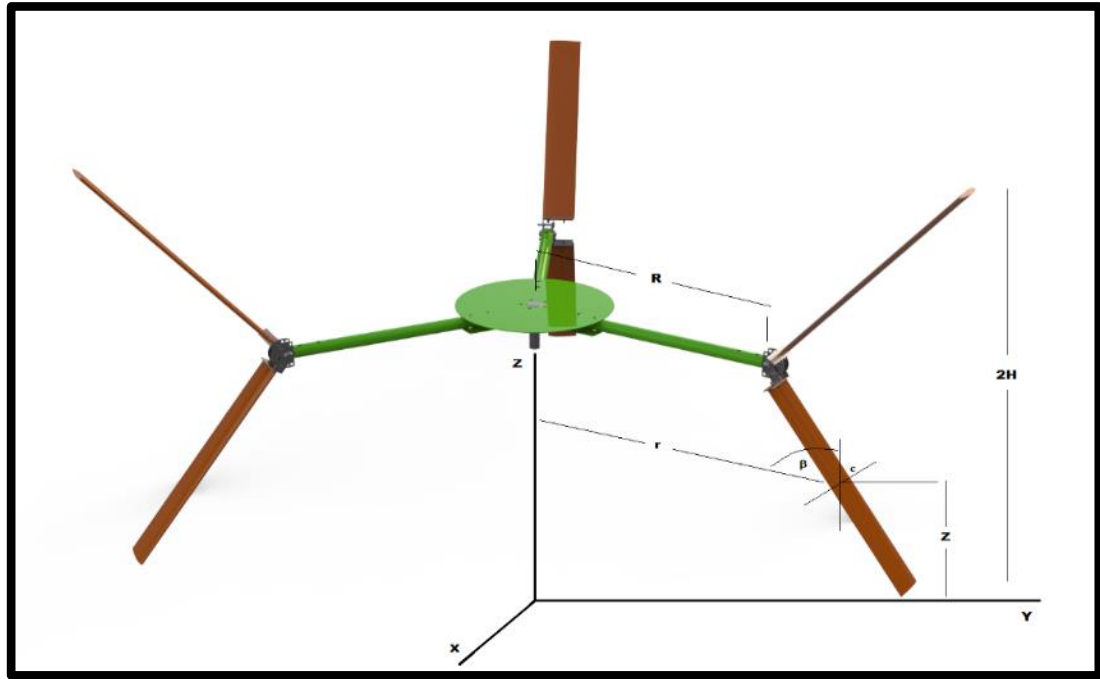


Figure 3.5. Blade-element position.

First let the rotor blade be subdivided into a number of blade-element. Consider one such blade-element of length ds and cord C situated at a height z , a radial distance (r) and azimuth angle θ as shown in Figure 3.6. The air velocity V at the blade element may be split into two components, a tangential component ($V \cos\theta$) and a normal component equal to ($V \sin\theta \sin\beta$) as shown in Figures 3.6 and 3.7. Here, β denotes the blade angle measured relative to the horizontal as shown in Figure (3.6). Relative to the blade-element there is yet another velocity component namely (ωr) which is due to its rotational motion.

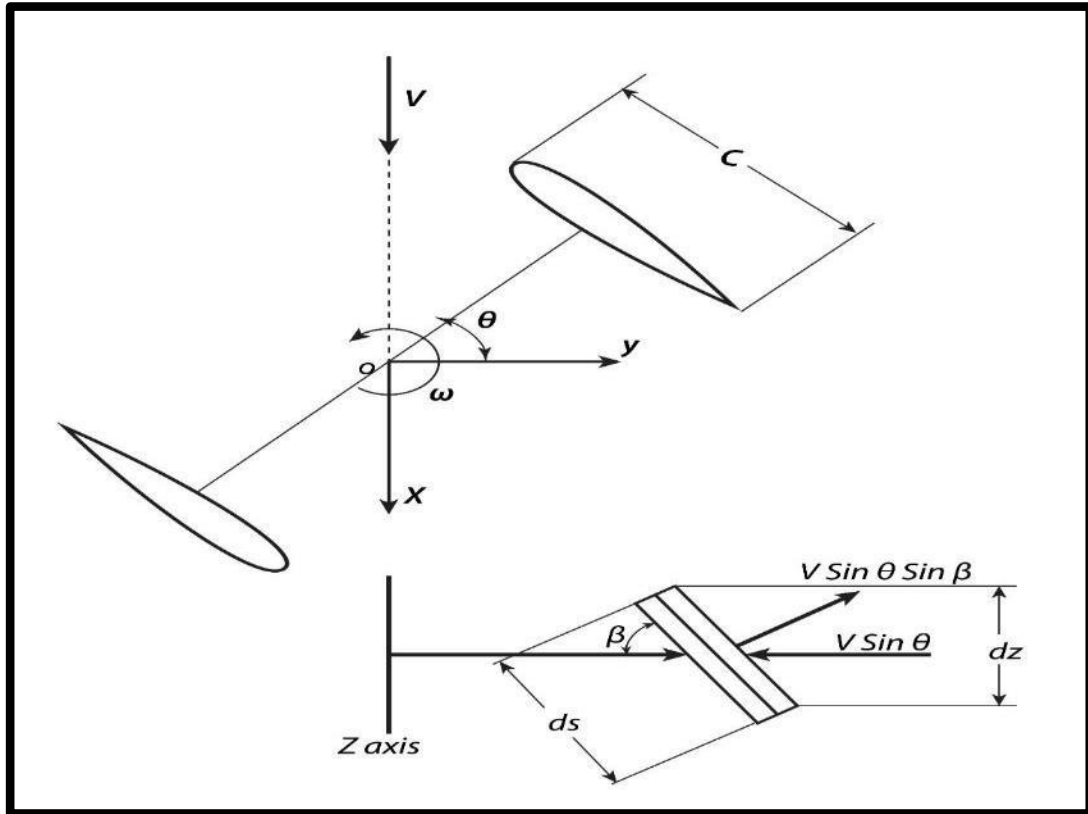


Figure 3.6. Wind velocity component normal to blade element surface ($V \sin \theta \sin \beta$).

The resultant velocity, W , may be determined from the velocity triangle shown in Figure 3.7. The resultant velocity " W " is seen to make a geometrical angle of attack " α " with respect to the chord line. This in turn leads to the generation of aerodynamic lift and drag forces dL and dD respectively as shown in Figure 3.8. It is well known in aerodynamics that dL and dD may be expressed in the following forms

$$dL = \frac{1}{2} \rho W^2 C_l C ds \quad (3.3)$$

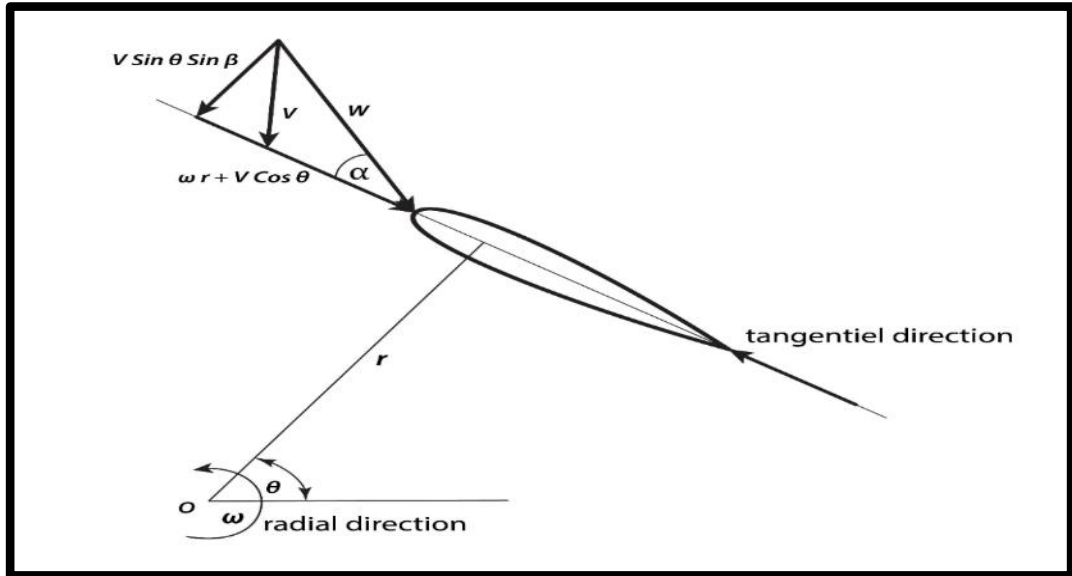


Figure 3.7. Velocity Triangle at a Blade-Element.

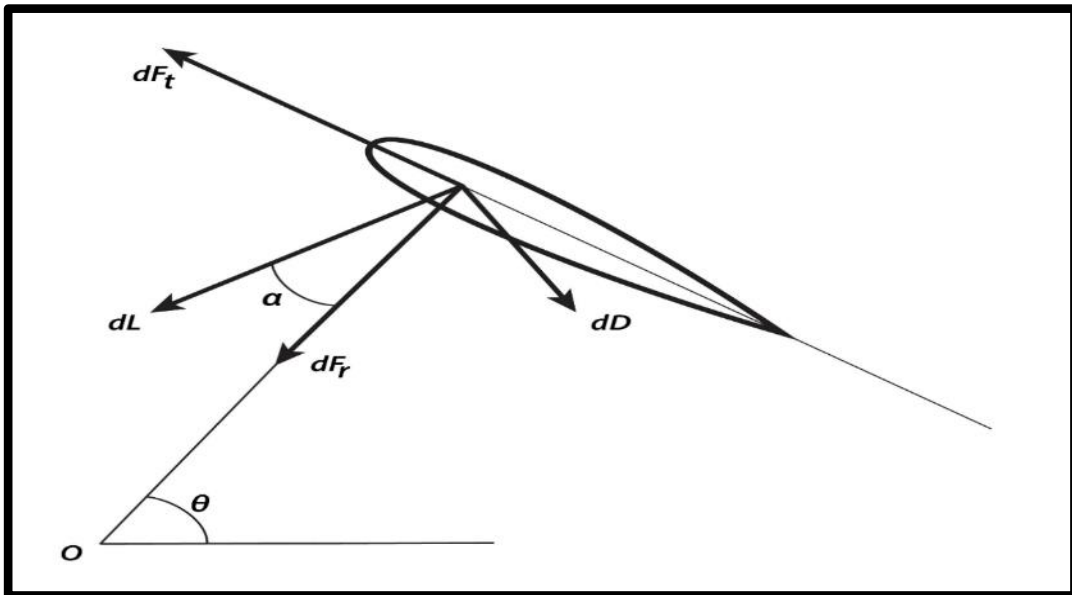


Figure 3.8. Forces Acting on a Blade-Element.

$$dD = \frac{1}{2} \rho W^2 C_d C_d s \quad (3.4)$$

where: $\rho \equiv$ air density (Kg/m^3), $C_l \equiv$ lift force coefficient and $C_d \equiv$ drag force coefficient.

As shown in figure (3.8), the radial and tangential forces dF_r and dF_t acting on the blade element may be written as follows:

$$dF_r = (dL \cos \alpha + dD \sin \alpha) \sin \beta \quad (3.5)$$

$$dF_t = (dL \sin \alpha - dD \cos \alpha) \quad (3.6)$$

From the same figure it is noted that the elemental axial force df acting on the blade-element is given by:

$$df = dF_r \sin \theta - dF_t \cos \theta \quad (3.7)$$

Combining equations (3.3), (3.4), (3.5), and (3.6) leads to

$$df = \frac{1}{2} \rho W^2 C \left(C_n \sin \theta - \frac{C_t \cos \theta}{\sin \beta} \right) dz \quad (3.8)$$

where: $ds = dz / \sin \beta$

$$C_n = C_l \cos \alpha + C_d \sin \alpha \quad (3.9)$$

$$C_t = C_l \sin \alpha - C_d \cos \alpha \quad (3.10)$$

Now the mean elemental axial force, df_x , acting on a number n of blade-elements passing through a given streamtube is given by:

$$df_x = \left(\frac{\Delta \theta}{\pi} \right) n df \quad (3.11)$$

where: $\left(\frac{\Delta \theta}{\pi} \right)$ represents the percentage of time spent by a blade-element within a streamtube, and df is as given by equation (3.8)

Using “axial momentum theorem”, the elemental axial force, df_x , acting over a given streamtube may be expressed as follows

$$df_x = \rho A_s V \Delta V \quad (3.12)$$

Where: (A_s) \equiv cross-sectional area of streamtube which is equal to ($r d\theta \sin \theta dz$) and $\Delta V \equiv$ net change in axial velocity which is equal to ($V_1 - V_2$) = $2aV_1 = 2(V_1 - V)$

Hence:

$$df_x = 2\rho r V (V_1 - V) \sin \theta . d\theta dz \quad (3.13)$$

The elemental axial forces given by equations (3.11) and (3.13) refer to the same force component, there for equating the two expressions yields:

$$\frac{ndf}{2\pi r \rho V_1^2 \sin \theta dz} = \frac{V}{V_1} \left(1 - \frac{V}{V_1}\right) \quad (3.14)$$

Denoting:

$$\left(\frac{ndf}{2\pi r \rho V_1^2 \sin \theta dz}\right) \text{ by } f_x^* \quad (3.15)$$

hence:

$$f_x^* = \frac{V}{V_1} \left(1 - \frac{V}{V_1}\right) \quad (3.16)$$

substituting for (V/V_1) from equation (3.1) yields $f_x^* = a(1 - a)$ or:

$$a = f_x^* + a^2 \quad (3.17)$$

3.2.2.3. Torque and Power Generated by the Rotor:

The elemental torque generated by a blade-element situated at a given point (r, θ, z) on the rotor blade is given by:

$$dM = r df_t \quad (3.18)$$

Substituting for df_i from equation (3.6) into equation (3.18) yields

$$dM = \frac{1}{2} \rho W^2 C C_t r \frac{dz}{\sin \beta} \quad (3.19)$$

It can be shown that the mean torque, M , acting on a rotor having N blades is given by:

$$M = \frac{\rho N C}{2\pi} \int_0^h \int_0^\pi W^2 r \frac{C_t}{\sin \beta} d\theta dz \quad (3.20)$$

Since the elemental power, dP , is equal to ωdM therefore it can be shown that power P is given by:

$$P = \frac{\rho N C}{2\pi} \int_0^h \int_0^\pi W^2 r \frac{\omega C_t}{\sin \beta} d\theta dz \quad (3.21)$$

3.2.2.4. Rotor Performance Parameters

Rotor performance data is always presented in a non-dimensional form which enables the use of such data no matter how large the wind rotor is, provided geometrical similarity between the different-size rotors is maintained. Therefore, tables or curves of power coefficients as functions of what is known as tip speed ratio, λ , are normally presented, as shown in Figure 3.9. The tip speed ratio is defined as follows:

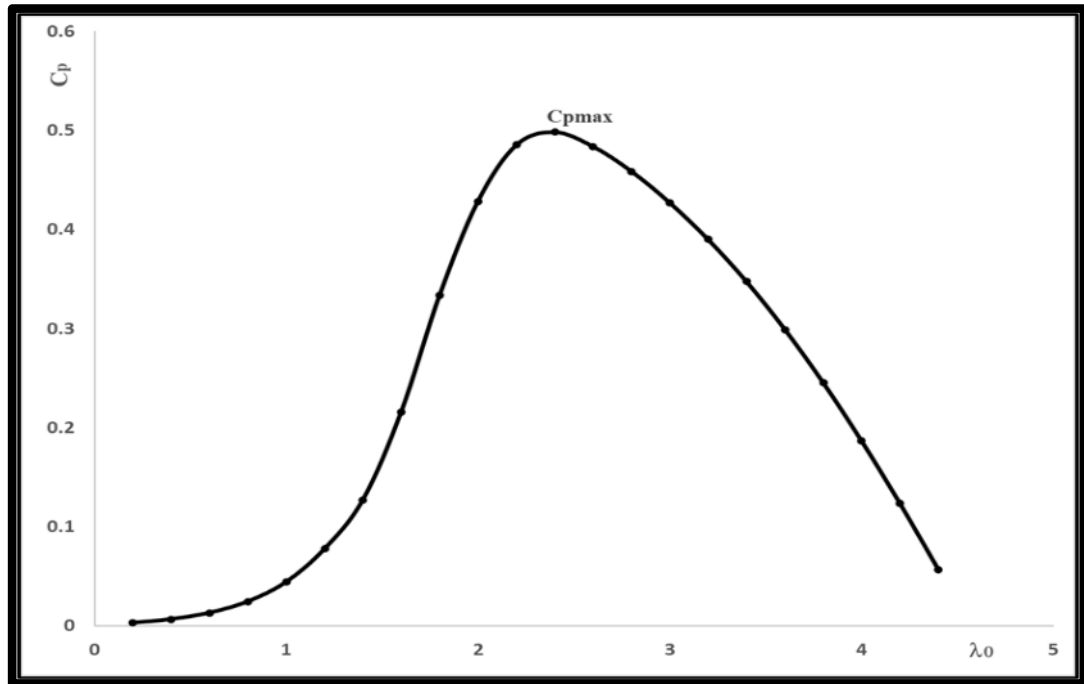


Figure 3.9. Power Coefficient as Function of Tip Speed Ratio.

$$\lambda_0 = \frac{\omega R}{V_1} \quad (3.22)$$

Where: $R \equiv$ maximum rotor radius

Now the torque coefficient, C_m , is defined as follows:

$$C_m = \frac{M}{\frac{1}{2}\rho V_1^2 AR} \quad (3.23)$$

Where: $A \equiv$ rotor swept area

Similarly, the power coefficient, C_p , is defined by:

$$C_p = \frac{P}{\frac{1}{2}\rho V_1^3 A} \quad (3.24)$$

Substituting for P from equation (3.21) yields

$$C_p = \frac{NC}{\pi A} \int_0^h \int_0^\pi \left(\frac{W}{V_1}\right)^2 \lambda_0 \frac{r}{R} \frac{c_t}{\sin \beta} d\theta dz \quad (3.25)$$

Now since $dM = \frac{dP}{\omega}$, it can be easily shown that:

$$C_m = \frac{C_p}{\lambda_0} \quad (3.26)$$

3.2.2.5. Determination of Induced Velocity Factor "a":

In order to determine the values of C_m and C_p at a given value of λ_0 , it is necessary to determine the velocity distribution through the disc or rotor. This in turn requires the determination of the induced velocity factor for each individual streamtube. To do so, the following iterative procedure was followed:

- Given the rotor geometrical shape and "a" certain value of λ_0 , then "a" certain streamtube position (r, θ, z) is selected.
- A starting value for "a" lying between zero and 0.5 is then assumed (choosing "a" = 0 at this step is good enough).
- The value of (V/V_1) is then computed from equation (3.1).
- Given the value of (V/V_1) , the angle of attack, α , is computed. From figure (3.4), it is seen that:

$$\alpha = \tan^{-1} \left[\frac{(V/V_1) \sin \theta \cdot \sin \beta}{(V/V_1) \cos \theta + \lambda_0 (r/R)} \right] \quad (3.27)$$

- Using $C_l(\alpha)$ and $C_d(\alpha)$ data relevant to the airfoil used to make the rotor blades, the values of C_l and C_d for the particular "a" computed in the previous step are then determined.
- Given α , C_l and C_d , the values of C_n and C_t may then be computed using equations (3.9) and (3.10) respectively.

- The value of $(W/V_1)^2$ is next computed noting that $(W/V_1) = (W/V) (V/V_1)$. As to (W/V) , it may be deduced from the velocity triangle in Figure 3.4

$$W^2 = V^2 \left[\left(\frac{r\omega}{V} + \cos \theta \right)^2 + (\sin \theta \cdot \sin \beta)^2 \right]$$

or:

$$(W/V)^2 = \left[\lambda_0 \frac{r}{R} (V_1/V) + \cos \theta \right]^2 + [\sin \theta \cdot \sin \beta]^2 \quad (2.28)$$

- combining equations (3.15) and (3.8) yields

$$f_x^* = \frac{nC}{4\pi r} (W/V_1)^2 \left(C_n - \frac{C_t \cos \theta}{\sin \theta \sin \beta} \right) \quad (2.29)$$

Thus f_x^* may readily be computed.

- A new value of "a" is then obtained from equation (3.17) by substituting for "a²" appearing on the right-hand side by the previous value of "a". The new value of "a" thus obtained is then utilized in the first step of the iterative procedure. This procedure is then repeated a number of times until the required accuracy of "a" is achieved.

3.3. DESIGNED ANALYSIS SOFTWARE

3.3.1. Overview

A computer program was designed as an application of the model of the “*multi-streamtube*” (MST) which was illustrated in section (3.2.2). And it is worth noting that (MST) model has been modified in line with the purposes of this thesis, that is, the designed computer program, which is called, *AL-Hashem-VAWT Soft*, can analyze the aerodynamic performance of the original Darrieus rotor (Parabolic Darrieus), Darrieus straight-blade (H-Darrieus) and in addition to Darrieus modified

and developed during this thesis and called it “*slant-straight blade vertical axis wind turbine*” (SS-VAWT). This program was designed using “*Microsoft Visual*” program, its inputs are: wind rotor type (PB-VAWT, H-VAWT or SS-VAWT), rotor height ($2H$), rotor diameter ($2R$), number of rotor blades (N), length of blade chord (C), Airfoil type and Reynolds number value (Re), as shown in Figure 3.10.

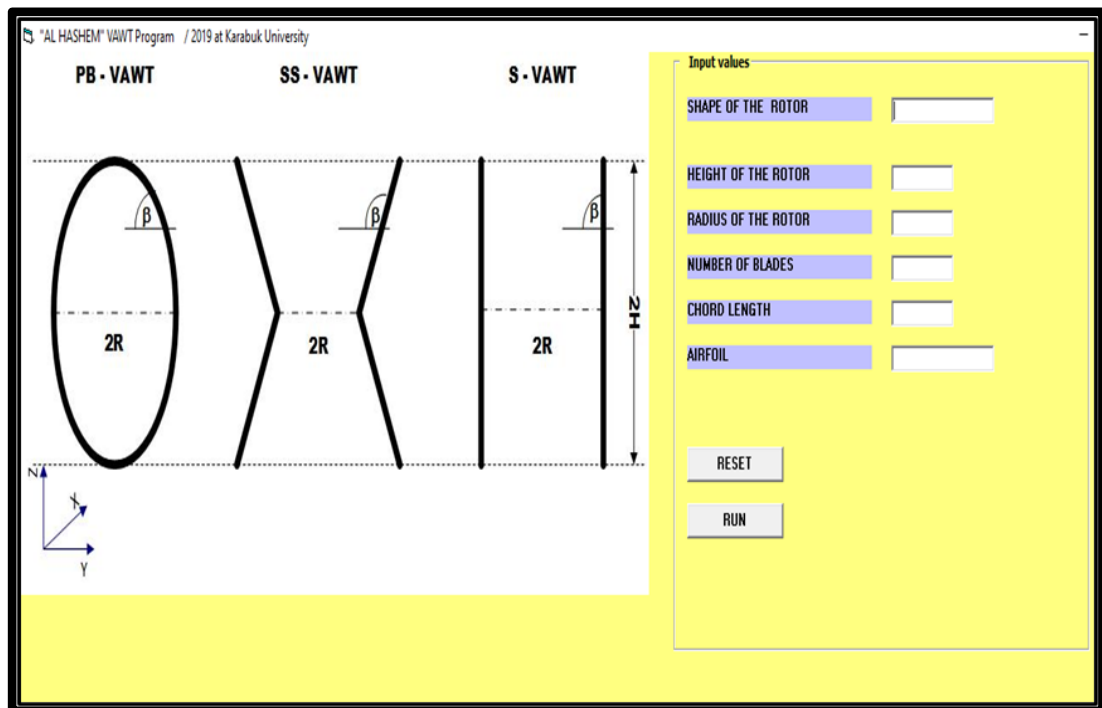


Figure 3.10. Input Window of AL Hashem VAWT Program.

The program performs a long and complex set of integrations, iterations, calls to process data pre-placed in external files such as “*Microsoft Access Database*” and calculations. Where any laboratory or field process data related to the air rotor are placed in external files to be recalled, analyzed and used according to the purpose. The data is extracted into external Microsoft Excel files. The results presented in values and curves. Where any laboratory or field process data related to the wind rotor testing are placed in external files to be recalled, analyzed and used according to the purpose. The data is extracted into external “*Microsoft Excel*” files. The results include values and curves. Flow chart of the program is shown in Figure 3.11.

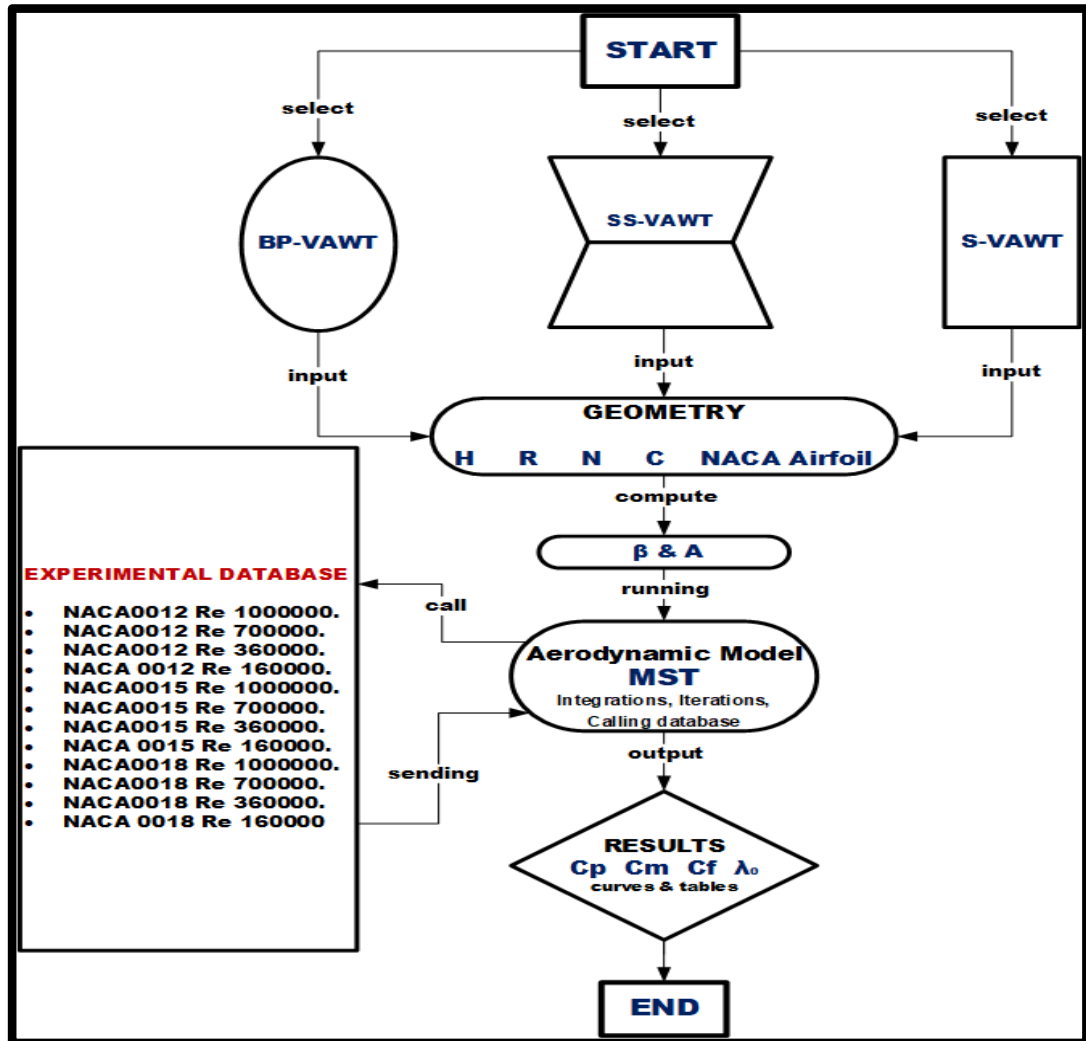


Figure 3.11. AL Hashem VAWT Program Flowchart.

The results are the behaviors of power coefficient as a function of tip speed ratio $C_p(\lambda_0)$ As previously shown in Figure 3.9. The program can also extract behaviors of torque coefficients and axial force coefficients, as well as behaviors of changing the angle of attack α with the rotation angle θ , in addition to the possibility of extracting the behaviors of the lift coefficients and the drag coefficients as a function of the angle of attack.

As this program is designed to be applied to several types of vertical axis wind cycles, and to verify its effectiveness, efficiency and accuracy, (i.e., conducting what is known as validation). As see in Figure 3.12, its results were compared with experimental results in the form of the change in the power factor with the change in

the relative terminal velocity. These experimental results represent wind tunnel tests of a wind rotor of known shape at flow velocities of 7, 9, 11 m/s. The curvature of each rotor blade is governed by the following two mathematical relationships, through which the general geometry of the rotor is determined:

$$\left(\frac{r}{R}\right) = \sin\left(\frac{\pi z}{h}\right) \quad (3.30)$$

$$\beta = \tan^{-1}\left\{\frac{\left(\frac{h}{R}\right)}{\cos\left(\frac{\pi z}{h}\right)}\right\} \quad (3.31)$$

Figure 3.12 represents the validation process, as the blue line is the power action curve extracted from the program designed in this thesis using the modified "*Multi streamtube*" mathematical model. While the points represent the power factor values extracted from the results of a wind tunnel for a rotor of known dimensions and the data was previously tested by researchers. Clearly, it is possible to see a very large congruence between the two cases, and therefore *Al-Hashem Software* was approved to perform the analyzes and studies of the first phase of this thesis.

It is worth mentioning and that is already known, that general geometry equations of *straight blade- Darrieus* (S-Darrieus) or (H-Darrieus) are:

$$\left(\frac{r}{R}\right) = 1 \quad (3.32)$$

$$\beta = 90(\text{Deg}) \quad (3.33)$$

In this thesis, special equations were created to determine the general and basic dimensions of the geometric shape of the SS-VAWT, which takes the shape of a trapezoid:

$$\left(\frac{r}{R}\right) = \left(\frac{\left(\frac{Z}{H}\right)}{\left(\frac{1}{\left(\frac{H}{R}\right)*\tan\left(\beta*\frac{\pi}{180}\right)}\right)}\right) + 1 \quad (3.34)$$

Where: $\beta = \text{Constant}$

3.3.2. Mathematical Commands Used in AL Hashem VAWT Soft

1. Input Geometric shape.
2. Input H, R, N , Airfoil Digit.
3. Compute: A .
4. Select: λ_0 .
5. Select: Z . ($0 \leq Z \leq H$)
6. Compute: r and δ .
7. Select: θ . ($0 \leq \theta \leq \pi$)
8. Set: $a = 0$
9. Compute: $(V/V_1) \rightarrow (V/V_1)=1-a$
10. Set: $\beta = (\pi/2) - \delta$.
11. Compute: α .
12. Determine: C_l and C_d
13. Compute: C_n and C_t .
14. Compute: (W/V_1) .
15. Compute: f_x^* .
16. Compute: new value of 'a'. $\rightarrow a = a^2 + f_x^*$
17. Substitute this value "a" in step (6) : $a = a$.
18. Repeat steps (6) to (15) until "a" converges.
19. Compute: (V/V_1) .
20. Set: $\beta = (\pi/2) - \delta$.
21. Compute: α .
22. Determine : C_l and C_d .
23. Compute: C_n and C_t .
24. Compute: (W/V_1) .
25. Compute: $C_{F\theta}$ and $C_{P\theta}$.
26. Repeat steps (5) to (23) for other values of θ .
27. Compute: C_{FZ} and C_{PZ} .
28. Repeat steps (3) to (25) for other values of Z .

29. Compute C_f , C_p and C_m .
30. Repeat steps (2) to (27) for other values of λ_o .

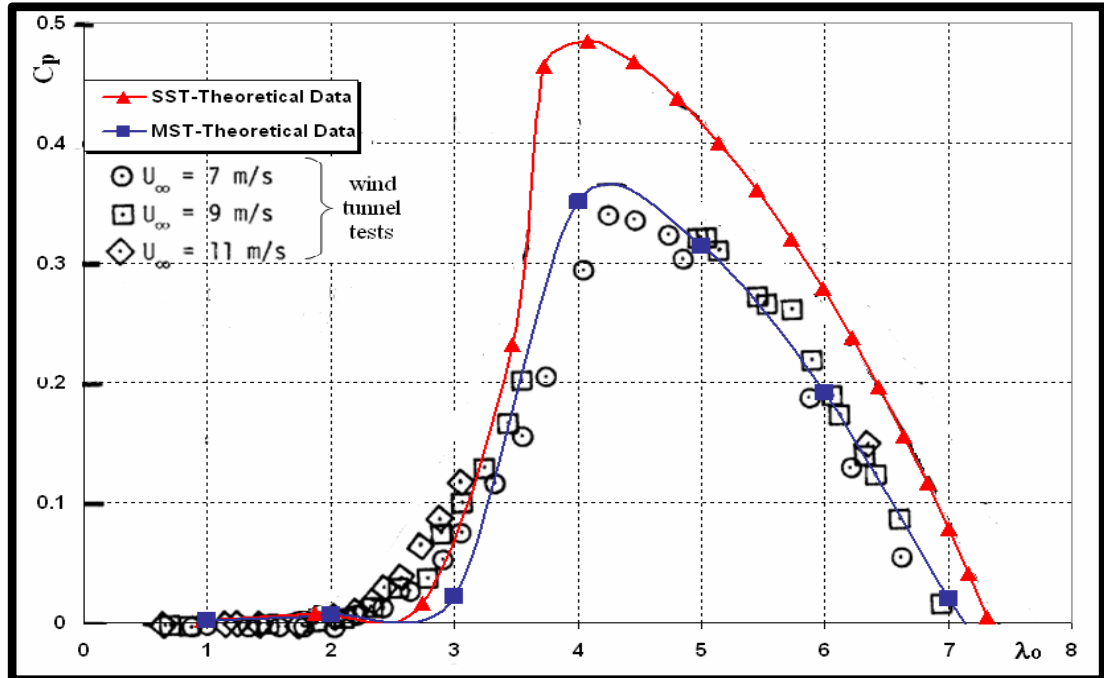


Figure 3.12. Validation of the Results of the Al-Hashem program.

3.4. PERFORMANCE COMPARISON OF PARABOLIC-DARRIEUS, STRAIGHT BLADE DARRIEUS AND SLANTING STRAIGHT BLADE-DARRIEUS

As explained in section (3.3) computer program was developed to be able to study three types of vertical axis wind turbines Figure 3.13, which are, parabolic blades rotor PB -VAWT, straight blades rotor S-VAWT or (H-VAWT) and slant straight blades rotor SS-VAWT. Consequently, previously, what were applied to both of twelve configurations of PB-VAWT and twelve configurations of S-VAWT, it is also applied to twelve configurations of SS-VAWT with the aim of comparing the three shapes under the similar condition of the geometric shape parameters.

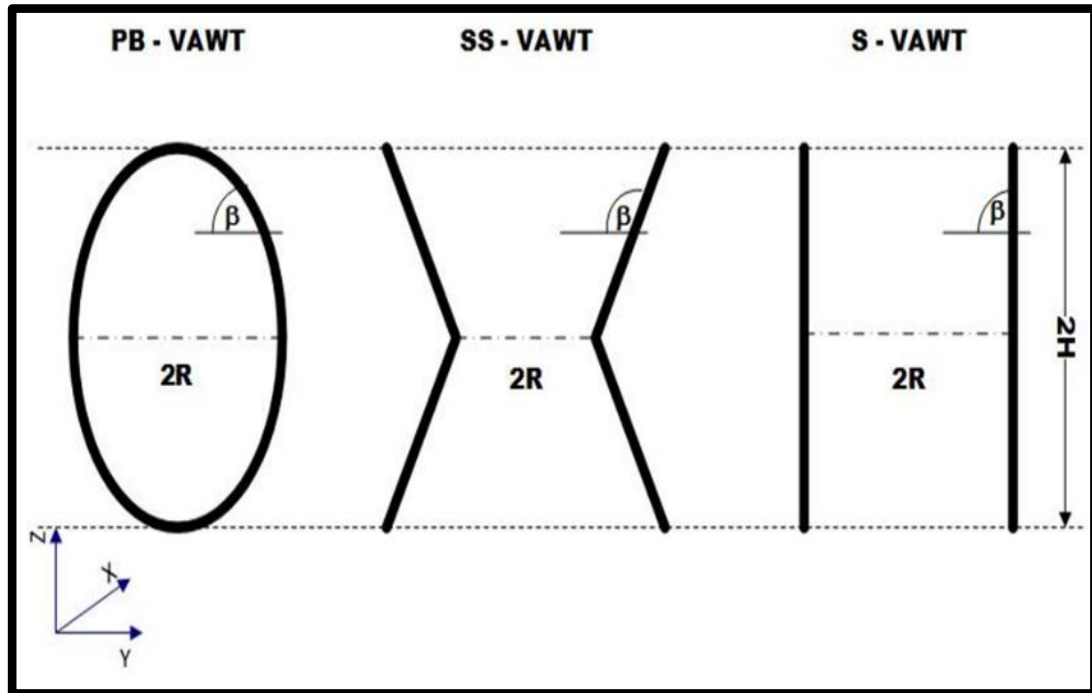


Figure 3.13. Sketch for Three Types of Vertical Wind Rotor.

A comparison was made between the three types in terms of aerodynamic performance, so the comparison resulted in the selection of the SS-VAWT type to move to the next stage of the thesis, due to its superiority in overcoming the problem of starting movement and the high values of the maximum power factor.

The dimensions of the geometry of the SS-VAWT, to be transferred to the next stage of the thesis, were determined. Also, the ideal geometric shape was determined according to many satisfactory and reliable results.

3.5. SIMULATION USING ANSYS FLUENT

This simulation is following the procedure of what if analysis as only one geometrical design parameter changed and focusing on the corresponding changes in the aerodynamic forces and moment acting on the turbine using the sliding mesh method. For the three cases the standard simulation steps was done, as following:

- Pre-Processing: Geometry preparations, Mesh Creation and setting the numerical model.
- Processing: Solving the three cases in Ansys Fluent Solver.
- Post-Processing: Extracting Results from CFD Post and analyzing data in Excel

3.5.1. Pre-Processing

3.5.1.1. Geometry Preparations

The turbine structure was created using *SolidWorks* in the part modeling environment as shown in Figure 3.14, then moved into the assembly environment to create the flow domain as shown in Figure 3.15, finally the turbine and the domain was exported as step part ready to be imported in “*Ansys Design Modeler*” as shown in Figures 3.16 and 17.

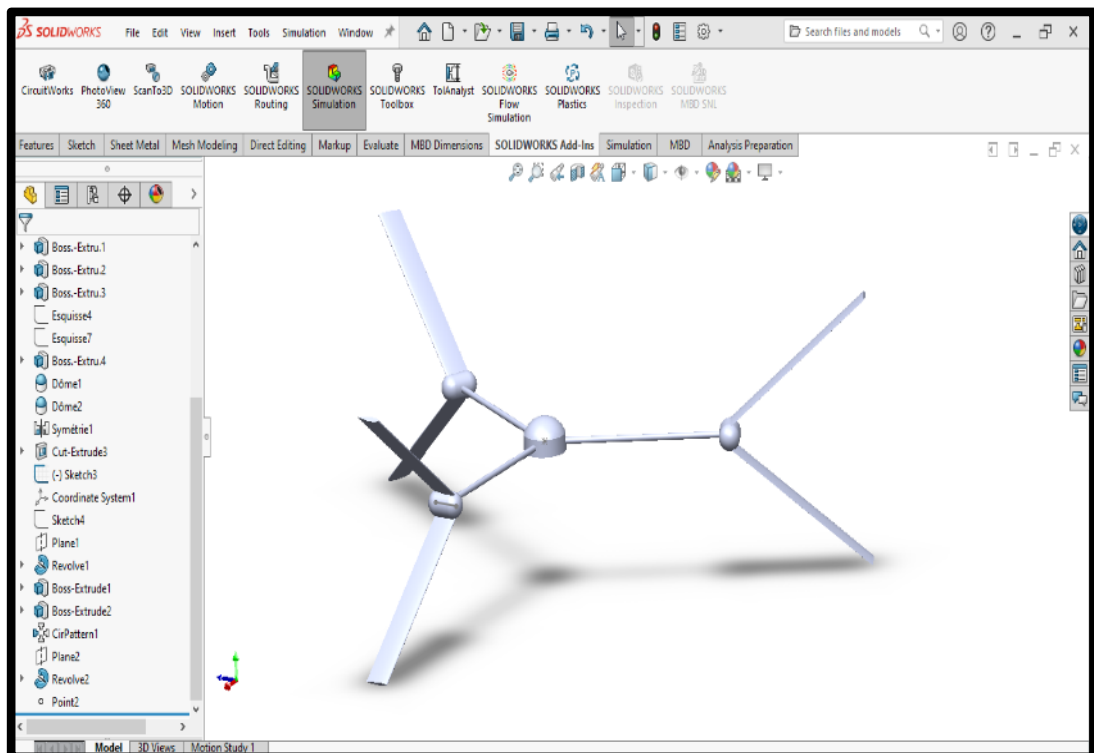


Figure 3.14. The model before mesh step.

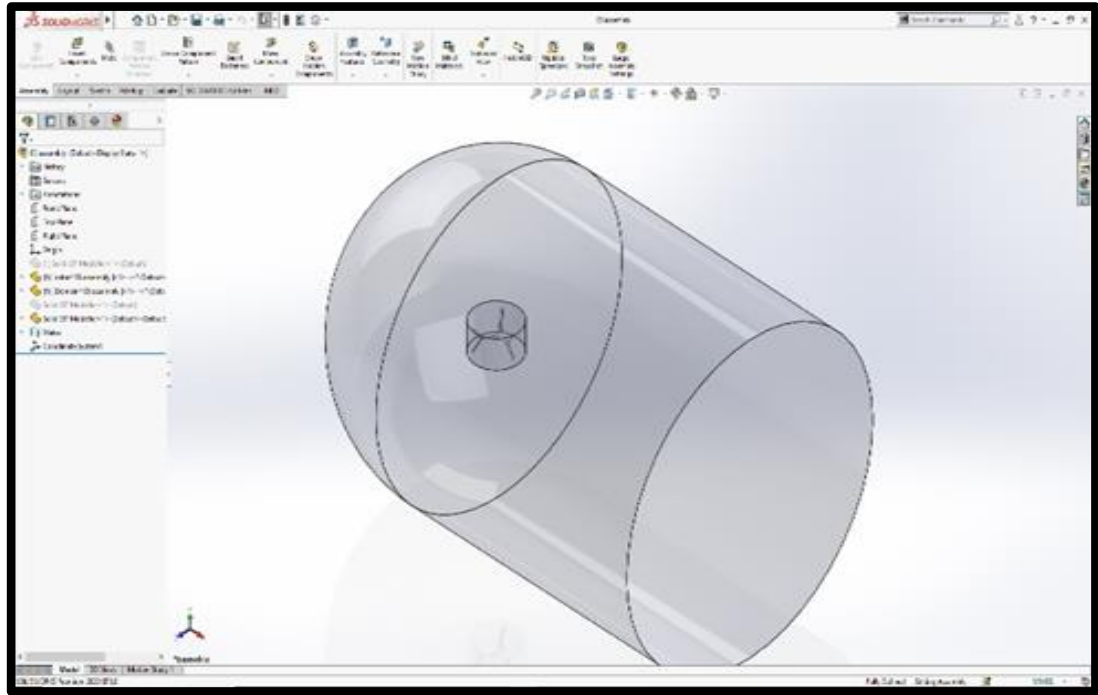


Figure 3.15. Creating Domine for the Model.

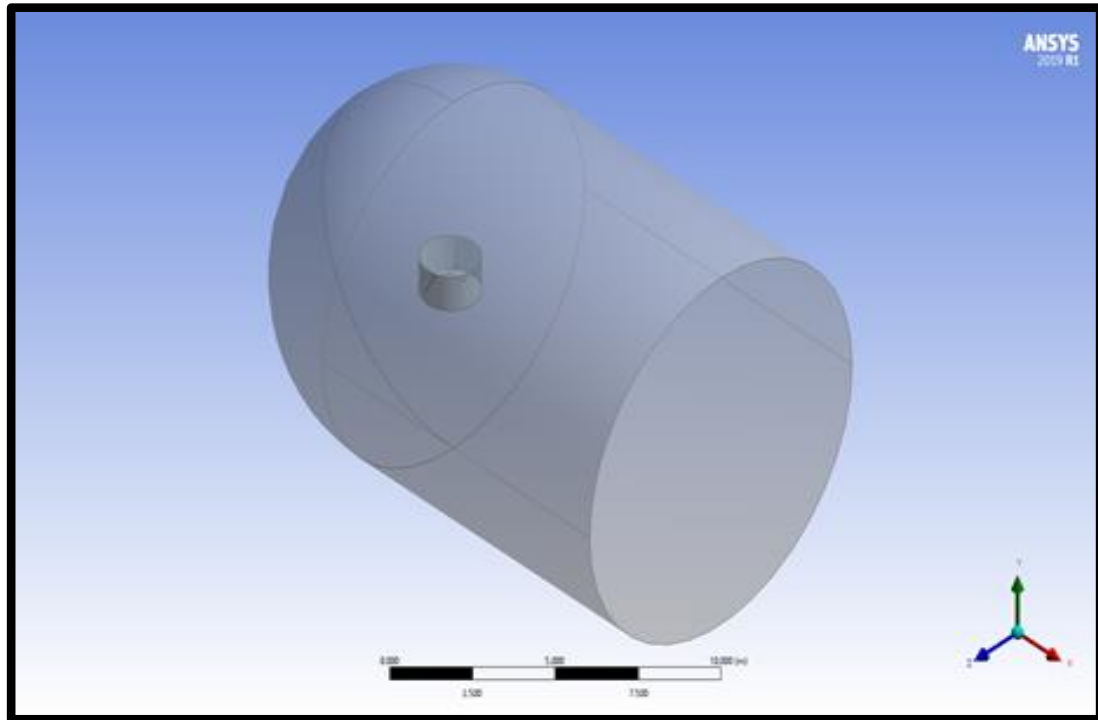


Figure 3.16. Imported the Model into “Ansys Design Modeler”.

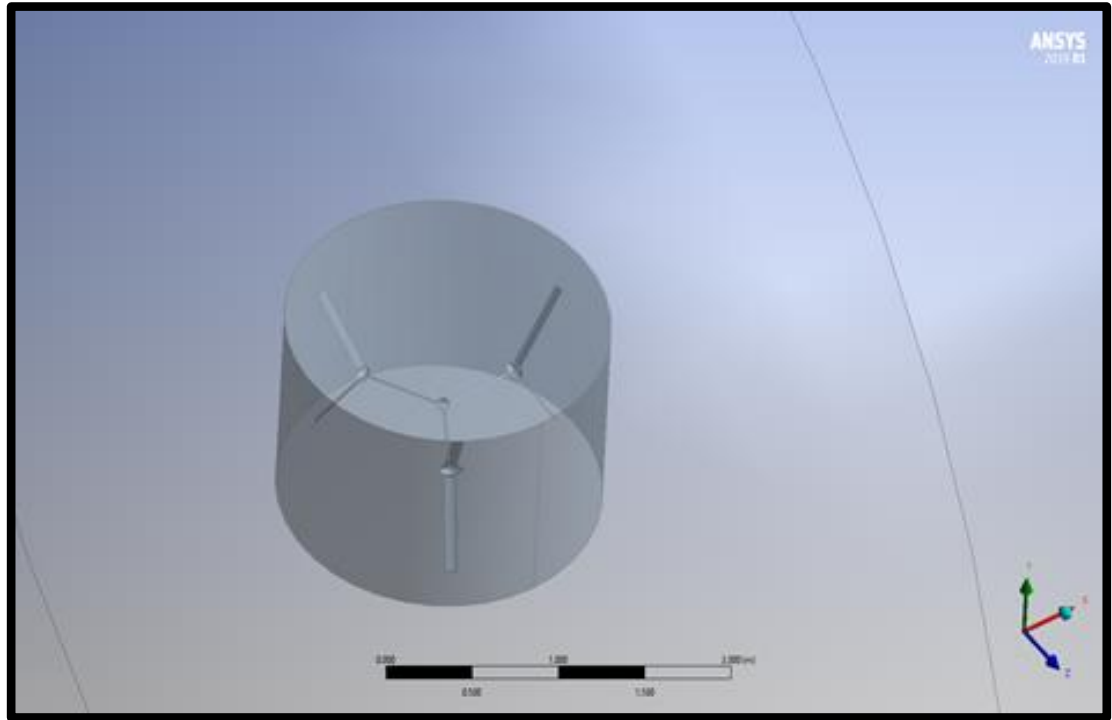


Figure 3.17. The model in “*Ansys Design Modeler*”.

Then two preparing Actions were done:

- Creating Booleans: As illustrate in Figure 3.18, In the sliding mesh-method the solid turbine extracted from the fluid domain leaving a cavity. In addition, second Boolean was created to generate the sliding interface.
- Creating named selections to set the boundary conditions on.

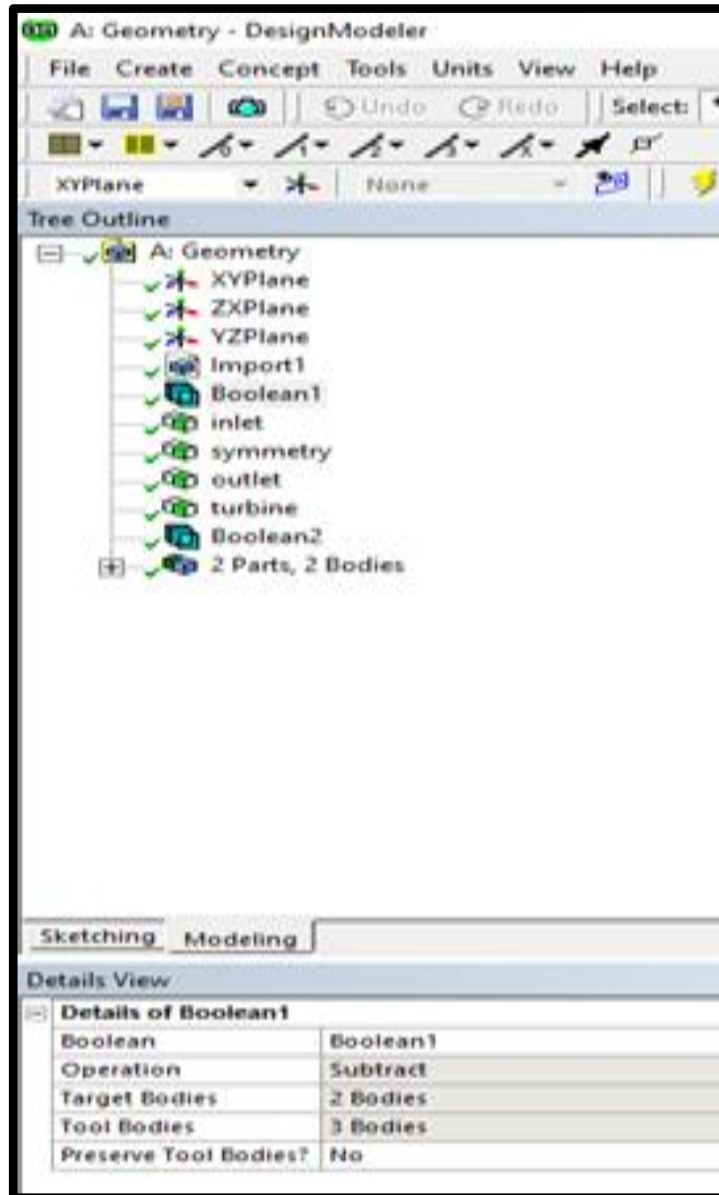


Figure 3.18. Creating *Booleans* for the model.

3.5.1.2. The Meshing

For the three Cases, (35° , 55° and 85°) *Ansys Meshing* was used to create the CFD mesh for the flow domain.

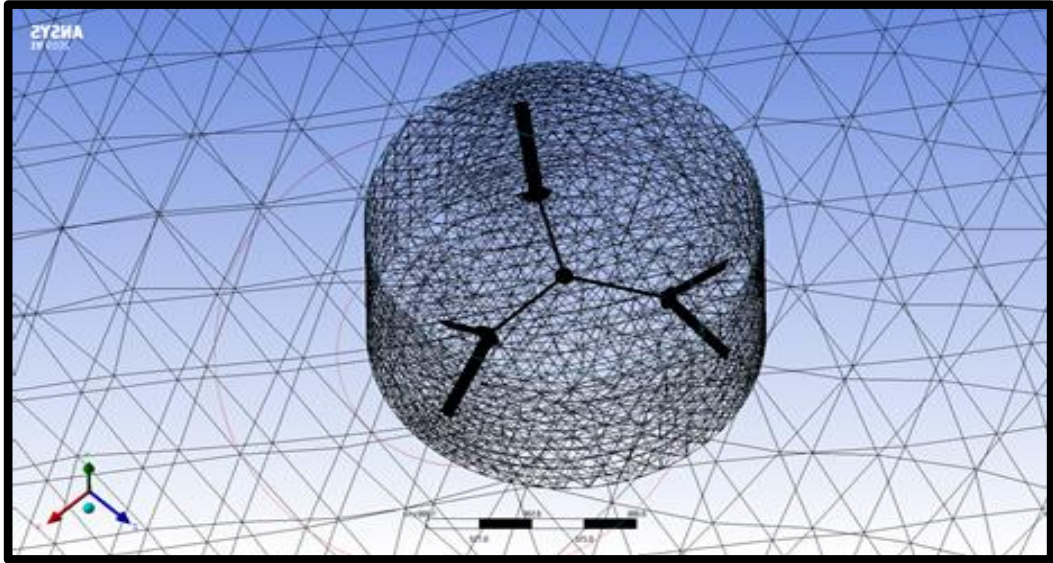


Figure 3.19. *CFD mesh* for the flow domain.

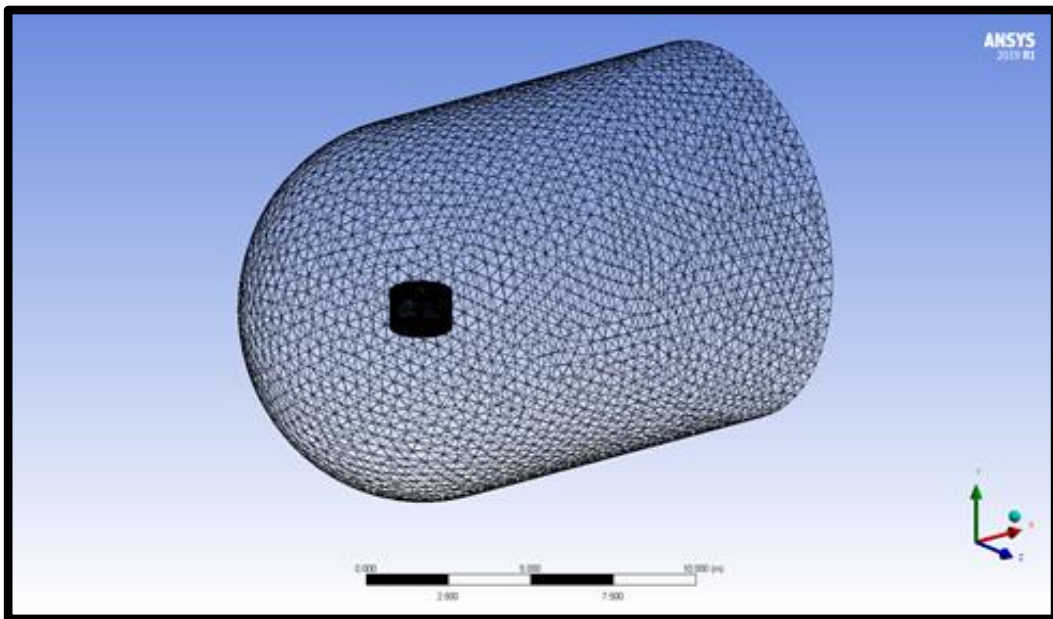


Figure 3.20. Primary surface mesh.

In meshing the refinement tool was used to create more fine mesh on the turbine and the sliding interfaces. A Body sizing tool was used to control the gross rate of the outer domain mesh. Then after creating the primary surface mesh refinement was repeated 2 times for the turbine and three times for the sliding interface to get a smooth transition of the variables across the interface.

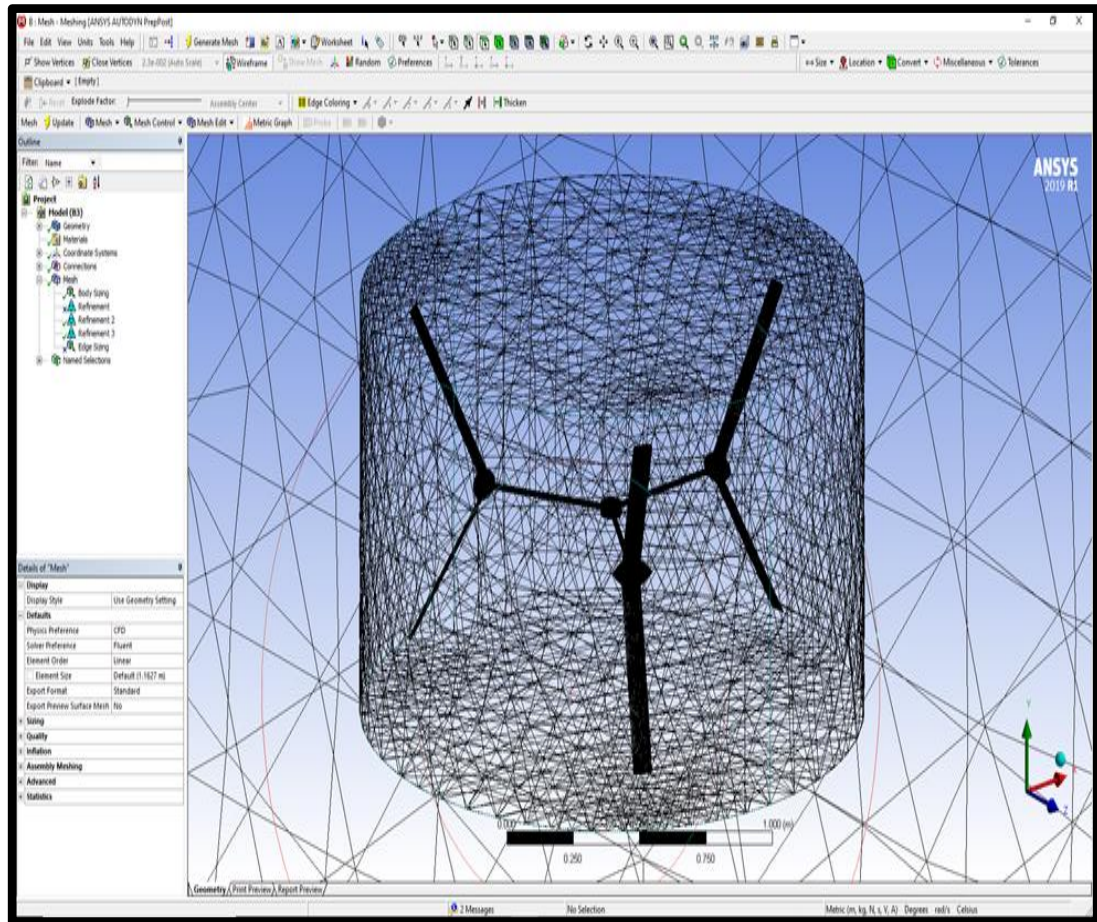


Figure 3.21. Mesh refinement the turbine and sliding interface.

Hence, the mesh elements had high quality for the Aspect Ratio and Skewness Metrics due to use of refinement tools of program This is illustrated in graphs 3.22, 3.23 and 3.24.

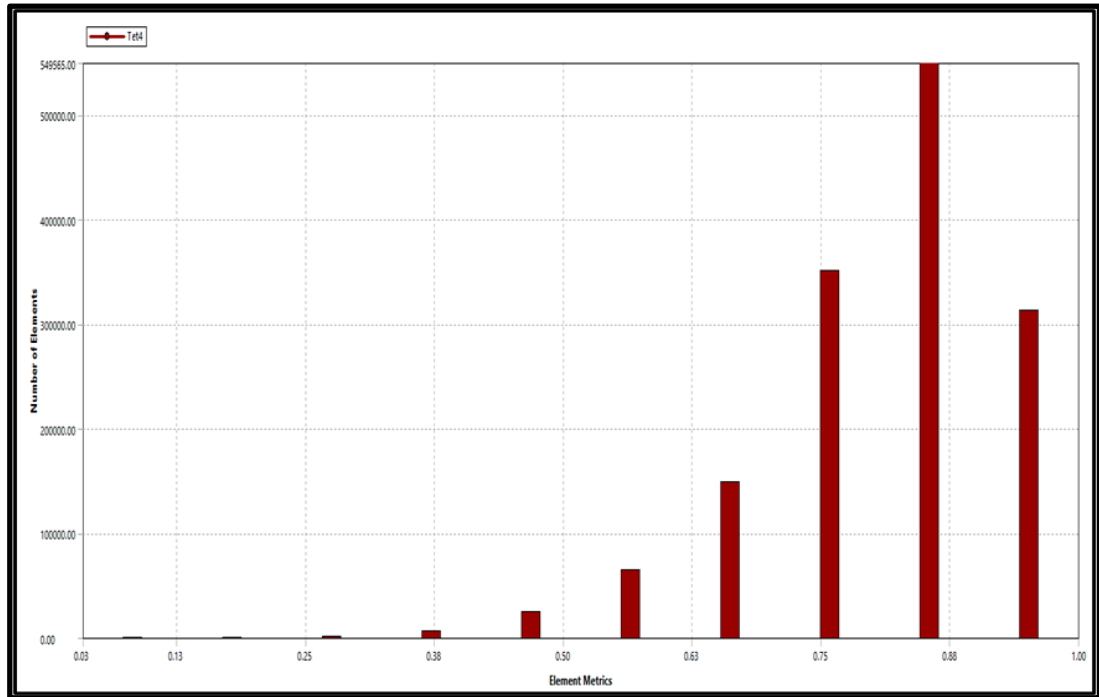


Figure 3.22. Element quality.

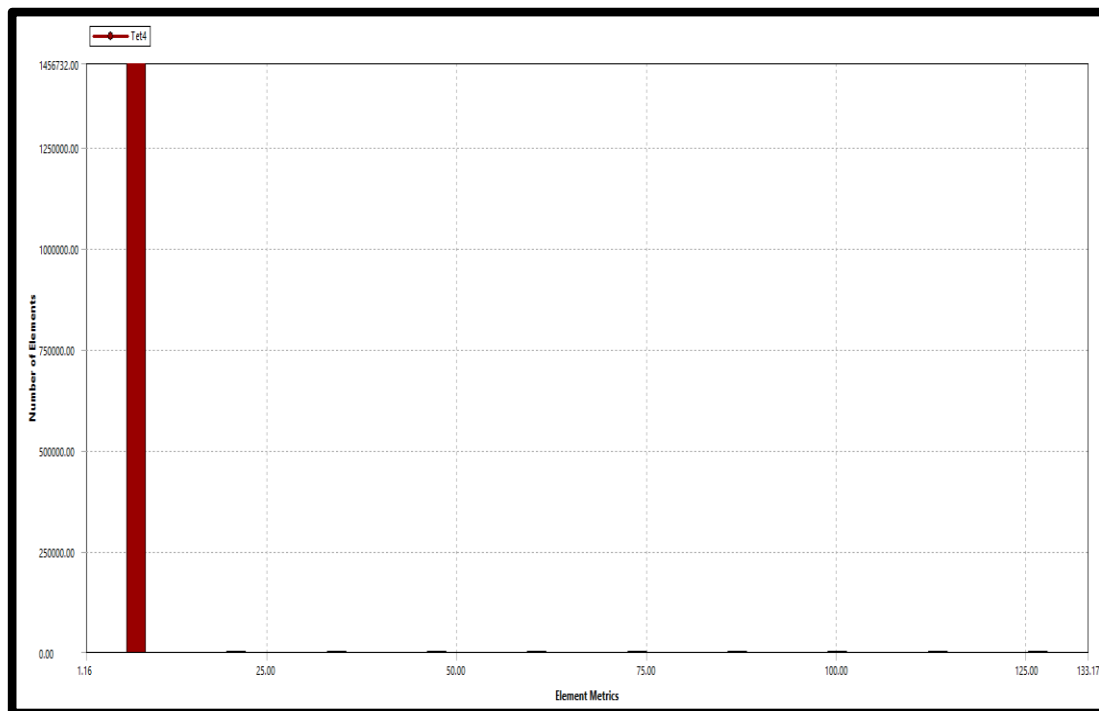


Figure 3.23. Aspect ratio.

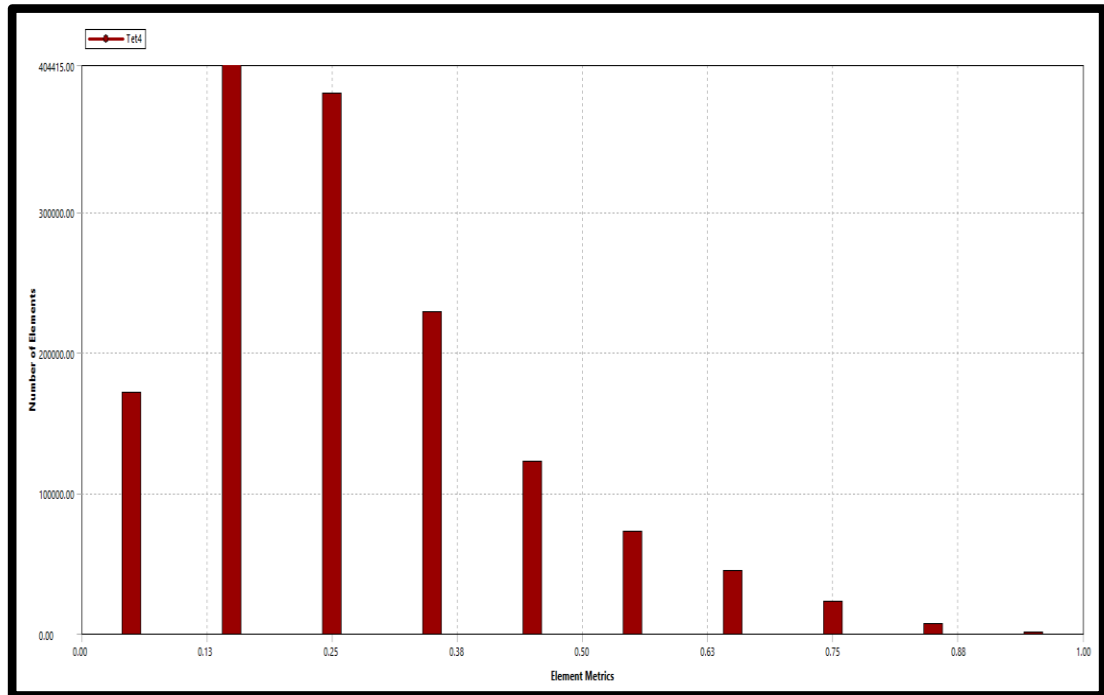


Figure 3.24. Skewness.

3.5.1.3. The Numerical Model Setup

The two following steps were applied to the three cases of SS-VAWT.

- The case was imported in *Ansys Fluent* solver.
- In the General option perform a transient simulation on a pressure-based solver was chosen, as shown in Figure 3.25.

Solver Technologies

“*Ansys Fluent*” consist of two main solver technologies which are:

- Pressure-based
- Density-based

Most solvers could handle a wide spectrum of flows, however, one formulation might perform much better for example “provide solutions faster or resolves specific

flow characteristics faster over the other in particular circumstances”. The momentum, continuity, and “where necessary energy”, as well as species computations, are calculated differently in the species as well as energy techniques, as stated in the review of flow solvers in the theoretical Guide.

Regarding incompressible and weakly compressible flows, the solver based on pressure has generally been utilized. The method relay on density, on the other hand, was created with high-speed compressed flows in mind. Either technique is currently suitable for a wide spectrum of flows (through compressed to extremely compress), although the based-on density formulation's beginnings may offer it an edge over through the based-on pressure solver in terms of precision (or shock resolution) for compressible flows of high-speed.

The solver based on density has two formulations: explicit as well as implicit. The equations involving extra scalars, such as radiation quantities or turbulence, are solved progressively using density-based implicit and explicit formulations. The linearization of the paired equations differs between the implicit as well as explicit formulations based on density. In Theory, Manual, see Introduction of Flow Solvers for further information on the solver formulations.

The implicit formulation, instead of the explicit formulation, could yield a converged steady-state solution significantly quicker according to the implicit formulation's greater stability properties. The formulation known as implicit, on the other hand, necessitates more storage than the formulation of explicit.

In ANSYS Fluent, a solver based on pressure has two techniques: a couple as well as a segregated algorithm. The regulating equations are then solved consecutively, separated from each other, throughout the segregated method, whereas the momentum equations, as well as the continuity equation based on pressure, are solved together in the coupled way throughout the coupled algorithm. The connected algorithm outperforms the segregated method in terms of speedy convergence; nevertheless, the coupled approach requires more space/memory than that of the segregated algorithm.

The following considerations must be taken while choosing an algorithm and solver:

- The availability of a model for a certain solver
- The effectiveness of the solver under the given flow circumstances
- The mesh size in question, as well as the amount of storage on the system

These considerations may play a role in selecting whether to utilize an implicit or explicit approach when using a solver which is based on density, or a segregated or linked algorithm when using a solver which is based on pressure.

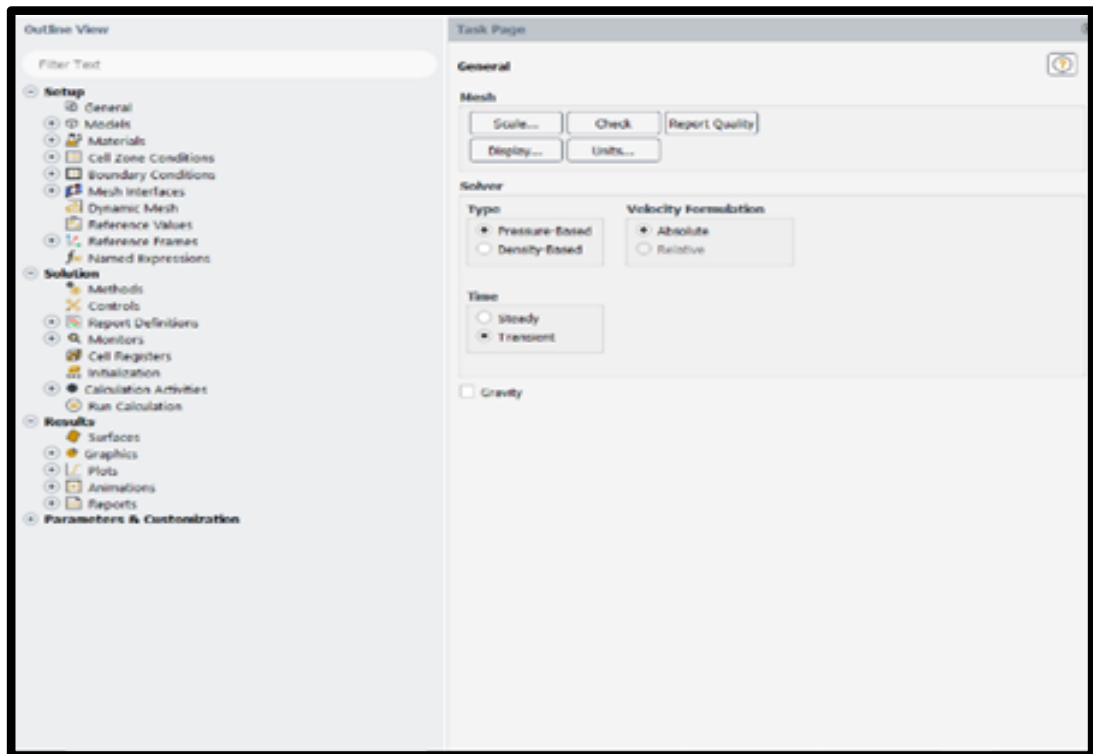


Figure 3.25. The step of choosing the type of solver.

Turbulence Model

At reasonably excessive Reynolds values, turbulence is indeed the 3-dimensional unstable random movement encountered in fluids. Mostly all technological flows are typically turbulent since they are often based on lower fluids of viscosity. Turbulence affects a wide range of technical variables, including:

- There is a mixture of species, energy as well as momentum.
- Transfer of heat
- Efficiency and pressure losses
- Forces acting on aerodynamic objects

Whereas the Navier-Stokes equations in concept characterize turbulence, this is not attainable to settle the broad variety of settings in spacetime using Direct Numerical Simulation (DNS) throughout most circumstances because the CPU prerequisites really would surpass the obtainable power of computing for the near future. As a result, to filter out all, and at minimum sections of the turbulent spectrum, aggregating processes must be employed to the Navier-Stokes equations. Reynolds-averaging (which would be, for any and all practical reasons, averaging of time) of the equations produces the Reynolds Averaged Navier-Stokes (RANS) equations, which are the most extensively used averaging approach. This method removes all turbulent characteristics from the flow, resulting in a smooth fluctuation of the median pressure and velocity domains. Furthermore, the averaged procedure brings new undetermined components (Reynolds Fluxes and Stresses) through into the equations of transport, which must be represented by appropriate turbulence closures and models. The simulation effectiveness can be heavily influenced by the turbulence model chosen, thus it's critical to establish the right selection and also supply an appropriate numerical grid again for the chosen model. Scale-Resolving Simulation (SRS) models are an alternative to RANS. At a minimum, a piece of the turbulent spectrum is rectified at a minimum of a flow domain part using SRS approaches. Large Eddy Simulation (LES) is the best methodology, but several novel hybrids (models that combine RANS and LES) are emerging. Because all SRS approaches involve simulations that are time-settled with minimal time stages, it's crucial to realize that they're far more computationally costly than RANS simulations.

Unfortunately, a turbulence model with no signal is generally recognized as also being preferable for all types of issues. The flow physics, recognized practice for a certain type of issue, the precision level demanded, attainable processing capabilities, as well as the time available again for simulation would all influence the

turbulence model chosen. You must grasp the strengths and constraints of the different alternatives in order to select the best model decision for your application.

Reynolds Averaged Navier-Stokes (RANS) Turbulence Models

For analyzing complicated turbulent industrial flows, RANS models (Reynolds (Ensemble) Averaging in the Theory Guide) are the most cost-effective option. The k - ϵ or the k - ω models in their various variants are typical instances of these kinds of models. To estimate the Reynolds Stresses, those models reduce the issue to the solutions of two extra equations of transport and incorporate an Eddy-Viscosity (turbulent viscosity). RANS models with more complexity (Reynolds Stress Models – RSM) and a scale equation (ϵ -equation or ω -equation) exist, which solve an individualized equation in each of the six separate Reynolds Stress directly. RANS models are appropriate for a wide range of engineering applications and often give the desired rate of precision. Because neither of the models is generic, you must choose the one that is best suited to your needs.

k - ω Models

In comparison to the ϵ -equation, the ω -equation has numerous benefits. The most notable advantage would be that the ω -equation could be incorporated into the viscous sublayer without even any additional conditions. As a result, creating a robust +-insensitive Enhanced Wall Treatment (EWT) is fairly simple. For further information, see the Theory Guide's Enhanced Wall Treatment ω -Equation (EWT- ω). In addition, k - ω models are superior at anticipating adverse pressure gradient boundary layers separation and flows.

The disadvantage of the usual ω -equation is that the solution is quite sensitive to the freestream values of k - and ω - outside the layer of shear. As a result, using the conventional k - ω model in ANSYS Fluency is not normally suggested. By merging features of the ω -equation and the ϵ -equation, the SST k - ω model has been constructed to overcome the freestream sensitivities of the conventional k - ω model. The SST model has also been tuned to calculate flow separation from flat surfaces

properly. It is accordingly advised to employ the SST model within the $k-\omega$ model category as shown in Figure 3.26. Among the most extensively employed models describing aerodynamic flows is the SST model. It is usually a little more precise than the Spalart-Allmaras model at forecasting the features of the layer of wall boundary characteristics. The improved wall solution is used by the standard in the SST model (as it is in all ω -equation-based models). Wilcox suggested the so-called low Reynolds number terms (low Re) for the $k-\omega$ models. These would be provided as a choice in ANSYS Fluent. It's worth noting that even these factors aren't necessary for integrated equations via the viscous sublayer. Their primary influence stems from their ability to simulate laminar-turbulent transition mechanisms.

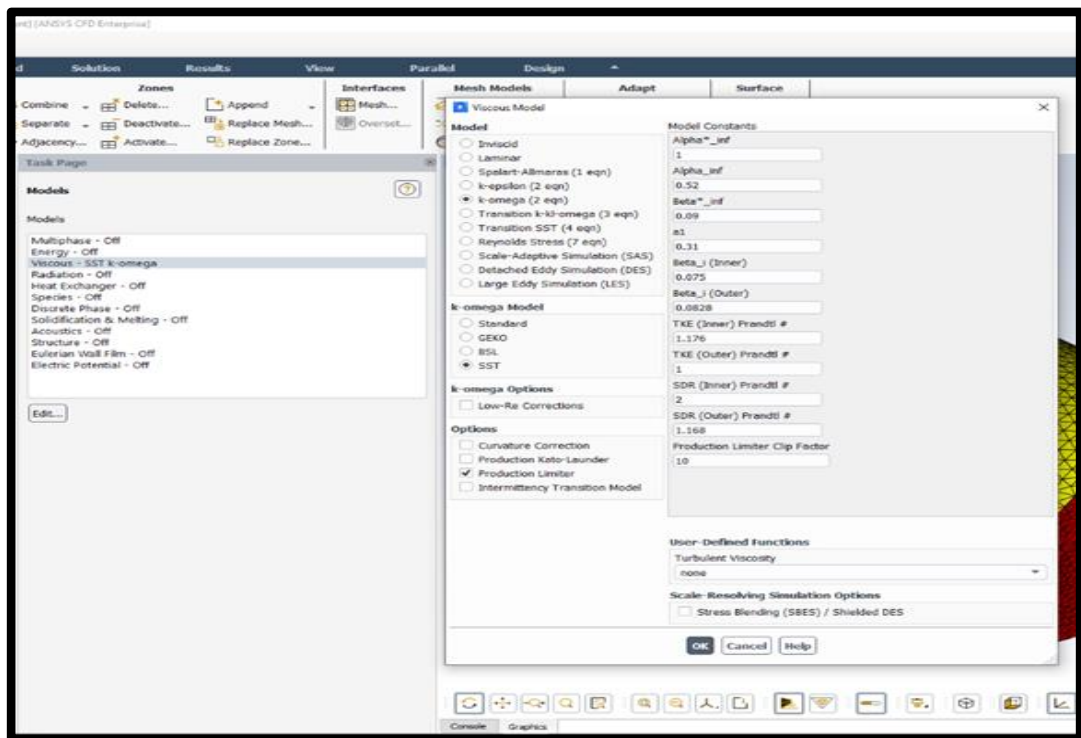


Figure 3.26. Step of choosing the type of physical model.

However, because this functionality isn't widely precise and accurate, combining the SST model with both the Transition SST model (Transition SST Model within Theory Guide), the Transition -model ($k-k_l-\omega$ Transition Model in the Theory Guide) or Intermittency Transition model (Intermittency Transition Model in the Theory Guide) is more accurate for wall-boundary layer transformation. As a result, the usage of low-Re keywords is discouraged.

Setting the Materials.

Specifying the materials as well as their mechanical characteristics, in which you can input values for the attributes that are pertinent to the issue context you defined within Models Activity, is indeed an essential phase in the model configuration. The following are examples of such properties:

- Heat capacity
- Viscosity
- Standard state enthalpies
- Thermal conductivity
- Kinetic theory parameters
- Mass diffusion coefficients
- Molecular weights or density
- UDS diffusion coefficients

Individual component parameters might well be described by you or computed using kinetic theory, including polynomial-based temperature dependency, piecewise-linear, as well as piecewise-polynomial function, and composition dependence depending on a polynomial, piecewise-linear, as well as piecewise-polynomial function.

Setting the Cell Zones Conditions According to the Sliding Mesh Method

The sliding mesh model lets you create an issue in which different zones shift around concerning one another. Translational and rotational motions are both possible. Transient contacts are caused by the relative stationary motion and moving parts (for example, in a spinning machine). A time-periodic transitory solution is frequently explored in a sliding mesh simulation. The transient solutions, in other words, repeat at a period proportional to the velocity of the moving sectors.

Two or even more cell zones are being used in the sliding mesh approach. (If you produce the mesh for each zone separately, you must integrate the mesh files before

beginning the computation, as stated in the User's Guide's Reading Multiple Mesh/Case/Data Files). Each zone of the cell is separated from the adjacent cell region from at least one "interface region." A "mesh interface" is formed when the interface regions of neighboring cell regions are linked together. Along with the mesh connection, the two cell regions will shift marginally to one another.

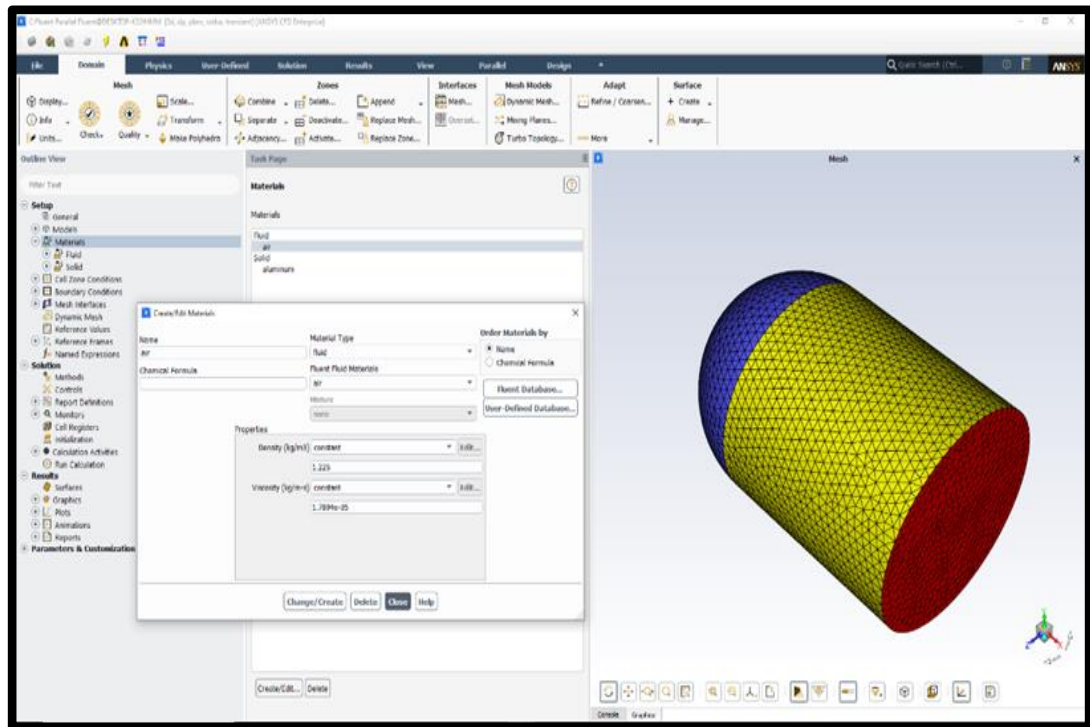


Figure 3.27. Step of choosing materials and properties.

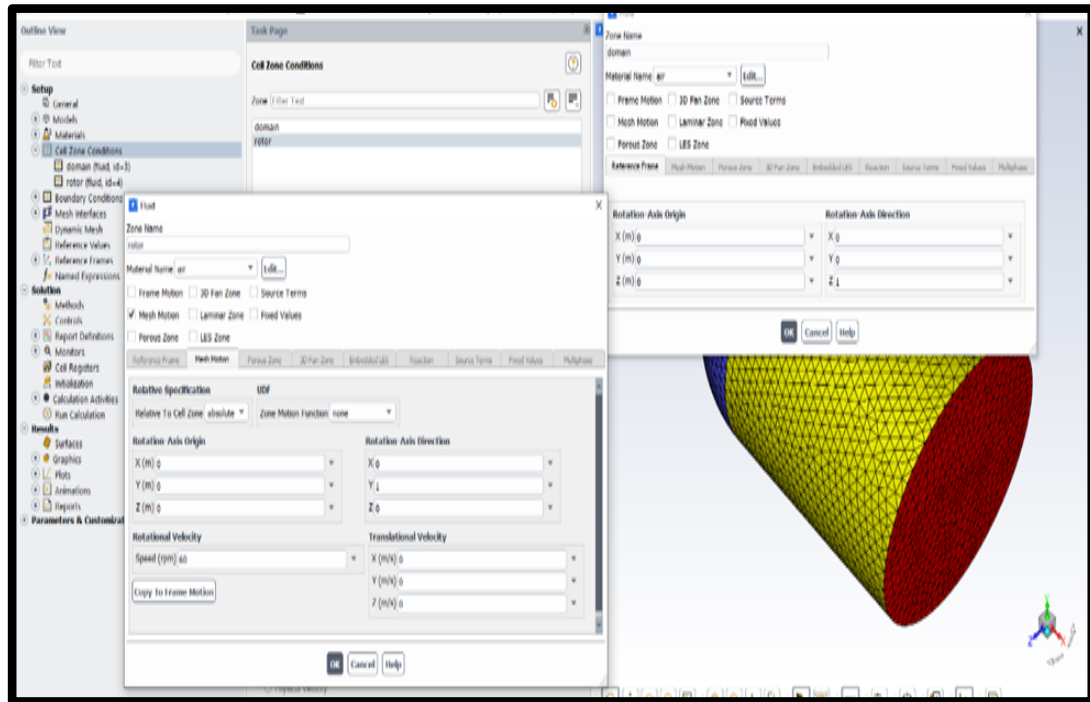


Figure 3.28. The cell zones slide.

The cell regions slide "translate as well as rotate" relative to each other along with the mesh contact in discrete stages during the computation and display the original positions of two meshes as well as their orientations after translating. When the mesh is changed, If needed, ANSYS Fluent would update automatically all non-conformal connections. Node synchronization along the mesh interface is not necessary as the translation or rotations occurs. A flow domain and a rotational domain were chosen for the two geometry components. In above, Figure 3.28 display cell zone steps.

Requirements and Constraints

Make sure the mesh you've built fits the following conditions before starting the scenario configuration in ANSYS Fluent:

- Each piece of the domain that's also sliding at such a variable pace requires a distinct cell region in the mesh.
- The mesh interface should be placed in such a way that there is no ordinary motion.

- The mesh interface could be any shape (even a non-planar area in three dimensions), as long as the two interface edges have the same layout. If the mesh has sharp angles (such as 90° angles), it is critical that both ends of the interface precisely follow that characteristic.
- If you make a single mesh with several cell regions, make ensuring that each cell region on the sliding boundaries has its face region. The placement and shape of the face regions for two nearby cell regions would be identical, but one will correlate to one cell region and one to the other. (Note that each of the cell regions can be created as a distinct mesh file, which can later be merged.)
- If you're utilizing periodicity to simulate stator/rotor geometry, the mesh across the rotor blades should have the same periodical angle as the mesh across the stationary vane (s).
- Whenever you build the mesh interface, make sure all periodical regions are properly oriented (translational or rotational).
- If you intend to utilize the periodic repetitions choice in the mesh interface, keep in mind the following constraints:
 - ❖ The borders of the second interface region must always be offset by such a consistent amount, whether it's a constant translational movement or a uniform rotation angle, from the respective edges of the very first interface region.
 - ❖ The two interface regions must coincide, or even be spatially contemporaneous, in some way.
 - ❖ Throughout mesh motion, the non-overlapping sections of the interface regions should have the same shape and size at all moments.
 - ❖ Each one of the interface regions must have a pair of conformal periodical regions adjacent to it. For example, when calculating just one blade and channel of a fan, turbine, or another device, you would have to have conformal periodic on both sides of the interface threads. With non-conformal periodic, this would not work. It's worth noting that in 3D scenarios, each interface region can only have one set of conformal periodical regions adjacent to it.

- ❖ You shouldn't have a solitary sliding mesh interface with a linked two-sided wall on one side and an uncoupled two-sided wall on another (that is, the ordinary interface treatment). In that kind of instance, the interface must always be split into two parts: a linked interface and a regular fluid-fluid interface. In ANSYS Fluent, see Utilizing a Non-Conformal Mesh.

Boundary Conditions

Flowing inlets, as well as exit borders pole barriers, repeating and also walls and internal face boundaries and face boundaries whereas internal are all examples of boundary conditions.

Flow Inlet and Exit Boundary Conditions Applied on the Domain Inlet

Flow inlets and exit borders, wall, recurring, pole barriers, and internally facing barriers are all examples of boundary situations. As shown in Figure 3.29.

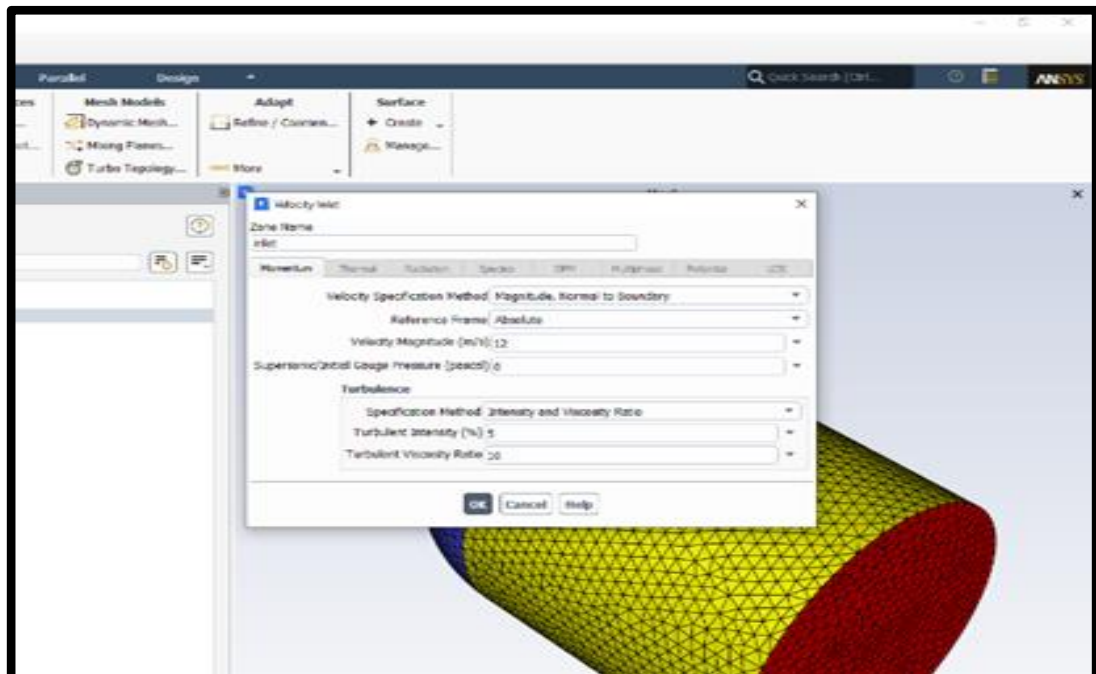


Figure 3.29. Velocity inlet in boundary condition step.

The boundary conditions in ANSYS Fluent allow flow to enter and exit the solution area in a variety of ways. This part gives details of how each type of the condition of boundary is used and what data is provided for each one to aid in the selection of the most suitable boundary condition for applicability. There are also suggestions for evaluating the inlet turbulence values parameters.

Pressure Outlet Boundary Conditions on the Outlet

The definition of a static (gauge) pressure there at the outlet boundaries is required by pressures outlet boundary conditions. Only when the flow is subsonic is the value of the given static pressure employed. The given pressure would no longer be utilized if the flow becomes locally supersonic; instead, the pressure would be extrapolated from the flow within the interior. The interior is used to extrapolate all those other flow parameters. Then would the flow opposite direction there at pressure outlet barrier throughout the solution operation, a set of "backflow" constraints is also given. Convergence problems will be reduced if the backflow amounts are given realistic values. Figure 3.30 display pressure outlet step.

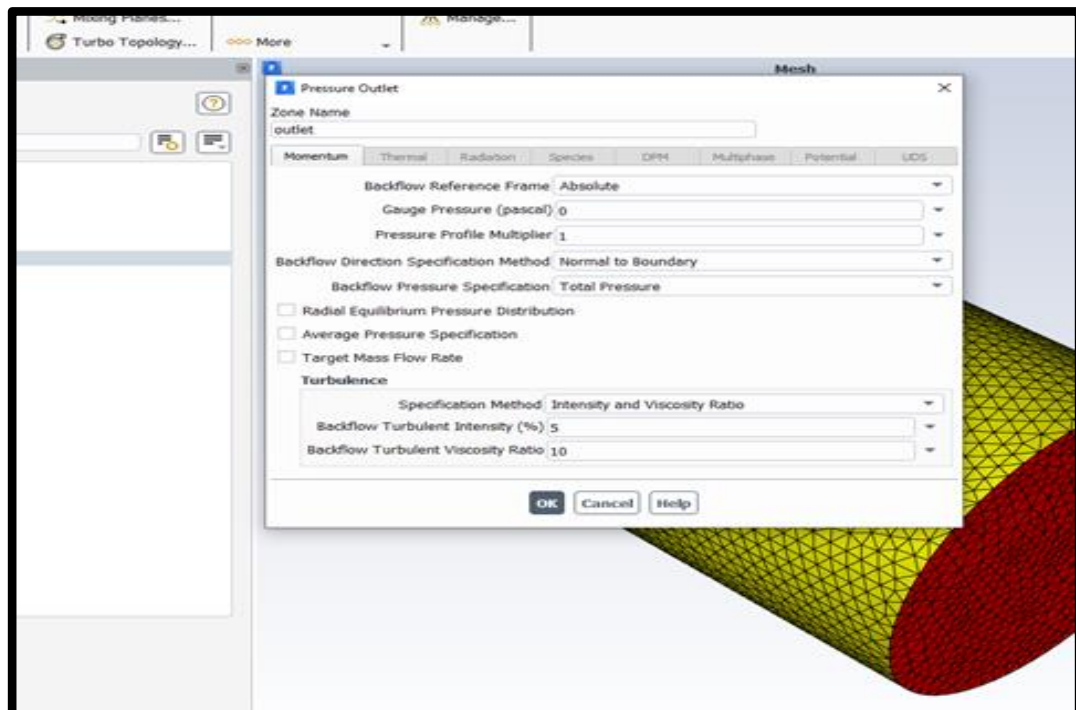


Figure 3.30. Pressure output in boundary condition step.

Symmetry Boundary Conditions on the Side Walls

Whenever the physical geometry of interest and the predicted sequence of the thermal/flow solution are mirror-symmetric, symmetry boundary conditions are being used. In viscous flows, they could also be utilized to model zero-shear slip walls. This part explains how to treat flow at symmetrical planes and gives examples of how to employ symmetry. At symmetrical boundaries, there are no boundary requirements to describe, but you should be careful to identify your symmetry boundary positions accurately. The turbine walls were given a moving wall (rotating around). Figure 3.31 illustrate boundary condition step.

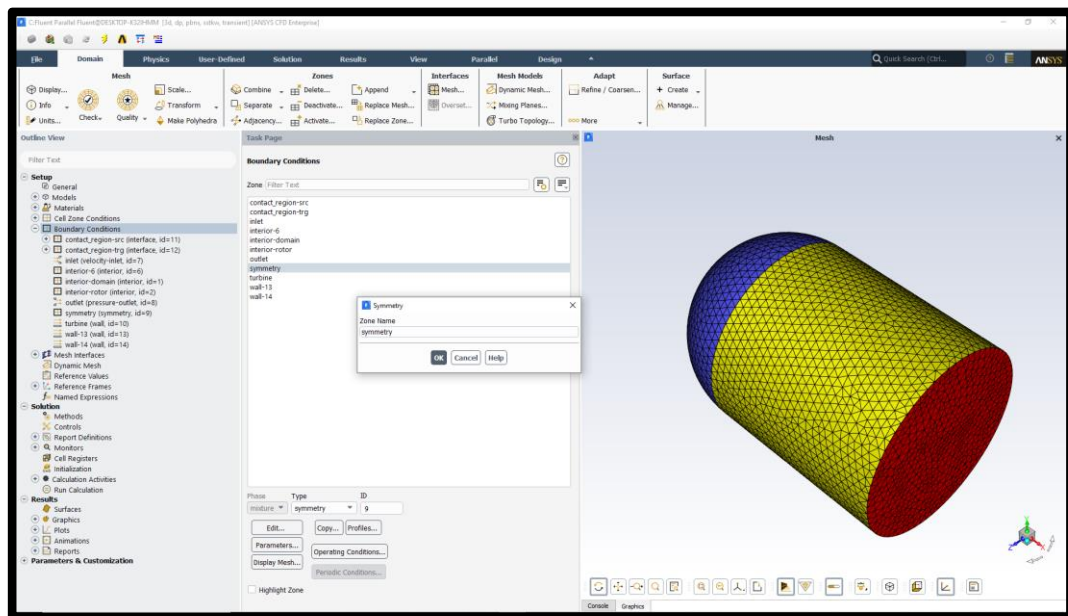


Figure 3.31. Symmetry boundary conditions.

Solution Methods

Pressure-Velocity Coupling Method

SIMPLEC, SIMPLE as well PISO, and Fractional Step (for flows that are timely dependent utilizing the Non-Iterative Time Advancement option (NITA) are the four kinds of algorithms available in *ANSYS Fluent* (FSM). The pressure-based segregated algorithm is the name given to these techniques. SIMPLE or SIMPLEC are suggested for steady-state computations, while PISO is suggested for transient

calculations. On heavily skewed meshes, PISO may be beneficial for steady-state and transient calculations. The Coupled algorithm in *ANSYS Fluent* allows for full pressure-velocity coupling, hence the name "pressure-based coupled algorithm."

The Coupled Algorithm

When you choose Coupled from the Pressure-Velocity Coupling drop-down list, you're employing the coupled algorithm based on pressure defined in the Theory Guide's Coupled Algorithm. Compared to the *segregated algorithm based on pressure*, this solver has a few advantages. For steady-state flows, *coupled method based on pressure* yields a more resilient and economical single-phase approach. For cases utilizing the Non-Iterative Time Advancement (NITA) choice, it is not enabled. Figure 3.32 show solution method step

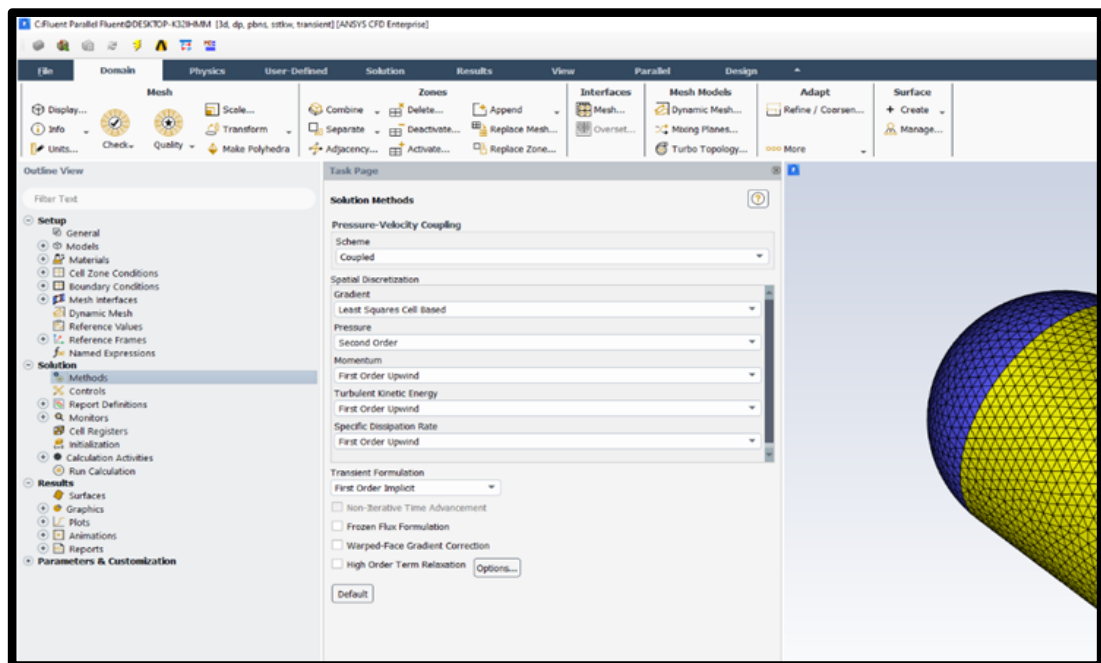


Figure 3.32. Solution method step.

Solution Initialization.

You must give *ANSYS Fluent* a preliminary "guess" for the solution flow field before actually beginning your CFD simulation. Throughout many circumstances, you'll

need to take the necessary precautions to give a preliminary solution that would help to accomplish the preferred final solution. If the backpressure is merely reduced to its operational value, a real-life supersonic wind tunnel would not "start"; the flow would choke somewhere at the tunnel throat and would not transition to supersonic speeds. In a numerical simulation, the flow must always be initialized to a supersonic flow otherwise it will choke as well as stay subsonic. When hybrid was picked, there are two approaches for initializing the solution. Figure 3.33 present solution initialization method.

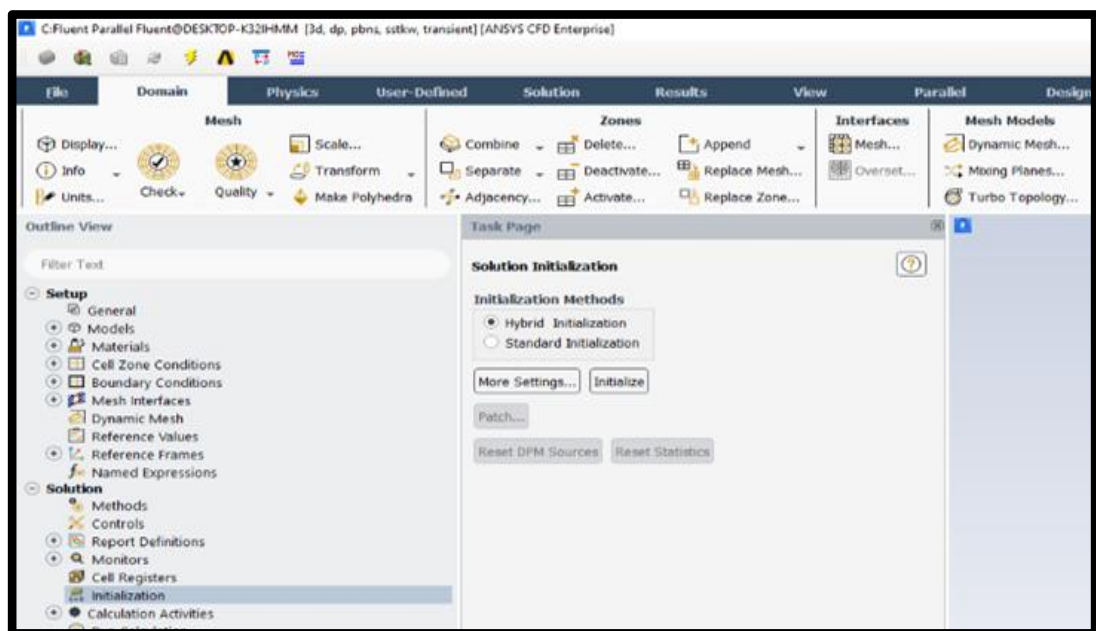


Figure 3.33. Solution initialization step.

Hybrid Initialization

Hybrid initialization seems to be another *ANSYS Fluent* initialization approach. Standard initialization and *FMG initialization* are the two initialization strategies. The term "hybrid initialization" refers to a set of recipes and boundary interpolation techniques. It determines the pressure and velocity fields by solving "*Laplace's Equation*". Turbulence, volume as well species fractions, Temperature, and other parameters would be interpolated automatically depending on domain averaged values or a specific interpolation recipe.

3.5.2. Processing

Solving the case until reaching a stable converged solution at about 2000 iterations. Figure 3.34 show the run step.

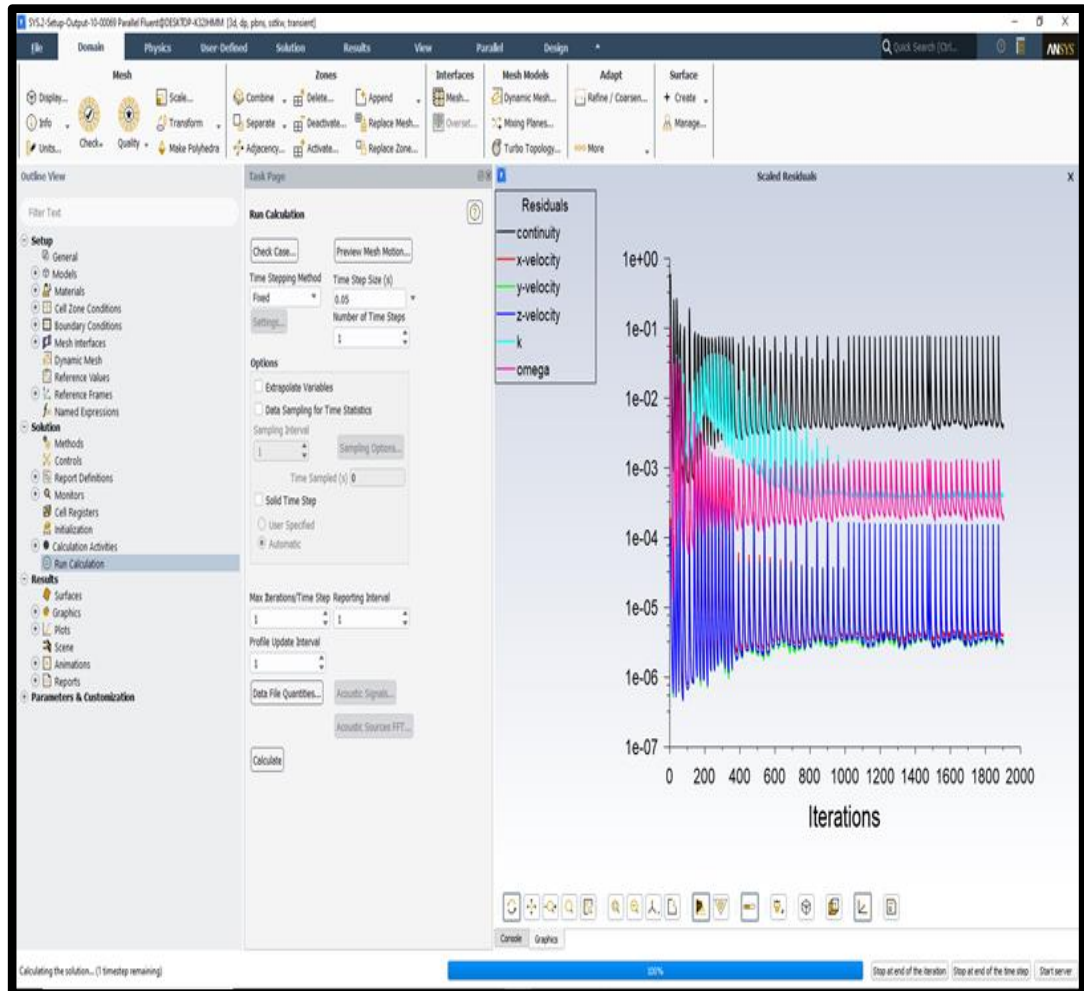


Figure 3.34. Run calculations step.

3.5.3. Post-Processing

The stage of “*post-processing*” in the “ANSYS Fluent” is for showing the results, so it is explained in the fourth part of the thesis.

3.6. DETAILED ENGINEERING DESIGN OF (SS-VAWT)

3.6.1. Using the Wind Energy Equation for (SS-VAWT)

Determining the geometry of the rotor consists in determining the number of blades and the length of each one of them, the height and diameter of the rotor, as well as the geometry of the blade section. In this context, the value of the biased area, "A" or what is known as the "rotor swept area", must first be determined. The value of "A" depends on a number of factors represented in: design power P_r (wind turbine rated power), design wind speed V_r (rated wind speed), design power factor C_{pr} (rated power coefficient), gearbox efficiency ζ_{GB} , generator efficiency ζ_{EG} , air density ρ . These six factors connect the following mathematical relations:

$$P_r = \left(\frac{1}{2} \rho A V_r^3 \right) C_{pr} \eta_{GB} \eta_{EG} \quad (3.36)$$

It is worth noting that the quantity enclosed in parentheses on the right side of equation (3.36) represents what is known as the wind energy available through an area A that is blown by a wind at a speed of V_r . Therefore, C_{pr} represents the efficiency of the rotor in converting this available energy into mechanical energy or "shaft power". The $(\zeta_{GB} \zeta_{EG})$ represents the efficiency of converting this mechanical energy into electrical energy. Therefore, to determine the biased area, the values of the six factors must be known, which are usually specified as follows:

- The value of P_r is determined according to the purpose of using the rotor.
- The value of V_r is determined by the prevailing wind pattern at the site.
- An average value of C_{pr} is chosen according to the level of scientific, technical and production maturity, and this value usually ranges between 0.27 and 0.4.
- It is possible to choose a modest value for the product of the two competencies $(\zeta_{GB} \zeta_{EG})$ in the range of approximately 0.9.
- Standard atmospheric conditions can be used to calculate the density of air as $\rho \approx 1.225$ (kg/m³), for example.

- When the biased area "A" is determined, the role of determining the geometric shape of the rotor comes in some detail.

3.6.2. Determine the Value of the Rotor Area (A)

In order to determine the value of (A) the following data in Table 3.2 was used:

Table 3.2. Initial design input

Rated power	P_r	= 400 (W)
Rated speed	V_r	= 10 (m/s)
Rated power coefficient	C_{p_r}	= 0.3
density of air	ρ	= 1.2 (kg/m ³)
generator efficiency	ζ_{EB}	= 0.92
gearbox efficiency	ζ_{GB}	None

By substituting in equation (3.36) for the variables shown above, it is found that the biased area is $2.42m^2$.

The areas of five cases of SS-VAWT are shown in table 3.3, which were determined by used following equation:

Table 3.3. Value of aera for each case.

CASE 1 35°35°	1.04m ²
CASE 2 55°55°	1.34m ²
CASE 3 85°85°	1.36m ²
CASE 4 105°55°	1.02m ²
CASE 5 55°105°	1.02m ²

$$A' = \left[\frac{2R + b}{2} \right] * H \quad (3.37)$$

Whereas, the (A') is the area of only upper part or lower part of the rotor and (b) is maximum diameter. Then, after using it for the upper part, it can be combined in two if the both parts of the rotor are symmetric, however, if the rotor unsymmetric it must use the equation (3.37) for the lower part and add the value of the area with the result of calculating the upper part to get the total area (A) of the wind rotor.

Where $(35^{\circ}35^{\circ})$ means that the blades of the upper part of the rotor tilt at an angle of 35° and the blades of the lower part of the rotor tilt at an angle of 35° . In the same manner, the cases symbols 2, 3, 4 and 5 express the angles of inclination of the blades in the upper and lower parts of the rotor. The engineering drawing in Figure 3.36 details the five cases.

The value of V_r is usually determined according to a specific study of the wind pattern in the region, but it can be calculated that V_r is approximately 1.5 of the value of the annual average wind speed in that region. Since the annual average wind speed in “Bala” town does not exceed 3 m/s [136], Where this value extracted from the Figure 3.37, which express the average wind speeds from *November 2020* to *November 2021*, i.e., during a whole year. Therefore, based on the foregoing, the value of rated speed (V_r) was chosen to be about 5 m/s.

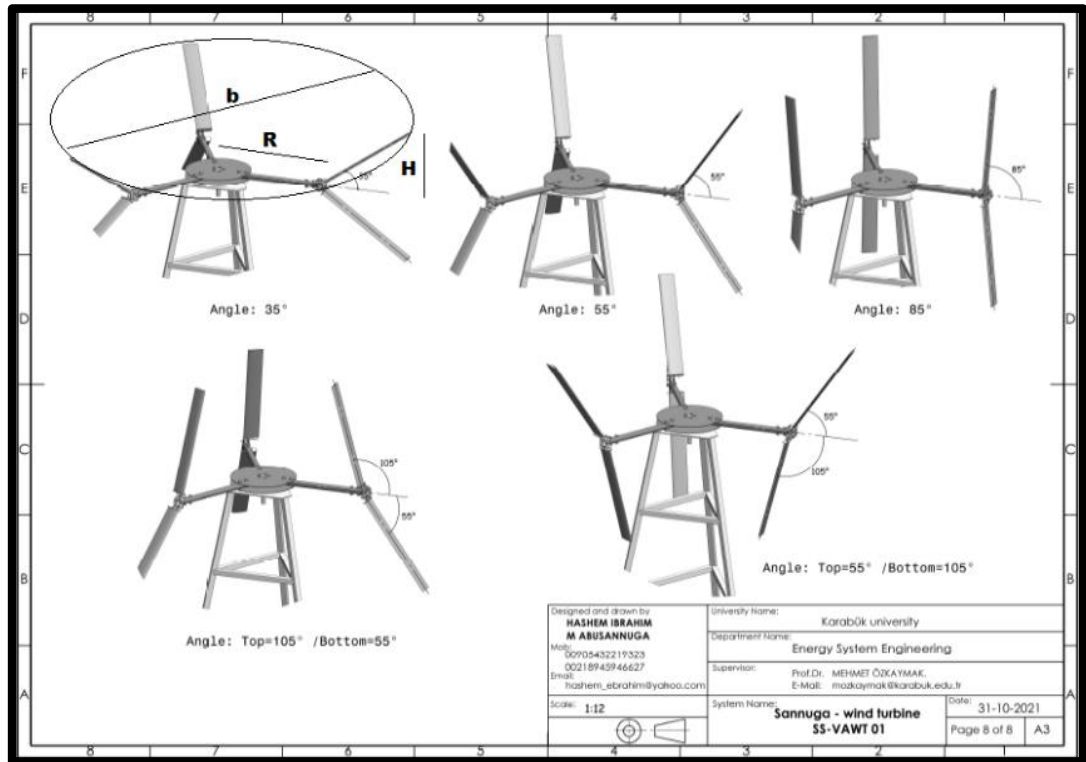


Figure 3.35. Five different geometrical shape of SS-VAWT.

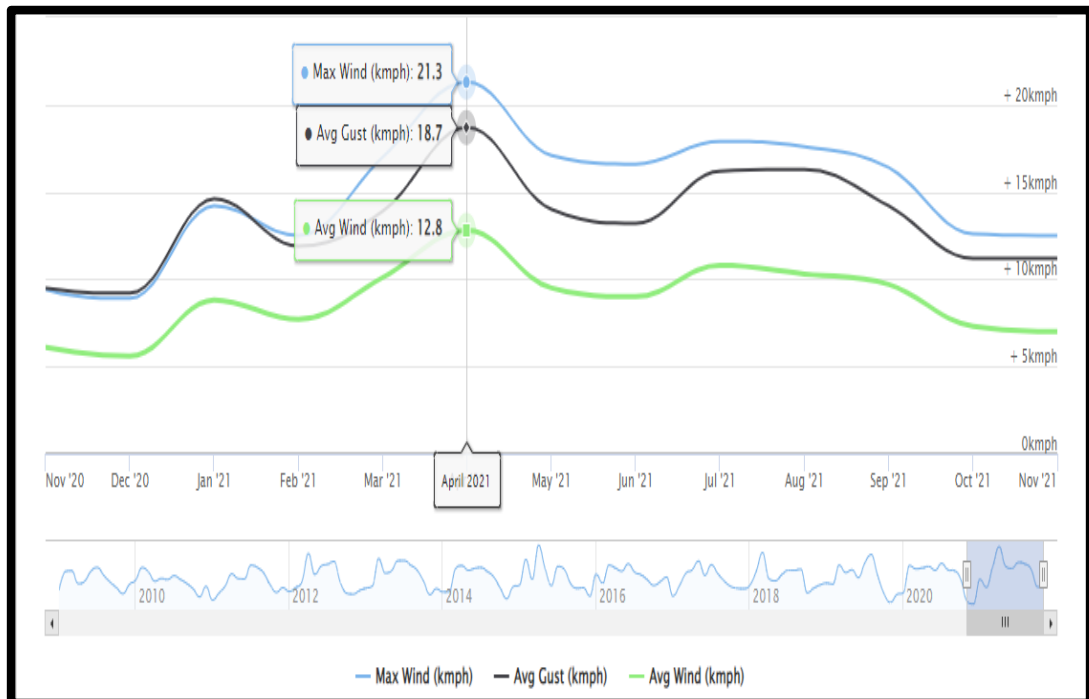


Figure 3.36. Average wind speeds for a year in the "Bala" region.

“Bala” is a town and district of “Ankara” province in the Central “Anatolia” region of “Turkey”, 67 km south-east of the city of Ankara, Figure 3.38 indicate its location on the map. It was chosen because it is an open area, free of obstacles, and close to the place of manufacture of the system.

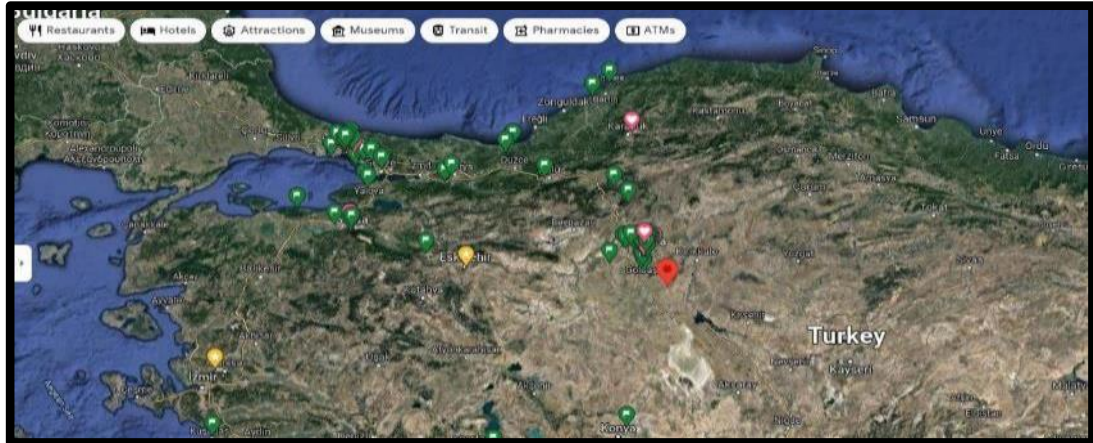


Figure 3.37. “bala” Location on the Map.

3.6.3. Choosing the Type of Airfoil

The Airfoil "NACA 0015" was chosen due to its ease of fabrication and the availability of aerodynamic data over the range $360 \geq \alpha \geq 0$ at different Reynolds numbers (Re). Figure 3.39 shows the section of blade section (Airfoil) with its dimensions.

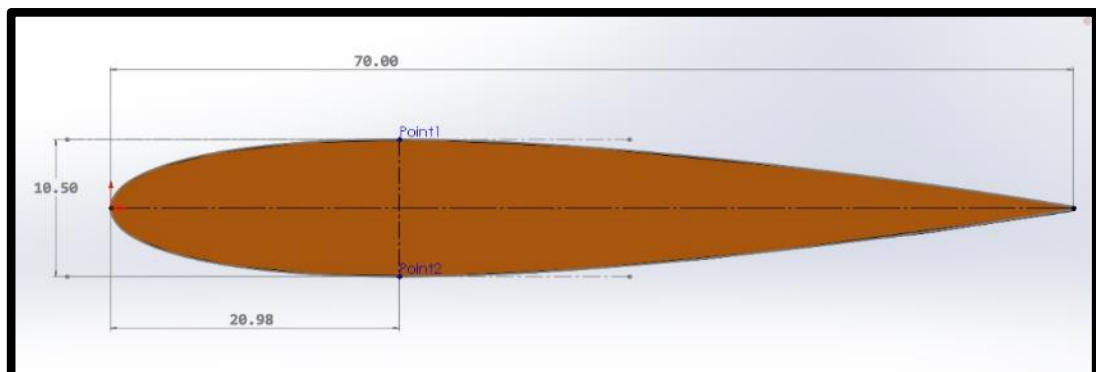


Figure 3.38. Airfoil "NACA 0015" with Dimensions.

3.6.4. Geometric Dimensions Values of the SS-VAWT

Concerning the geometric dimensions of the rotor, Table 3.4 lists them in detail.

Table 3.4. Value of aera for each case.

	2H (m)	2R (m)	N	C (m)
CASE 1 35°35°	0.62	1.22	3	0.07
CASE 2 55°55°	0.88	1.22	3	0.07
CASE 3 85°85°	1.07	1.22	3	0.07
CASE 4 105°55°	0.97	1.22	3	0.07
CASE 5 55°105°	0.97	1.22	3	0.07

3.7. SANNUGA SYSTEM SS-VAWT 01

The previous stages of this thesis included an analysis using a “*Microsoft Visual Software*” specially designed for this thesis project, in addition a physical modelling using the “*Fluent Ansys*” program. Accordingly, it was conceived to manufacture the wind rotor to be a prototype. As a first step, “*SolidWork*” was used to conduct a detailed design of the system with all its parts in preparation for the manufacturing process. Figure 3.40 and 3.41 show generally samples of designed by “*SolidWorks*” parts, the entire design information is available in Appendix B. Then the trend began to laboratories and workshops inside and outside the university, as needed, for the manufacture of the prototype. Within the framework of this thesis, the name “*Sannuga System SS-VWAT 01*” was given to the prototype. “*Sannuga*” is the title of the researcher who authored this thesis, “*SS*” meaning slant straight blade, “*VAWT*” abbreviation for vertical axis wind turbine and “*01*” meaning first version.

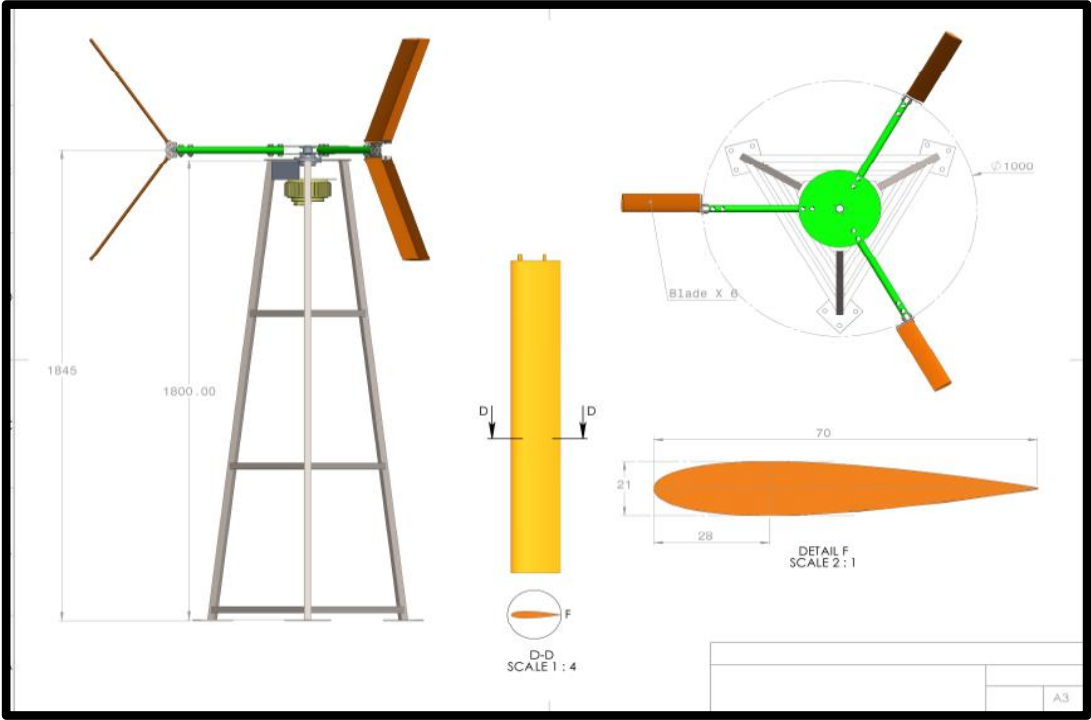


Figure 3.39. General design details of the system.

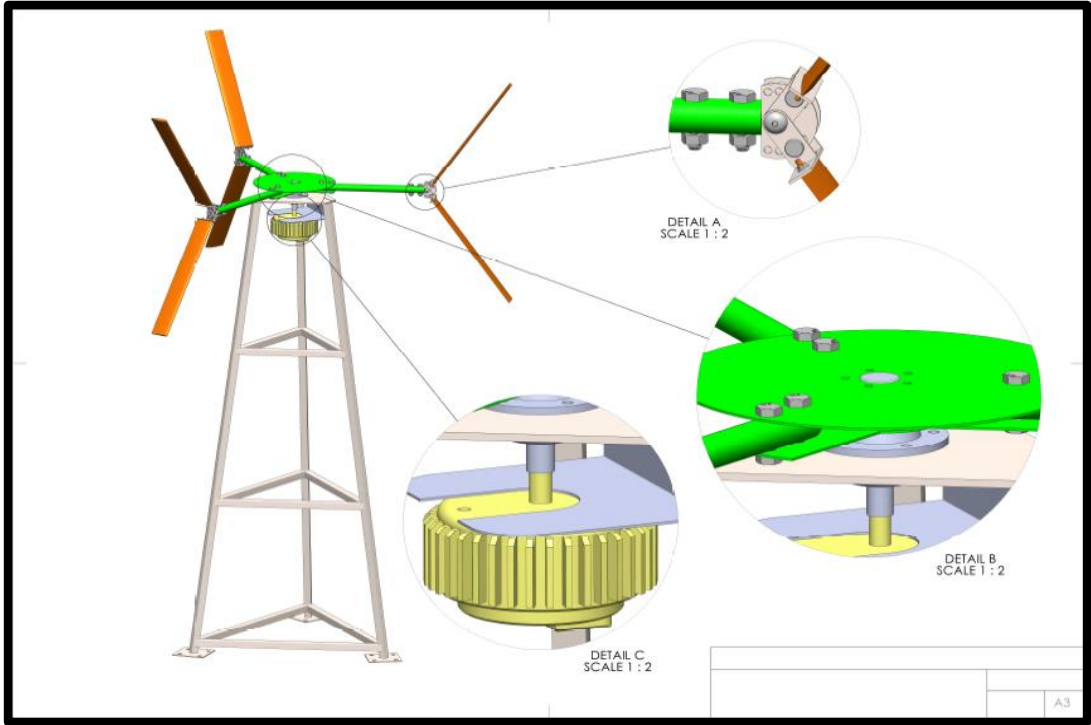


Figure 3.40. Some Important parts of the system.

3.7.1. Solidworks Software Design

The “*SolidWorks*” CAD software is a mechanical design automation application that lets designers quickly sketch out ideas, experiment with features and dimensions, and produce models and detailed drawings. This document discusses concepts and terminology used throughout the “*SolidWorks*” application. It familiarizes you with the commonly used functions of “*SolidWorks*” [137]. A complete design of the SS-VAWT system was carried out by SolidWorks software so that the result was a detailed integrated design ready for the manufacturing process. All design information is provided in Appendix B.

3.7.2. System Manufacturing Process

It took about four months to make the prototype. In the manufacturing process, the outputs of the previous stages of design were applied, such as performance analysis in Visual Basic, physical modeling in “*Ansys Fluent*” and detailed engineering design in “*Solid Work*”. Within the framework of this thesis, the prototype was named “*Sannuga System SS-VWAT 01*”, where “*Sannuga*” is relative to the surname of the author of this thesis, “*SS*” stands for Slant Street Blade, “*VAWT*” is a vertical axis wind turbine and “*01*” indicates that this is the first version of the design.

This system consists of a pneumatic rotor with six blades, three of which are in the upper part of the rotor and the other three are in the lower part of it. These blades are made of fiberglass, each blade is 50 cm long, has a cross section of 0.07 cm, and its Airfoil type is “*NACA 0015*”. Each upper and lower blades are connected by a joint made of aluminum. The functions of this joint are to connect each two blades to work as one blade, control the angle of inclination of each blade to the horizontal so that it can be adjusted in the range 0° to 120° , in addition to controlling the number of blades where the upper or lower blades can be moved without effort and simply. successively to the above, the joints was connected by hollow aluminum cylindrical shields, 20 mm in diameter and 2 mm in wall thickness. Then the aluminum shields are connected to two iron round discs, 30 mm in diameter and 2 mm thick each. Successively. The metal discs are connected to the shaft, which is made of iron and

designed to connect the wind rotor to the electric generator, two rollers are engaged with it to gain smooth rotation, the shaft length is *12 mm* and during this distance it has three different diameters with values of *55 mm*, *30 mm* and *22 mm*. The shaft passes through two bearing sandwiched between iron covers and thus the shaft, the two caps and the rollers become one unit. As for the tower that carries the wind rotor, it was designed in a lattice form and made of iron with a triangular base and its height is *125 mm*. Figures 3.42 and 3.43 shows the Sannuga System SS-VAWT 01 in several geometrical configurations.

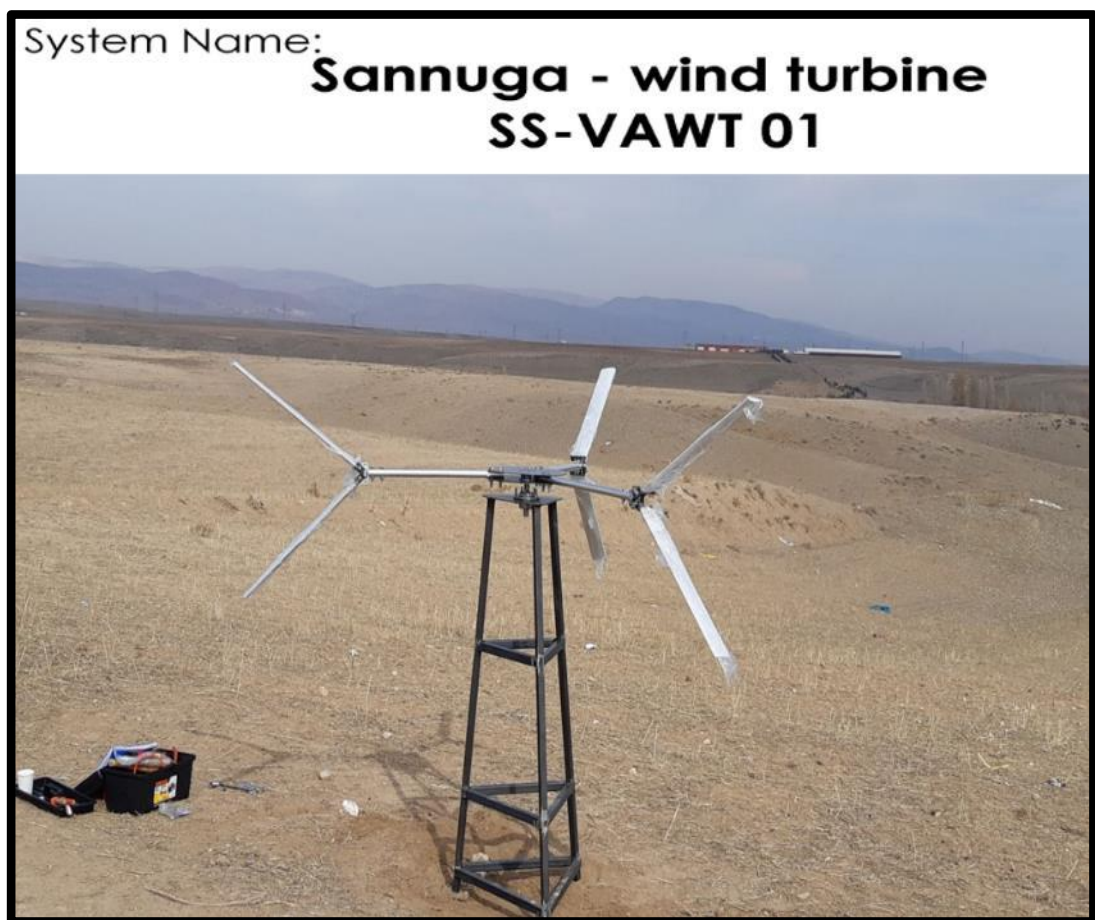


Figure 3.41. Sannuga system SS-VAWT 01.

PART 4

RESULTS AND DISCUSSION

4.1. EFFECT OF GEOMETRIC SHAPE OF SS-VAWT ON ITS PERFORMANCE (Case: 25DEG)

4.1.1. Rotor Hight Effect (H)

Figure 4.1. illustrates the following, an increase in the C_{pmax} value with a decreasing H value, an increase in the energy range under each curve with a decreasing H value, and the initial rotational velocity decreases as the H value decreases.

4.1.2. Rotor Radius Effect (R)

Figure 4.2. shows a decrease in the value of C_{pMax} with an increase in the value of R , the energy range specified by the area under each curve increases with an increase in the value of R and the value of the initial rotational speed decreases with an increase in the value of R .

4.1.3. Number of Blade Effect (N)

Figure 4.3. shows the following, the increase in the value of C_{pMax} with an increase in the value of N , a slight increase in the value of the rotational initial velocity with N increase and an increase in the energetic range confined under each curve with an increase in the value of N .

4.1.4. Airfoil Chord Length Effect (C)

Figure 4.4 shows the behavior of power factor curves C_p as a function of the tip speed ratio λ_o when changing the values of the Chord line C . There is a high similarity between these behaviors and the behaviors in Figure 4.3.

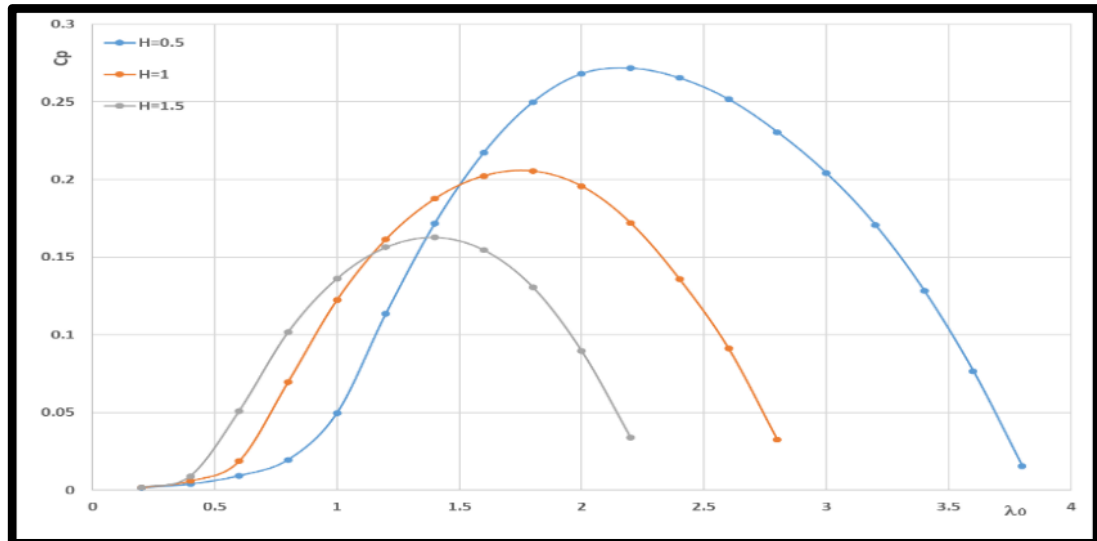


Figure 4.1. Height change effect, case: 25Deg.

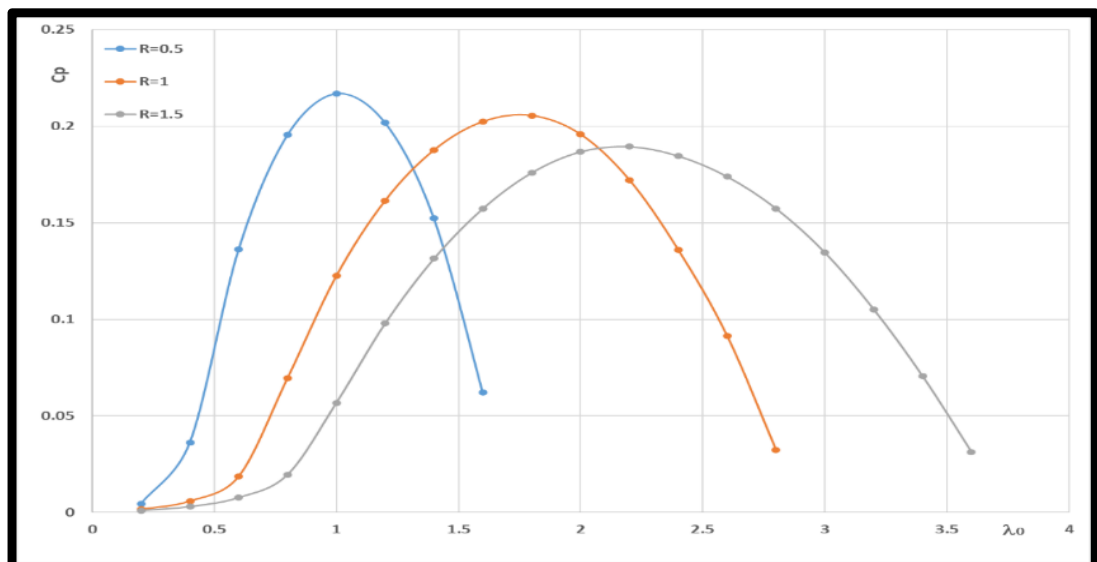


Figure 4.2. Radius change effect, case: 25Deg.

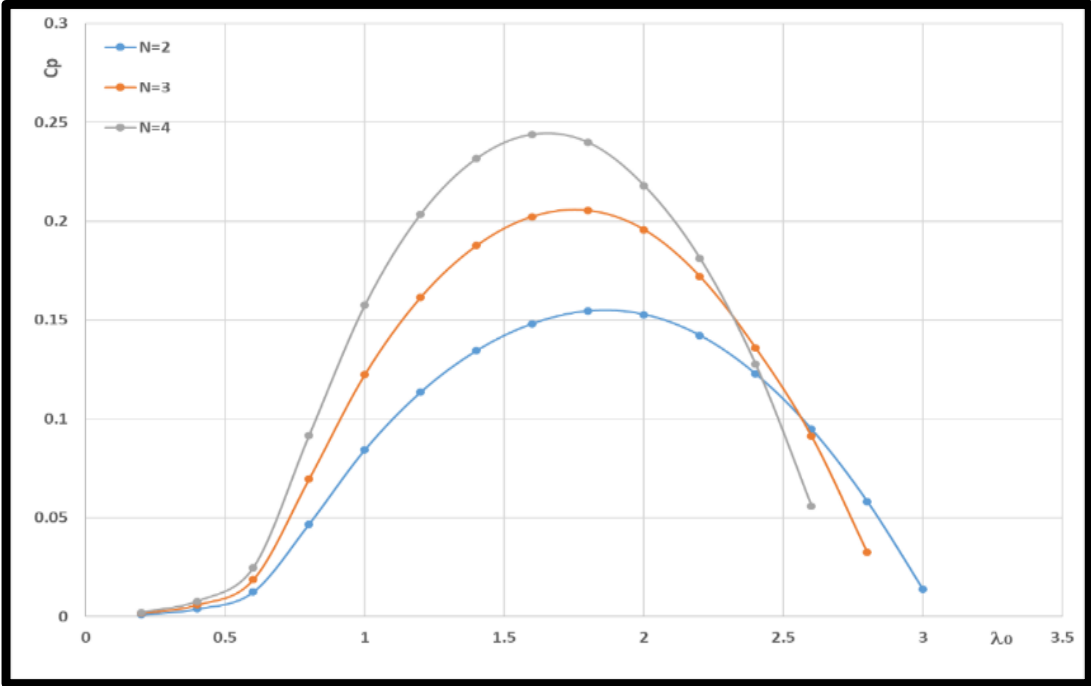


Figure 4.3. Blades number change effect, case: 25Deg.

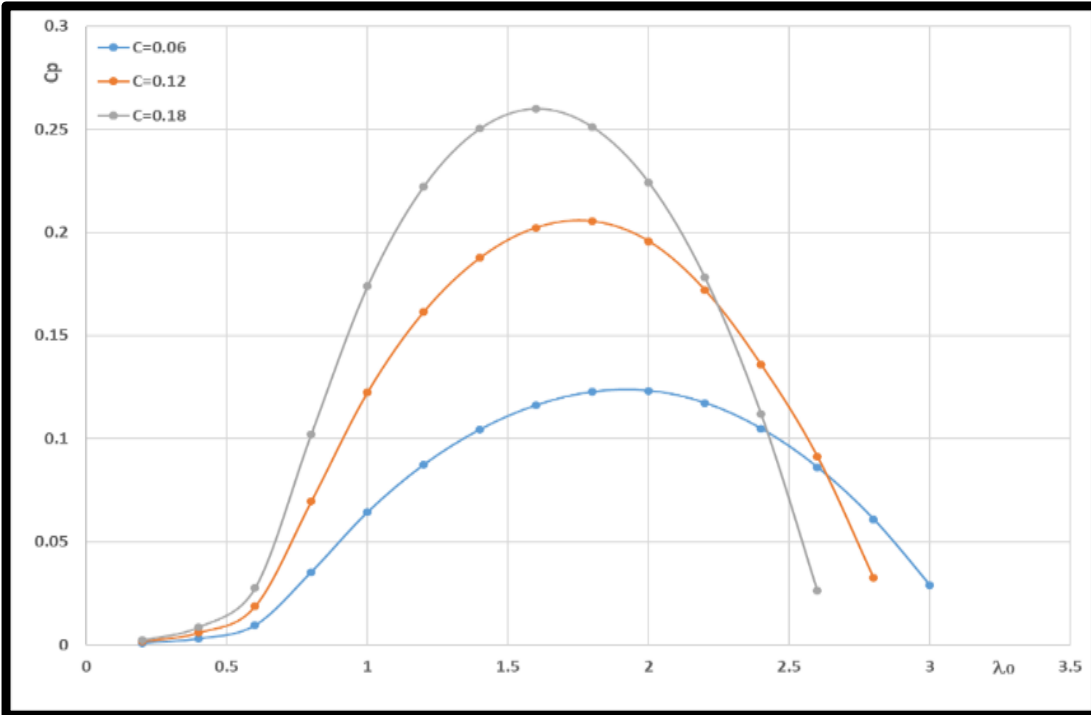


Figure 4.4. Chord length change effect, case: 25Deg.

4.2. EFFECT OF GEOMETRIC SHAPE OF SS-ROTOR ON ITS PERFORMANCE (Case: 45DEG)

4.2.1. Rotor Hight Effect (H)

Figure 4.5. illustrate that as the value of H decreases, the value of $CpMax$ decreases, but with a less decreasing intensity than in the case section 4.1.1. An increase in the value of H leads to an increase in the value of the initial rotational speed. It can also be seen that the energy range confined under each curve decreases with the increase in the value of H .

4.2.2. Rotor Radius Effect (R)

In the two cases, R equals 0.5 and R equals 1 , the $CpMax$ value is almost equal, while in the third case, when R equals 1.5 , the $CpMax$ value is less. Also, the lower the R value, the faster the $CpMax$ occurs on the X-axis (Tip Speed Ratio λ_0). As the value of R reduces, the value of the energy range under each curve reduces.

4.2.3. Number of Blade Effect (N)

Figure 4.7 mentioned that by increasing the value of N from 2 to 3 and then 4, the following appears: the $CpMax$ value increases, it decreases, the $CpMax$ value occurs early, the energy range decreases, and the starting point of energy generation occurs faster at one value for the three cases of λ_0 .

4.2.4. Airfoil Chord Length Effect (C)

Figure 4.8 illustrates a great similarity in the behavior of its variable curves with a change in the value of C with the behavior of the Figure 4.7 curves.

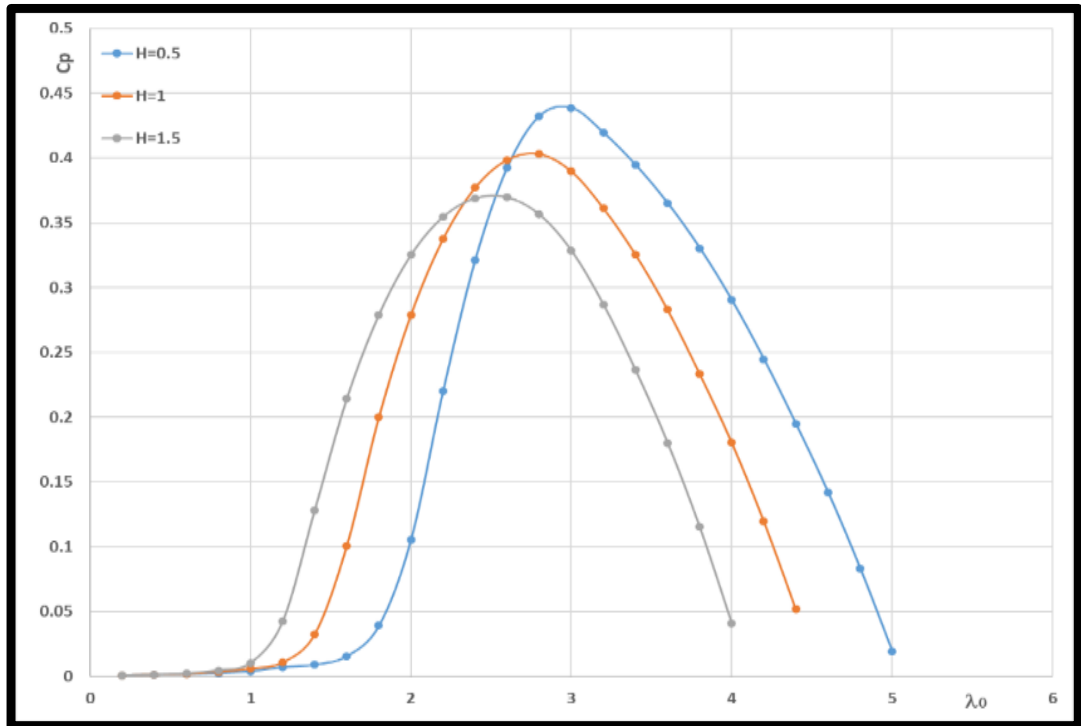


Figure 4.5. Hight change effect, case: 45Deg.

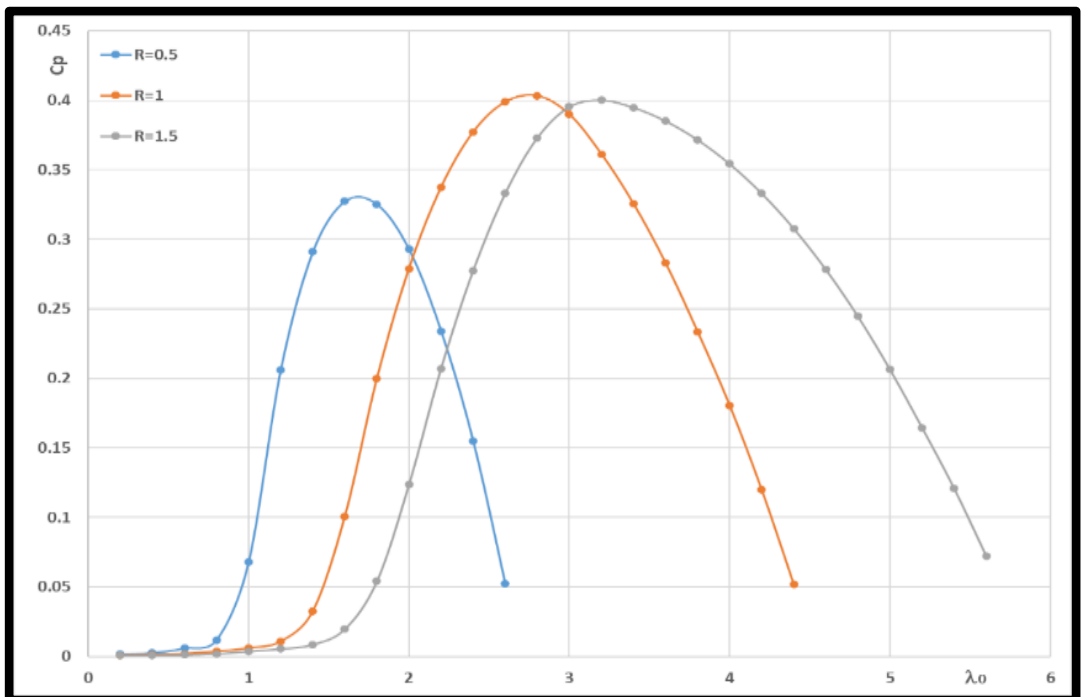


Figure 4.6. Radius change effect, case: 45Deg.

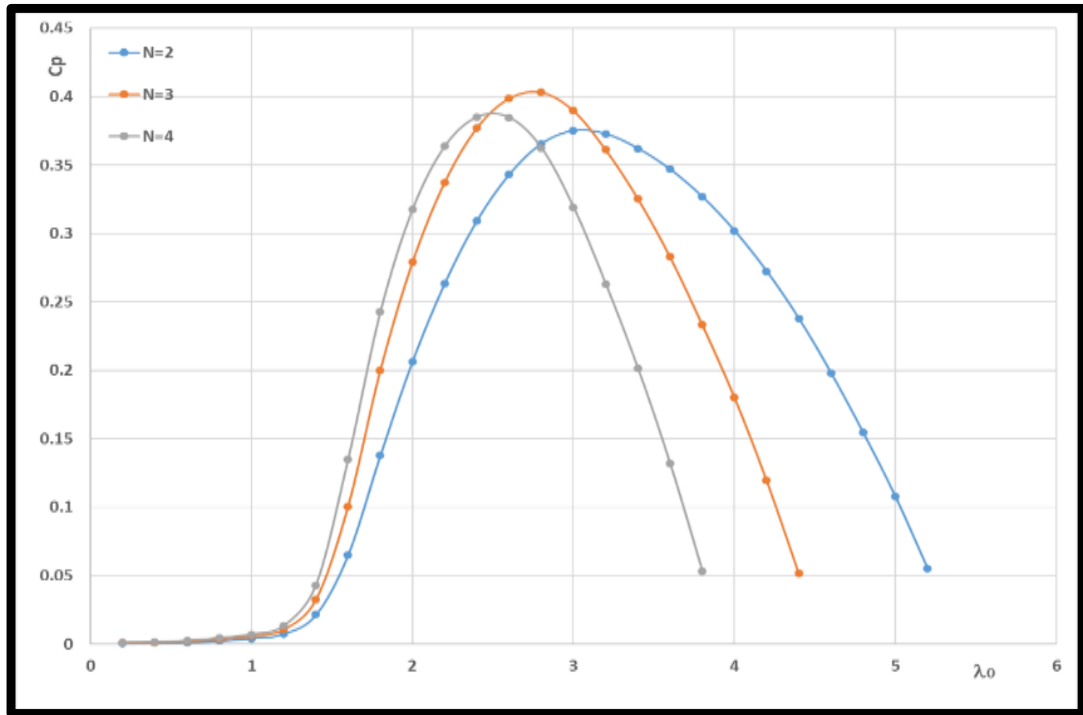


Figure 4.7. Blades number change effect, case: 45Deg.

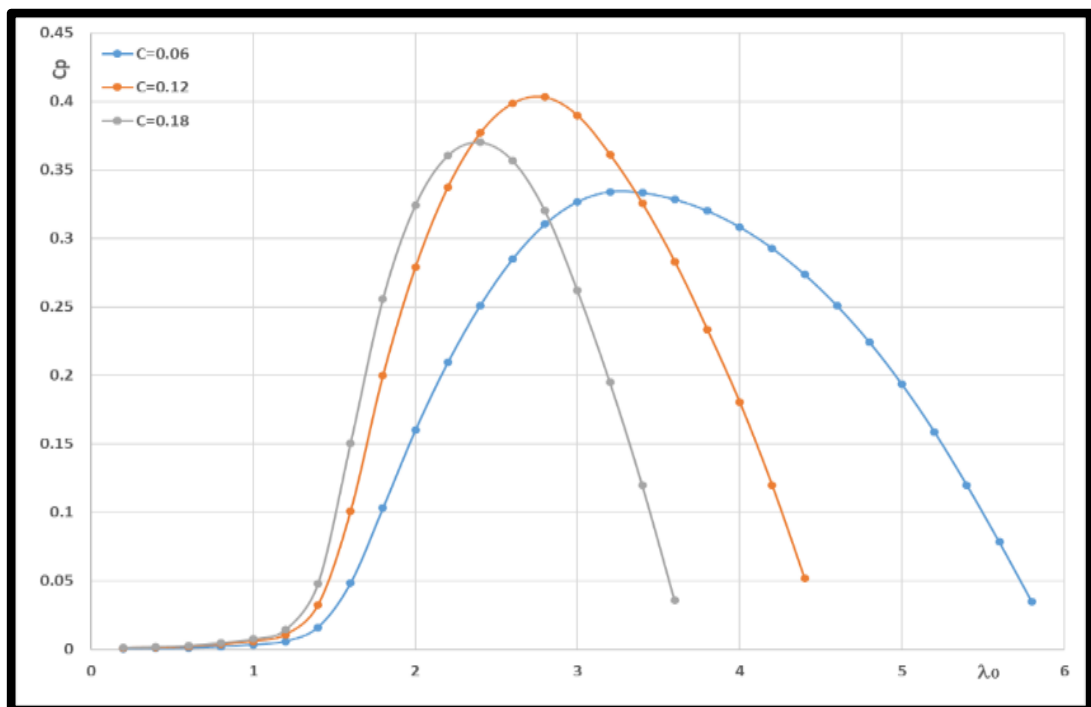


Figure 4.8. Chord length change effect, case: 45Deg.

4.3. EFFECT OF GEOMETRIC SHAPE OF SS-ROTOR ON ITS PERFORMANCE (Case: 65DEG)

4.3.1. Rotor Hight Effect (H)

As the value of H increases, there is a small decrease in the value of $CpMax$, the rotor reaches this value early, the power range decreases slightly and the start of power generation occurs faster. It is worth noting that this figure shows the aggravation of the problem of self-initiation in the state of beta equal to 65 in general, where it can be observed that the zero value of Cp extends to a $\lambda_0=2$.

4.3.2. Rotor Radius Effect (R)

In Figure 4.10, an increase in H value leads to an increase in the $CpMax$ value, an increase in the energy range, a delay in reaching the $CpMax$ value in the λ_0 range and finally an exacerbation of the spontaneous initiation problem. In addition, it can be easily seen that in the case H equal to 0.5 of the poorly-efficient case.

4.3.3. Number of Blade Effect (N)

Figure 4.11 shows that, with an increase in the value of H , a decrease in the $CpMax$ values occurs, a decrease in the energy range occurs, and there is no difference in terms of the start of the self-movement, as indicated by the curves in the range from $\lambda_0 = 0$ to $\lambda_0=2$.

4.3.4. Airfoil Chord Length Effect (C)

Figure 4.12 above is concerned with the effect of changing the value of C , it is very similar by up to 98% with what happened in Figure 4.11 regarding the effect of changing the values of N .

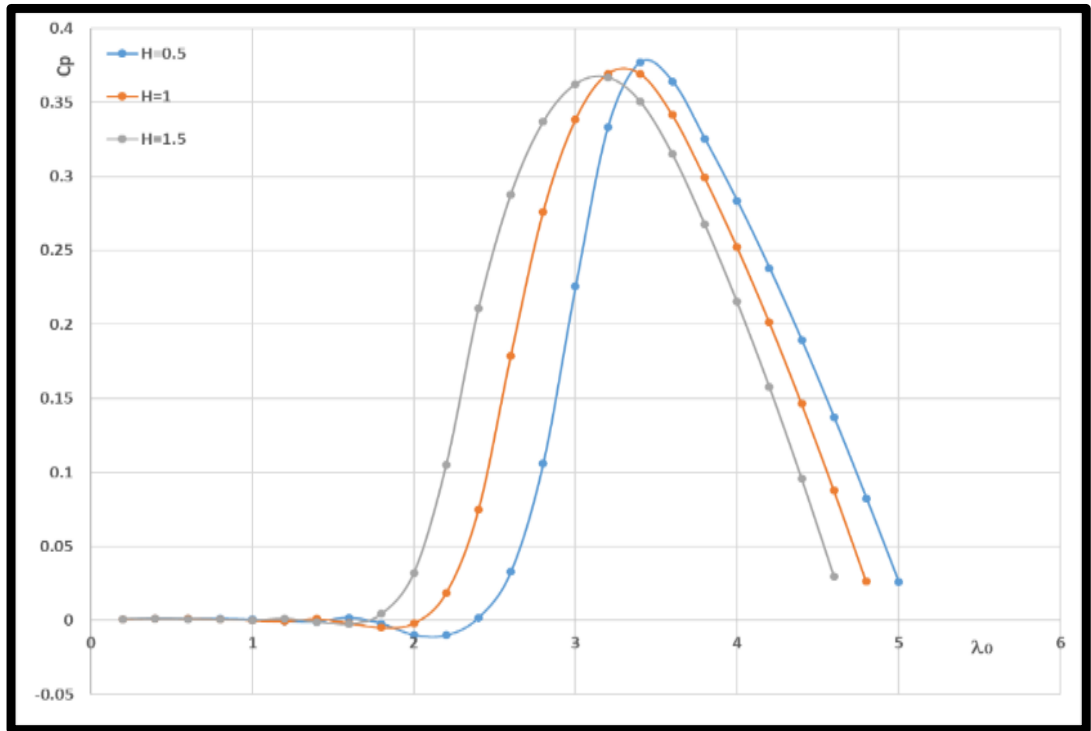


Figure 4.9. Height change effect, case: 65Deg.

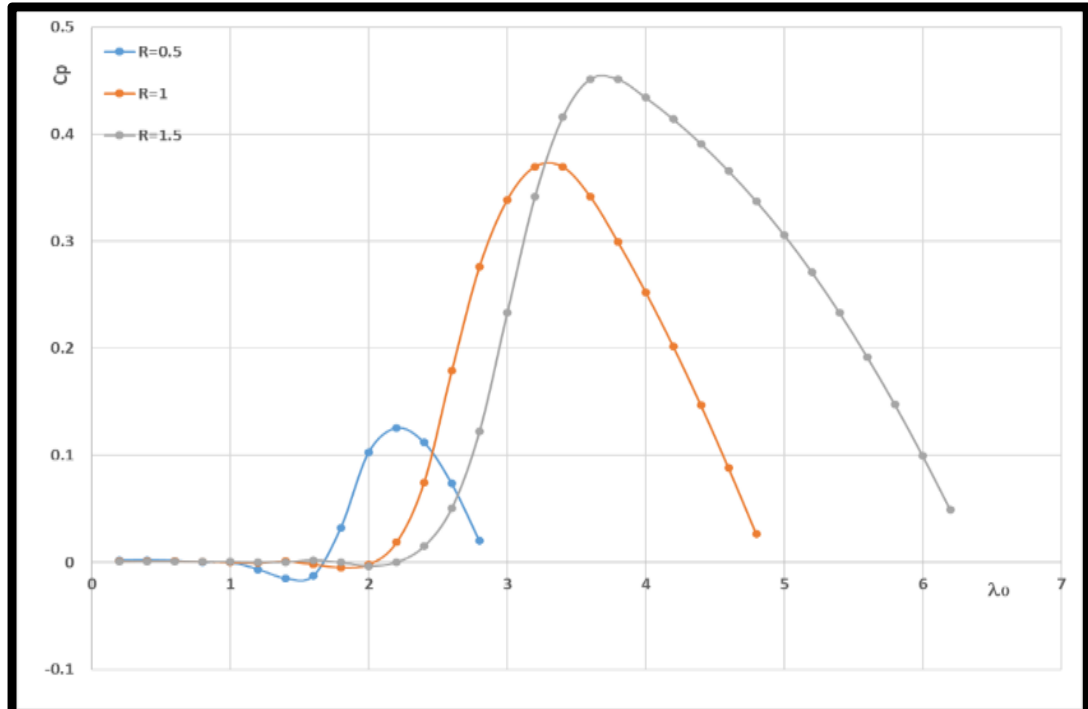


Figure 4.10. Radius change effect, case: 65Deg.

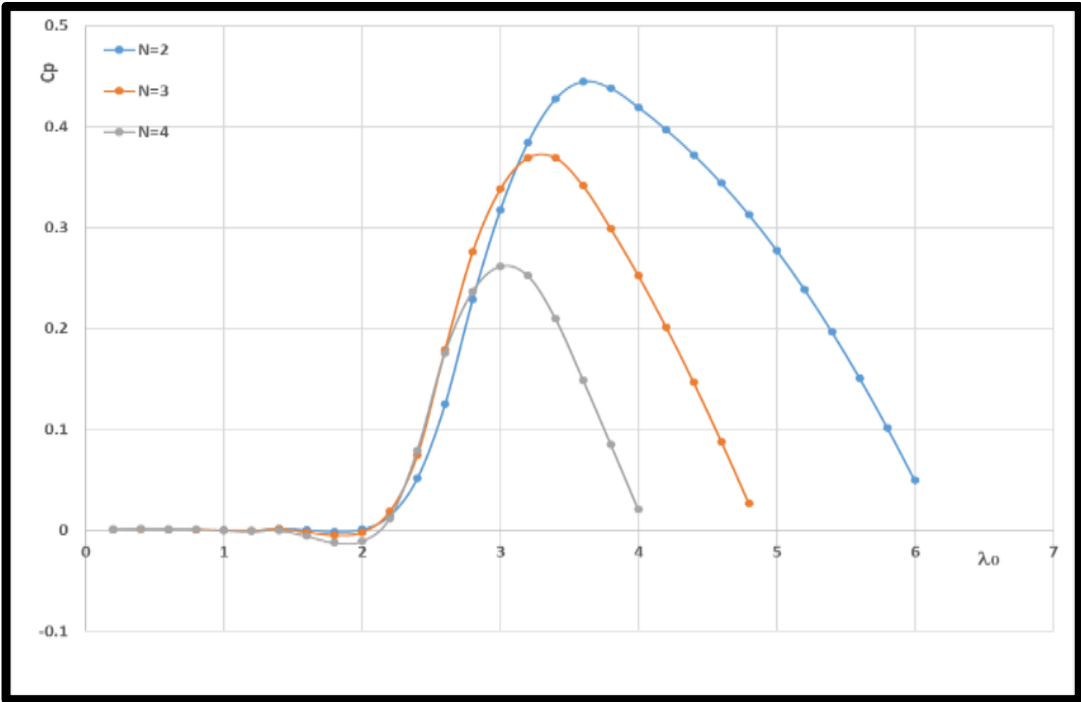


Figure 4.11. Blades number change effect, case: 65Deg.

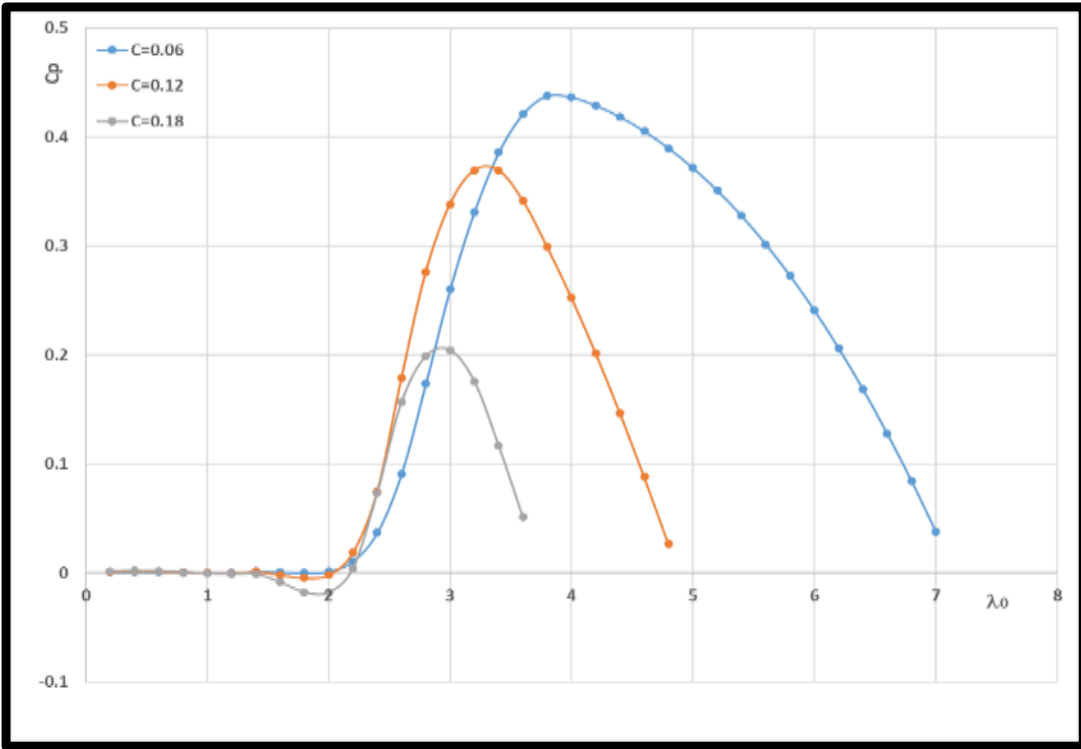


Figure 4.12. Chord length change effect, case: 65Deg.

4.4. EFFECT OF GEOMETRIC SHAPE OF SS-ROTOR ON ITS PERFORMANCE (Case: 85DEG)

4.4.1. Rotor Hight Effect (H)

In Figure 4.13, increasing the value of H causes very little change in the behavior of the curves and is negligible.

4.4.2. Rotor Radius Effect (R)

Figure 4.14 illustrate, an increase in the value R leads to a rise in the value of C_pMax and an increase in the range of energy range.

4.4.3. Number of Blade Effect (N)

Figure 4.15 figure out that in this case, the rise in the number of blades N causes a decrease in the value of C_pMax and a decrease in the energy range confined under each curve along the λ_o range. Case N equals 4 is very poor in terms of efficiency and can be neglected. At all values of N , the problem of self-starting appears in a large way, consisting of negative and zero C_p values along λ_o equal to 0 - λ_o equal to 3.

4.4.4. Airfoil Chord Length Effect (C)

This Figure in below expresses the effect of changing C on aerodynamic performance. The changes in the behavior of the power factor curves C_p are very similar to what happened in Figure 4.16 when studying the effect of changing N .

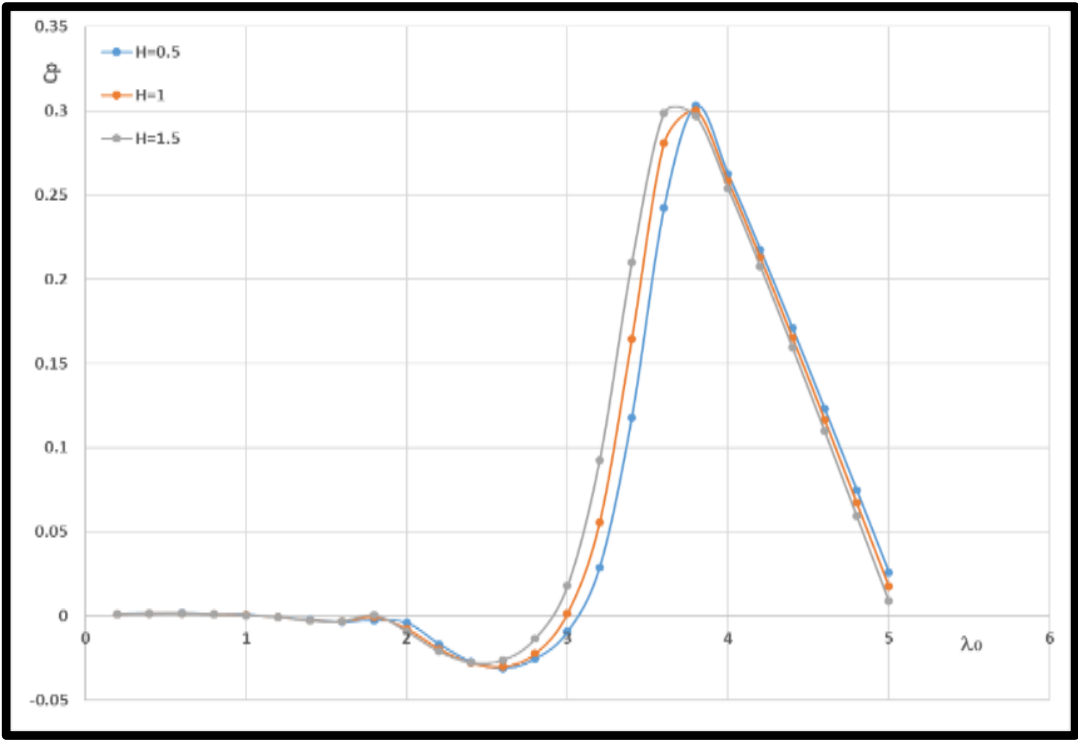


Figure 4.13. Height change effect, case: 85Deg.

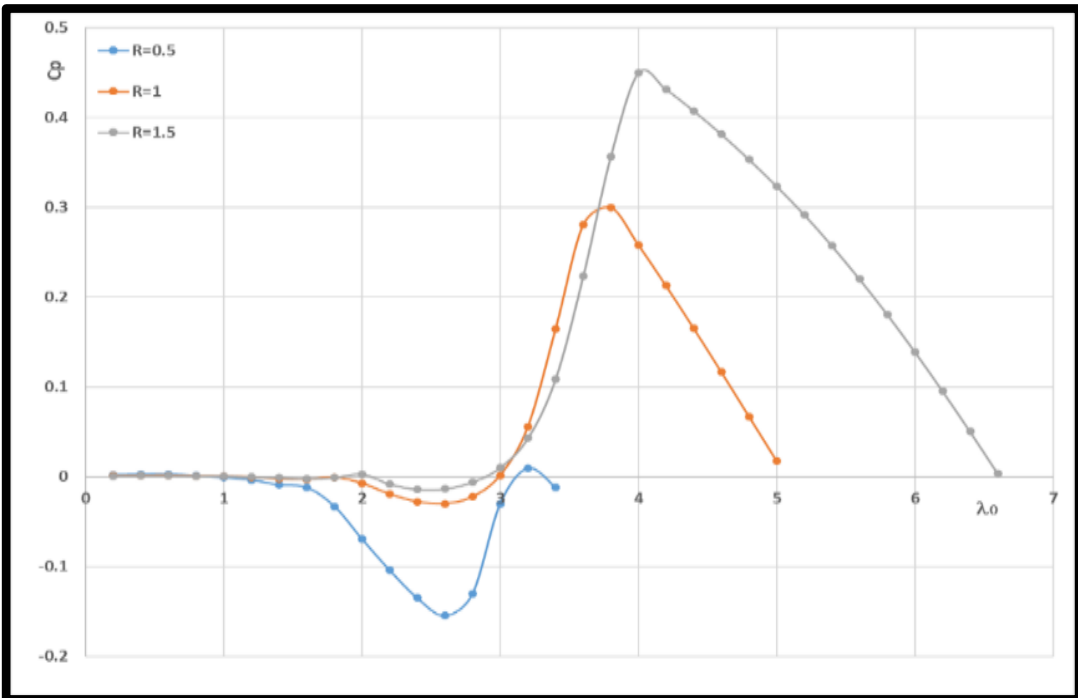


Figure 4.14. Radius change effect, case: 85Deg.

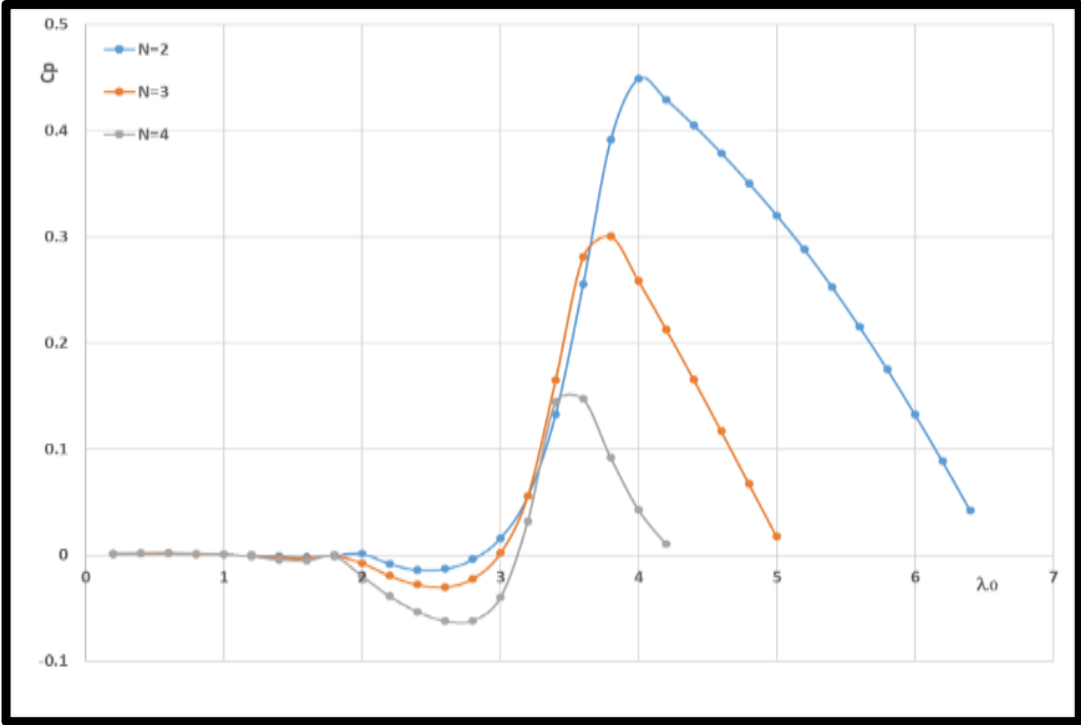


Figure 4.15. Blades number change effect, case: 85Deg.

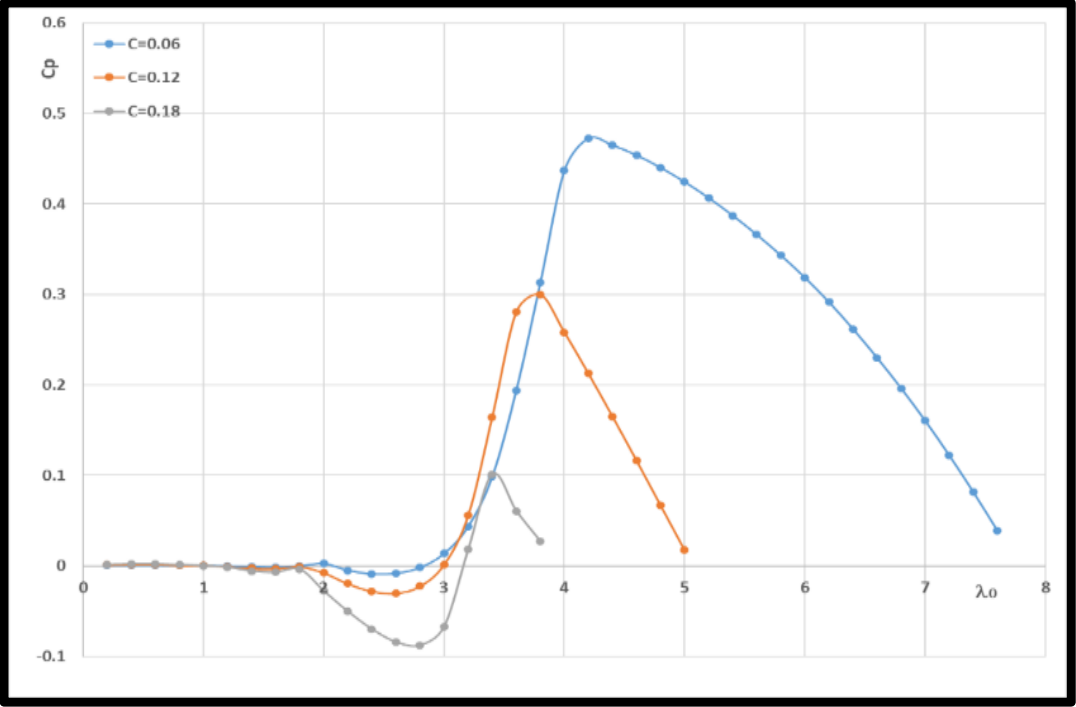


Figure 4.16. Chord length change effect, case: 85Deg.

4.5. FOUR CASES COMPARISON FOR THE SS-VAWT ROTOR

4.5.1. Influence of β On C_p at Different H Values

Some of the patterns for the curves are similar in Figure 4.17 Therefore, the analysis was done in groups, the cases that include H is equal to 0.5, 1, and 1.5, and β varied from 85° to 25° with an amount of change equal to 20° , so it is noticeable that at β equal to 85° results in a low $C_{p_{Max}}$ between 0.26 - 0.29 and it occurs much later when the λ_0 is 3.8-3.6, and C_p values are negative in the λ_0 range from 0.2 to 3. Towards a β value of 65° , the $C_{p_{MAX}}$ value increases significantly to 0.36 with a corresponding λ_0 value of 3.2-3.4, and in the λ_0 range of 0.2-2 the C_p values are negative or very close to zero. Consequently, by moving to the β states equal to 45° , in this mode the air rotor reaches a very high-power factor of between 0.36 and 0.43, and a wide and close operating range for the three states $H=0.5$, $H=1$ and $H=1.5$. Moreover, the region in which C_p values are negative or very close to zero is diminishes to be confined to the range of λ_0 within 0.2-1.5. Finally, looking at the $\beta = 25^\circ$ state, it is clear here that all C_p values including $C_{p_{Max}}$ are reduced to 0.27 and corresponding to λ_0 values equal to 2.2, and for negative C_p values or close to zero, they are confined to a range of λ_0 between 0.2 and 0.8.

4.5.2. Influence of β On C_p at Different R Values

To facilitate the explanation, Figure 4.18 was detailed with five curves confined to the range of λ_0 from 0.2 to 3.6 as a maximum, where the $C_{p_{MAX}}$ value did not exceed 0.21 in a best case. These curves Represent the performance of the air cycles ($\beta = 85^\circ - R = 0.5$), ($\beta = 65^\circ - R = 0.5$), ($\beta=45^\circ - R=1$), ($\beta=25^\circ - R=1$) and ($\beta = 25^\circ - R = 0.5$). And all of these cases are not suitable for the purpose of generating electric power due to the low C_p values in particular and C_p in general. Easily, it can be seen that both the turbines ($\beta=85^\circ - R =1$) and ($\beta =85^\circ - R=1.5$) suffer from the problem of self-movement starting because the C_p values are negative or close to zero in the boundary of the λ_0 0.2 - 3.2. As for the rest of the rotors represented by the curves ($\beta =45^\circ - R=0.5$), ($\beta =45^\circ - R=1$), ($\beta =45^\circ - R =1.5$), ($\beta =65^\circ - R=1$) and ($\beta =65^\circ -$

$R=1.5$) They are characterized by high $C_{p_{MAX}}$ values, where $C_{p_{MAX}}$ values range between 0.32 and 0.44. Moreover, they have a relatively high operating range with a rotor preference ($\beta=45^0 - R = 1.5$), which Its energy range extends from $\lambda_0 = 1.8$ to $\lambda_0 =$ about 6, with the exception of the case ($\beta = 45^0 - R = 0.5$), which showed a very low energy range extending from $\lambda_0 = 1$ to $\lambda_0 = 2.6$ only.

4.5.3. Influence of β on C_p at different N values

The curves in Figure 4.19 are divided into 4 groups, where these groups represent the angles $\beta = 85^0$, $\beta = 65^0$, $\beta = 45^0$ and β equals 25^0 . And each group includes 3 curves, these three curves represent the change in the number of rotor blades, $N = 2$, $N = 3$ and $N = 4$. The group $\beta = 25^0$ shows that the $C_{p_{MAX}}$ value is between 0.15 and 0.24, and the C_p values are generally low despite the change in the value of N in each case. Moreover, the energy range of the $\beta = 25^0$ group extends from $\lambda_0 = 0.8$ to about $\lambda_0 = 2.8$. Moving to the group $\beta = 45^0$, it is evident that the values of C_p and $C_{p_{MAX}}$ are high, ranging between 0.38 and 0.40, and the operational energy range of the turbine is very reasonable, as it extends from a λ_0 equal to 1.5 to a λ_0 equal to 5.2. Next comes the $\beta = 65^0$ state, which showed high inequality in the $C_{p_{MAX}}$ values, where at $N = 2$ it reached 0.44, and decreased to 0.36 at $N = 3$ and decreased dramatically to 0.26 at $N = 4$. also, when increased the value of N , the operational range is decreased in the λ_0 range. Finally, in the situation in which the rotor blades are tilted at an angle of $\beta = 85^0$, the problem of self-starting appears greatly and clearly, as the C_p values are negative or close to zero to the λ_0 boundary equal to 3.3 regardless of whether the value of $N = 2$ Or 3 or 4. In the same context, the $C_{p_{MAX}}$ values for $\beta = 85^0$ are highly variable, so when $N = 2$ the $C_{p_{MAX}} = 0.43$, when $N = 3$ the $C_{p_{MAX}} = 0.29$, and when $N = 4$, then $C_{p_{MAX}} = 0.14$.

4.5.4. Influence of β On C_p at Different R Values

Figure 4.20 shows the results of the effect of C changes on the rotor performance at β equal to 85^0 , 65^0 , 45^0 and 25^0 . The results revealed that the behavior of the C_p curves

as a function of λ_0 is almost identical to the previous case presented in Section 3.3. In other words, shapes 7 and 8 are nearly identical.

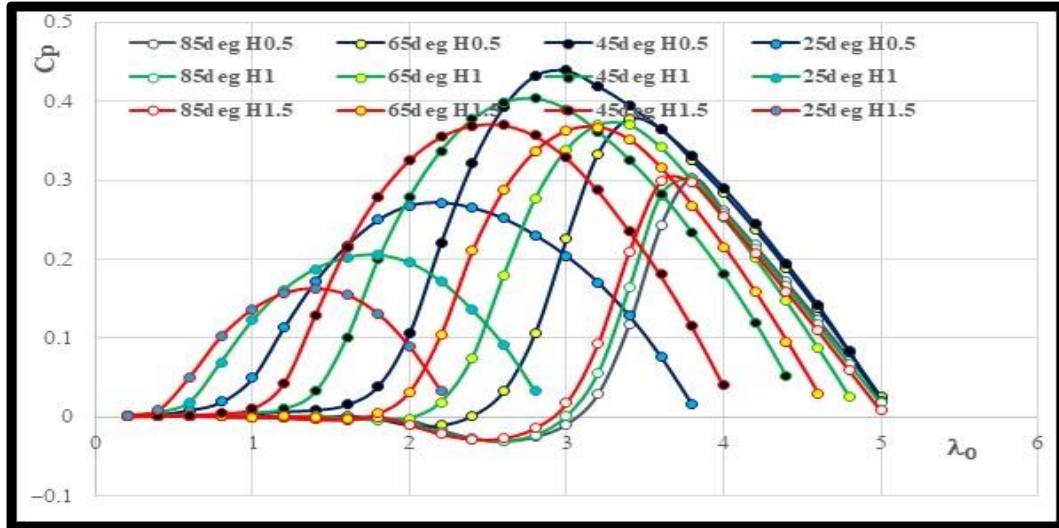


Figure 4.17. Influence of β on C_p at different H values.

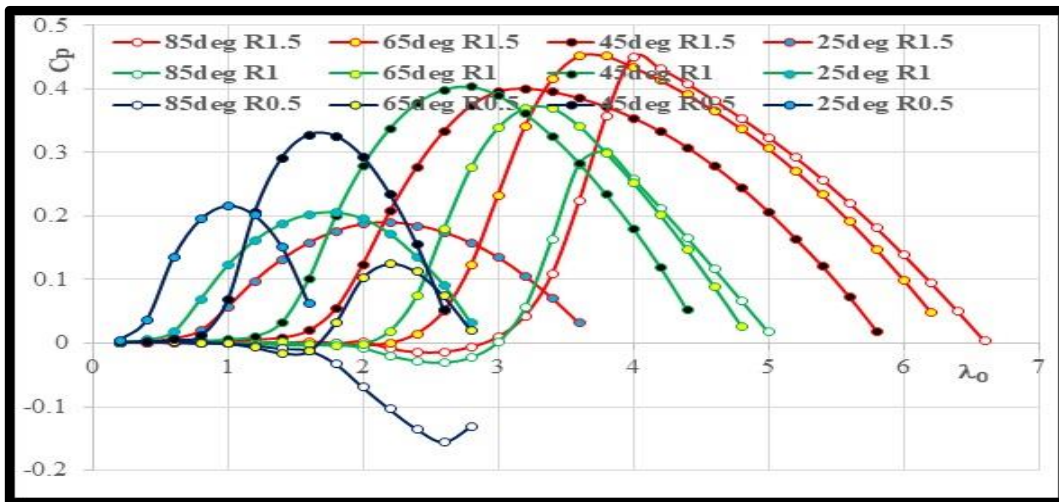


Figure 4.18. Influence of β on C_p at different R values.

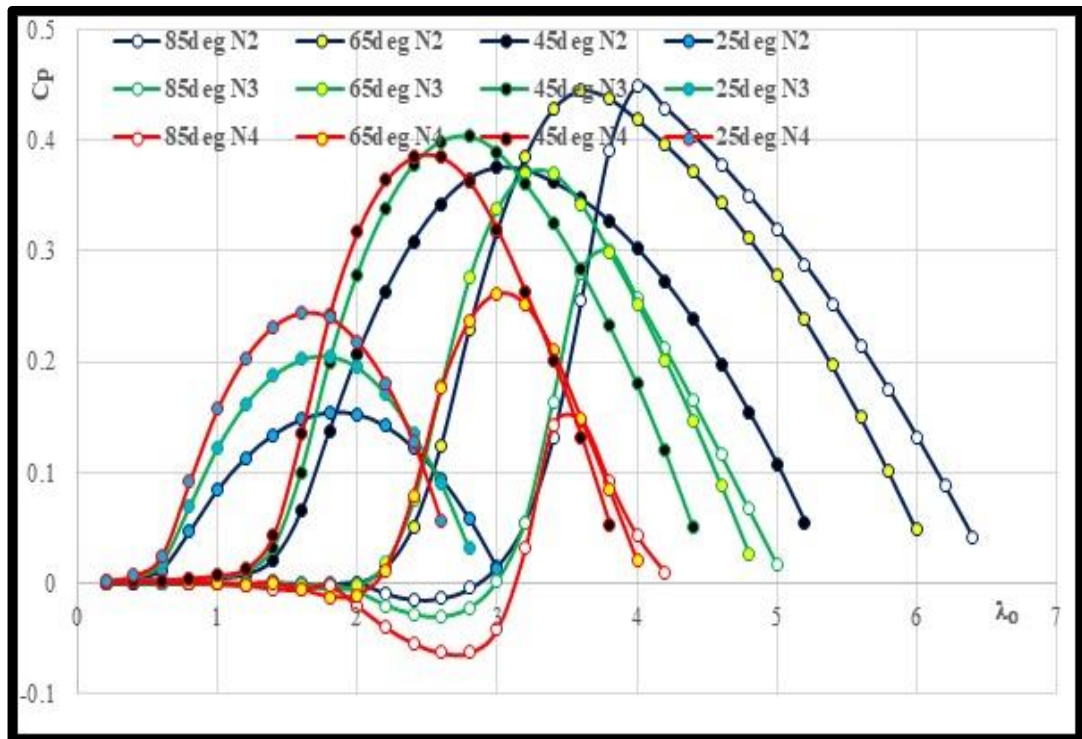


Figure 4.19. Influence of β on C_p at different N values.

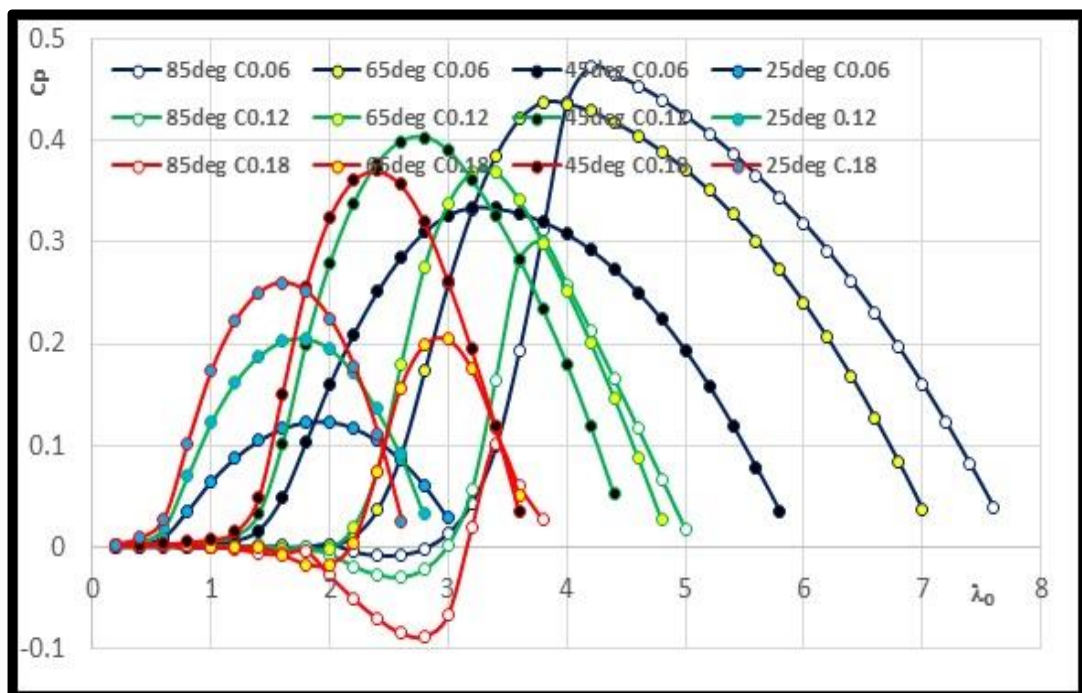


Figure 4.20. Influence of β on C_p at different C values.

4.6. REYNOLDS NUMBER EFFECT

Figure 4.21 displays that the values of the power factor C_p increase along the tip speed ratio λ_0 with the increase in the value of the Reynolds number Re . Where the lowest values of power factor were recorded when Reynolds Number equals 160000 and the highest values when Reynolds number equals 1000000.

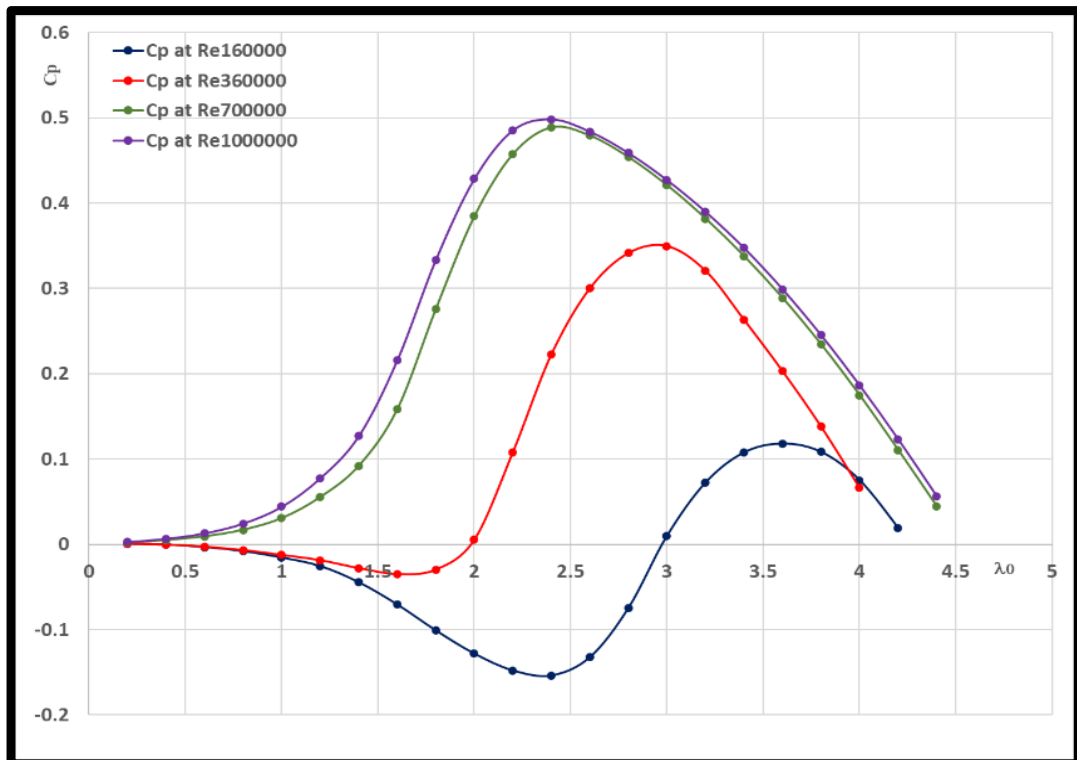


Figure 4.21. Reynolds number effect on power factor.

4.7. PERFORMANCE OF SS-VAWT vs, S & PB-DARRIEUS

The graphs from Figure 4.22 to Figure 4.25 show comparisons between the three wind turbines, Parabolic Darrieus PB-VAWT, H-Darrieus or (S-VAWT) and SS-VAWT turbine. A comparison between them shows the superiority of the SS-VAWT case with its blades inclined at an angle of *45 degrees*. Where the preference was based on achieving the highest value of the power factor C_p and the high values of C_p in the first range extending between λ_0 equal to zero and λ_0 equal to 2, in addition to the large area confined under the C_p curves. The comparison was made by

changing the geometric shape variables for the three cases represented by H , R , N and C in order to verify their influence on the power factor C_p .

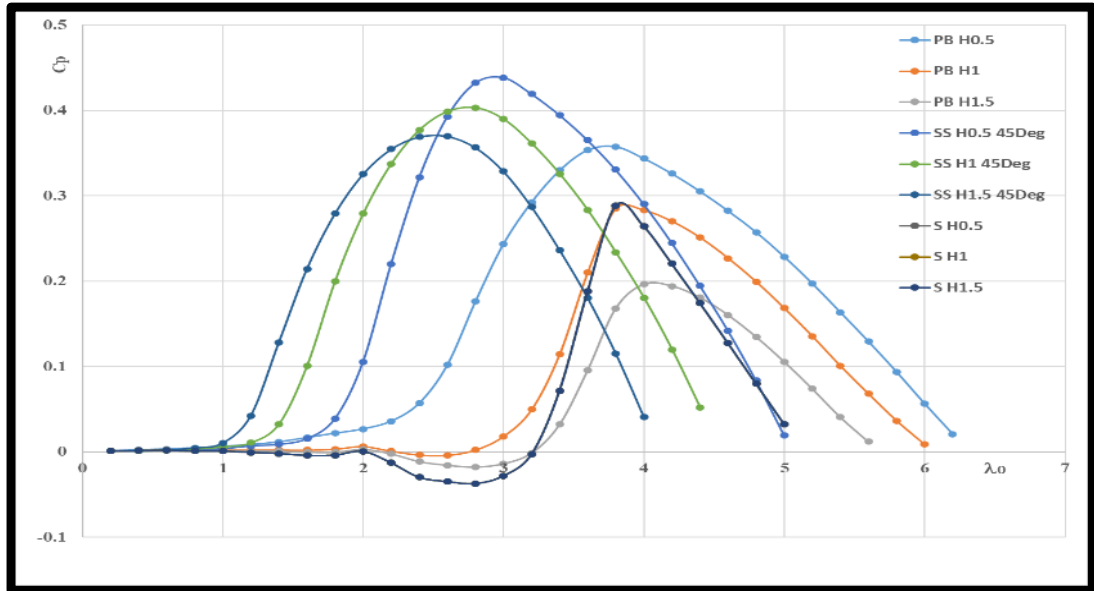


Figure 4.22. Comparison when changing the height of the three models.

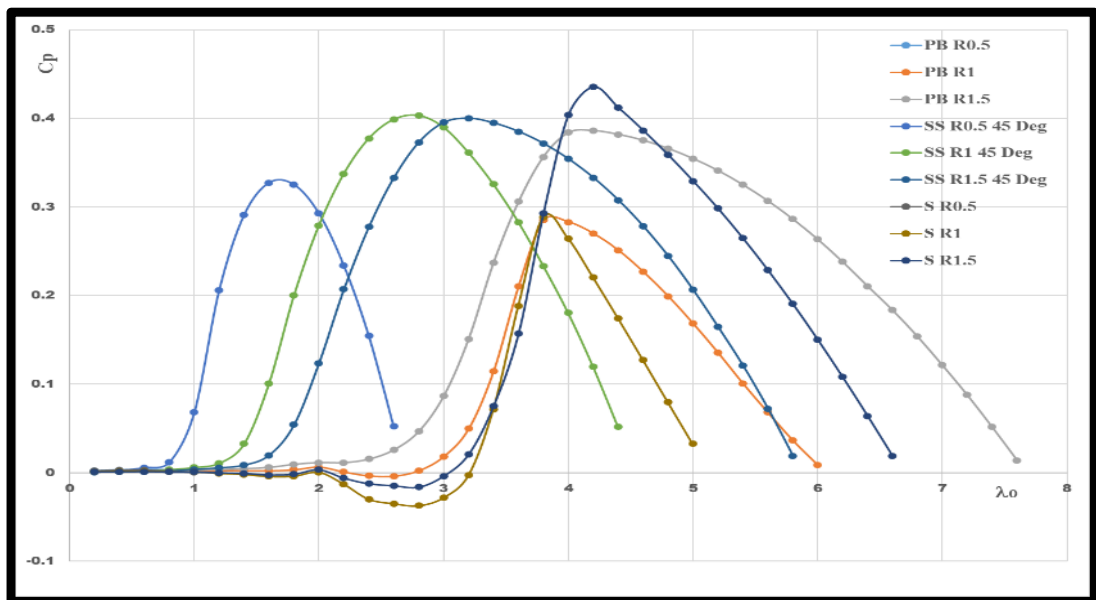


Figure 4.23. Comparison when changing the radius of the three models.

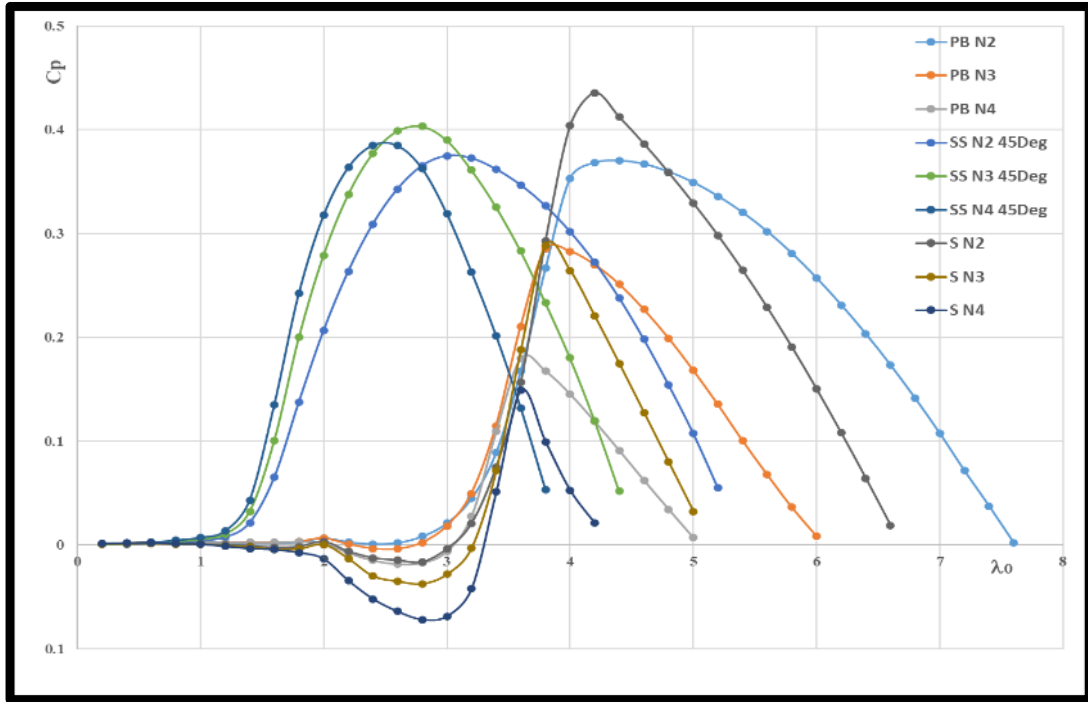


Figure 4.24 Comparison when changing the blades number of the three cases.

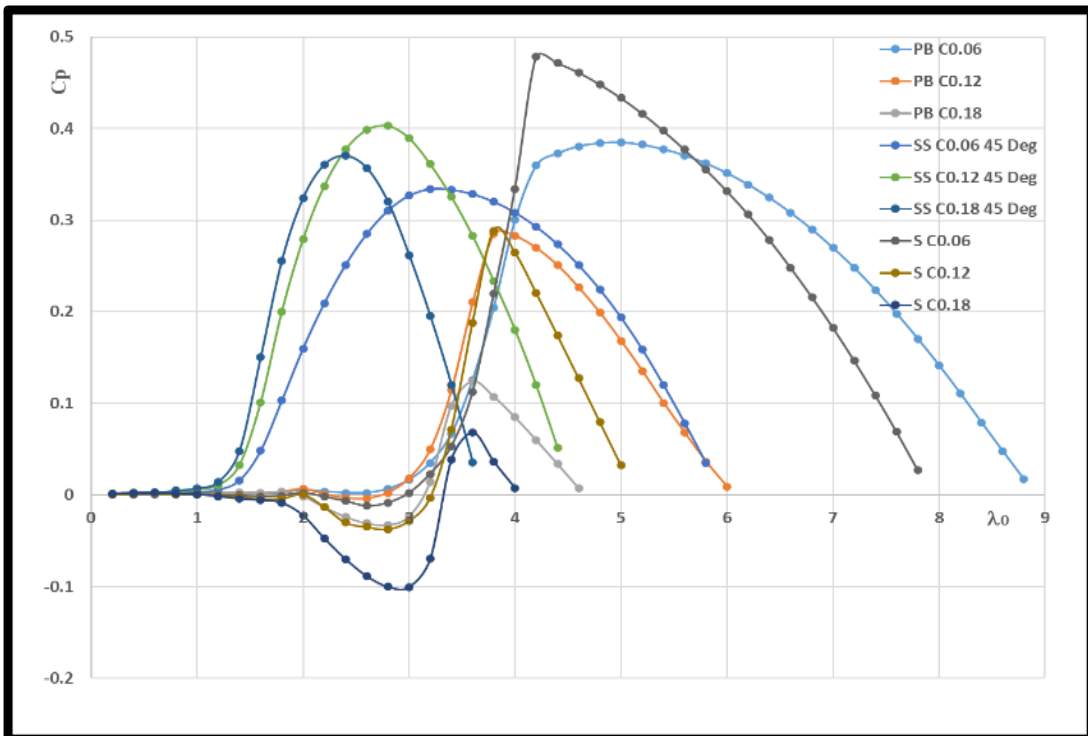


Figure 4.25. Comparison when changing the chord length of the three models.

4.8. WORK WITHIN THREE SPECIFIC ANGLES [35Deg 55Deg 85Deg]

4.8.1. The Case Study 35Deg

Figure 4.26 shows the relationship between the terminal relative velocity and the power factor C_p . The maximum power factor C_{pMax} value of 0.33 is achieved at a λ_0 value of 2.6, The starting torque is achieved when the value of the power factor C_p reaches 0.09 corresponding to the value of λ_0 equal to 1.7.

4.8.2. The Case Study 55Deg

Figure 4.27 shows the relationship between the terminal relative velocity and the power factor C_p . The maximum power factor C_{pMax} value of 0.39 is achieved at a λ_0 value of 3.2, The starting torque is achieved when the value of the power factor C_p reaches 0.09 corresponding to the value of λ_0 equal to 2.6.

4.8.3. The Case Study 85Deg

Figure 4.26 shows the relationship between the terminal relative velocity and the power factor C_p . The maximum power factor C_{pMax} value of 0.29 is achieved at a λ_0 value of 3.8, The starting torque is achieved when the value of the power factor C_p reaches 0.09 corresponding to the value of λ_0 equal to 3.4.

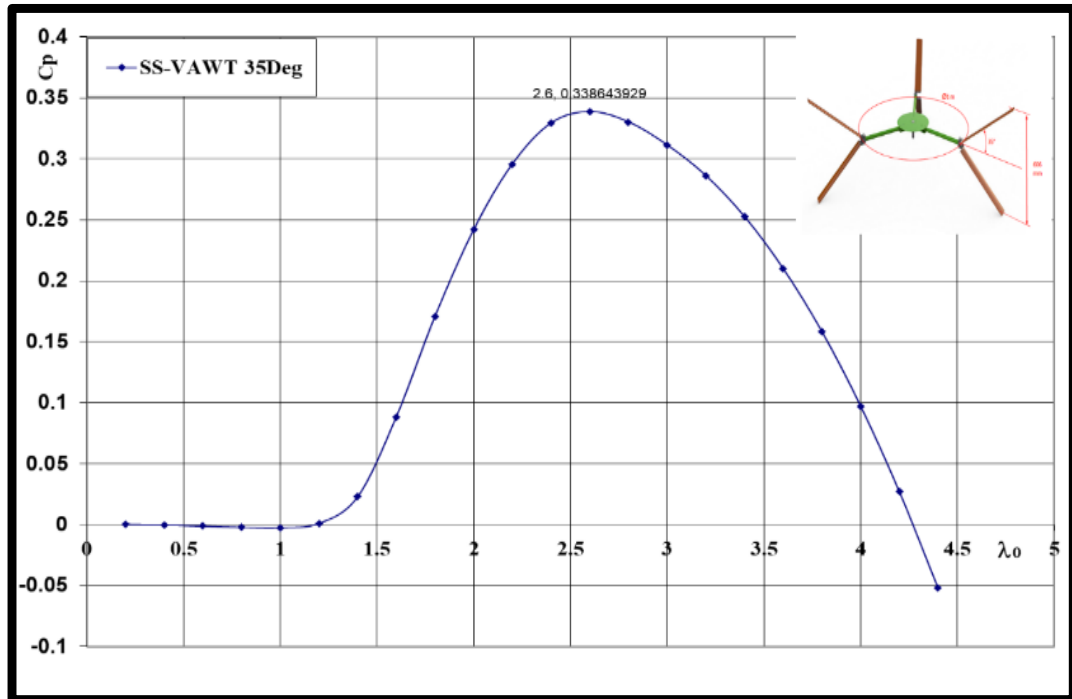


Figure 4.26. Power factor behavior in case of 35Deg.

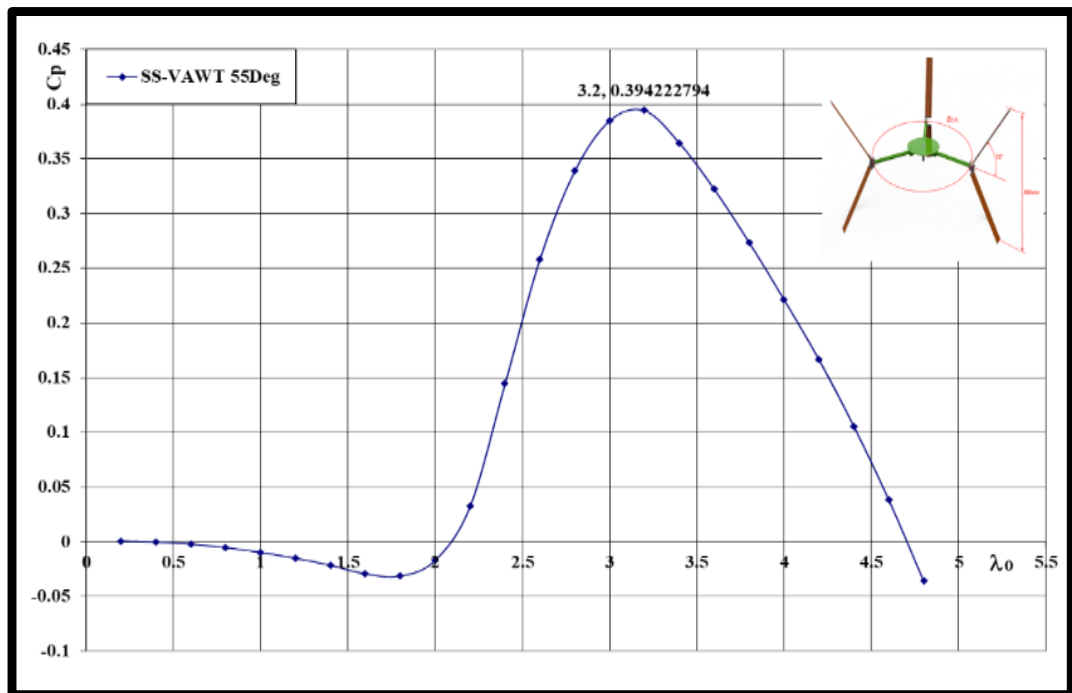


Figure 4.27. Power factor behavior in case of 55Deg.

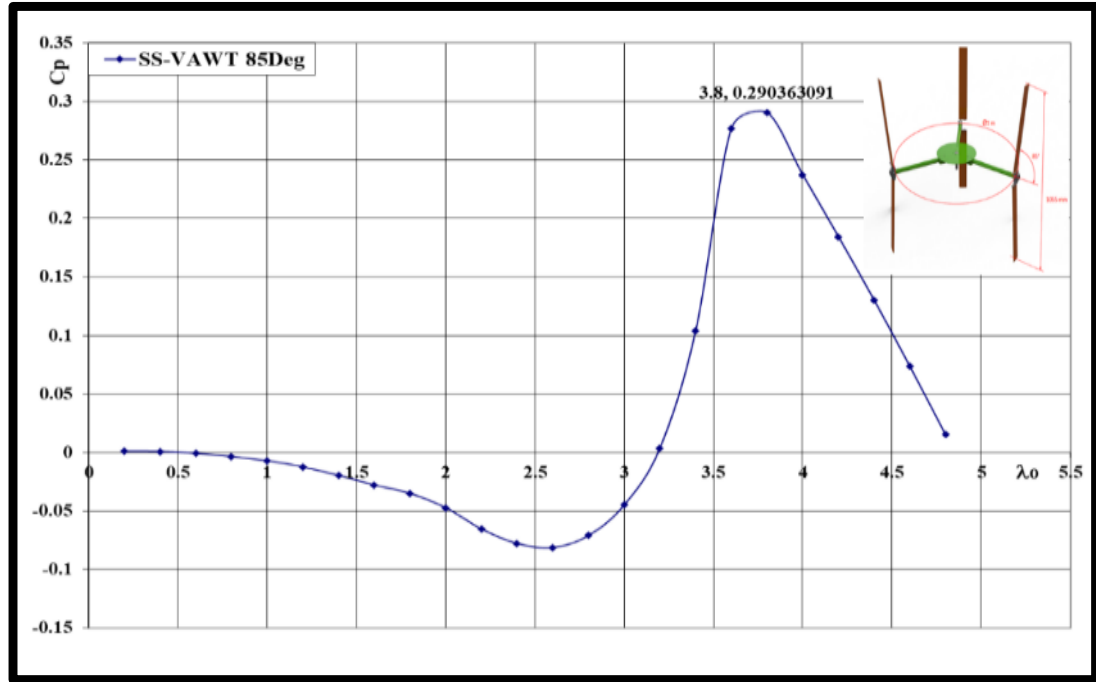


Figure 4.28. Power factor behavior in case of 85Deg.

4.9. ANSYS FLUENT POST PROCESSING

4.9.1. Aerodynamic Investigations of Physical Phenomena

Figure 4.29 expresses the effect of air hitting the SS-VAWT body in terms of air velocities and their change according to the place of contact with the turbine. Where the air velocities decrease at the arms of the fixing blades and increase at edges of the blades. Figure 4.30 shows the water flow lines through the turbine inside the domain, where its speed changes in the green area at each blade. Figure 4.31 shows the wind speed vectors, where the speed values change inside the turbine domain according to the position, where the speed increases at the surface of one of the blades and decreases behind the blades in the wake region. The reason is the inclination of the angle of flow on the body and the shape of the body in terms of aerodynamic. Figure 4.32 shows the distribution of air pressure on the turbine, where the pressure varies from one location to another on the turbine body. The reason for this difference is the shape of the body and the angle of collision of the flow with the body.

Figure 4.33 shows the different values of air pressure passing through the turbine inside the domain, where the flow pressure values differ due to the rotation of the wind rotor and also due to air attach the turbine body, especially the area behind the edge of the airfoil trailing edge moreover the upper surface for each blade. Figure 4.34 present the different flow velocities within the rotor field of the turbine, where the acceleration of the flow at the front edges of the airfoil and its deceleration at the cylindrical support parts, in addition to a severe speed drop in the wake region, but the area of this region varies from one blade to another according to the angle of rotation θ . Figure 4.35 shows the effect of the tangential force generated by the aerodynamic kinetics of the flow on the turbine body at different positions. Where the values of the tangential forces, or what is known as the stress of the wall, differ according to the shape of the part acting on it, the type of material it is made of, and the angle of contact with the stream.

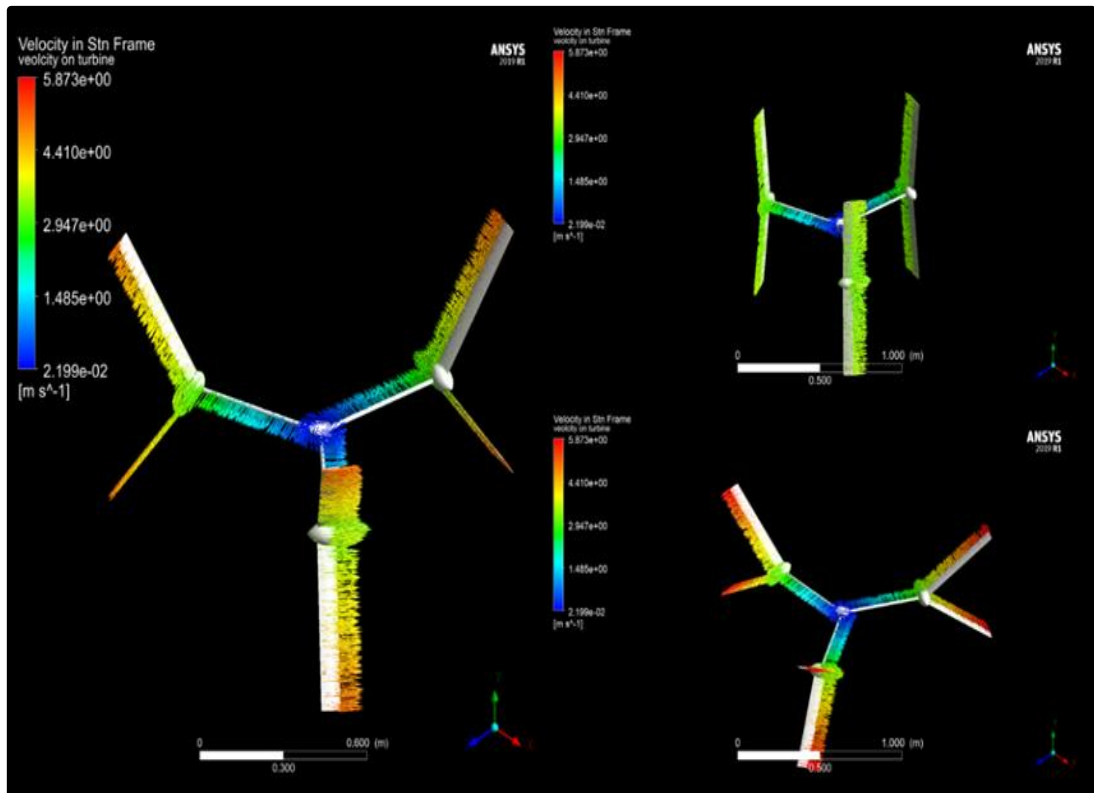


Figure 4.29. Velocity vectors behavior for three cases of SS-VAWT.

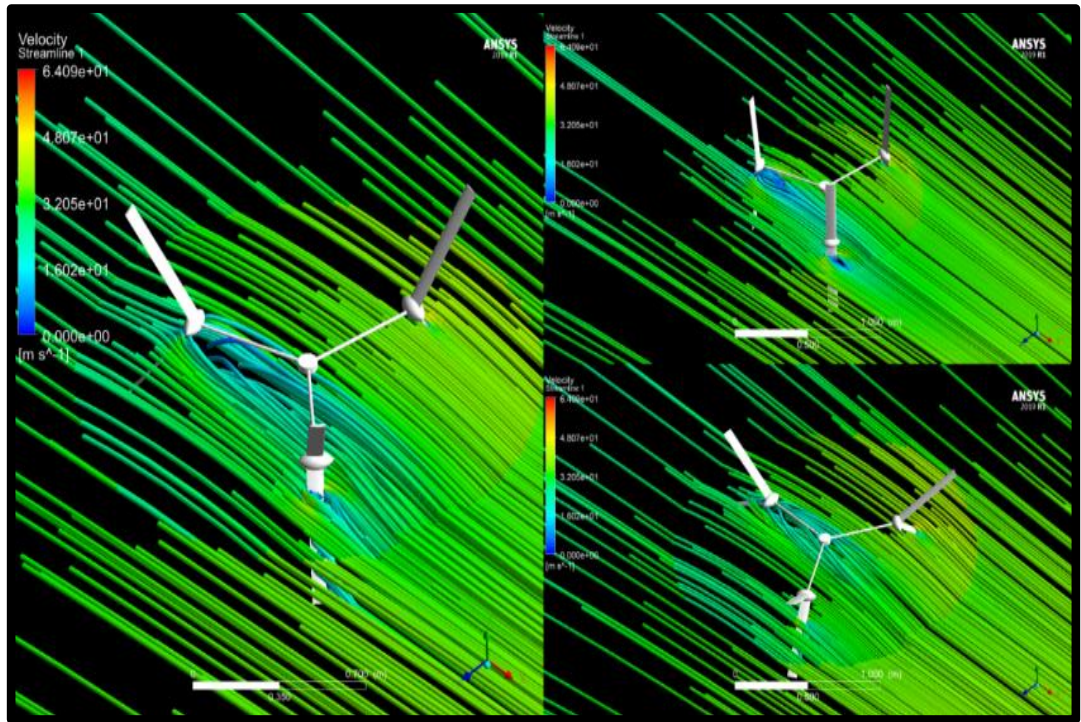


Figure 4.30. Stream lines behavior for three cases of SS-VAWT.

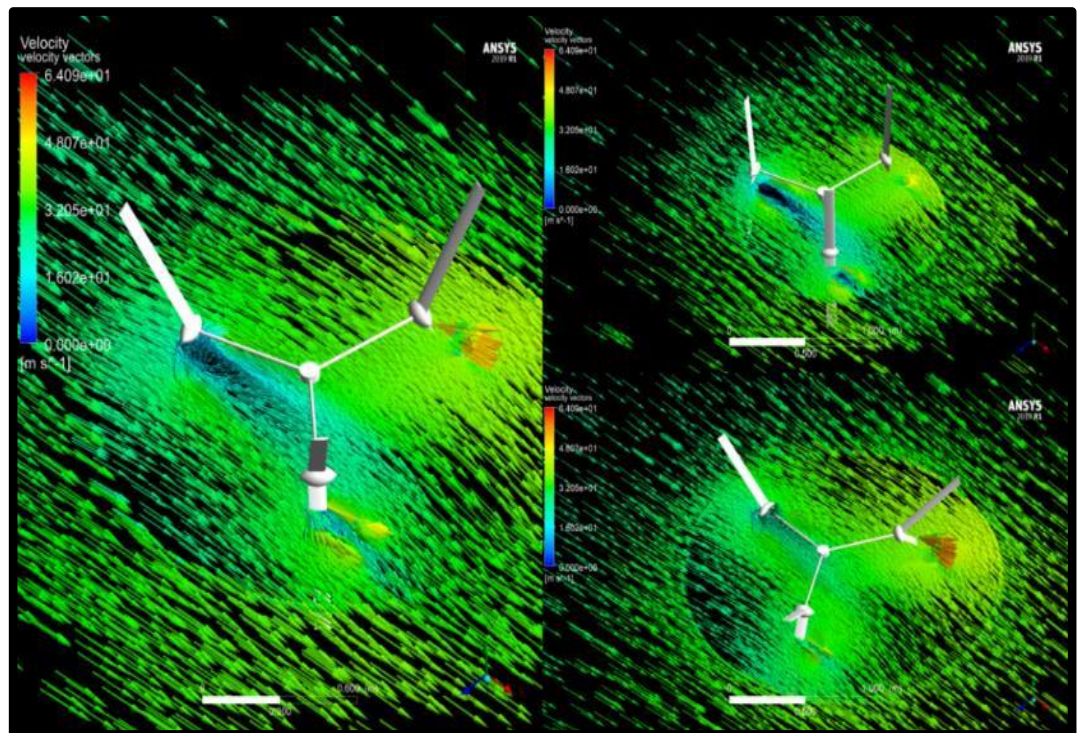


Figure 4.31. Velocity vectors behavior for three cases of SS-VAWT domine.

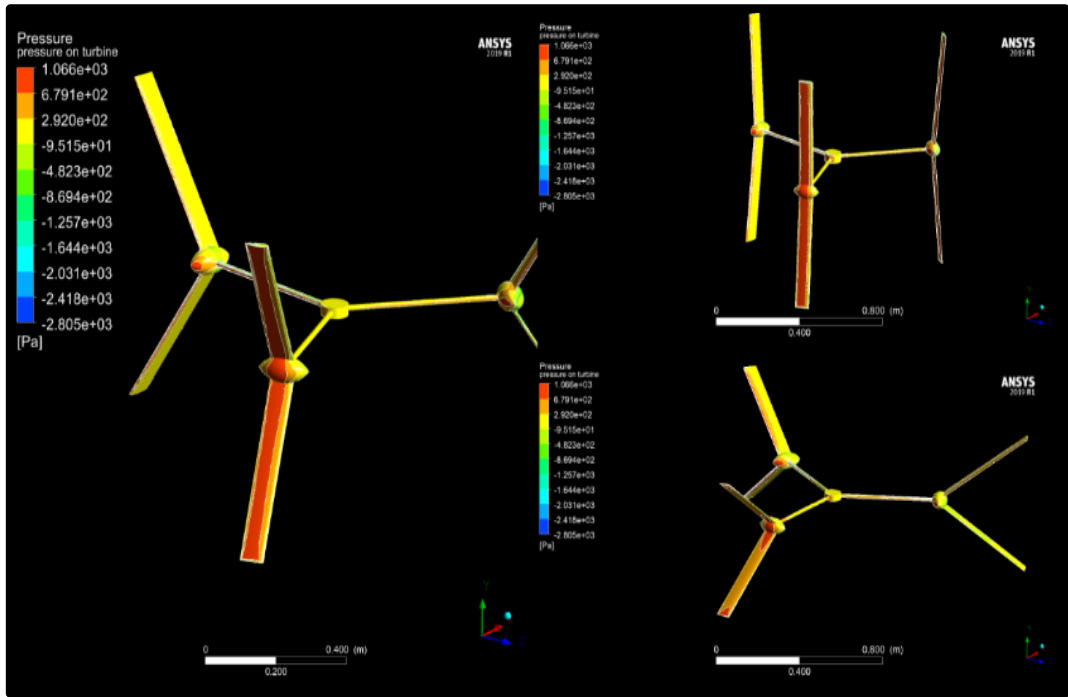


Figure 4.32. Pressure behavior for three cases of SS-VAWT.

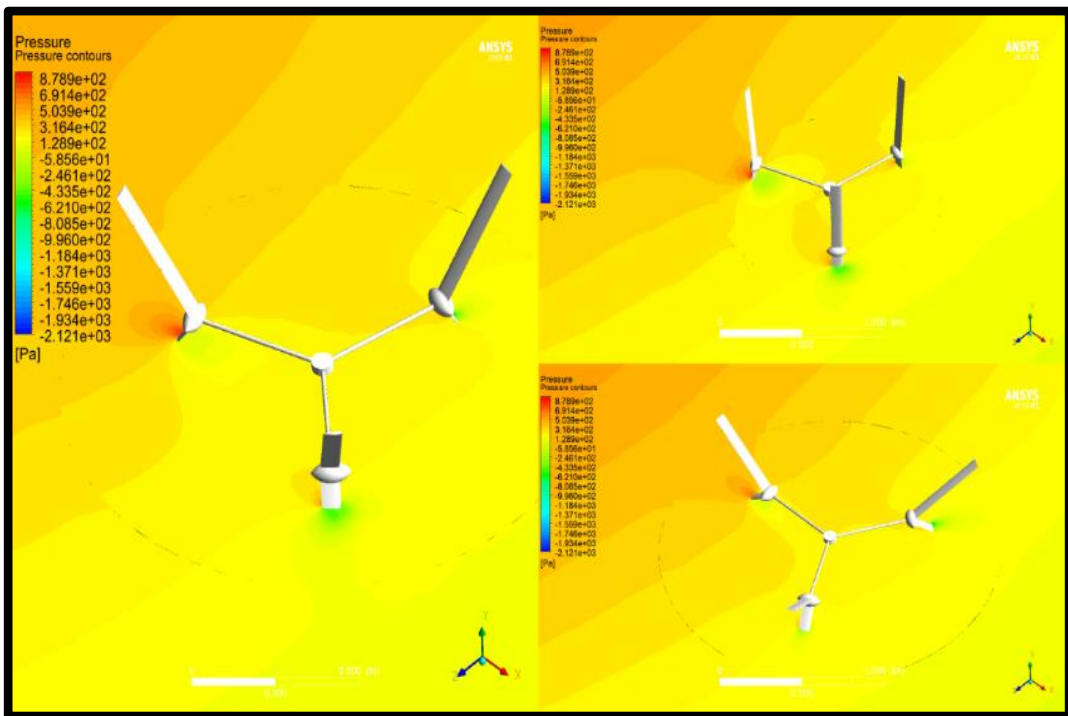


Figure 4.33. Pressure counter of three cases of SS-VAWT.

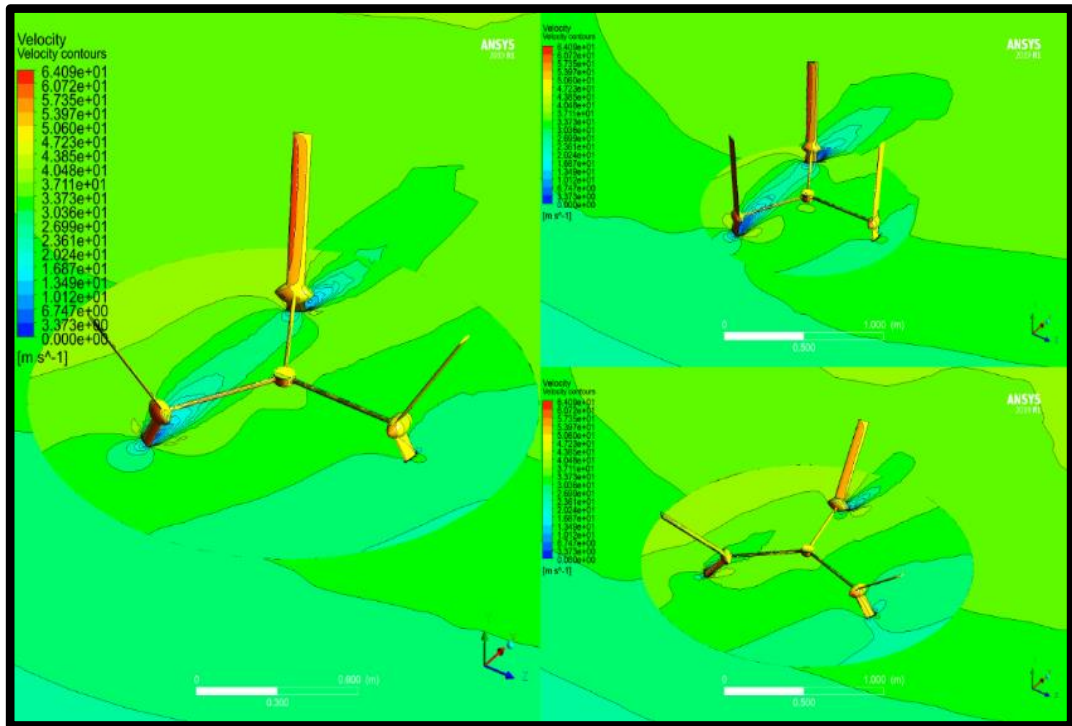


Figure 4.34. Velocity counter of three cases of SS-VAWT.

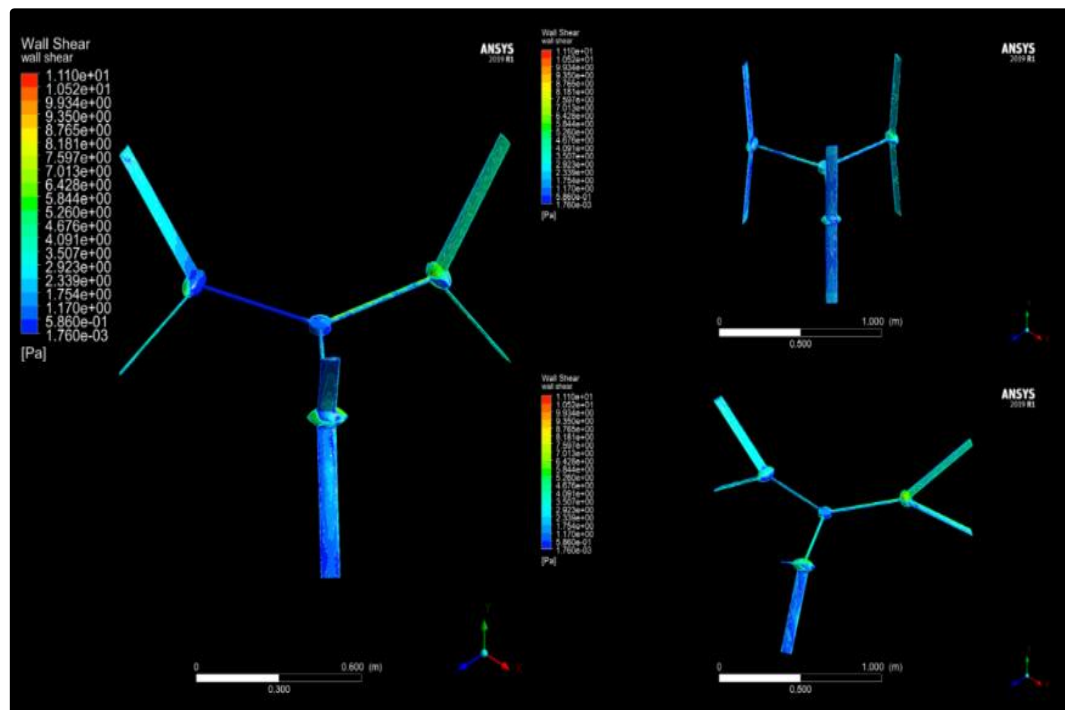


Figure 4.35. Wall shear due to aerodynamic forces.

4.9.2. Aerodynamic Forces for the Three Cases [35Deg, 55Deg, 85Deg]

Figures 4.36, 4.37 and 4.38 show the effect of aerodynamic forces on blades of the rotor in the three directions X, Y and Z. Where the effect of these forces changes according to the angle of inclination β of the blades only, to expose the three turbines of the turbine to the same physical conditions during the simulation process.

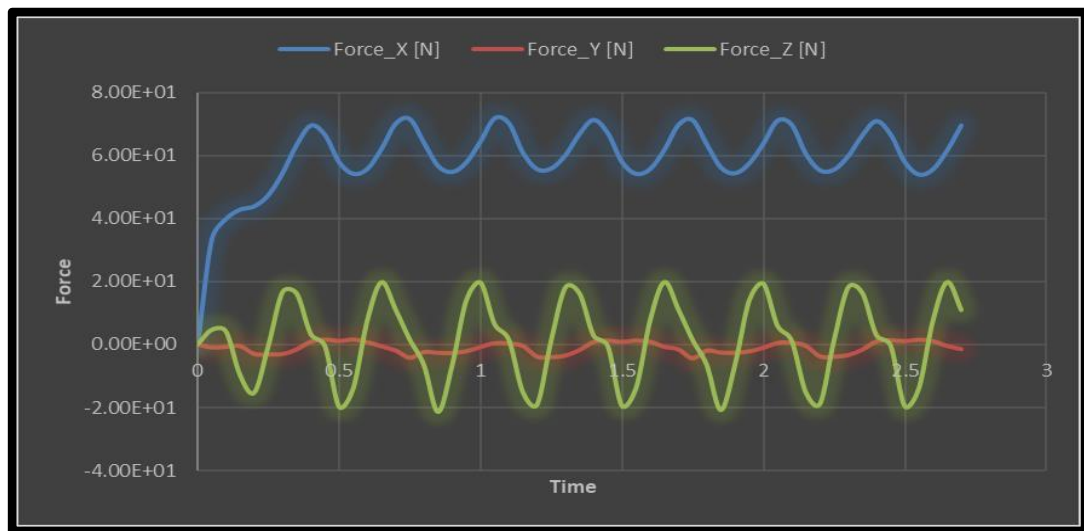


Figure 4.36. Force effect in three directions for case study 35deg.

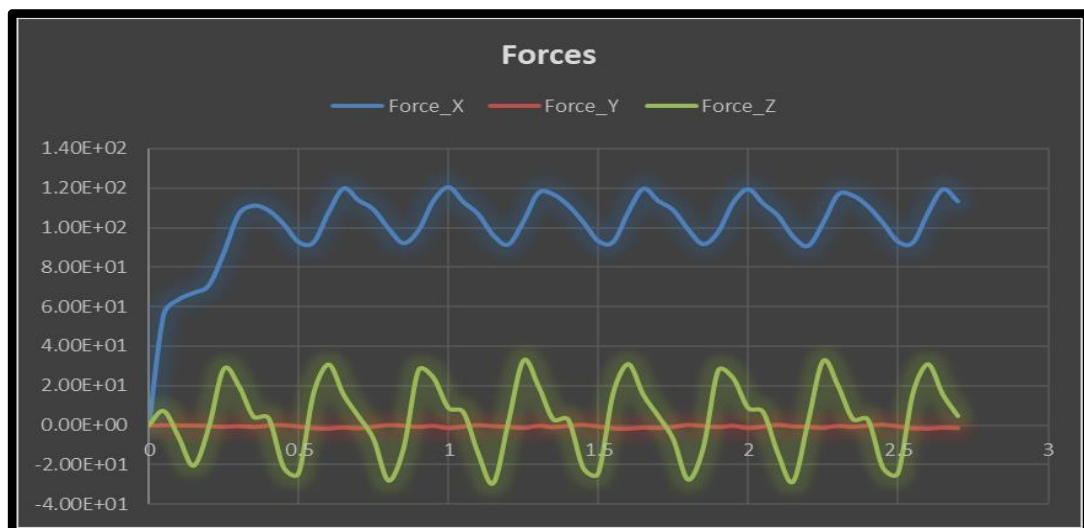


Figure 4.37. Force effect in three directions for case study 55deg.

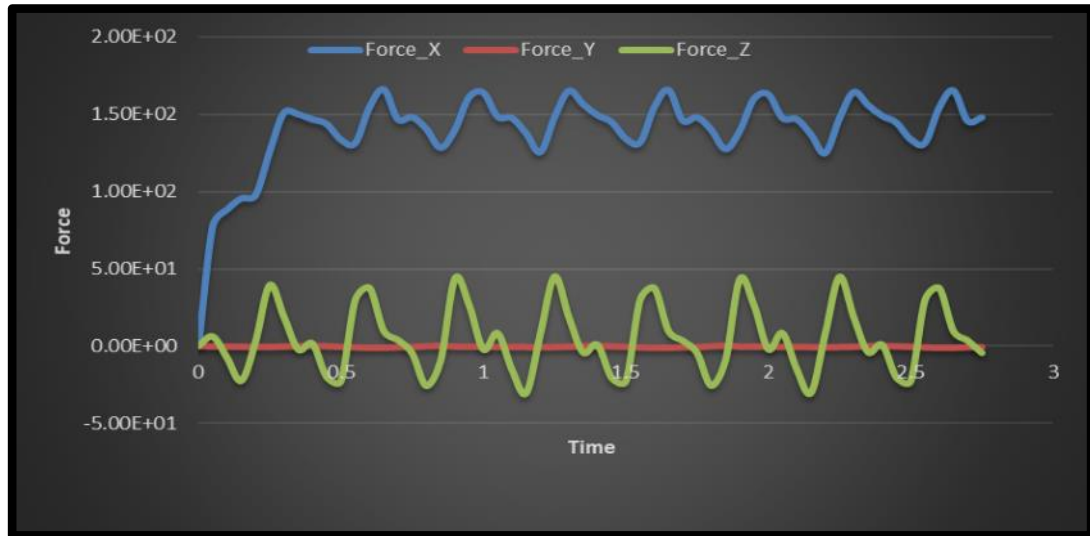


Figure 4.38. Force effect in three directions for case study 85deg.

4.9.3. Forces Effects Comparison of Three Cases [35Deg, 55Deg, 85Deg]

Forces in X directions differ according to the normal projected area to the flow direction. Case 85 has the largest area then comes case 55 finally case 35. This is shown in the pressure concentration figure. Large X-force is not preferable as it acts to bend the turbine axis so the minimum the best. Y-force is not preferable too as it acts to make the turbine fly away acting like a propeller. The order of cases here is reversed as case 85° has the minimum horizontal area then comes 55° finally 35° . Z-Force is acting in the same way as X-Force to bend the turbine axis. But it is much lower because it results from the side flow stream and the main flow stream is in the x-direction. The minimum Z-Force is the best too. Our main criteria here is the power output. Power results from the spin of the turbine due to the aerodynamic moment on the blades.

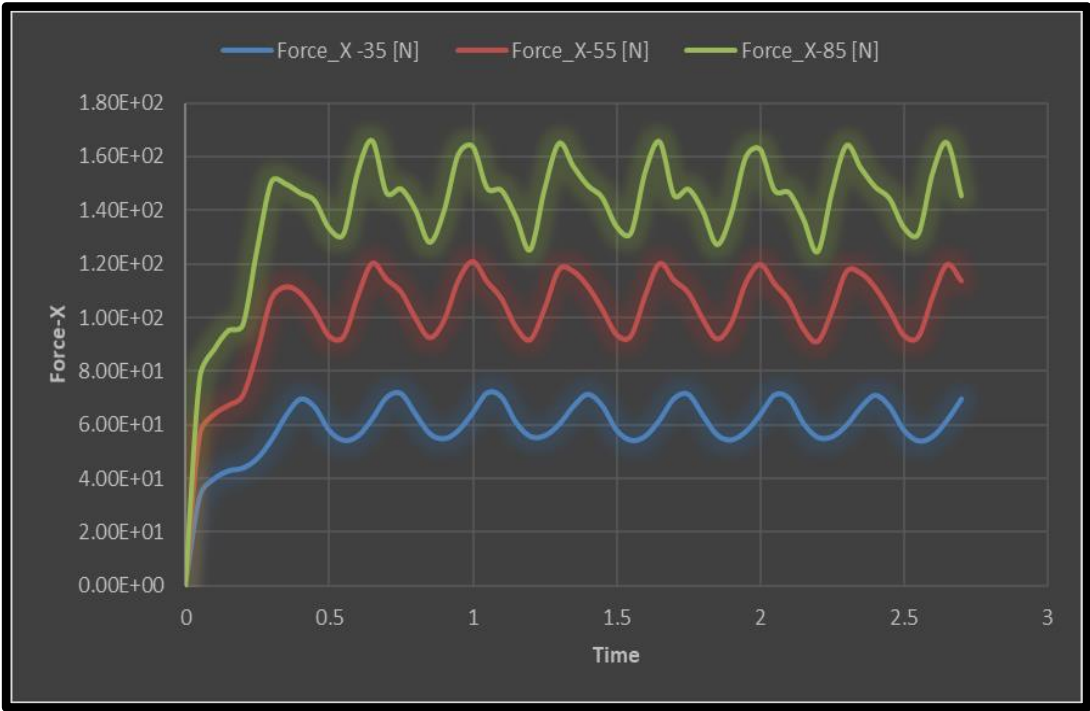


Figure 4.39. X-Force comparison.

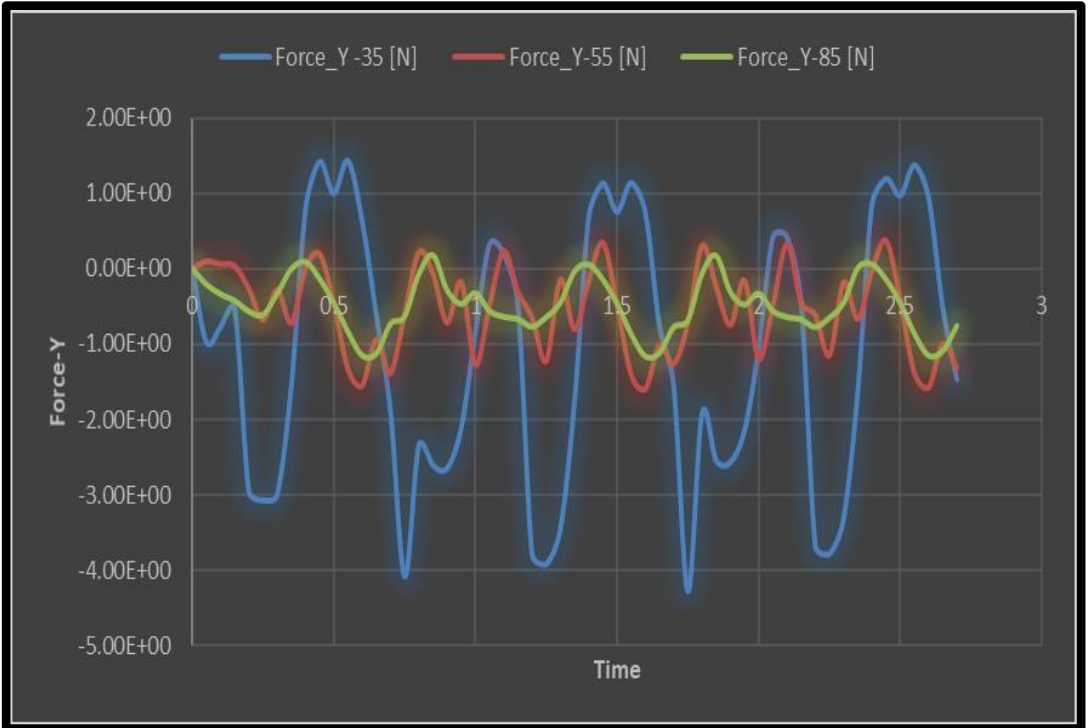


Figure 4.40. Y-Force comparison.

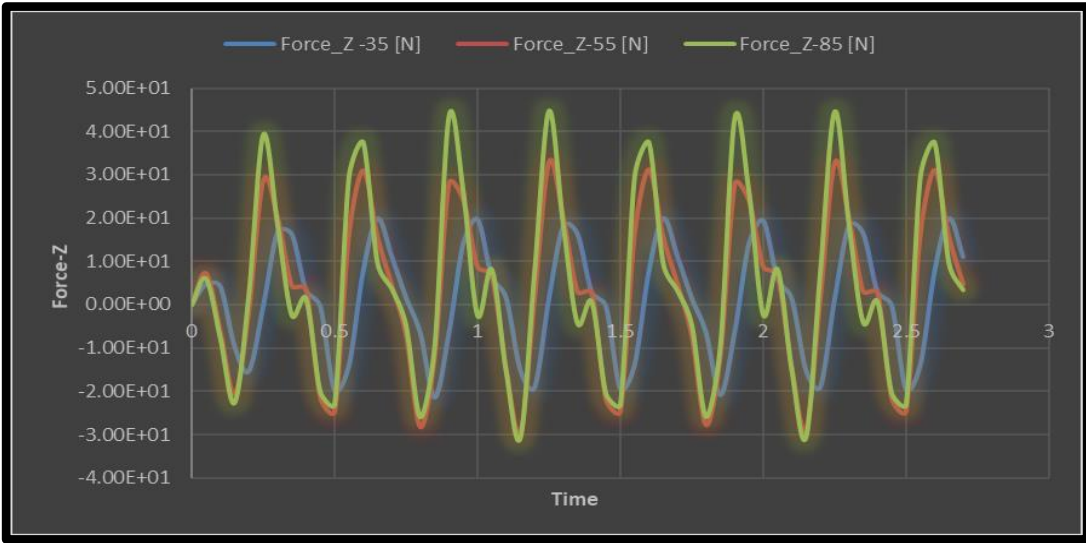


Figure 4.41. Z-Force comparison.

4.9.4. Power Output for The Three Cases [35Deg, 55Deg, 85Deg]

Figures 4.42, 4.43 and 4.44 show the power curves P as a function of time for cases 35° , 55° and 85° respectively, while Figure 4.45 shows a comparison between them and the superiority of case 55° is evident through the higher values of power represented in the red curve.

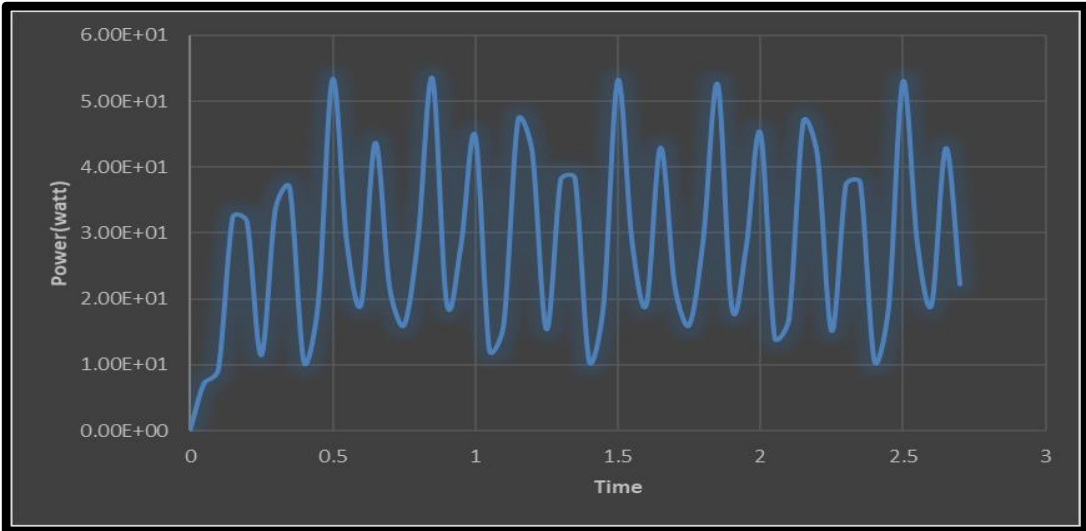


Figure 4.42. Power output for case 35Deg.

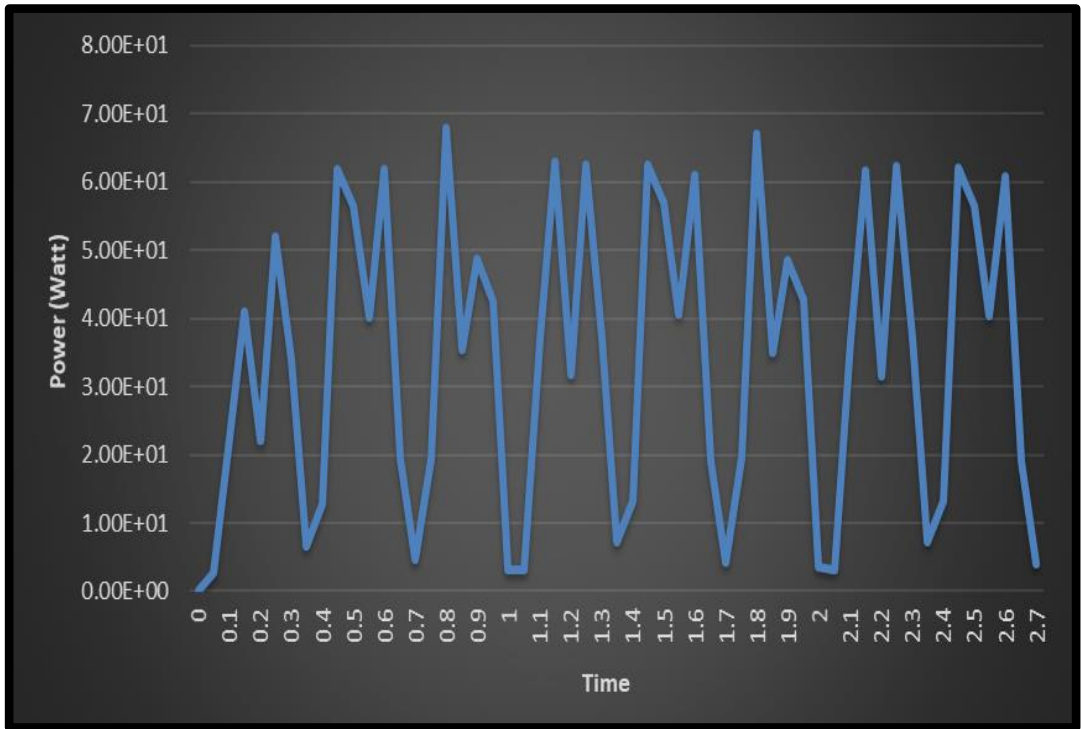


Figure 4.43. Power output for case 55Deg.

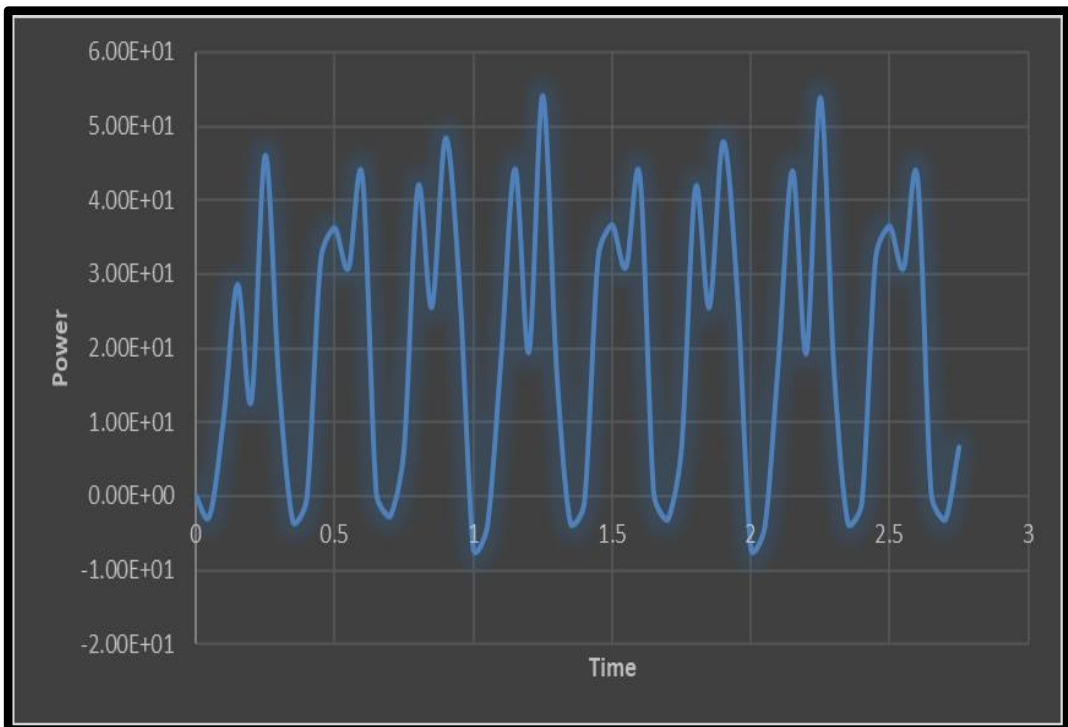


Figure 4.44. Power output for case 85Deg.

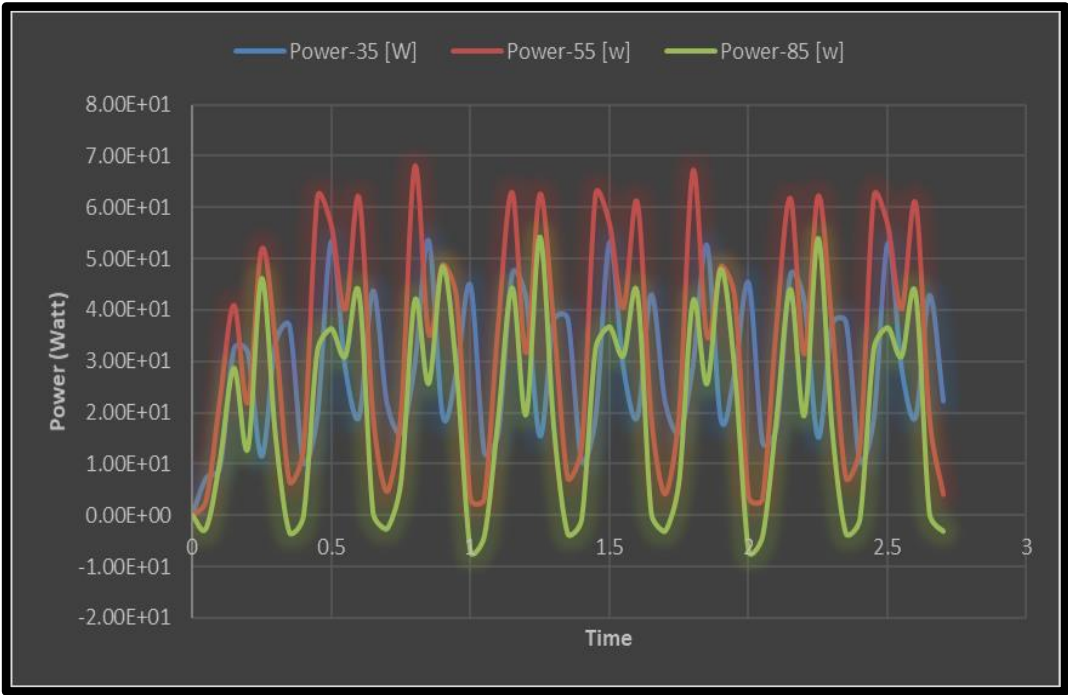


Figure 4.45. Output power comparison of cases [35Deg, 55Deg, 85Deg].

PART 5

CONCLUSION

- Within the framework of this thesis, the computer program which called “*Al-Hashem VAWT Soft*” that was designed works very effectively in terms of the quality of the results, the accuracy and the speed of the analysis processes. It can successfully predict the power factories of three types of vertical aerodynamic cycles: *Parabolic-Darrieus*, *H-Darrieus* and *Slant Straight Blade Vertical Axis Wind Turbine SS-VAWT*.
- The highest value of the power factor of the rotor is achieved in the angular range of blades $\beta=45^\circ$ to $\beta=55^\circ$.
- The greatest energetic range is achieved when the angles of inclination of the blades are between $\beta=45^\circ$ to $\beta=55^\circ$.
- The SS-VAWT achieves the best starting torque when the blades are inclined between 25° and 45° , so this range has the advantage in reducing self-starting problem.
- Theoretically, according to computer program results, the geometrical variables N and C can be dealt with as one geometric variable “ $N*C$ ” when studying their effect on the performance SS-VAWT rotor whose blades are angled outward.
- The value of the diameter of the rotor R had the strongest effect on the performance C_p of the SS-VAWT rotor compared to the effect of changing other dimensions such as the number of blades N , the length of the blade section C and the height H of the SS-VAWT rotor.
- Under the same conditions in terms of the geometric similarity of the cases Darrieus, H Darrieus and SS-VWAT, the latest system is the best in terms of maximum power factor value, energy range and start of rotational motion.

- When studying the effect of aerodynamic forces on the rotor structure, the revolution per minute *RPM* and power output using the *Ansys Fluent*, it was found that the case *55 Degree* is the best design available here for many reasons:
 1. Case *35⁰*:
 - ✓ Has the minimum Z-Force (preferable)
 - ✓ Has the minimum X-Force (preferable)
 - ✓ Has the maximum Y-Force (Not preferable)
 - ✓ Has an average power output.
 2. Case *85⁰*:
 - ✓ Has the maximum Z-Force (Not preferable).
 - ✓ Has the minimum Y-Force (preferable).
 - ✓ Has the maximum X-Force (Not preferable).
 - ✓ Has the minimum power output.
 - ✓ Case *85Deg.* has another critical problem that it has a reversed moment in some part of the revolution that causes noise and increases the dangers of fatigue failure due to the twisting moments applied on the axis. Due to this problem case *85Deg* is suspended from the comparison.
 3. Case *55⁰*:
 - ✓ It has an average accepted range of forces in the three directions.
 - ✓ It has the maximum Power output.
 - ✓ It does not have a reversed direction moment as in case *85Deg.*

5.1. FUTURE WORK

- The *Sannuga System SS-VAWT 01* can be developed by conducting practical experiments in the *Wind Tunnel* for several different geometric shapes.
- Structural analyzes can be performed in *Wind Tunnel* to determine the extent to which aerodynamic and mechanical loads affect the rotor in terms of stresses, strain, crack, buckling and torsion.

- *Field tests* can be carried out by connecting a generator with a rated capacity of 300-400 watts and connecting other basic units, electronic and electrical, such as inverter, charge regulator, batteries and electrical loads for a purpose to conduct studies from the electrical side, such as the practical calculation of the energy extracted from the system, by connecting the *Sannuga System SS-VAWT 01* with a *full-diagram* in an area with suitable winds during a period of time not less than six months.
- *Solar panels* can be connected to the *Sannuga System SS-VAWT 01* to become a *hybrid system*, and then studies can be carried out on it.

REFERNCES

1. IRENA, "Future of wind: Deployment, investment, technology, grid integration and socio-economic aspects," *International Renewable Energy Agency*, Abu Dhabi, 2019.
2. J. Lee and F. Zhao, "GLOBAL WIND REPORT 2021," *Global Wind Energy Council*, Belgium, 2021.
3. Tony Burton, Nick Jenkins, David Sharpe and Ervin Bossanyi, *Wind Energy Handbook*, Second Edition, U.S.: John Wiley & Sons, Ltd, 2011.
4. R. N. Thomas Corke, *Wind Energy Design*, vol. ISBN 9781138096028, U.S.: CRC Press, 2018, p. 352.
5. J. Damota, I. Lamas, A. Couce, J. Rodríguez, "Vertical Axis Wind Turbines: Current Technologies and Future Trends," in *International Conference on Renewable Energies and Power Quality (ICREPQ'15)*, Coruna, 2015.
6. Z. Shahan, "History of Wind Turbines," 2014. [Online]. Available: <https://www.renewableenergyworld.com/storage/history-of-wind-turbines/#gref>.
7. P. Schaffarczyk, Introduction to Wind Turbine Aerodynamics, Vols. ISBN 978-3-642-36409-9, Kiel, Germany: *Springer*, 2014.
8. S. Rehman, M. Alam, L. Alhems and M. Rafique, "Horizontal Axis Wind Turbine Blade Design Methodologies for Efficiency Enhancement—A Review," *Energies*, vol. 11, no. <https://doi.org/10.3390/en11030506>, p. 506, 2018.
9. Kumar, P.M., Sivalingam, K., Narasimalu, S., Lim, T.-C., Ramakrishna, S. and Wei, H, "A Review on the Evolution of Darrieus Vertical Axis Wind Turbine: Small Wind Turbines," *Journal of Power and Energy Engineering*, vol. 7, pp. 27-44, 2019.
10. Muhammad Bhutta, Nasir Hayat, Ahmed Farooq, Zain Ali, Sh. Rehan Jamil, Zahid Hussain, "Vertical axis wind turbine – A review of various configurations and design techniques," *Renewable and Sustainable Energy Reviews*, vol. 16, no. 4, pp. 1926-1939, 2012.
11. T. Dang, "Introduction, history, and theory of wind power," in *41st North American Power Symposium*, Starkville, MS, 2009.

12. Tjiu, Willy & Marnoto, Tjukup & Sohif, Mat & Ruslan, M.H. & Sopian, Kamaruzzaman, "Darrieus vertical axis wind turbine for power generation I: Assessment of Darrieus VAWT configurations," *Renewable Energy*, vol. 75, p. 50–67, 2015.
13. Thomas D. Ashwill, Timothy M. Leonard, "Developments in Blade Shape Design for a Darrieus Vertical Axis Wind Turbine," *Sandia National Laboratories*, Albuquerque, New Mexico, 1986.
14. Emil G. Kaldlec, "Characteristics of Future Vertical Axis Wind Turbines," *Sandia National Laboratories*, Albuquerque, New Mexico, 1982.
15. B. F. BLACKWELL, "THE VERTICAL-AXIS WIND TURBINE "HOW IT WORKS"," *Sandia Laboratories*, Albuquerque, New Mexico, 1974.
16. R. Templin, "Aerodynamic Performance Theory for the NRC Vertical-Axis Wind Turbine," *National Aeronautical Establishment*, LTR-LA-160, Canada, 1974.
17. G. Darrieus, "Turbine Having Its Rotating Shaft Transverse to the Flow of the Current," *Patent* 1835018, 8, U.S., 1931.
18. R. Templin and R. Rangi, "Vertical-axis wind turbine development in Canada," *IEE Proc*, Canada, 1983.
19. Adamek and S. Tudor, "A Brief History of Wind Power Development in Canada 1960–1990s," *Canada Science and Technology Museum: Ottawa, ON, Canada*, 2015.
20. J. Naar, "The new wind power," *Passive and Low Energy Alternatives I; Elsevier*, pp. pp. 12-11–12-16., 1982.
21. Paraschivoiu, *Wind Turbine Design: With Emphasis on Darrieus Concept*, QC, CANADA: *Presses Internationals Polytechnique*: Montréal, 2002.
22. L. Schienbein, "Development and testing of the DAF Indal 6400–6500 kW VAWT," *Intersol Eighty-Five; Elsevier*, p. pp. 2172–2176, 1986.
23. P. Penna, "The DAF Indal ltd. series 6400 VAWT at the Atlantic wind test site: Performance and structural dynamic test data," *Intersol Eighty-Five; Elsevier*, p. pp. 2167–2171, 1986.
24. D. Malcolm, "Structural Response of the DAF Indal 6400 VAWT," in *Fourth Asme Wind Energy Symposium*, NY, USA, 1985.
25. L. Schienbein and D. Malcolm, "Design, performance, and economics of 50-kW and 500-kW vertical axis wind turbines," *J. Sol. Energy Eng*, vol. 105, p. 418–424, 1983.

26. D. Indal., "<http://www.wind-works.org/cms/index.php?id=501>," 2019. [Online].
27. M. Wehrey and S. Yinger, "Demonstration testing of the daf indal ltd, 50 kw vertical axis wind turbine generator—A fourteen-month experience," in *ASME Wind Energy Symposium*, Amer Society of Mechanical: New York, 1983.
28. H. Sutherland, D. Berg and T. Ashwill, "A Retrospective of VAWT Technology," *Sandia National Laboratories*: Albuquerque, NM, USA, 2012.
29. P. Klimas, H. Dodd and R. Clark, "An overview of the DOE/SANDIA/USDA vertical axis wind turbine Test Bed Project," in In *Proceedings of the Windpower '87*, San Francisco, CA, USA, 1987.
30. J. S. F. Johnston, "Proceedings of the Vertical Axis Wind Turbine (VAWT) Design Technology Seminar for Industry," *Sandia Laboratories*: Albuquerque, NM, USA, 1980.
31. W. Liu, I. Paraschivoiu and R. Martinuzzi, "Calculation of dynamic stall on sandia 34-m VAWT using an indicial model," *Wind Engineering*, vol. 16, p. 313–325, 1992.
32. H. Dodd, T. Ashwill, D. Berg, M. Ralph, W. Stephenson and P. Veers, "Test Results and Status of the DOE/Sandia 34-M VAWT Test Bed," *Sandia National Laboratories*: Albuquerque, NM, USA, 1989.
33. M. Ralph, "Control of the variable speed generator on the Sandia 34-metre vertical axis wind turbine," *Windpower'89*, no. San Francisco, CA, USA, p. 24–27, 1989.
34. D. Berg, "Structural Design of the Sandia 34-Meter Vertical-Axis Wind Turbine," *Sandia National Laboratories*: Albuquerque, NM, USA, 1985.
35. T. Ashwill, "Structural design and fabrication of the Sandia 34-meter Vertical Axis Wind Turbine," in *ASME/JSME/ISES Solar Energy Conference*, Honolulu, HI, USA, 1987.
36. T. Ashwill, "Measured Data for the Sandia 34-Meter Vertical Axis Wind Turbine," *Sandia National Laboratories*: Albuquerque, NM, USA, 1992.
37. J. Damota, I. Lamas, A. Couce and J. Rodriguez, "Vertical Axis Wind Turbines: Current Technologies and Future Trends," in In *Proceedings of the International Conference on Renewable Energies and Power Quality (ICREPQ'15)*, La Coruña, Spain, 2015.
38. A. A. 5. kW, "<http://www.wind-works.org/cms/index.php?id=504>," 2019. [Online].

39. E. Möllerström, P. Gipe, J. Beurskens and F. Ottermo, "A historical review of vertical axis wind turbines rated 100 kW and above," *Renew. Sustain. Energy Rev*, vol. 105, p. 1–13, 2019.
40. V. 6. kW, "<http://www.wind-works.org/cms/index.php?id=719>," 2019. [Online].
41. V. 9. kW, "<http://www.wind-works.org/cms/index.php?id=505>," 2019. [Online].
42. K. Touryan, J. Strickland and D. Berg, "Electric power from vertical-axis wind turbines," *J. Propuls. Power*, vol. 3, p. 481–493, 1987.
43. FloWind, "<http://www.wind-works.org/cms/index.php?id=509>," 2019. [Online].
44. S. Eriksson, H. Bernhoff and M. Leijon, "Evaluation of different turbine concepts for wind power," *Renew. Sustain Energy Rev*, vol. 12, p. 1419–1434, 2008.
45. J. Hulls, "Vertical Axis Wind Turbine with Blade Tensioner," *Patent* 5531567A, U.S., 1996.
46. M. D'Ambrosio and M. Medaglia, "Vertical Axis Wind Turbines: History, Technology and Applications. Master's Thesis," *Halmstad University*, Halmstad, Sweden, 2010.
47. V. Wallace, M. McMullen and W. Archibald, "Vertical Axis Wind Turbine with Pultruded Blades," *Patent* 5375324A, U.S, 1994.
48. T. Carne, J. Lauffer and A. Gomez, "Modal Testing the EOLE," *Sandia National Laboratories*: Albuquerque, NM, USA, 1987.
49. Eole, "<http://www.wind-works.org/cms/index.php?id=506>," 2019. [Online].
50. H.VAWT, "<https://www.mwps.world/market/offered/industrial-wind-turbines/heidelberg-wind-turbines-for-sale-refurbishing-available/>," 2019. [Online].
51. P. Musgrove, Wind Power, UK: *Cambridge University Press*: Cambridge, 2009.
52. T. Price, "UK large-scale wind power programme from 1970 to 1990: The Carmarthen Bay experiments and the musgrove vertical-axis turbines," *Wind Eng*, vol. 30, no. <https://doi.org/10.1260/030952406778606214>, p. 225–242, 2006.

53. C. Morgan, P. Gardner, I. Mays and M. Anderson, "The demonstration of a stall regulated 100 kW vertical axis wind turbine," in In *Proceedings of the European Wind Energy Conference*, Glasgow, UK, 1989.
54. P. Musgrove, "Wind energy conversion: Recent progress and future prospects," *Solar Wind Technol*, vol. 4, no. [https://doi.org/10.1016/0741-983X\(87\)90006-3](https://doi.org/10.1016/0741-983X(87)90006-3), p. 37–49, 1987.
55. P. Kumar, S. Rashmitha, N. Srikanth and T.-C. Lim, "Wind Tunnel Validation of Double Multiple Streamtube Model for Vertical Axis Wind Turbine," *Smart Grid and Renewable Energy*, vol. 8, no. 10.4236/sgre.2017.812027, p. 412–424, 2017.
56. M. VAWT, "https://www.researchgate.net/figure/Major-components-of-Musgroverotor-rotor-49_fig16_266799978," 2019. [Online].
57. I. Mays, C. Morgan, M. Anderson and S. Powles, "The 500 kW VAWT 850 is now operating," *Mod. Power Syst*, vol. 10, p. 53–55, 1990.
58. "Aerogenerator Turbine Sets Sail for a Greener Future," 2019. [Online]. Available: <http://www.guardian.co.uk/technology/2008/jan/29/wind.energy.aerogenerator>.
59. A. VAWT, 2019. [Online]. Available: <http://eprints.whiterose.ac.uk/79230/1/ener166-007.pdf>.
60. A. X. L. b. W. P. L. W. P. Ltd, "<https://www.scribd.com/document/155485918/Aerogenerator-X-Release-26-07-10>," 2019. [Online].
61. A. Shires, "Design optimization of an offshore vertical axis wind turbine," *Proceedings of the Institution of Civil Engineers -Energy*, vol. 166, no. <https://doi.org/10.1680/ener.12.00007>, pp. 7-18, 2013.
62. V. W. AB, 2019. [Online]. Available: <http://www.verticalwind.se/teknik/>.
63. S. Apelfröjd, S. Eriksson and H. Bernhoff, "A review of research on large scale modern vertical axis wind turbines at Uppsala University," *Energies*, vol. 9, no. <https://doi.org/10.3390/en9070570>, p. 570, 2016.
64. J. Kjellin and H. Bernhoff, "Electrical starter system for an H-rotor type VAWT with PM-generator and auxiliary winding," *wind energy*, vol. 35, no. <https://doi.org/10.1260/0309-524X.35.1.85>, p. 85–92, 2011.
65. E. Möllerström, F. Ottermo, J. Hylander and H. Bernhoff, "Eigen frequencies of a vertical axis wind turbine tower made of laminated wood and the effect upon attaching guy wires," *wind energy*, vol. 38, no. <https://doi.org/10.1260/0309-524X.38.3.277>, p. 277–289, 2014.

66. E. Möllerström, F. Ottermo, J. Hylander and H. Bernhoff, "Noise emission of a 200-kW vertical axis wind turbine," *Energies*, vol. 9, no. <https://doi.org/10.3390/en9010019>, 2016.
67. F. Ottermo, E. Möllerström, A. Nordborg, J. Hylander and H. Bernhoff, "Location of aerodynamic noise sources from a 200-kW vertical-axis wind turbine," *Journal of Sound and Vibration*, no. <https://doi.org/10.1016/j.jsv.2017.03.033>, p. 154–166, 2017.
68. E. Möllerström, S. Larsson, F. Ottermo, J. Hylander and L. Bååth, "Noise propagation from a vertical axis wind turbine," in In Proceedings of the **43rd International Congress on Noise Control Engineering**, Melbourne, Australia, 2014.
69. Skwid, 2019. [Online]. Available: <https://newatlas.com/skwid-wind-tidal-power-japan/27559/>.
70. P. Mohan Kumar, M. Surya, S. Narasimalu and T.-C. Lim, "Experimental and numerical investigation of novel Savonius wind turbine," *wind energy*, vol. 43, no. <https://doi.org/10.1177/0309524X18780392>, p. 247–262, 2019.
71. H. F. V. S. o. J. Coast, 2019. [Online]. Available: <https://www.windpoweroffshore.com/article/1327126/japanese-hybrid-floating-turbine-sinks>.
72. M. R. S. S. Unit, 2019. [Online]. Available: <https://marineenergy.biz/2015/06/03/moderetrieves-sunken-skwid-unit/>.
73. P. Kumar, M. Surya, R. Kethala and N. Srikanth, "Experimental Investigation of The Performance of Darrieus Wind Turbine with Trapped Vortex Airfoil," in In Proceedings of the 2017 **3rd International Conference on Power Generation Systems and Renewable Energy Technologies (PGSRET)**, Johor Bahru, Malaysia, 2017.
74. VertAxWind, 2019. [Online]. Available: <http://vertaxwind.com>.
75. V. W. Blades, 2019. [Online]. Available: <http://vertaxwind.com/technology.php#blades>.
76. O. Keysan, A. McDonald, M. Mueller, R. Doherty and M. C.-G. Hamilton, " a lightweight direct drive generator for marine energy converters," in In Proceedings of the **5th IET International Conference on Power Electronics, Machines and Drives (PEMD)**, Brighton, UK, 2010.
77. V. W. E. Generation, <http://vertaxwind.com/technology.php#electrical>, 2019.
78. V. W. Crane, 2019. [Online]. Available: <http://vertaxwind.com/technology.php#crane>.

79. VertiWind, 2019. [Online]. Available:
<http://www.sunwindenergy.com/news/vertical-axis-turbines-mediterranean>.
80. [Vertiwind-Data, 2019. [Online]. Available:
<https://www.windpowerengineering.com/design/floating-vertical-axis-turbine-makes-waves-in-europe/>.
81. Vertiwind, 2019. [Online]. Available:
<https://www.windpoweroffshore.com/article/1462375/vertical-axis-firm-nenuphar-enters-liquidation>.
82. A. 1. ANEW-S1, 2019. [Online]. Available:
<https://www.anew-institute.com/vertical-wind-turbine.html>.
83. A. 2. ANEW-M1, 2019. [Online]. Available:
<https://www.anew-institute.com/anev-m1-vawt.html>.
84. S. Eriksson, H. Bernhoff and M. Bergkvist, "Design of a unique direct driven PM generator adapted for a telecom tower wind turbine," *Renewable Energy*, vol. 44, no. https://doi.org/10.1016/j.renene.2012.01.090, p. 453–456, 2012.
85. A. 1. ANEW-B1, 2019. [Online]. Available:
<https://www.anew-institute.com/anev-b1-vawt.html>.
86. M. R.J And Guillotte.R. J, "Wind Tunnel Investigation of A 14' Vertical Axis Windmill," *National Aeronautics and Space Administration Mncley Research Center*, Virginia, 1976.
87. Dominy, R., Lunt, P., Bickerdyke, A., Dominy, J, "Self-starting capability of a Darrieus turbine," *Journal of Power and Energy*, vol. 221, no. 1, p. 111–120, 2007.
88. Zhu, J., Huang, H., & Shen, H, "Self-starting aerodynamics analysis of vertical axis wind turbine," *Advances in Mechanical Engineering*, vol. 7, no. 12, 2015.
89. Omar S. Mohamed, Ahmed A. Ibrahim, Ahmed K. Etman, Amr A. Abdelfatah, Ahmed M.R. Elbaz, "Numerical investigation of Darrieus wind turbine with slotted airfoil blades," *Energy Conversion and Management: X*, vol. 5, no. 100026, 2020.
90. J. Krishnaraj, Sivakumar Ellappan, M. Anil Kumar, "Additive Manufacturing of a Gorlov Helical Type Vertical Axis Wind Turbine," *International Journal of Engineering and Advanced Technology (IJEAT)*, vol. 9, no. 2, 2019.
91. R. Gupta and A. Biswas, "Performance Measurement of a Twisted Three-Bladed Airfoil-Shaped H-Rotor," *International Journal of Renewable Energy Technology*, vol. 1, no. 3, pp. 279-300, 2010.

92. W. Moran, "Giromill Wind Tunnel Test and Analysis," *McDonnell Aircraft Corporation*, St. Louis, Missouri, 1977.
93. J. Baker, "Features to Aid or Enable Self Starting of Fixed Pitch Low Solidity Vertical Axis Wind Turbines," *Journal of Wind Engineering and Industrial Aerodynamics*, vol. 15, no. [https://doi.org/10.1016/0167-6105\(83\)90206-4](https://doi.org/10.1016/0167-6105(83)90206-4), pp. 369-380, 1983.
94. S. Worasinchai, G. Ingram and R. Dominy, "The Physics of H-Darrieus Turbine Starting Behaviour," in Proceedings of the *ASME Turbo Expo 2014*, Düsseldorf, Germany, 2014.
95. R. Bos, "Self-Starting of a Small Urban Darrieus Rotor," *Delft University of Technology*, Delft, Netherlands, 2012.
96. S.-M. Hwang, J.-B. Eom, Y.-H. Jung, D.-W. Lee and B.-S. Kang, "Various Design Techniques to Reduce Cogging Torque by Controlling Energy Variation in Permanent Magnet Motors," *IEEE Transactions on Magnetics*, vol. 37, no. <https://doi.org/10.1109/20.951313>, pp. 2806-2809, 2001.
97. A. Hansen, F. Iov, F. Blaabjerg and L. Hansen, "Review of Contemporary Wind Turbine Concepts and Their Market Penetration," *Wind Engineering*, vol. 28, no. <https://doi.org/10.1260/0309524041590099>, pp. 247-263, 2004.
98. H. Li and Z. Chen, "Overview of Different Wind Generator Systems and Their Comparisons," *IET Renewable Power Generation*, vol. 2, no. <https://doi.org/10.1049/iet-rpg:20070044>, pp. 123-138, 2008.
99. B. Blackwell, R. Sheldahl and L. Feltz, "Wind Tunnel Performance Data for the Darrieus Wind Turbine with NACA 0012 Blades," *Sandia National Laboratories*, Albuquerque, New Mexico, Livermore, CA, 1976.
100. M. Islam, D. Ting and A. Fartaj, "Desirable Airfoil Features for Smaller Capacity Straight-Bladed VAWT," *Wind Engineering*, vol. 31, no. <https://doi.org/10.1260/030952407781998800>, pp. 165-196, 2007.
101. C. Ferreira and B. Geurts, "Aerofoil Optimization for Vertical-Axis Wind Turbines," *Wind Energy*, vol. 18, no. <https://doi.org/10.1002/we.1762>, pp. 1371-1385, 2015.
102. R. Gupta and K. Sharma, "Flow Physics of a Combined Darrieus-Savonius Rotor Using Computational Fluid Dynamics (CFD).," *International Research Journal of Engineering Science*, Technology and Innovation, vol. 1, pp. 1-13, 2012.
103. "<https://en.wind-turbine-models.com/turbines/358-dornier-darrieus-savonius-5-5-kw>," 1979. [Online].

104. Y. Kyojuka, "An Experimental Study on the Darrieus-Savonius Turbine for the Tidal Current Power Generation," *Journal of Fluid Science and Technology*, vol. 3, pp. 439-449, 2008.
105. T. Wakui, Y. Tanzawa, T. Hashizume and T. Nagao, "Hybrid Configuration of Darrieus and Savonius Rotors for Stand-Alone Wind Turbine-Generator Systems," *Electrical Engineering in Japan*, vol. 150, no. <https://doi.org/10.1002/eej.20071>, pp. 13-22, 2005.
106. S. Rassoulinejad-Mousavi, M. Jamil and M. Layeghi, "Experimental Study of a Combined Three Bucket H-Rotor with Savonius Wind Turbine," *World Applied Sciences Journal*, vol. 28, pp. 205-211, 2013.
107. R. Gupta, R. Das and K. Sharma, "Experimental Study of a Savonius-Darrieus Wind Machine," in Proceedings of the *International Conference on Renewable Energy for Developing Countries*, Washington, 2006.
108. I. Chopra, "Review of State of Art of Smart Structures and Integrated Systems," *AIAA Journal*, vol. 40, no. <https://doi.org/10.2514/2.1561>, pp. 2145-2187, 2002.
109. P. Jain and A. Abhishek, "Performance prediction and fundamental understanding of small-scale vertical axis wind turbine with variable amplitude blade pitching," *Renewable Energy*, Vols. ISSN 0960-1481, no. <https://doi.org/10.1016/j.renene.2016.05.056>., pp. 97-113, 2016.
110. B. Kirke and L. Lazauskas, "Enhancing the Performance of Vertical Axis Wind Turbine Using a Simple Variable Pitch System," *Wind Engineering*, vol. 15, pp. 187-195, 1991.
111. P. Chougule, S. Nielsen and B. Basu, "Active Blade Pitch Control for Straight Bladed Darrieus Vertical Axis Wind Turbine of New Design," *Key Engineering Materials*, vol. 569, no. <https://doi.org/10.4028/www.scientific.net/KEM.569-570.668>, pp. 668-675, 2013.
112. I. Hwang, S. Min, Y. Lee and S. Kim, "Efficiency Improvement of a New Vertical Axis Wind Turbine by Individual Active Control of Blade Motion," in Proceedings of *SPIE—The International Society for Optical Engineering*, San Diego, California, United States, 2006.
113. M. Elkhoury, T. Kiwata and E. Aoun, "Experimental and Numerical Investigation of a Three-Dimensional Vertical-Axis Wind Turbine with Variable-Pitch.," *Journal of Wind Engineering and Industrial Aerodynamics*, vol. 139, no. <https://doi.org/10.1016/j.jweia.2015.01.004>, pp. 111-123, 2015.
114. I. Paraschivoiu, O. Trifu and F. Saeed, "H-Darrieus Wind Turbine with Blade Pitch Control," *International Journal of Rotating Machinery*, vol. 505343, no. <https://doi.org/10.1155/2009/505343>, 2009.

115. A. Gorlov, "Development of the Helical Reaction Hydraulic Turbine," *Northeastern University*, Boston, 1998.
116. M. Shiono, K. Suzuki and S. Kiho, "Output Characteristics of Darrieus Water Turbine with Helical Blades for Tidal Current Generations," in The *Twelfth International Offshore and Polar Engineering Conference*, Kitakyushu, Japan, 2002.
117. B. Blackwell and G. Reis, "Blade Shape for a Troposkien Type of Vertical Troposkien Type of Vertical-," *Sandia National Laboratories*, New Mexico, Livermore, CA., 1974.
118. M. Kumar, M. Surya, N. Sin and N. Srikanth, "Design and Experimental Investigation of Airfoil for Extruded Blades," *International Journal of Advances in Agricultural and Environmental Engineering (IJAAEE)*, vol. 3, no. <https://doi.org/10.15242/IJAAEE.U1216208>, 2017.
119. P. Purser and M. Spearman, "Wind-Tunnel Tests at Low Speed of Swept and Yawed Wings Having Various Plan Forms," *The National Aeronautics and Space Administration*, Washington DC., 1951.
120. Q. Revolution, "Quiet Revolution," 2009. [Online]. Available: <https://www.quietrevolution.com/>.
121. M. Castelli, A. Dal Monte, M. Quaresimin and E. Benini, "Numerical Evaluation of Aerodynamic and Inertial Contributions to Darrieus Wind Turbine Blade Deformation," *Renewable Energy*, vol. 51, no. <https://doi.org/10.1016/j.renene.2012.07.025>, pp. 101-112, 2013.
122. Turby, 2009. [Online]. Available: <https://www.turby.nl/>.
123. D. E. Berg, "Vertical-axis wind turbines -- The current status of an old technology," 1996. [Online]. Available: <https://www.osti.gov/biblio/432928>.
124. R. E. Wilson, P. B. S. Lissaman and S. N. Walker, "Aerodynamic Performance of Wind Turbines. *Final Report*," United States: N. p., 1976. Web. doi:10.2172/7315651, 1976.
125. P. N. Shankar, "On the aerodynamic performance of a class of vertical shaft windmills," Proceedings of the Royal Society of London. Series A, *Mathematical and Physical Sciences*, vol. Vol. 349, no. No. 1656, pp. 35-51, 1976.
126. P. C. Klimas and R. E. Sheldahl, "Four aerodynamic prediction schemes for vertical-axis wind turbines: a compendium," United States: N. p., 1978. Web., 1978.
127. Strickland, J H, "The Darrieus Turbine: A Performance Prediction Model Using Multiple Streamtubes," *Sandia Laboratories*, Albuquerque, New Mexico, 1975.

128. Paraschivoiu, I., "Double-Multiple Streamtube Model for Darrieus Wind Turbines," in *Institute de Recherche* de l'Hydro-Quebec, Quebec, 1981.
129. Brownlee and B. Gene, "A vortex model for the vertical axis wind turbine," *Texas Tech University*, <http://hdl.handle.net/2346/10123>, 1988.
130. A. Allet, M. Brahim and I. Paraschivoiu, "On the Aerodynamic modeling of a VAWT," *Wind Engineering*, vol. 21(6), no. <http://www.jstor.org/stable/43749657>, pp. 351-365, 1997.
131. C. Liang, D. Xi, S. Zhang, B. Chen, X. Wang and Q. Guo, "Optimization on Airfoil of Vertical Axis Wind Turbine Based on CST Parameterization and NSGA-II Aigorithm," *Preprints*, doi: [10.20944/preprints201608.0136.v1](https://doi.org/10.20944/preprints201608.0136.v1), 2016.
132. R. E. Sheldahl and P. C. Klimas, "Aerodynamic characteristics of seven symmetrical airfoil sections through 180-degree angle of attack for use in aerodynamic analysis of vertical axis wind turbines," doi:[10.2172/6548367](https://doi.org/10.2172/6548367), United States: N. p, 1981.
133. K. Rogowski, M. O. Hansen and R. Maroński, "Steady and Unsteady Analysis Of NACA 0018 Airfoil In Vertical-Axis Wind Turbine," *Journal of Theoretical and Applied Mechanics*, vol. 56, no. 10.15632/jtam-pl.56.1.203, pp. 203-212, 2018.
134. N. C. Batista, R. Melicio and V. M. Mendes, "Darrieus vertical axis wind turbines: methodology to study the self-start capabilities considering symmetric and asymmetric airfoils," *Research on Engineering Structures and Materials*, vol. 4(3), no. DOI: <http://dx.doi.org/10.17515/resm2017.39ds0108>, pp. 189-217, 2018.
135. Hirsch, Ir. H; Mandal, A. C.; "A Cascade Theory for the Aerodynamic Performance of Darrieus Wind Turbines," *Wind Engineering*, vol. 11, no. 3, p. 164–175, 1987.
136. [Online]. Available: <https://www.worldweatheronline.com>.
137. [Online]. Available: www.solidworks.com.
138. P. Kumar, K. Ajit, N. Srikanth and T. Lim, "On the Mathematical Modelling of Adaptive Darrieus Wind Turbine," *Journal of Power and Energy Engineering*, vol. 5, no. <https://doi.org/10.4236/jpee.2017.512015>, pp. 133-158, 2017.
139. Y. Li, "Straight-Bladed Vertical Axis Wind Turbines: History, Performance, and Applications," *IntechOpen*, London, 2019.
140. "Hi-VAWT," 2010. [Online]. Available: http://www.hi-vawt.com.tw/en/ds1500w_photogallery.html.

141. "Cleanfield Energy," 2010. [Online]. Available: <http://savonius-balaton.hupont.hu/43/cleanfield-energy-ontariocanada>.
142. "Apple Wind," 2008. [Online]. Available: <http://www.kde-energy.fr/apple-wind.html>.
143. P. Kumar, M. Surya and N. Srikanth, "On the Improvement of Starting Torque of Darrieus Wind Turbine with Trapped Vortex Airfoil," in **2017 IEEE International Conference on Smart Grid and Smart Cities (ICSGSC)**, Singapore, 2017.
144. P. Kumar, K. Ajit, M. Surya, N. Srikanth and T.-C. Lim, "On the Self-Starting of Darrieus Turbine: An Experimental Investigation with Secondary Rotor," in **2017 Asian Conference on Energy, Power and Transportation Electrification (ACEPT)**, Singapore, 2017.

APPENDIX A.

“AL-HASHEM VAWT” MICROSOFT VISUAL SOFTWARE

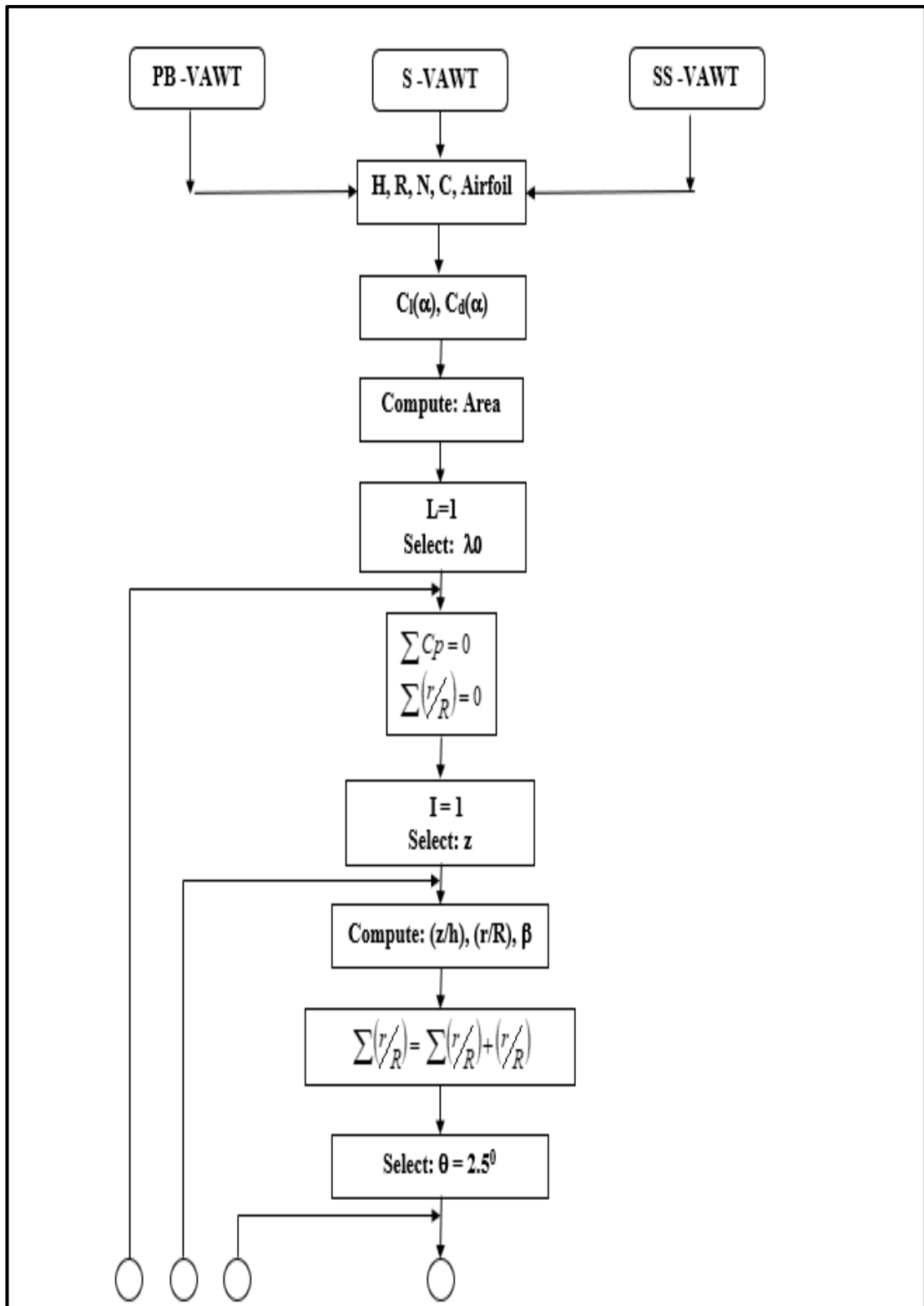


Figure Appendix A.1. AL-Hashem-VAWT Software Flochart.

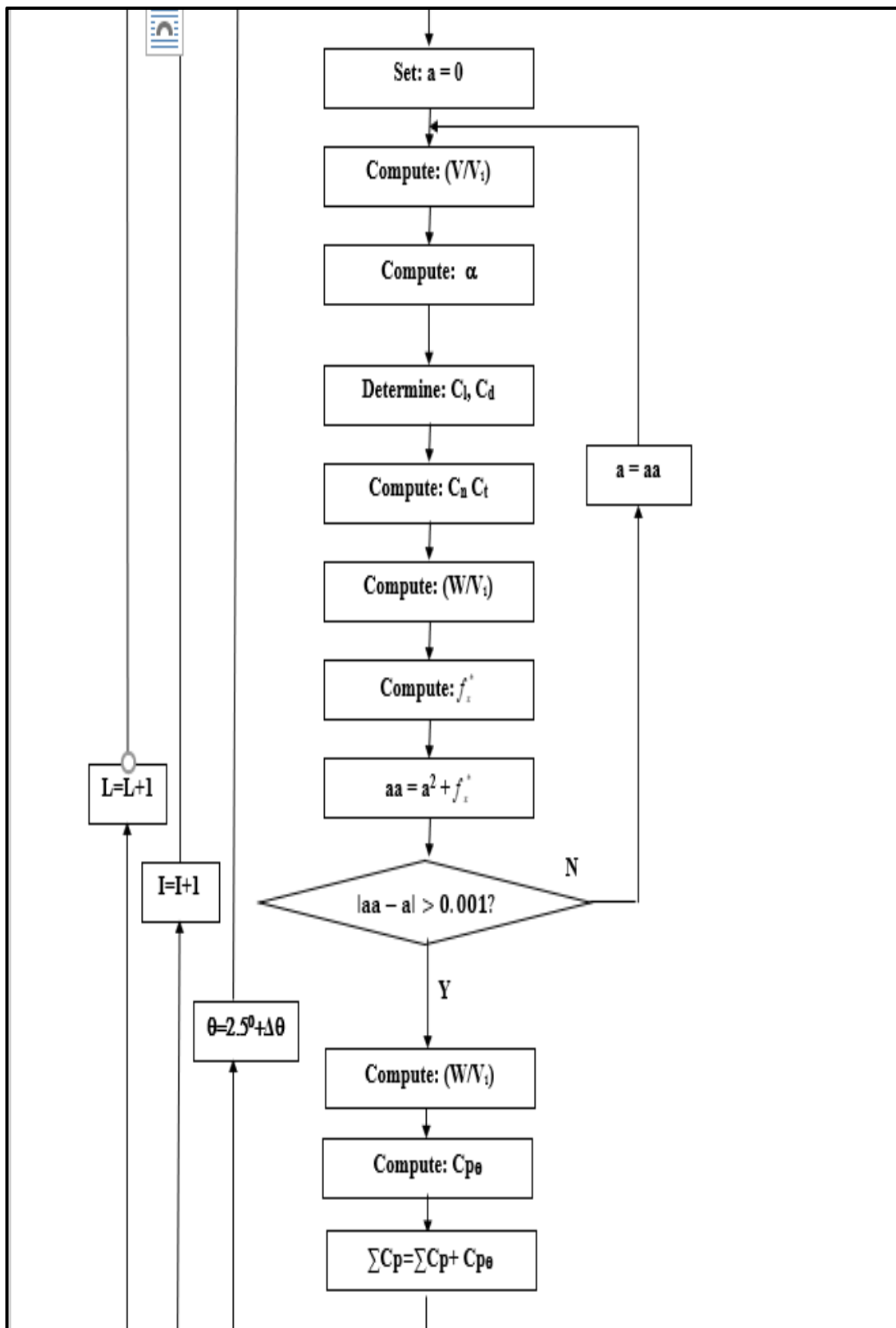


Figure Appendix A.1. Continuing.

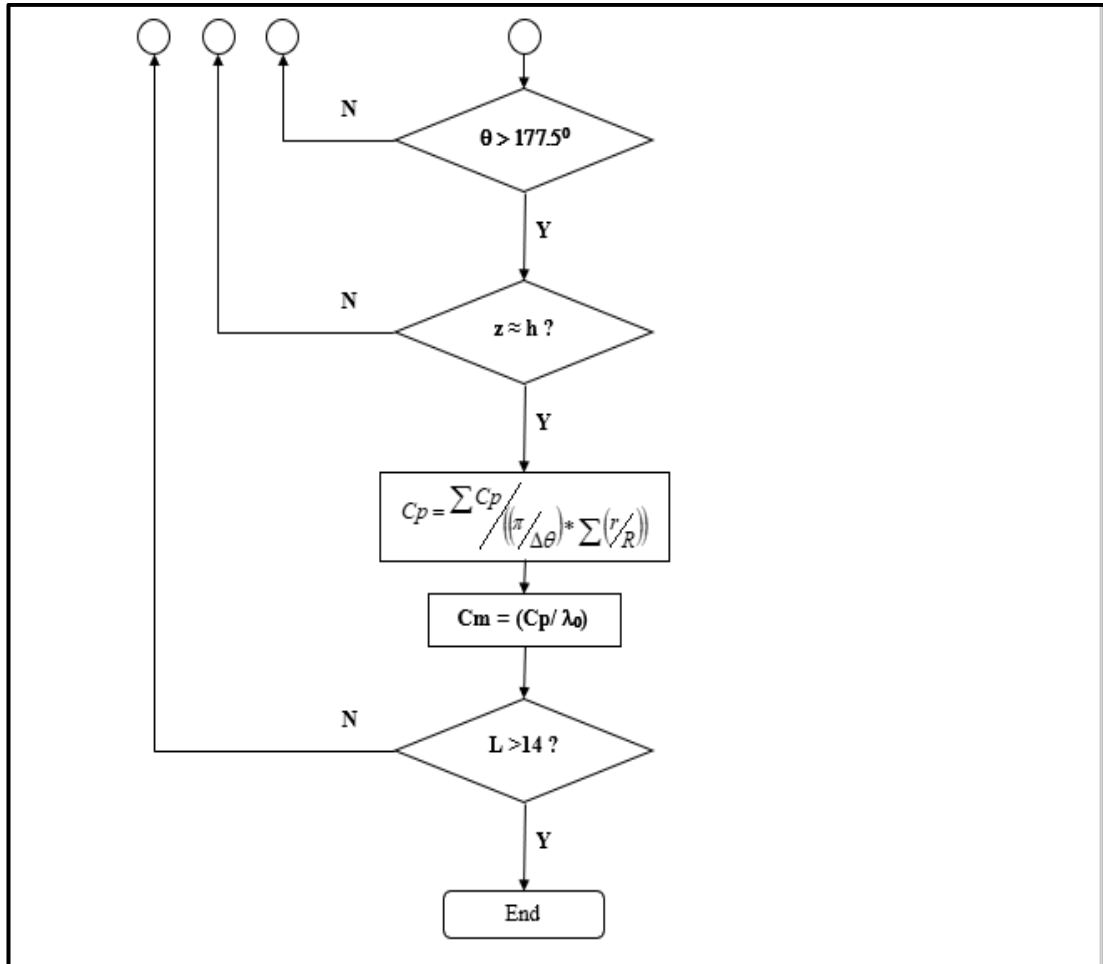


Figure Appendix A.1. (Continuing)

Commands Appendix A.2. AL-Hashem-VAWT Software Commands.

Dim t, S, HR, a, aa, UUinf, Beta, URUINF, Fxs, CFt, CPt, CFSUM, N, Betarad(80),
 k1, k2, row1, nel, dt, R, H, b, c, dz, dtrad, J, ZH(100), rR(100), ri(100), d(100), trad,
 aRad, aDeg, aDegAbs, CN, CT, CL, CD, Cp(30), Cf(30), Cm(30), CpSUM, L,
 rRSUM, Z(100) As Single

Dim X, Y, E, I, nt, M, falg As Integer

Dim xlApp As Excel.Application

Dim wb As Workbook

Dim ws As Worksheet

Dim result1 As Excel.Application

Dim wba As Workbook

Dim wsa As Worksheet

```

Dim var1, var2 As Variant
Private Sub Command2_Click()
Set r1 = db1.OpenRecordset(Text2.Text)
Set xlApp = New Excel.Application
Set result1 = New Excel.Application
Set wba = result1.Workbooks.Open("C:\R.xls")
Set wsa = wba.Worksheets("Sheet1")
H = Val(Text1(0).Text)
R = Val(Text1(1).Text)
N = Val(Text1(2).Text)
c = Val(Text1(3).Text)
nel = 70
nt = 35
dt = 180 / nt
HR = H / R
dtrad = (dt * 3.14159) / 180
S = (N * c) / R
L = 0.2
kkk = 1
Do Until L > 14
J = L
CpSUM = 0
rRSUM = 0
For I = 1 To (nel) Step 1
ZH(I) = (2 * (I - 1)) / (4 * nel)
Z(I) = H * ZH(I)
If Text3(4) = "curved blade" Then
If (I = 1) Then
rR(I) = 0.0001
Else ""
rR(I) = Sin(3.14159 * ZH(I))
End If ""
Else

```

```

If Text3(4) = "slant blade" Then
If (I = 1) Then ""
rR(I) = 1 ""
Else """"
rR(I) = (ZH(I) / ((1 / HR) * Tan(85 * 3.14 / 180))) + 1
End If """"
Else
If Text3(4) = "stright blade" Then
rR(I) = 1
End If
End If
End If
ri(I) = (rR(I)) * R
rRSUM = rRSUM + rR(I)
If Text3(4) = "curved blade" Then
Betarad(I) = Atn((HR) / (3.14159 * Cos(3.14159 * ZH(I))))
Else
If Text3(4) = "slant blade" Then
Betarad(I) = (85 * 3.14 / 180)
Else
If Text3(4) = "stright blade" Then
Betarad(I) = 1.570795
End If
End If
End If
If L = 0.2 Then
wsa.Cells(I + 1, 14).Value = ri(I)
wsa.Cells(I + 1, 15).Value = Z(I)
wsa.Cells(I + 1, 16).Value = (-1 * ri(I))
wsa.Cells(I + 1, 17).Value = ZH(I)
End If
row1 = 1
For t = 2.5 To 177.5 Step 5

```



```

trad = (t * 3.14159 / 180)
a = 0
M = 0
Iteration:
UUinf = 1 - a
aRad = Atn((Sin(trad) * Sin(Betarad(I))) / (Cos(trad) + (J / UUinf) * rR(I)))
If (aRad < 0) Then
aRad = 3.14159 + aRad
End If
aDegAbs = (aRad * 180) / 3.14159
Call CnCt
  URUINF = UUinf * ((Sin(trad) * Sin(Betarad(I))) / Sin(aRad))
  Fxs = S * (1 / (4 * 3.14159 * rR(I))) * (URUINF ^ 2) * (CN - ((CT * Cos(trad)) /
  (Sin(trad) * Sin(Betarad(I))))))
  aa = (a ^ 2) + Fxs
  M = M + 1
  If (M <= 100) And (aa > 1) Then
  UUinf = 0
  a = aa
  ElseIf (M > 100) Then
  UUinf = -UUinf
  a = aa
  ElseIf (M <= 100) And (aa < 1) And (Abs(aa - a) < 0.001) Then
  UUinf = UUinf
  a = aa
  ElseIf (M <= 100) And (aa < 1) And (Abs(aa - a) > 0.001) Then
  a = aa
  GoTo Iteration:
  End If
  URUINF = UUinf * ((Sin(trad) * Sin(Betarad(I))) / Sin(aRad))
  CPt = (CT * S * J * (rR(I)) * (URUINF) ^ 2) / (2 * Sin(Betarad(I)))
  CpSUM = CpSUM + CPt
Next t

```

```

Next I
Cp(J) = (CpSUM / (nt * rRSUM))
Cm(J) = (Cp(J) / J)
wsa.Cells(kkk, 1).Value = L "
wsa.Cells(kkk, 2).Value = Cp(J) ""
wsa.Cells(kkk, 3).Value = Cm(J) ""
wsa.Cells(kkk, 4).Value = Cf(J) ""
kkk = kkk + 1
L = L + 0.2 ""
Loop "
xlApp.Quit
Set ws = Nothing
Set wb = Nothing
Set xlApp = Nothing
wba.Close
result1.Quit
Set wsa = Nothing
Set wba = Nothing
Set result1 = Nothing
End Sub
Public Sub CnCt()
r1.MoveFirst
Do Until r1.EOF
If r1.Fields("no") = 180 Then Exit Do
k1 = Val(r1.Fields("no"))
cl1 = Val(r1.Fields("cl"))
cd1 = Val(r1.Fields("dl"))
r1.MoveNext
k2 = Val(r1.Fields("no"))
cl2 = Val(r1.Fields("cl"))
cd2 = Val(r1.Fields("dl"))
If aDegAbs = k1 Then
    r1.MovePrevious

```

```

CL = Val(r1.Fields("cl"))
CD = Val(r1.Fields("dl"))
Exit Do
Else
If aDegAbs = k2 Then
    CL = Val(r1.Fields("cl"))
    CD = Val(r1.Fields("dl"))
    Exit Do
Else
    If (aDegAbs > k1) And (aDegAbs < k2) Then
        CL = c11 - ((c11 - c12) * (k1 - aDegAbs)) / (k1 - k2)
        CD = cd1 - ((cd1 - cd2) * (k1 - aDegAbs)) / (k1 - k2)
        Exit Do
    End If
End If
End If
Loop
CN = (CL * Cos(aRad)) + (CD * Sin(aRad))
CT = (CL * Sin(aRad)) - (CD * Cos(aRad))
If I = 2 And L = 0.2 Then
wsa.Cells(row1, 5).Value = t
wsa.Cells(row1, 6).Value = aDegAbs
wsa.Cells(row1, 7).Value = CL
wsa.Cells(row1, 8).Value = CD
wsa.Cells(row1, 9).Value = CN
wsa.Cells(row1, 10).Value = CT
wsa.Cells(row1, 18).Value = a
row1 = row1 + 1
End If
If I = 2 And L = 3 Then
wsa.Cells(row1, 19).Value = a
row1 = row1 + 1
End If

```

```
If I = 2 And L = 5 Then
wsa.Cells(row1, 20).Value = a
row1 = row1 + 1
End If

If I = 2 And L = 7 Then
wsa.Cells(row1, 21).Value = a
row1 = row1 + 1
End If

If I = 2 And L = 9 Then
wsa.Cells(row1, 22).Value = a
row1 = row1 + 1
End If

End Sub

Private Sub Form_Load()
Set db1 = OpenDatabase("c:\DATA BASE OF AIRFOIL.mdb")
End Sub

Private Sub Frame1_DragDrop(Source As Control, X As Single, Y As Single)
End Sub

Private Sub Text2_Change()
End Sub

Private Sub Text3_Change(Index As Integer)
End Sub
```

APPENDIX B.

“SANNUGA SYSTEM SS-VAWT 01” SOLIDWORKS DESIGN

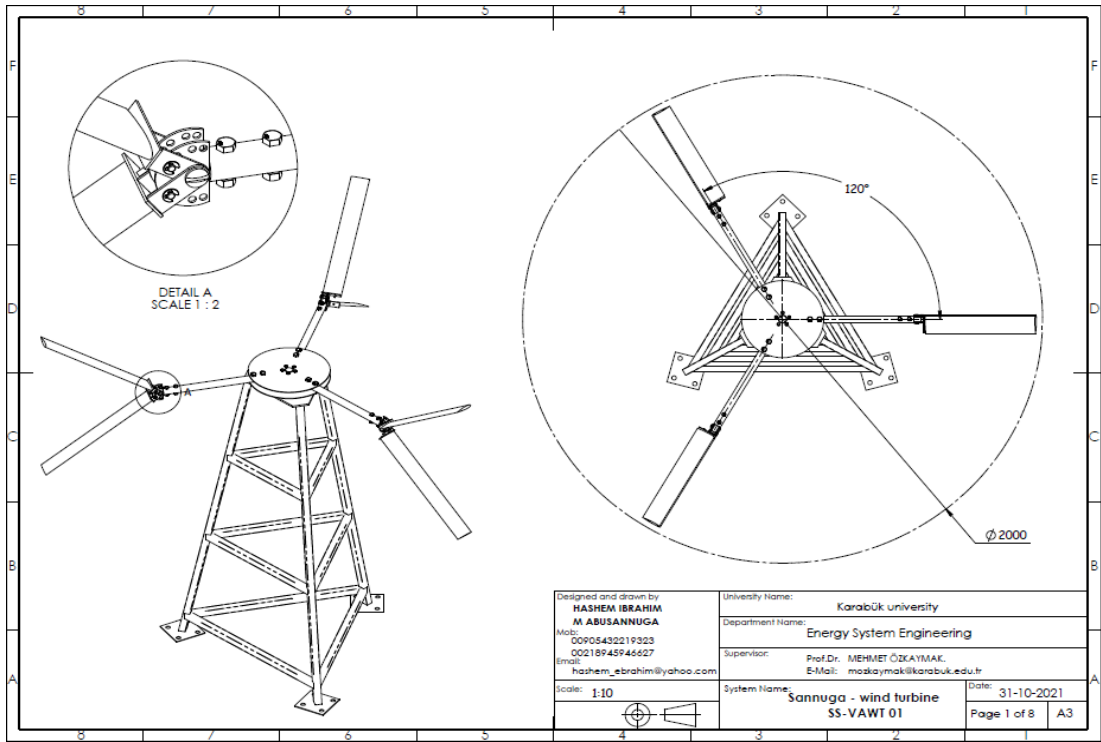


Figure Appendix B.1. “Sannuga System VAWT 01” Engineering Drawings.

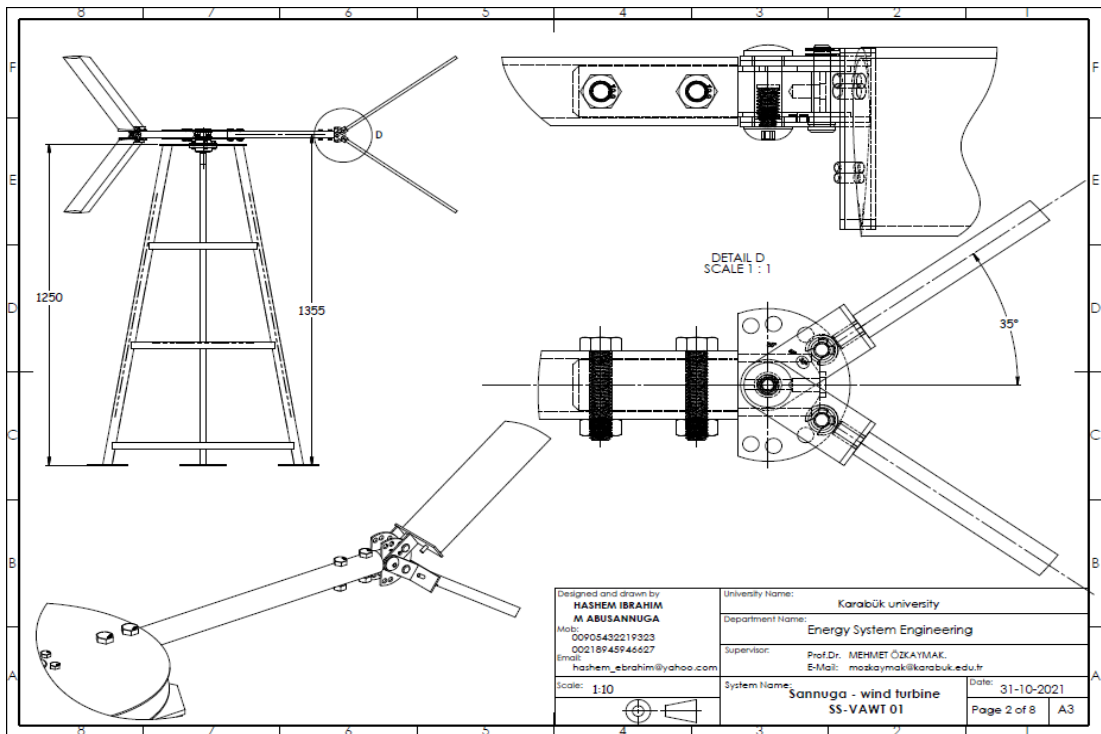


Figure Appendix B.1. (Continuing)

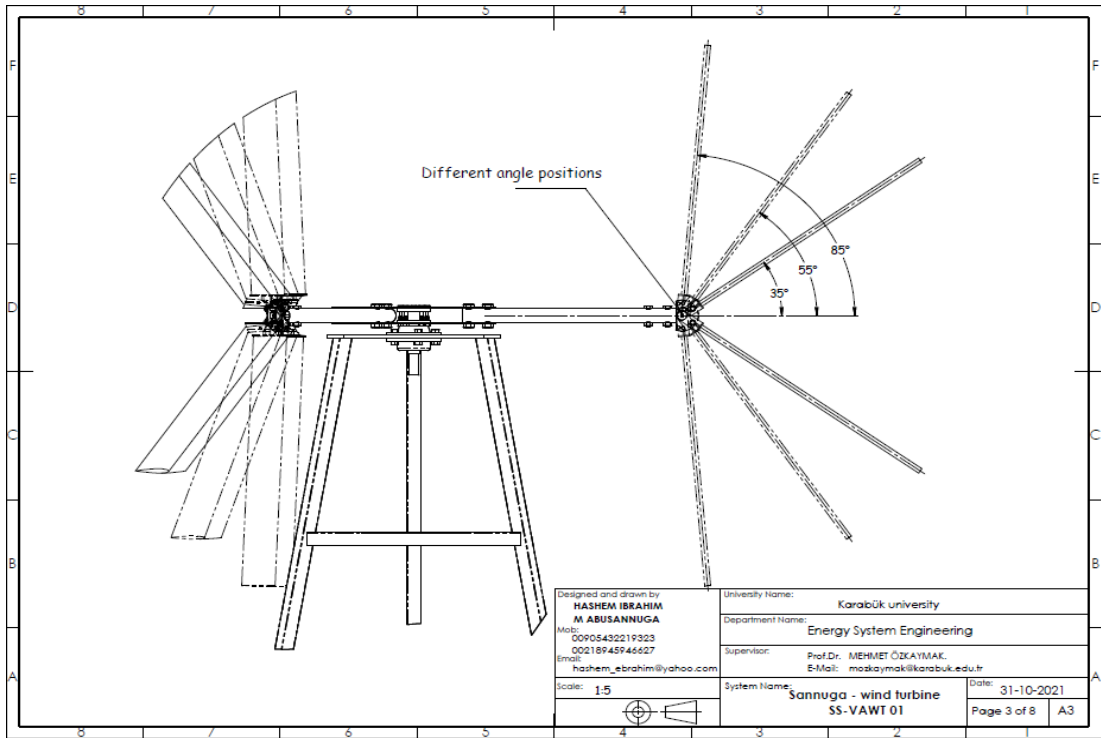


Figure Appendix B.1 (Continuing)

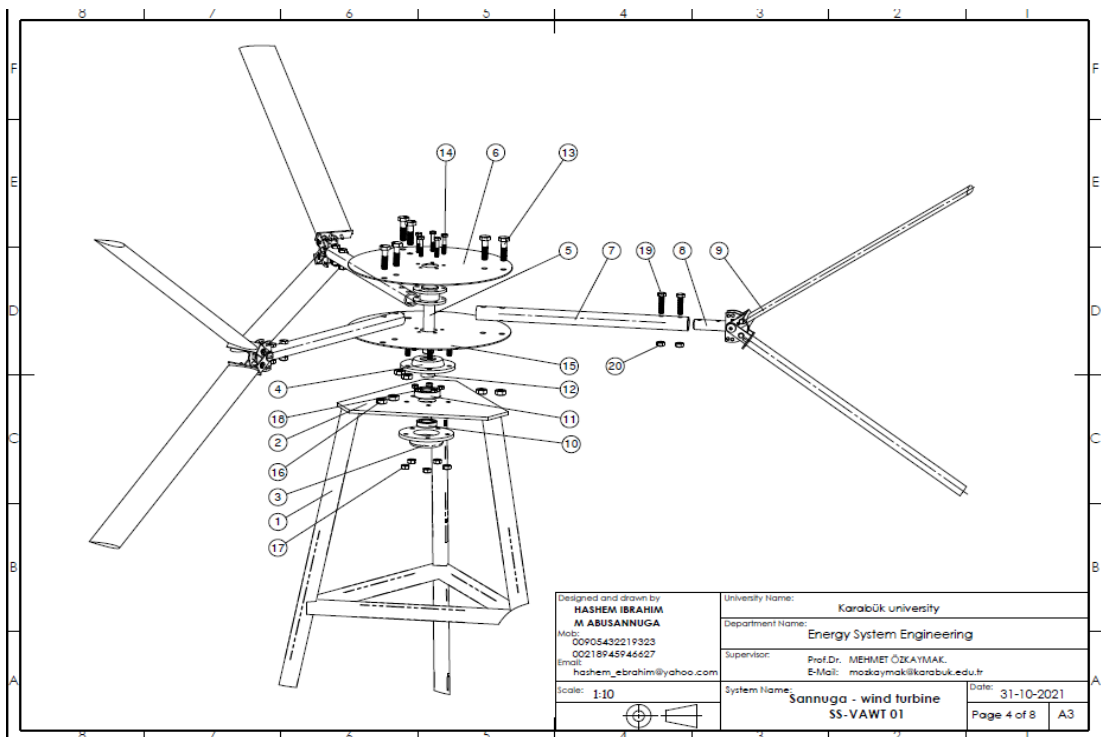


Figure Appendix B.1. (Continuing)

ITEM	Qty	DESCRIPTION	MATERIAL	NOTE
1	1	lattice tower	Steel	
2	1	tower base	Steel	Thickness 6 mm
3	1	Bottom Cover	Steel	
4	1	Top Cover	Steel	
5	1	Rotor Shaft	Steel	
6	2	rotor disk	Steel	Thikness 2 mm
7	3	Cylinder strut $\phi 22 \times 500 \text{mm}$	Aluminium	Thikness 1 mm
8	3	Movable joint	Aluminium	
9	6	Rotor blades	Fiber Glass	Airfoil: NACA 0015
10	1	Ball Bearing $\phi 20 \times 37 \times 9$		
11	1	Ball Bearing $\phi 20 \times 47 \times 13$		
12	1	Inner ring	Steel	
13	6	Hex Screw HM10 x 40		
14	5	Hex Screw HM6 x 35		
15	5	Hex Screw HM8 x 22		
16	6	Hex Nut HM10		
17	5	Hex Nut HM6		
18	5	Hex Nut HM8		
19	6	Hex Screw HM8 x 35		
20	6	Hex Nut HM8		

Figure Appendix B.1. (Continuing)

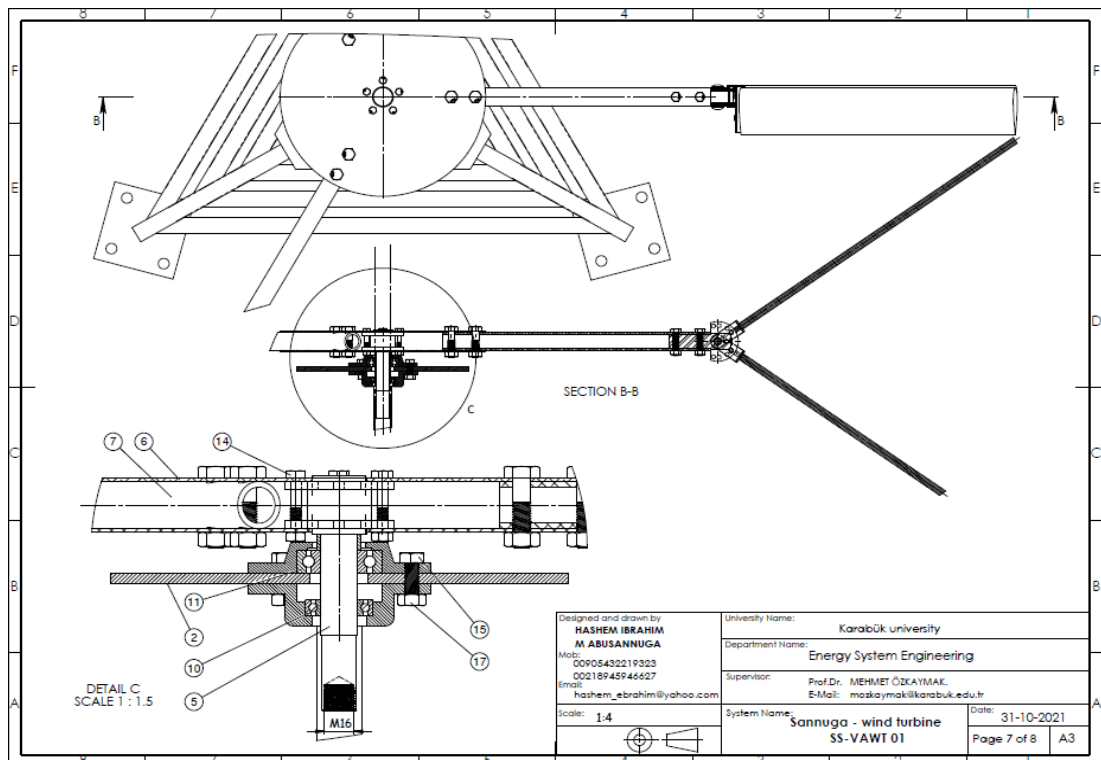


Figure Appendix B.1 (Continuing)

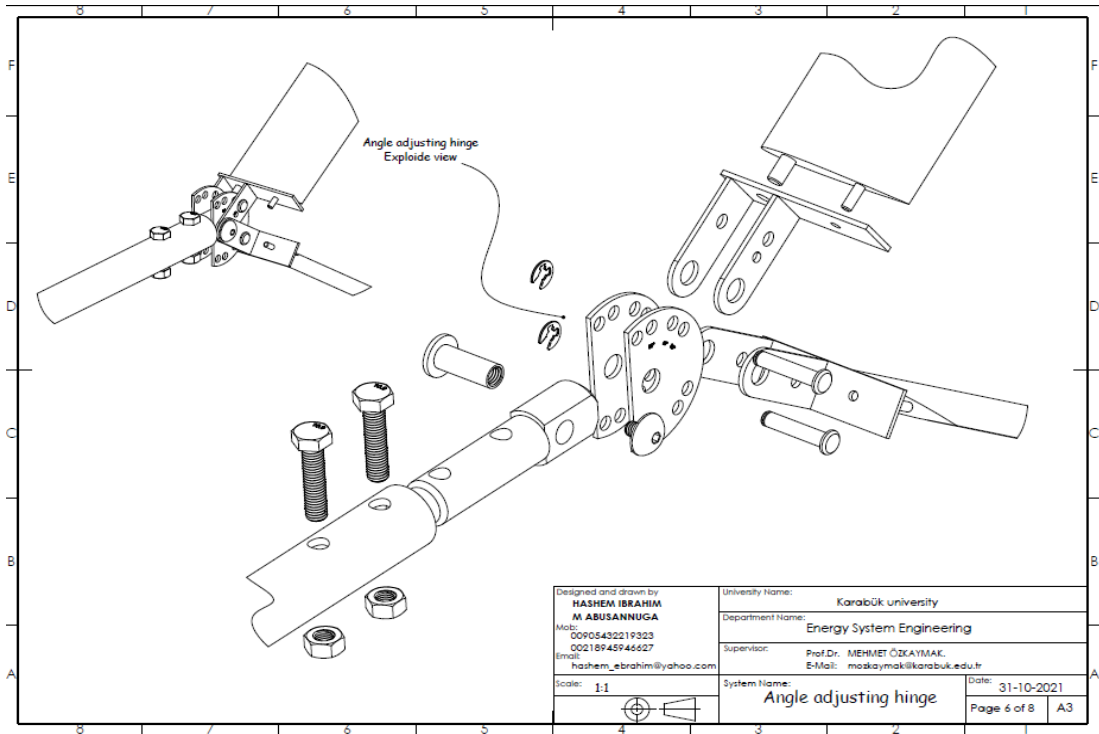


Figure Appendix B.1. (Continuing)

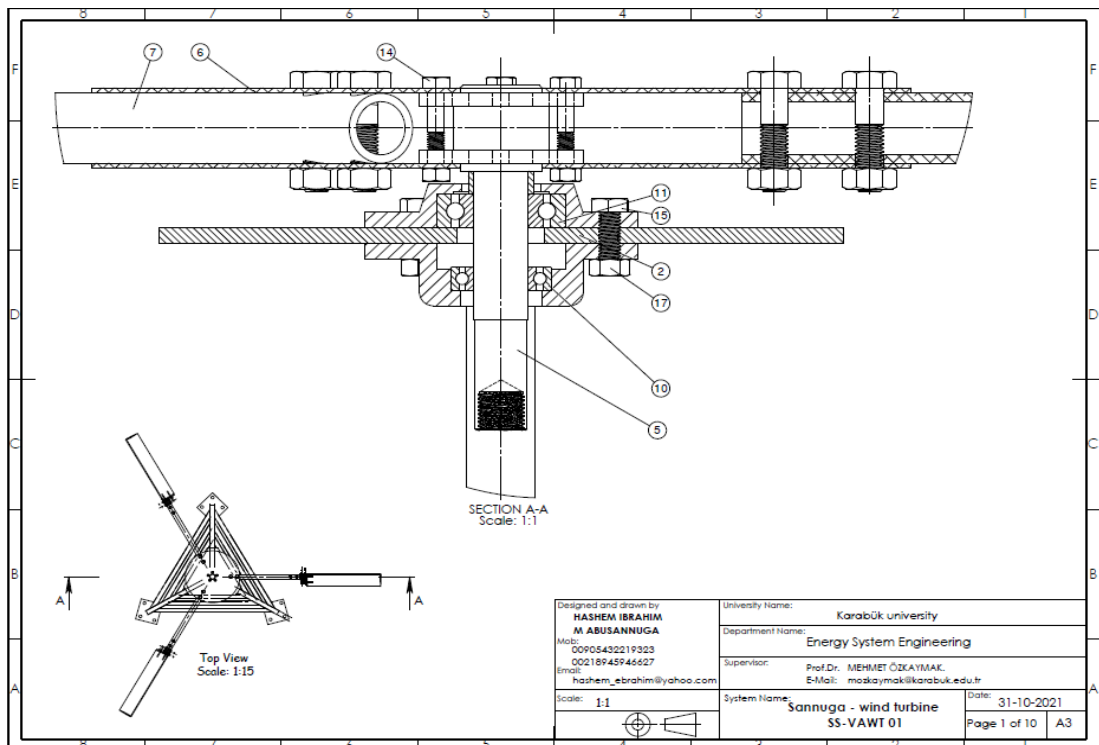


Figure Appendix B.1. (Continuing)

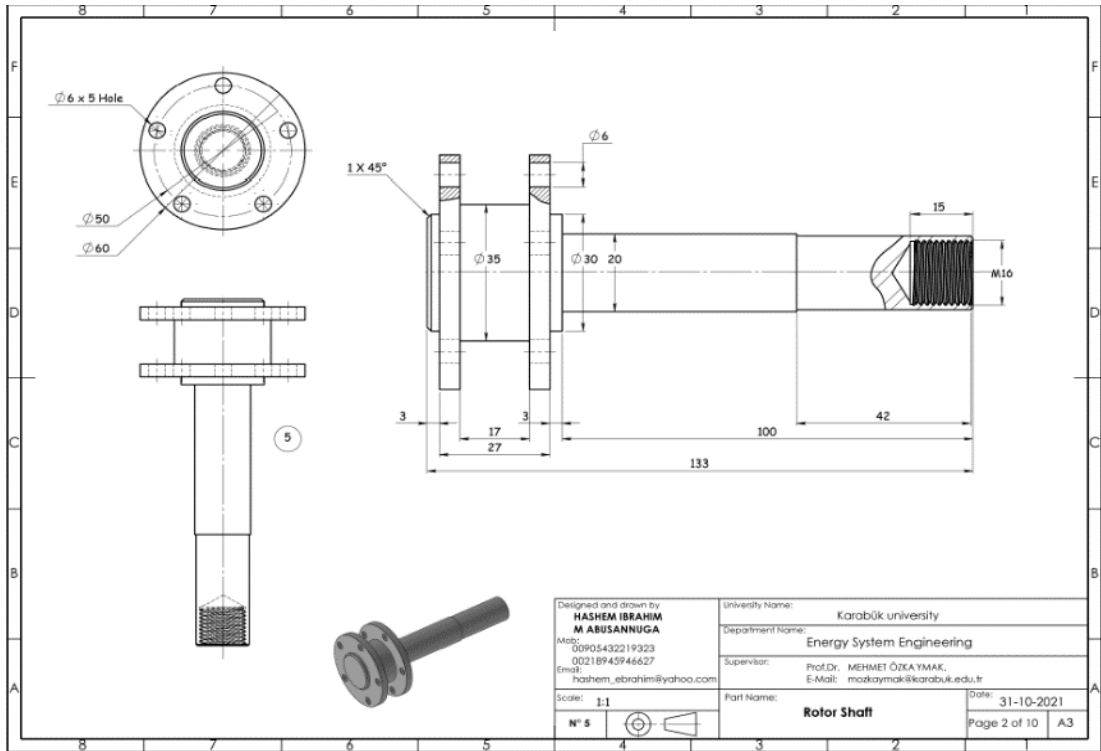


Figure Appendix B.1. (Continuing)

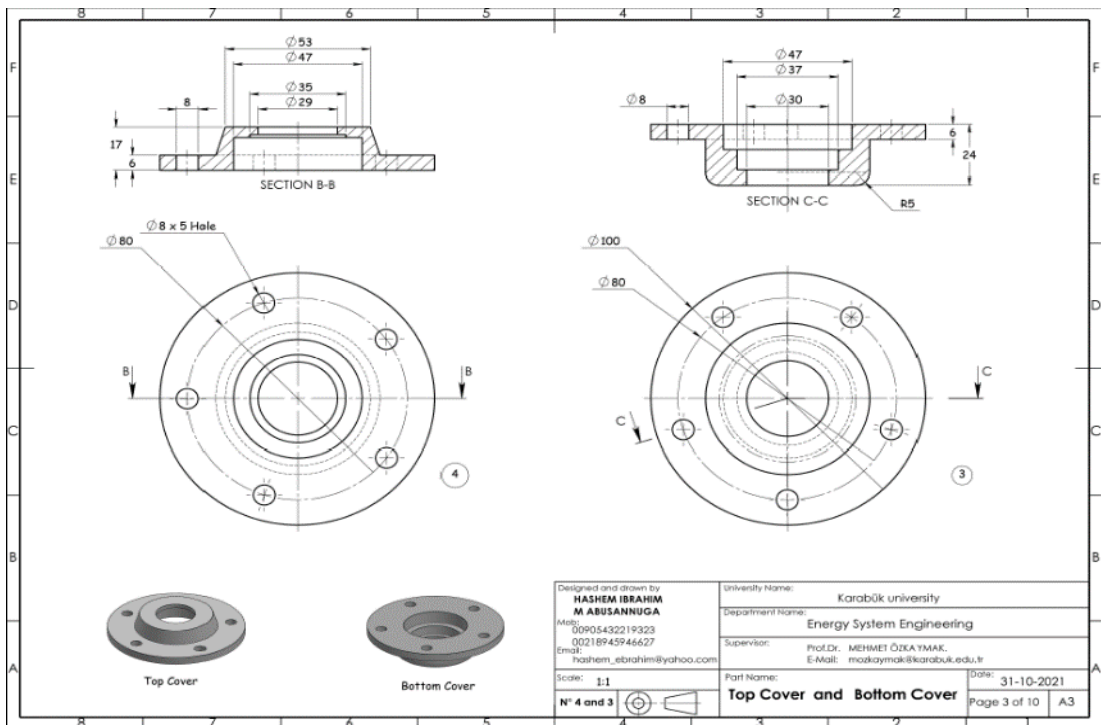


Figure Appendix B.1. (Continuing)

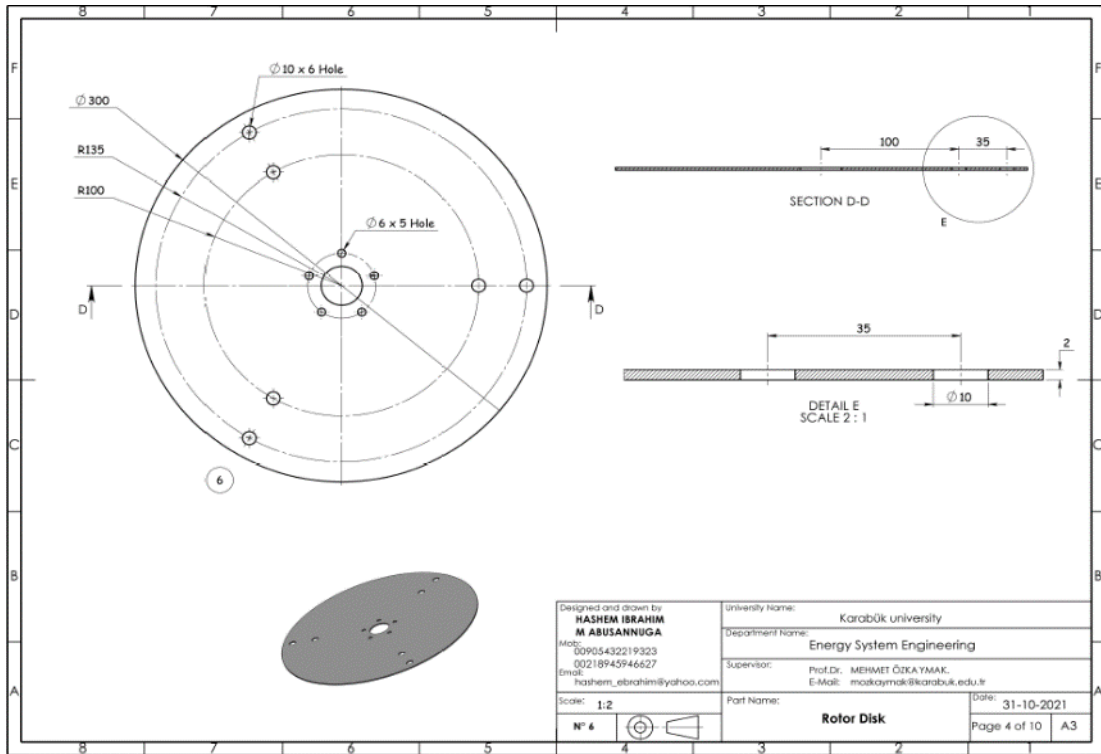


Figure Appendix B.1. (Continuing)

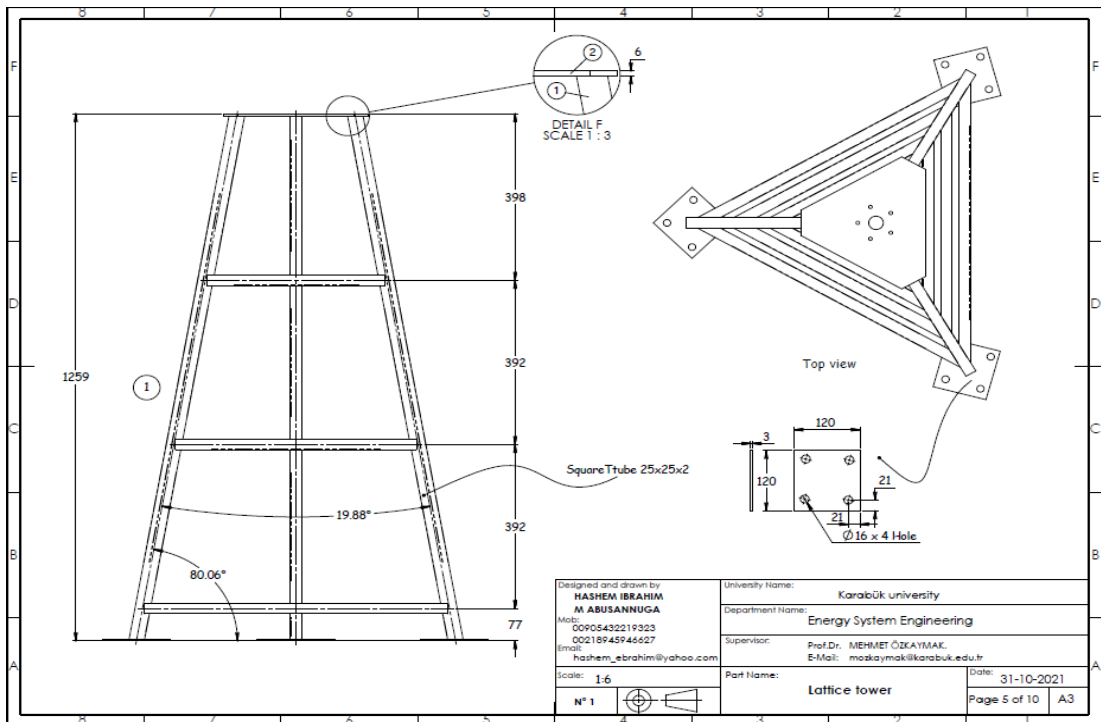


Figure Appendix B.1. (Continuing)

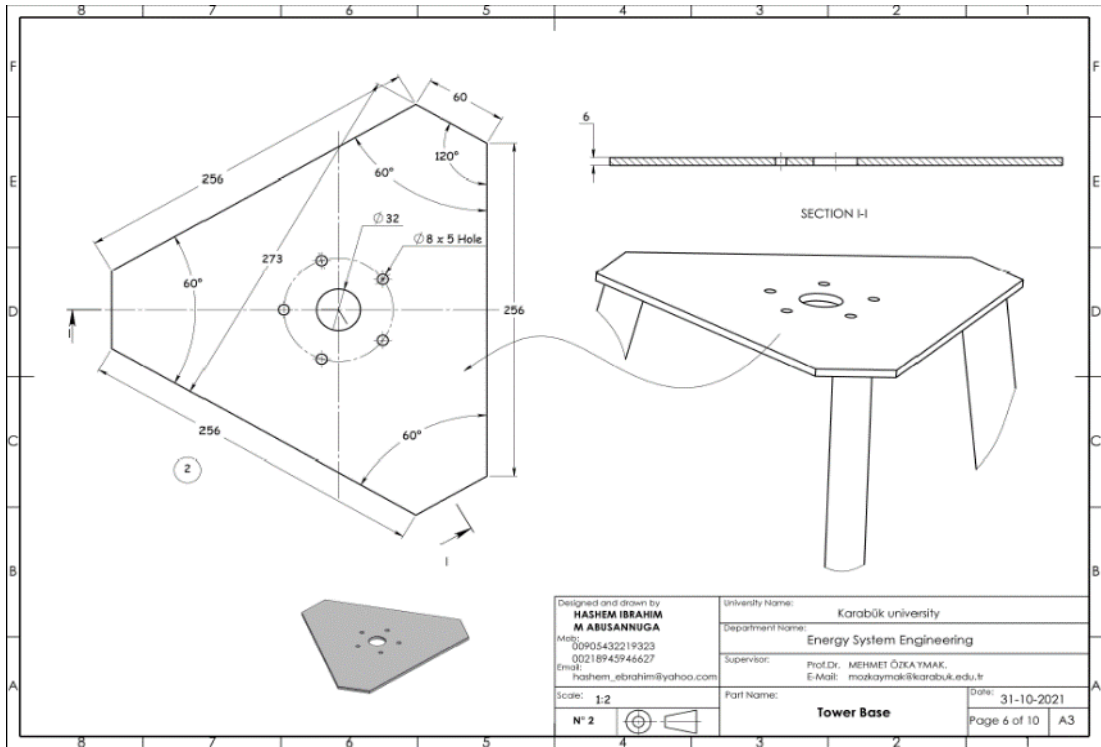


Figure Appendix B.1. (Continuing)

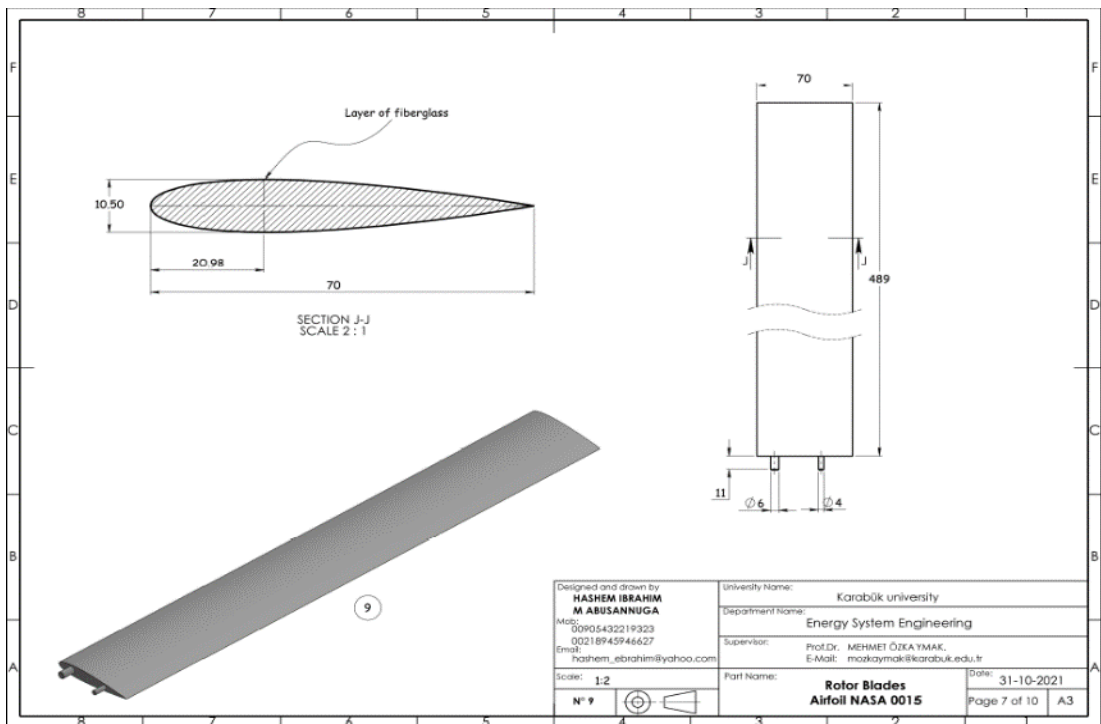


Figure Appendix B.1. (Continuing)

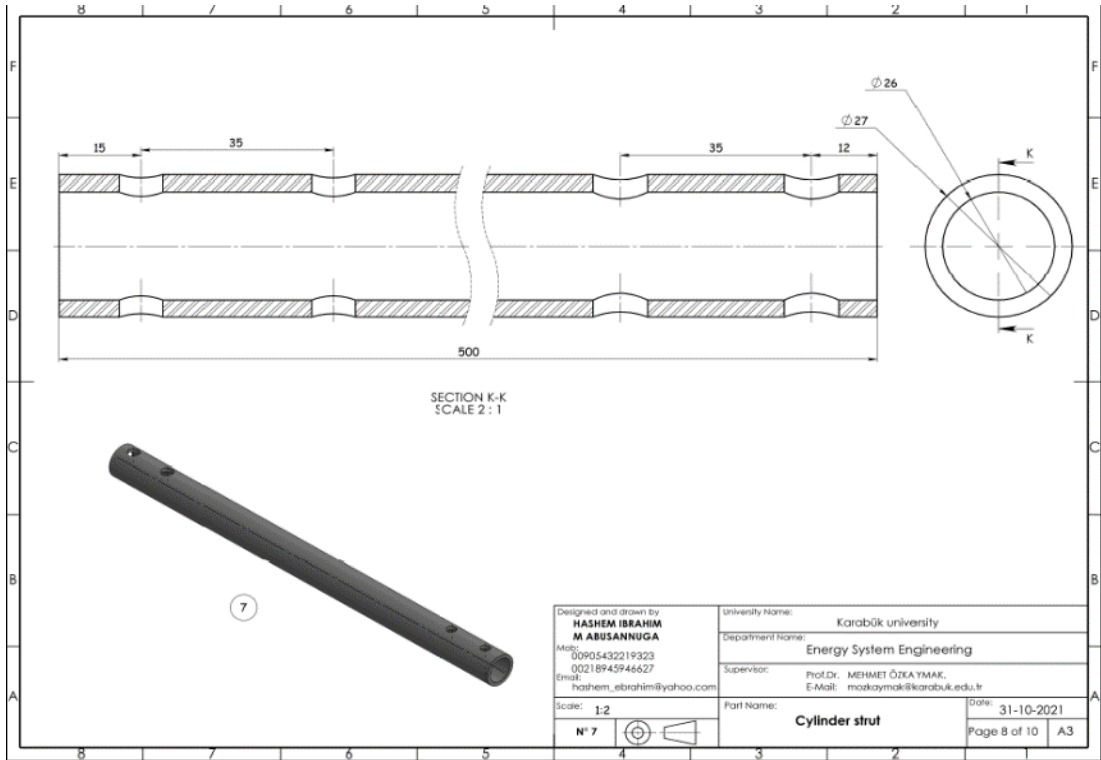


Figure Appendix B.1. (Continuing)

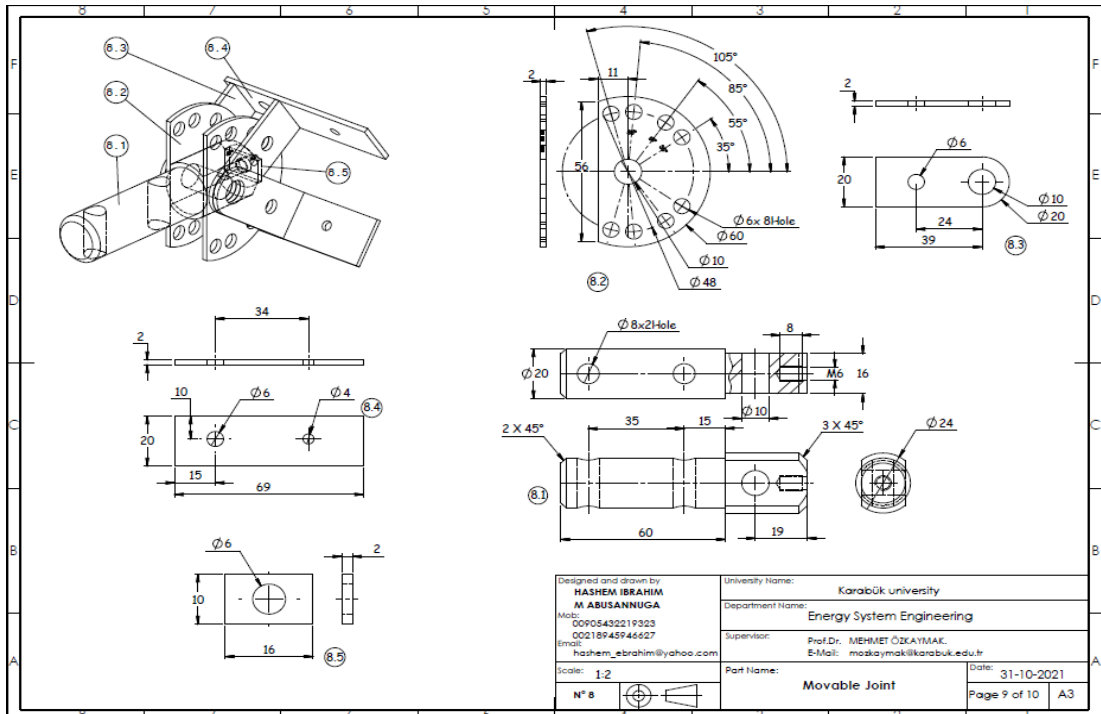


Figure Appendix B.1. (Continuing)

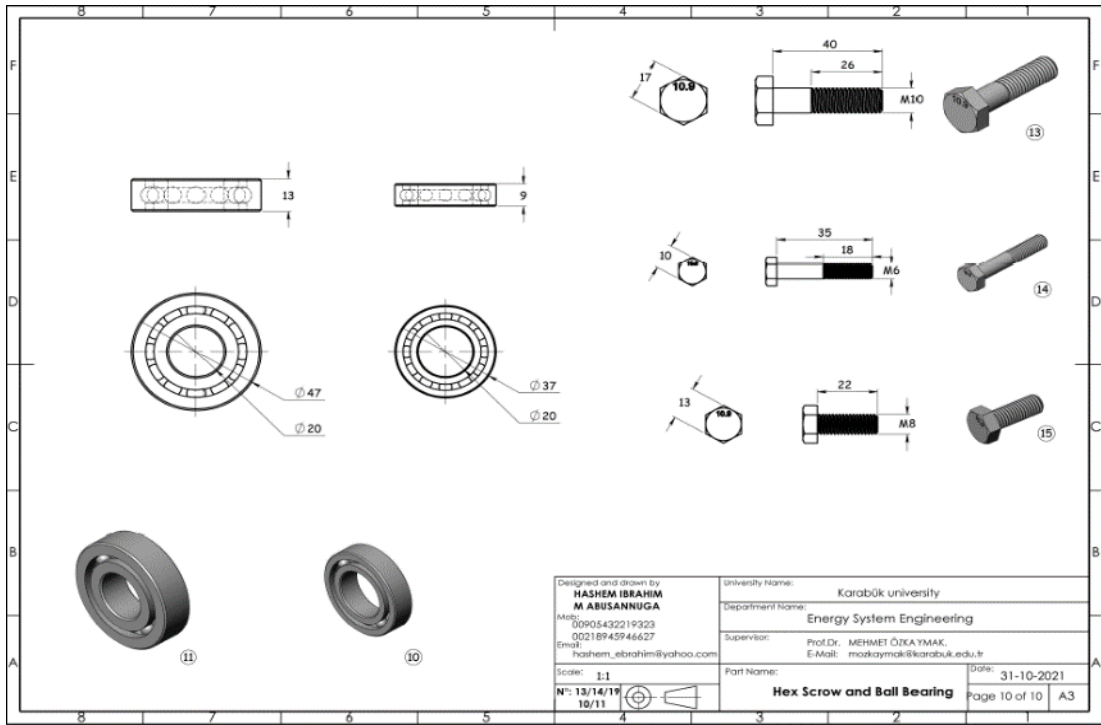


Figure Appendix B.1. (Continuing)

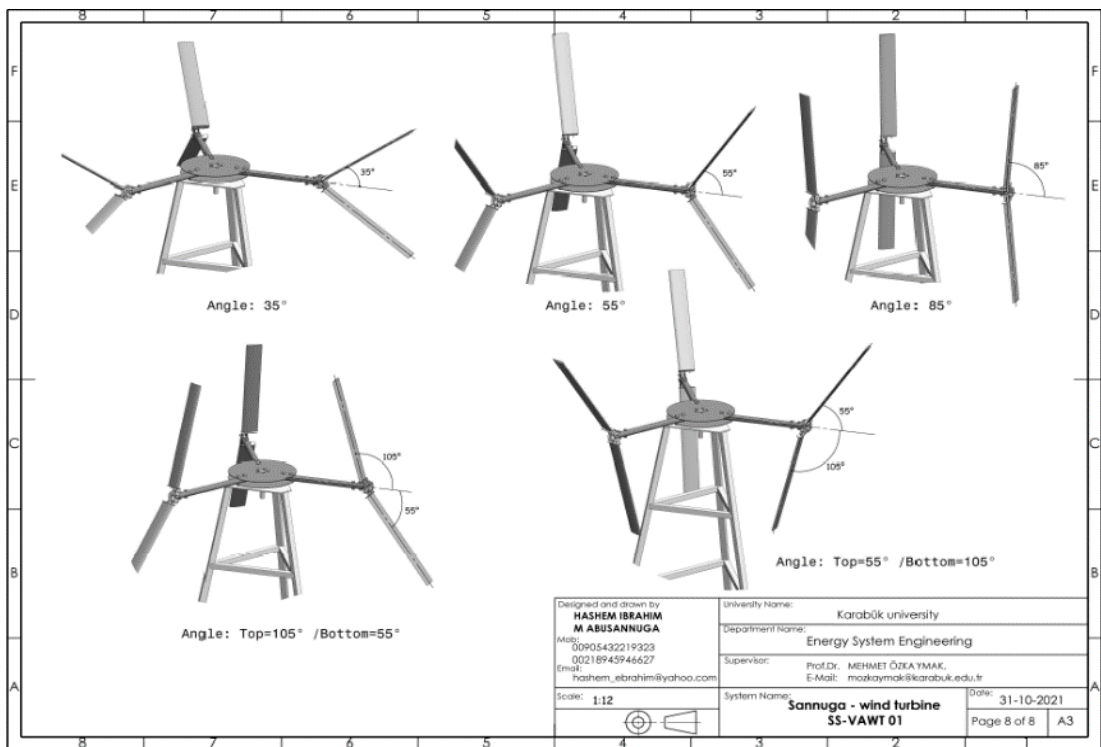


Figure Appendix B.1. (Continuing)

APPENDIX C.

PROTOTYPE MANUFACTURING

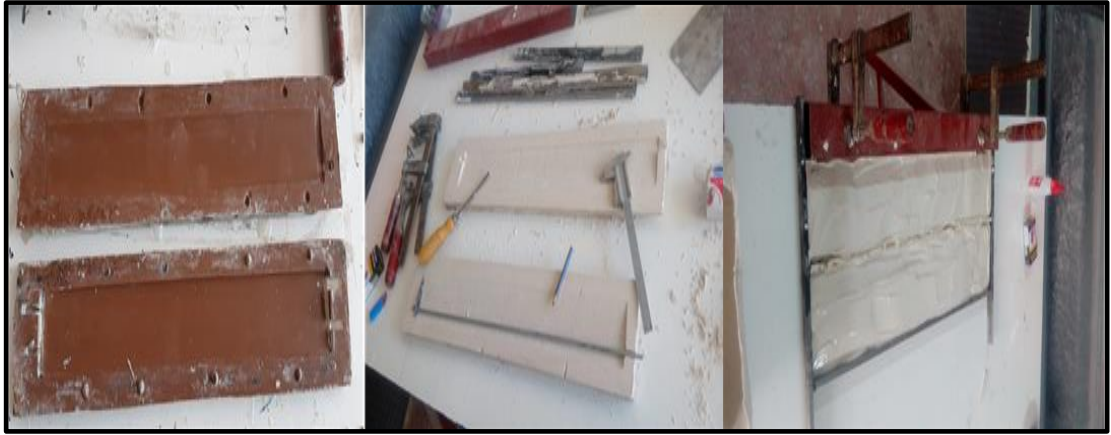


Figure Appendix C.1. Blades Tamblet.



Figure Appendix C.2. Initial Blade.



Figure Appendix C.3. Airfoil Tamblets.

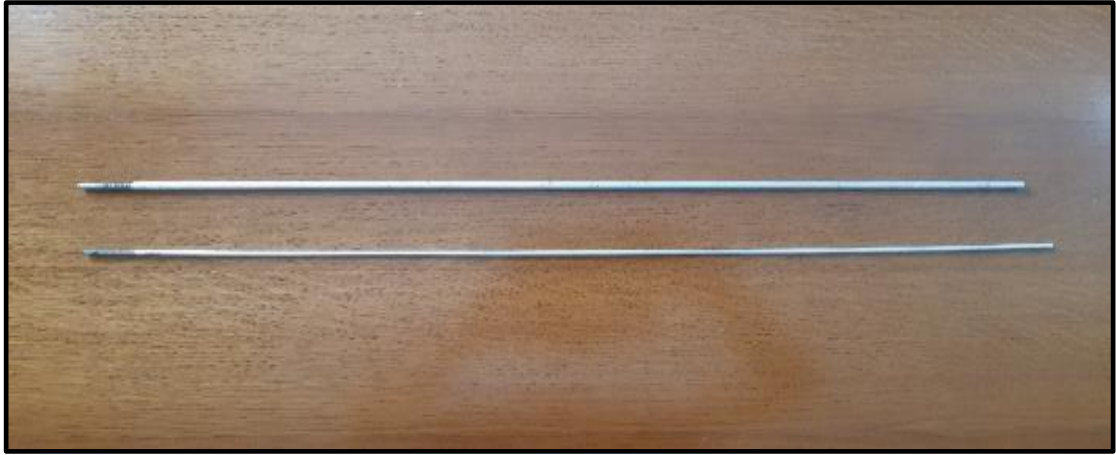


Figure Appendix C.4. Aluminyum Supports.



Figure Appendix C.5. Blades Production.



Figure Appendix C.6. Blades are Ready.

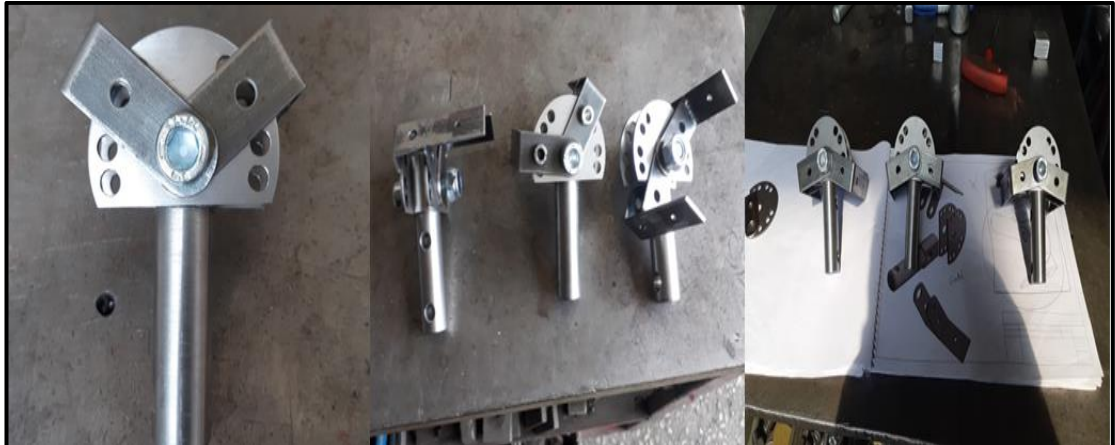


Figure Appendix C.7. Metal joints for fixing blades.



Figure Appendix C.8. Aluminum Struts Connecting Blades to the Discs.



Figure Appendix C.9. Iron Discs Connecting Struts to the Shaft.



Figure Appendix C.10. Iron Rotating Shaft.



Figure Appendix C.11. Bearing Covers.



Figure Appendix C.12. The Tower and Its Upper Base.

APPENDIX D.

SANNUGA SYSTEM SS-VAWT 01



Figure Appendix D.1. Multi Shape of “Sannuga System SS-VAWT 01”.

APPENDIX E.

PUBLICATIONS

PUBLICATIONS

1. H. Abusannuga and M. Özkaymak, "Towards Evaluating the Performance of Vertical Axis Wind Turbine Consist of Slant Straight Blades," 2020 IEEE International Conference on Environment and Electrical Engineering and 2020 IEEE Industrial and Commercial Power Systems Europe (EEEIC / I&CPS Europe), 2020, pp. 1-5, doi: 10.1109/EEEIC/ICPSEurope49358.2020.9160815.
2. H. Abusannuga and M. Özkaymak, "The effect of geometry variants on the performance of VAWT-rotor with incline-straight blades", AIP Advances 11, 045307 (2021), doi: <https://doi.org/10.1063/5.0042399>.
3. H. Abusannuga, M. Özkaymak, "Performance of Vertical Axis Wind Turbine Type of Slant Straight Blades", Advances in Science, Technology and Engineering Systems Journal, vol. 6, no. 4, pp. 292-297 (2021). DOI: 10.25046/aj060432.
4. H. Abusannuga, M. Özkaymak, "Investigation of Power Coefficient Behaviors of the Parabolic Wind Rotor Due to its Variable Geometry Parameters", International Journal of Renewable Energy Research (IJRER), Vol 10, No 1 (2020) DOI: <https://doi.org/10.20508/ijrer.v10i1.10363.g7901>
5. H. Abusannuga and M. Özkaymak, "Sannuga System-Slant Straight Blade Vertical Axis Wind Turbine", 3rd International Conference on Industrial Engineering and Industrial Management (IEIM 2022), ID: U2104-A, Spain, 13th January 2022.
6. H. Abusannuga and M. Özkaymak, "Whether the Darrieus Rotor with Straight-Blades or Curved blades is the Best, in Terms of Aerodynamic Effect", 12th International Conference on Future Environment and Energy, ID: TK6010, Tokyo, Japan, 20-22 January 2022.

RESUME

Hashem Ibrahim BUSANNUGA was born in Tripoli in 1979 and he graduated first and elementary education in this city. He completed high school education in Ali Warieth School, after that, he started undergraduate program in Tripoli University at Department of Aeronautical Engineering in 1998. Then in 2005, he started master program in the same Department. In 2006 HASHEM started assignment as a Research Assistant at the Center for Solar Energy Research and Studies (CSERS) in Tajoura city in Libya. To complete Ph.D. education, he moved to Karabük University in Turkey in 2017, where he has started his program at Energy System Engineering Department.